USC
UNIVERSIDADE
DE SANTIAGO
DE COMPOSTELA

ESCOLA DE DOUTORAMENTO
INTERNACIONAL EN CIENCIAS
E TECNOLOXÍA DA USC

Saray
Busto Ulloa

Tese de doutoramento

Contributions to the numerical solution of heterogeneous fluid mechanics models

Santiago de Compostela, 2017

PD en Métodos Matemáticos e Simulación Numérica en Enxeñaría e Ciencias Aplicadas

USC
UNIVERSIDADE
DE SANTIAGO
DE COMPOSTELA

CENTRO INTERNACIONAL DE ESTUDOS
DE DOUTORAMENTO E AVANZADOS
DA USC (CIEDUS)

TESE DE DOUTORAMENTO

Contributions to the numerical solution of heterogeneous fluid mechanics models

Saray Busto Ulloa

ESCOLA DE DOUTORAMENTO EN CIENCIAS E TECNOLOXÍA DA USC

PROGRAMA DE DOUTORAMENTO EN MÉTODOS MATEMÁTICOS E SIMULACIÓN NUMÉRICA EN ENXEÑARÍA E CIENCIAS APLICADAS

SANTIAGO DE COMPOSTELA

2017

USC
UNIVERSIDADE
DE SANTIAGO
DE COMPOSTELA

DECLARACIÓN DA AUTORA DA TESE

[**Contributions to the numerical solution of heterogeneous fluid mechanics models**]

Dna. Saray Busto Ulloa

Presento a miña tese, seguindo o procedemento adecuado ao Regulamento, e declaro que:

1. A tese abarca os resultados da elaboración do meu traballo.
2. No seu caso, na tese faise referencia ás colaboracións que tivo este traballo.
3. A tese é a versión definitiva presentada para a súa defensa e coincide coa versión enviada en formato electrónico.
4. Confirmo que a tese non incorre en ningún tipo de plaxio de outros autores nin de traballos presentados por min para a obtención de outros títulos.

En Santiago de Compostela, 20 de decembro de 2017

Asdo. Saray Busto Ulloa

USC
UNIVERSIDADE
DE SANTIAGO
DE COMPOSTELA

AUTORIZACIÓN DOS DIRECTORES DA TESE

[Contributions to the numerical solution of heterogeneous fluid mechanics models]

D. José Luis Ferrín González

Dna. María Elena Vázquez Cendón

INFORMAN:

Que a presente tese, se corresponde co traballo realizado por Dna. Saray Busto Ulloa, baixo a nosa dirección, e autorizamos a súa presentación, considerando que reúne os requisitos esixidos no Regulamento de Estudos de Doutoramento da USC, e que como directores desta non incorre nas causas de abstención establecidas na Lei 40/2015.

En Santiago de Compostela, 20 de decembro de 2017

Asdo. José Luis Ferrín González

Asdo. María Elena Vázquez Cendón

USC
UNIVERSIDADE
DE SANTIAGO
DE COMPOSTELA

Agradecementos

Ao longo destes anos foron moitas as persoas que me axudaron a percorrer o meu camiño. O seu apoio e ensinanzas foron esenciais para que este proxecto chegase a bo fin.

Gustaríame comezar agradecéndolles aos meus directores: *Elena Vázquez Cendón* e *José Luis Ferrín*, toda a súa dedicación, paciencia e confianza. Os seus coñecementos e experiencia foron decisivos para a consecución desta tese. Grazas por contaxiarme o voso entusiasmo e por abrirme as xanelas a mundos completamente novos para min.

Quixera, tamén, mencionar a *Alfredo Bermúdez* e a *María Luisa Seoane* pois sen eles esta andaina pola Matemática Aplicada nunca tería sido posible. Marisa, grazas por axudarme dende os meus primeiros pasos. Alfredo, grazas por ter sempre a porta aberta para min, é todo un privilexio aprender de ti.

Neste tempo tiven a sorte de poder realizar dúas estancias de investigación cuns magníficos directores, *Eleuterio Toro* da Università degli Studi di Trento e *Gianluigi Rozza* da SISSA. Tito, es un lujo poder trabajar contigo, gracias por recibirme con los brazos abiertos. Gianluigi e Giovanni, grazie mille per aver trovato il tempo dove non c'era e per i vostri consigli. Vorrei anche ringraziare i miei compagni di lavoro sia a Trieste che a Trento. Le pause a pranzo, le gite, le conference, i viaggi in bus, le lezione improvisate d'Italiano... mi avete fatto sentire felice tra di voi. Arigatō. Xièxiè. Grazie.

Se ben é certo que estiven uns meses fora, a maior parte desta etapa paseina na Facultade de Matemáticas de Santiago de Compostela. Non podo por menos que agradecerlles a todos os membros do Departamento de Matemática Aplicada o tempo compartido, o seu exemplo e o seu apoio. *Fran*, *Carmen* e *Jerónimo*, grazas por compartirdes todos os vosos coñecementos cando me inciciáchedes nesa aventura de aprender a ensinar. *Laura*, grazas polas túas achegas, por estar sempre disposta a botarme unha man. *Dolores* e *Patricia* grazas polos vosos constantes ánimos e consellos. *Marta*, grazas polas discusións improvisadas, por compartir experiencias e opinións. *Carlos*, *Elisa* e *Manolo*, grazas por resolverme os meus infinitos problemas informáticos, lingüísticos e administrativos.

Por suposto nunca me poderei esquecer dos meus compañeiros de tese e proxectos: *Mercedes*, *Ibán*, *Pedro*, *Chuco*, *Fran*, *Cris*, *Víctor*, *Gonzálo*, *Enrique*, *Cristina*, *Begoña*, *Juan Carlos*, *Luis*, *Jorge*... con vós tiven a sorte de poder compartir esta aventura: lecturas cruzadas de correos, papeleo, cafés, comidas, excursións, dúbidas, sesións de terapia, éxitos, congresos, reencontros... grazas por permitirme percorrer este camiño

en tan extraordinaria compañía. Quero darlles as grazas especialmente a *Miriam* e a *Maribel*, porque compartides conmigo o bo e o malo, porque me entendedes, porque ás veces sabedes máis cousas de min que eu mesma.

Moitas grazas á miña *familia* e *amigos*, por creer en min e animarme a superar cada novo reto. *Mercedes*, ti transmitíchesme dende o primeiro momento a túa paixón polas matemáticas e despertaches en min a curiosidade pola investigación. *David*, grazas pola túa paciencia e por axudarme a poñer as cousas en perspectiva. *Avós*, de vós aprendín o significado de esforzo e constancia. A meus pais débolles o que son. Grazas *Papá* por animarme sempre a loitar polos meus soños e por ensinarme a non rendirme nunca. *Mamá*, merci de toujours m'écouter, d'être sincère, de trouver les mots justes. Aos dous: grazas por estar sempre ahí.

This work was financially supported by Spanish MECD under grant FPU13/00279; by Xunta de Galicia Consellería de Cultura Educación e Ordenación Universitaria under grant *Axudas de apoio á etapa predoutoral do Plan I2C*, PRE/2013/031, and under project GRC2013-014 2013-PG082, by Fundación Barrié under grant *Becas de posgrado en el extranjero 2013* and by Spanish MINECO under project MTM2013-43745-R.

A meus pais, Ángeles e Jesús.

Ás estrelas que iluminan o meu camiño.

USC
UNIVERSIDADE
DE SANTIAGO
DE COMPOSTELA

Contents

Preface

Fluids play a primal role in numerous industrial and environmental problems. Therefore, an increasing number of researchers have focused, during the last decades, on better understanding their behaviour. Several mathematical models and various numerical methods have been developed willing to solve specific fluid mechanics problems.

This PhD thesis deals with two specific kinds of flows: incompressible flows and compressible low Mach number flows. Accounting for the features of the flows we are modelling, the derivation of incompressible and compressible Navier-Stokes equations is recalled (see [Ber05] and [CL14]).

Previous works in fluid mechanics have shown us that a wide variety of problems involve not only laminar but also turbulent flows. That could be observed, for instance, when analysing the flow around an object (see [Bus14], [Bus15] and [BBFF15]). Numerical simulation of turbulence is thus of great interest. However, it comprises a large range of scales in non-linear iteration with each other. This fact makes performing direct numerical simulation unaffordable. Therefore, to compute the effect the smallest scales have on the mean flow, we use turbulence models. In particular, in this thesis, we will couple Navier-Stokes equations with a RANS $k-\varepsilon$ turbulent model (see [LS72], [Wil88], [MP94] and [CL14]).

Another kind of problems involving additional variables appears, for example, in the design of a gas network (see [BLVC16], [BLVC17b] and [BLVC17a]) or when analysing the mixture of diverse species in a furnace (see [FS13] and [CFS13]). Both of them entail the resolution of a new set of equations. More precisely, the mass fractions can be modelled using the transport of species equations whereas the energy conservation equation provides the temperature distribution.

The scope of this thesis is to develop high-order numerical methods to solve incompressible turbulent flows and compressible low Mach number flows. To this end, we extend the projection hybrid finite volume - finite element method first put forward in [BFSVC14].

The high complexity of the systems to be solved makes the theoretical study of numerical methods unaffordable in the three-dimensional case. Seeking to capture the main problematic of the three-dimensional models in a simplified equation, we define the unidimensional advection-diffusion-reaction equation with time and space dependent advection and diffusion coefficients. Diverse numerical high-order methods are introduced aiming to solve it. Furthermore, the accuracy and stability analysis are

carried out. Once the former methodologies are validated, they are extended to solve the governing equations of the three-dimensional models.

The projection hybrid finite volume - finite element methodology proposed decouples the computation of the pressure and the conservative variables. Therefore, we profit from the main strengths of the two numerical methods used. The finite volume methodology is applied to solve the advection-diffusion-reaction equations providing a high-order approximation of the conservative variables. On the other hand, a finite element method supplies the solution of the Laplace problem related to the pressure correction.

As final step, the method of manufactured solutions is applied in order to obtain analytical tests which asses the performance of the above methodology. Moreover, classical fluid dynamics problems are solved and some of the numerical results obtained are successfully compared with experimental data.

In what follows, we include a detailed description of the contents of each part of the thesis.

Part I. Mathematical modelling

Aiming to get a self-contained document, we devote the first part of this thesis to recall basic concepts of continuum mechanics and the mathematical models used to portray incompressible and compressible low Mach number flows. Following [Gur81] and [Ber05], we start by characterizing the behaviour of a mixture of Coleman-Noll fluids using the mass conservation law and the balances of momentum and energy. Next, the concept of incompressible Newtonian fluid is introduced and the related system of equations is presented. In order to obtain simplified mathematical models for the former types of fluids, a dimensional analysis is performed. The resulting systems of equations are called, respectively, compressible and incompressible Navier-Stokes equations. Finally, we derive the equations of the RANS $k - \varepsilon$ model which are coupled with the Navier-Stokes equations to solve turbulent flows (see [MP94] and [CL14]).

Part II. Numerical analysis of the unidimensional advection-diffusion-reaction equation

The goal of this part is to develop high-order finite volume schemes. Due to the complexity on deriving them for three-dimensional models, we focus on the unidimensional advection-diffusion-reaction equation. Following the works on [Kol11] and [CVC12], Kolgan and CVC Kolgan-type schemes are presented for the advection equation. To obtain second-order in space and time schemes, ADER, [TMN01], and MUSCL-Hancock, [vL97], methodologies are introduced and extended to solve the advection-diffusion-reaction equation. Furthermore, a modification of ADER methodology, LADER method, is proposed to reduce the stencils involved in the numerical scheme. Its extension to solve the advection-diffusion-reaction equation with time and space dependent advection coefficients is derived. Stability and accuracy analysis are carried out for the obtained schemes. Finally,

several test problems are presented in order to study the empirical convergence rates.

The extension of ADER and MUSCL-Hancock methodologies to solve the advection-diffusion-reaction equation were detailed in [BTVC16]. Besides, the studies related to LADER methodology were partially included in [BFTVC18].

Part III. Projection hybrid FV/FE method for Navier-Stokes equations

The projection hybrid finite volume - finite element method put forward in [BFSVC14] is proposed to solve Navier-Stokes equations. Three different stages are considered in the resolution of incompressible flows. At the transport diffusion stage, a first approximation of the conservative variables is computed. To obtain high-order schemes, the finite volume methods developed in Part II are extended to the three-dimensional case. At the projection stage, a finite element method provides the pressure correction needed to enforce the divergence free condition on the velocities. Their final values are computed at the post-projection stage. Finally, the production and source terms related to the turbulence, the species and the energy conservation equations are obtained. Regarding compressible low Mach number flows, a new pre-projection stage, in which the density is obtained from the temperature and the composition of the mixture, is added. Besides, special care is paid to the time and space dependency of the density. Consequently, a modified artificial viscosity is defined in order to stabilize the schemes. To analyse the order of accuracy of the former methodologies, several manufactured solution tests are studied. Moreover, some more realistic problems are posed and the results obtained are compared with those available in the bibliography.

Preliminary results concerning this part have been presented in [BBC$^+$15] and [BBF$^+$17c]. The methodology and analysis related to incompressible flows were introduced in [BFTVC18].

Appendices.

Appendix A is devoted to the analysis of the truncation error of Kolgan and CVC Kolgan-type schemes introduced in Part II.

Appendix B contains a summary of this dissertation in Galician.

USC
UNIVERSIDADE
DE SANTIAGO
DE COMPOSTELA

Part I

Mathematical Modelling

USC
UNIVERSIDADE
DE SANTIAGO
DE COMPOSTELA

Contents

USC
UNIVERSIDADE
DE SANTIAGO
DE COMPOSTELA

Introduction

Low Mach number flows are involved in a wide variety of natural phenomena and industrial processes. Therein, their study has been a major goal in the last centuries. From the mathematical point of view, the analysis of these problems starts with the development of a mathematical model which captures the main features of the flow. Depending on the process to be modelled, various systems of equations are obtained. Detailed information about mathematical models for continuum mechanics and thermomechanics can be found, for instance, in [Gur81] and [Ber05].

In this work, we focus on Navier-Stokes equations for both incompressible and compressible low Mach number flows. Seeking to provide the framework for this thesis, we recall basic concepts of fluid mechanics and we derive the systems of equations to be solved following the former publications.

Compressible flows are characterized by the mass, momentum and energy conservation equations and by the state equation. Moreover, if the fluid is a mixture, species transport equations are also included. On the other hand, incompressible fluids assume a constant value for the density. Herein, the system of equations to be solved reduces to the mass and momentum conservation equations.

The dimensional analysis of the obtained models leads to the compressible and incompressible Navier-Stokes equations. Besides, when dealing with a turbulent flow a RANS turbulent model can be coupled with the Navier-Stokes equations aiming to decrease the computational complexity of a direct numerical simulation. More precisely, we apply the $k-\varepsilon$ standard model. Classical references in which the equations related to the kinetic energy, k, and dissipation rate, ε, are deduced are [MP94], [CL14] or [Wil88].

This part is divided into two chapters. A careful introduction on the concepts of fluids and incompressible Newtonian fluids is accomplished in Chapter 1. Furthermore, the mathematical models for compressible low Mach number flows and incompressible flows are described and the related dimensional analysis is performed. Chapter 2 is devoted to the derivation of the RANS $k-\varepsilon$ model. Firstly, the election of this model to capture turbulent effects is motivated by its comparison with other models available in the literature. Then, the averaging of Navier-Stokes equations is tackled leading to the introduction of the eddy viscosity and the turbulent kinetic energy. Next, the partial differential equations needed to compute the turbulent variables are presented. Finally, the global schemes to model turbulent flows for both incompressible and compressible low Mach number flows are obtained.

USC
UNIVERSIDADE
DE SANTIAGO
DE COMPOSTELA

Chapter 1

Mathematical modelling in continuum thermomechanics

This chapter is devoted to recall some of the central concepts of fluid dynamics. Besides, the mathematical models for compressible and incompressible flows are presented following [Ber05] and [Gur81].

The outline of this chapter is as follows. We start reviewing some general notations and results from continuum mechanics. The mass conservation law and the balances of momentum and energy are recalled. Next, the concept of fluid is introduced and the equations needed to characterize compressible flows are developed. In Section 1.3, the system is extended to model a Coleman-Noll mixture and the state law is described. The definition of incompressible Newtonian fluids and the related conservation equations are presented in Section 1.4. Finally, the dimensional analysis of the obtained systems is performed in Section 1.5.

1.1 General definitions

In this section, we recall some definitions and results from continuum mechanics that will be used throughout this document.

Let us consider an affine space, $\mathcal{E}$, on a three-dimensional Euclidean vector space $\mathcal{V}$. Let Lin be the vector space of endomorphism of $\mathcal{V}$ (which is isomorphic to the space of second order tensors) and Sym the subspace of those which are symmetric.

Definition 1.1.1. A regular region is a closed region, that is, the closure of a connected open set in $\mathcal{E}$, with piecewise $\mathcal{C}^1$ boundary.

Definition 1.1.2. A body, or reference configuration, $\mathcal{B}$ is a regular region of the Euclidean space $\mathcal{E}$. Elements in $\mathcal{B}$ are called material points. A part $\mathcal{P}$ is a bounded regular subregion of $\mathcal{B}$.

Definition 1.1.3. A deformation of $\mathcal{B}$ is a smooth one-to-one mapping $\mathbf{f}$ which maps $\mathcal{B}$ onto a closed region in $\mathcal{E}$ and verifies $\det(\nabla \mathbf{f}) > 0$.

Definition 1.1.4. A motion of $\mathcal{B}$ is a class $\mathcal{C}^3$ mapping

$$X : \mathcal{B} \times \mathbb{R} \to \mathcal{E}$$

with $X(\cdot, t)$ a deformation of $\mathcal{B}$ for each fixed t. We will denote

$$\mathcal{B}_t := \{x \in \mathcal{E} : \exists p \in \mathcal{B} \text{ such that } X(p,t) = x\}$$

the region of space occupied by the body at time t.

Definition 1.1.5. Considering a material point $p \in \mathcal{B}$ and $x = X(p,t)$ its place at time t, the trajectory of the motion is the set

$$\mathcal{T} := \{(x,t) : x \in \mathcal{B}_t, t \in \mathbb{R}\}.$$

Definition 1.1.6. The reference map of the motion,

$$P : \mathcal{T} \to \mathcal{B}$$

is the inverse mapping of X. It provides the material point which occupies the place x at time t.

Definition 1.1.7. The displacement of p at time t is the vector $\mathbf{v}(p,t) = X(p,t) - p$.

Definition 1.1.8. The gradient of the motion is the tensor $F(p,t) := \nabla X(p,t)$.

Definition 1.1.9. The Green-Saint Venant strain tensor is defined by

$$G = \frac{1}{2}\left(F^t F - I\right) = \frac{1}{2}\left(\nabla \mathbf{v} + \nabla \mathbf{v}^t + \nabla \mathbf{v}^t \nabla \mathbf{v}\right).$$

Its linear part,

$$E = \frac{1}{2}\left(\nabla \mathbf{v} + \nabla \mathbf{v}^t\right), \tag{1.1}$$

is called infinitesimal strain tensor.

Definition 1.1.10. The fields defined on $\mathcal{B} \times \mathbb{R}$ are called material or Lagrangian fields while those defined on $\mathcal{T}$ are spatial or Eulerian fields.

We can swap between material and spatial fields using the movement and the reference mappings:

$$\begin{array}{rccc} \psi : & \mathcal{B} \times \mathbb{R} & \longrightarrow & \mathcal{T}, \\ & (p,t) & \longrightarrow & \psi(p,t) := (X(p,t),t), \end{array}$$

$$\phi_m := \phi_s \circ \psi,$$

Operator	Material field	Spatial Field
Time derivative	$\dot{\phi}$	$\dfrac{\partial \phi}{\partial t}$
Spatial derivative	$\nabla \phi$	$\operatorname{grad} \phi$
Divergence	$\operatorname{Div} \phi$	$\operatorname{div} \phi$
Curl	$\operatorname{Curl} \phi$	$\operatorname{curl} \phi$

Table 1.1: Notation of the differential operators.

$$\begin{aligned} \psi^{-1}: \quad \mathcal{T} &\longrightarrow \mathcal{B} \times \mathbb{R}, \\ (x,t) &\longrightarrow \psi^{-1}(x,t) := (P(x,t),t), \\ \phi_s &:= \phi_m \circ \psi^{-1}. \end{aligned}$$

Depending on whether the field is given in the material or the spatial description, different notations for the differential operators will be used (see Table 1.1 for further details). In particular, $\mathbf{u}(x,t) := \dot{X}(P(x,t),t)$ is the spatial description of the velocity.

After having introduced some general definitions and notations we can present the conservation laws for a body.

1.1.1 Conservation of mass

We denote $\rho : \mathcal{T} \to \mathbb{R}^+$ the density in the motion X and $\rho_0(p) = \rho(X(p,0),0)$ the reference density in the reference configuration. Then, the mass conservation law states that

$$\rho(x,t) \det\left(F(p,t)\right) = \rho_0(p). \tag{1.2}$$

Hence, the local equation in conservative form reads

$$\frac{\partial \rho}{\partial t} + \operatorname{div}\left(\rho\, \mathbf{u}\right) = 0. \tag{1.3}$$

Integrating equation (1.3) in a control volume $\mathcal{R} \subset \mathcal{B}_t$ and applying Gauss' Theorem we obtain the integral form of the mass conservation law used in finite volume methods:

$$\frac{d}{dt} \int_{\mathcal{R}} \rho \, dV + \int_{\partial \mathcal{R}} \rho\, \mathbf{u} \cdot \boldsymbol{\eta} \, dA = 0, \tag{1.4}$$

where $\boldsymbol{\eta}$ denotes the outward unit normal to $\partial \mathcal{R}$.

Equation (1.4) *asserts that the rate of increase of mass in* $\mathcal{R}$ *is equal to the mass flow into* $\mathcal{R}$ *across its boundary.*

1.1.2 Balance of linear momentum

Let us consider the system of forces defined by $\mathbf{s} : \mathcal{N} \times \mathcal{T} \to \mathcal{V}$, the density of surface force with $\mathcal{N}$ the set of unit normal vectors of $\mathcal{V}$, and $\mathbf{b} : \mathcal{T} \to \mathcal{V}$, the body force. Then, the balance of linear momentum laws reads

$$\frac{d}{dt}\int_{\mathcal{P}_t} \rho\,\mathbf{u}\,dV = \int_{\partial\mathcal{P}_t} \mathbf{s}(\boldsymbol{\eta})\,dA + \int_{\mathcal{P}_t} \mathbf{b}\,dV. \tag{1.5}$$

Moreover, we can take into account Cauchy's theorem which asserts that momentum balance laws are satisfied if and only if there exists a symmetric second order tensor field $T : \mathcal{T} \to Sym$ such that $\mathbf{s}(\boldsymbol{\eta}, x, t) = T(x,t)\,\boldsymbol{\eta}$ for all $\boldsymbol{\eta}$ and which satisfies the equation of motion

$$\frac{\partial(\rho\,\mathbf{u})}{\partial t} + \operatorname{div}(\rho\,\mathbf{u}\otimes\mathbf{u}) = \operatorname{div} T + \mathbf{b}. \tag{1.6}$$

Remark 1.1.1. The Cauchy stress tensor, T, can be expressed as linear combination of the principal stresses,

$$\tau_{\mathrm{p}} = \frac{1}{3}\operatorname{tr}(T)\,\mathbf{I},$$

and the deviatoric ones,

$$\tau = T - \tau_{\mathrm{p}}.$$

Like for the mass conservation equation, we can derive the integral form of the momentum conservation equation used in finite volume methods:

$$\frac{d}{dt}\int_{\mathcal{R}} \rho\,\mathbf{u}\,dV + \int_{\partial\mathcal{R}} \rho\,\mathbf{u}\,\mathbf{u}\cdot\boldsymbol{\eta}\,dA = \int_{\partial\mathcal{R}} T\,\boldsymbol{\eta}\,dA + \int_{\mathcal{R}} \mathbf{b}\,dV. \tag{1.7}$$

Equation (1.7) *states that the total force on the control volume $\mathcal{R}$ is equal to the rate at which the linear momentum of the material in $\mathcal{R}$ is increasing plus the rate of outflow of momentum across the boundary, $\partial\mathcal{R}$.*

1.1.3 Balance of energy

Let E be the specific total energy and consider the system of heat for the body, $\mathcal{B}$, defined by $g : \mathcal{N} \times \mathcal{T} \to \mathbb{R}$, the surface heat, and $f : \mathcal{T} \to \mathbb{R}$, the body heat. Then, the energy conservation law (also known as the First Principle of Thermodynamics) states that

$$\frac{d}{dt}\int_{\mathcal{P}_t} \rho E dV = \int_{\partial\mathcal{P}_t} \mathbf{s}(\boldsymbol{\eta})\cdot\mathbf{u}\,dA + \int_{\mathcal{P}_t} \mathbf{b}\cdot\mathbf{u}\,dV - \int_{\partial\mathcal{P}_t} g(\boldsymbol{\eta})dA + \int_{\mathcal{P}_t} f dV. \tag{1.8}$$

Applying Cauchy theorems for the momentum and energy balances, there exists a spatial vector field $\mathbf{q}$ called heat flux vector such that $g(\boldsymbol{\eta}) = \mathbf{q}\cdot\boldsymbol{\eta}$ and it is verified

$$\rho\dot{E} = \operatorname{div}(T\,\mathbf{u}) + \mathbf{b}\cdot\mathbf{u} - \operatorname{div}\mathbf{q} + f. \tag{1.9}$$

Definition 1.1.11. We denote by specific internal energy, e, the scalar field given by

$$e = E - \frac{|\mathbf{u}|^2}{2}.$$

Using Gauss' theorem, the Localization theorem and then adding the mass conservation equation multiplied by the specific internal energy, we obtain the conservative form of the energy conservation law

$$\frac{\partial(\rho e)}{\partial t} + \operatorname{div}(\rho e\,\mathbf{u}) = T \cdot D - \operatorname{div}\mathbf{q} + f, \tag{1.10}$$

where

$$D = \frac{1}{2}\left(L + L^T\right), \quad L = \operatorname{grad}\mathbf{u}.$$

Finally, the integral form of (1.10) reads

$$\frac{d}{dt}\int_{\mathcal{R}} \rho e\, dV + \int_{\partial\mathcal{R}} \rho e\,\mathbf{u}\cdot\boldsymbol{\eta}\, dA = \int_{\mathcal{R}} T \cdot D\, dV - \int_{\partial\mathcal{R}} \mathbf{q}\cdot\boldsymbol{\eta}\, dA + \int_{\mathcal{R}} f\, dV. \tag{1.11}$$

Equation (1.11) *asserts that the rate at which the internal energy in* $\mathcal{R}$ *is increasing is due to the rate of outflow of internal energy across the boundary, a contribution of the work of the internal forces, the balance of heat flux across the boundary and the internal heat sources.*

1.2 Fluids

In this section, we present a particular type of materials: fluids. As a consequence of the Second Principle of Thermodynamics two new scalar fields are introduced: the specific entropy, $s \in \mathbb{R}$, and the absolute temperature, $\theta \in \mathbb{R}^+$. Gathering together these fields with the already introduced in the previous section, we can define:

Definition 1.2.1. A thermodynamic process for a body with mass distribution ρ_0 is the set of mappings

$$X : \mathcal{B} \times \mathbb{R} \to \mathcal{E}, \tag{1.12}$$
$$T : \mathcal{T} \to Sym, \quad T \in \mathcal{C}^1(\mathcal{T}; Sym), \tag{1.13}$$
$$\mathbf{b} : \mathcal{T} \to \mathcal{V}, \quad \mathbf{b} \in \mathcal{C}^0(\mathcal{T}; \mathcal{V}), \tag{1.14}$$
$$e : \mathcal{T} \to \mathbb{R}, \quad e \in \mathcal{C}^1(\mathcal{T}; \mathbb{R}), \tag{1.15}$$
$$\theta : \mathcal{T} \to \mathbb{R}^+, \quad \theta \in \mathcal{C}^1(\mathcal{T}; \mathbb{R}), \tag{1.16}$$
$$\mathbf{q} : \mathcal{T} \to \mathcal{V}, \quad \mathbf{q} \in \mathcal{C}^1(\mathcal{T}; \mathcal{V}), \tag{1.17}$$
$$f : \mathcal{T} \to \mathbb{R}, \quad f \in \mathcal{C}^0(\mathcal{T}; \mathbb{R}), \tag{1.18}$$
$$s : \mathcal{T} \to \mathbb{R}, \quad s \in \mathcal{C}^1(\mathcal{T}; \mathbb{R}), \tag{1.19}$$

verifying equations (1.6) and (1.10).

This yields to an extended concept of material body.

Definition 1.2.2. A material body is a triple $(\mathcal{B}, \rho_0, \mathcal{C})$ consisting of a body, $\mathcal{B}$, a mass distribution, ρ_0, and a family of thermodynamic processes, $\mathcal{C}$, called the constitutive class of the body.

Now, we can introduce a particular material body called Colleman-Noll material (see [CN63] and [Ber05]).

Definition 1.2.3. A Coleman-Noll material is an hyperelastic material with heat conduction and viscosity whose constitutive class, $\mathcal{C}$, consists of all thermodynamic processes verifying

$$T(x,t) = \hat{T}\left(F(p,t), s(x,t), p\right) + \hat{l}\left(F(p,t), s(x,t), p\right)\left(L(x,t)\right), \tag{1.20}$$

$$e(x,t) = \hat{e}\left(F(p,t), s(x,t), p\right), \tag{1.21}$$

$$\theta(x,t) = \hat{\theta}\left(F(p,t), s(x,t), p\right), \tag{1.22}$$

$$\mathbf{q}(x,t) = \hat{\mathbf{q}}\left(F(p,t), s(x,t), \operatorname{grad}\theta(x,t), p\right), \tag{1.23}$$

for some smooth enough mappings,

$$\hat{T} : Lin^+ \times \mathbb{R} \times \mathcal{B} \to Sym, \tag{1.24}$$

$$\hat{l} : Lin^+ \times \mathbb{R} \times \mathcal{B} \to \mathcal{L}\left(Lin, Sym\right), \tag{1.25}$$

$$\hat{e} : Lin^+ \times \mathbb{R} \times \mathcal{B} \to \mathbb{R}, \tag{1.26}$$

$$\hat{\theta} : Lin^+ \times \mathbb{R} \times \mathcal{B} \to \mathbb{R}^+, \tag{1.27}$$

$$\hat{\mathbf{q}} : Lin^+ \times \mathbb{R} \times \mathcal{V} \times \mathcal{B} \to \mathcal{V}, \tag{1.28}$$

where Lin^+ denotes the subset of second order tensors with positive determinant

$$Lin^+ = \left\{G \in Lin : \det\left(G\right) > 0\right\}.$$

The mappings above are called response mappings of the body.

Definition 1.2.4. A material body satisfies the Principle of Material Frame-Indifference if its response is independent of the observer.

Definition 1.2.5. A material body is said to be isotropic at p if its symmetry group at this point contains all rotations.

Definition 1.2.6. A fluid is a Coleman-Noll material having the unimodular group

$$Unim = \left\{H \in Lin^+ : \det\left(H\right) = 1\right\}$$

as extended symmetry group.

Remark 1.2.1. Since $Orth^+ \subset Unim$, any fluid is isotropic.

Once we have introduced the concept of fluid, we can pose the constitutive laws and deduce more detailed expressions of the conservation equations.

Hypothesis 1.2.7. *For a Colemman-Noll material with constitutive class $\mathcal{C}$, there exists a smooth enough function, $\hat{s} : Lin^+ \times \mathbb{R} \times \mathcal{B} \to \mathbb{R}$, such that if $s \in \mathbb{R}$, $F \in Lin^+$, $\theta \in \mathbb{R}^+$ and $p \in \mathcal{B}$, then*

$$s = \hat{s}\,(F, \theta, p) \quad \Longleftrightarrow \quad \theta = \hat{\theta}\,(F, s, p)\,. \tag{1.29}$$

Theorem 1.2.8. *Supposing that Hypothesis 1.2.7 holds, then all thermodynamic processes in the constitutive class of a fluid satisfy the second law of thermodynamics if and only if*

$$\hat{\theta}\,(\nu, s, p) = \frac{\partial \hat{e}}{\partial s}\,(\nu, s, p)\,, \tag{1.30}$$

$$\hat{T}\,(\nu, s, p) = \frac{\partial \hat{e}}{\partial \nu}\,(\nu, s, p)\,I, \tag{1.31}$$

$$\hat{l}\,(\nu, s, p)\,(L) \cdot L \geq 0, \tag{1.32}$$

$$\hat{\mathbf{q}}\,(\nu, s, \boldsymbol{\varpi}, p) \cdot \boldsymbol{\varpi} \leq 0, \tag{1.33}$$

for all $\nu \in \mathbb{R}^+$, $\nu := \frac{\det F}{\rho_0}$, $s \in \mathbb{R}$, $p \in \mathcal{B}$, $L \in Lin$ and $\boldsymbol{\varpi} \in \mathcal{V}$.

Definition 1.2.9. The thermodynamic pressure is the scalar field

$$\mathrm{p}(\mathrm{x}, \mathrm{t}) = \hat{\mathrm{p}}\,(\nu(\mathrm{x}, \mathrm{t}), \mathrm{s}(\mathrm{x}, \mathrm{t}), \mathrm{p})\,,$$

with $\hat{\mathrm{p}}$ given by

$$\hat{\mathrm{p}}(\nu, s, p) = -\frac{\partial \hat{e}}{\partial \nu}\,(\nu, s, p)\,. \tag{1.34}$$

From now on, we will assume that any fluid satisfies the Principle of Material Frame-Indifference. Hence, the following proposition is verified.

Proposition 1.2.10. *For any fluid there exist two functions*

$$\hat{\mu} : \mathbb{R}^+ \times \mathbb{R} \times \mathcal{B} \to \mathbb{R}, \tag{1.35}$$

$$\hat{\xi} : \mathbb{R}^+ \times \mathbb{R} \times \mathcal{B} \to \mathbb{R}, \tag{1.36}$$

such that

$$\tau = 2\hat{\mu} D + \hat{\xi}\, tr\,(D)\, I, \quad D = \frac{1}{2}\left(grad\,\mathbf{u} + grad\,\mathbf{u}^t\right). \tag{1.37}$$

The corresponding scalar fields, μ and ξ are the dynamic viscosity and the second viscosity coefficient, respectively. Furthermore, $\zeta = \xi + \frac{2}{3}\mu$ is called bulk viscosity.

Hypothesis 1.2.11 (Stokes' hypothesis)**.** *The first and second viscosities verify*

$$\xi = -\frac{2}{3}\mu. \tag{1.38}$$

Corollary 1.2.12. *For a fluid the motion equation becomes*

$$\frac{\partial(\rho\,\mathbf{u})}{\partial t} + div(\rho\,\mathbf{u}\otimes\mathbf{v}) + grad\,\mathrm{p} - div\left(2\mu\mathrm{D} - \frac{2}{3}\mu\,div(\mathbf{u})\,\mathrm{I}\right) = \mathbf{b}. \tag{1.39}$$

In what follows, we will accept that the unique body forces are due to the gravity, $\mathbf{g}$. Thus, the motion equation reads:

$$\frac{\partial(\rho\,\mathbf{u})}{\partial t} + \mathrm{div}\,(\rho\,\mathbf{u}\otimes\mathbf{u}) + \mathrm{grad}\,\mathrm{p} - \mathrm{div}\left(2\mu\mathrm{D} - \frac{2}{3}\mu\,\mathrm{div}\,(\mathbf{u})\,\mathrm{I}\right) = \rho\mathbf{g}. \tag{1.40}$$

1.3 Mixtures of Coleman-Noll fluids

In the previous sections, we have considered a flow with only one species. Nevertheless, it is usual to find flows of mixture of species.

We consider a mixture of N_e species, E_i, related to N_e superposed motions, X_i, of N_e bodies $\mathcal{B}^i$ such that each of them occupies the same position at each time t. Let us suppose that each species is a Coleman-Noll fluid with the following properties:

- mass fraction: y_i,
- density: $\rho_i = \rho\mathrm{y}_i$,
- molecular mass: $\mathcal{M}_i$,
- velocity: $\mathbf{u}_i$,
- pressure: $\mathrm{p_i}$,
- concentration: $c_i = \dfrac{\rho_i}{\mathcal{M}_i}$,
- specific heat at constant pressure: $c_{\mathrm{p,i}}$.

We assume that the species satisfy the local thermodynamic equilibrium which implies that, at each (x,t), the temperature of all species is the same. Then, the variables related to the mixture are:

- density:

$$\rho = \sum_{i=1}^{N_e}\rho_i = \sum_{i=1}^{N_e}\rho\mathrm{y}_i, \tag{1.41}$$

- molecular mass:

$$\mathcal{M} = \frac{1}{\displaystyle\sum_{i=1}^{N_e}\frac{\mathrm{y}_i}{\mathcal{M}_i}}, \tag{1.42}$$

- velocity:

$$\mathbf{u} = \sum_{i=1}^{N_e} \mathrm{y}_i \, \mathbf{u}_i, \tag{1.43}$$

- pressure:

$$\mathrm{p} = \sum_{\mathrm{i}=1}^{\mathrm{N_e}} \mathrm{p_i}, \tag{1.44}$$

- concentration:

$$c = \sum_{i=1}^{N_e} c_i, \tag{1.45}$$

- specific heat at constant pressure:

$$c_{\mathrm{p}} = \sum_{i=1}^{N_e} \mathrm{y}_i c_{\mathrm{p,i}}. \tag{1.46}$$

Finally, the diffusion velocity of a species E_i is defined by

$$\mathbf{U}_i = \mathbf{u}_i - \mathbf{u}\,. \tag{1.47}$$

1.3.1 Mass conservation

Recalling the mass conservation equation (1.3) and assuming that there are not reactions and, so, the source due to chemical reactions and to an evaporating or combusting condensed phase are zero, it holds

$$\frac{\partial \rho_i}{\partial t} + \operatorname{div}(\rho_i \, \mathbf{u}_i) = 0 \tag{1.48}$$

for each species E_i. Adding (1.48) for all the species we obtain the mass conservation equation of the mixture

$$\rho' + \operatorname{div}(\rho \, \mathbf{u}) = 0. \tag{1.49}$$

We observe that equation (1.49) is equal to equation (1.3).

To obtain a closed system of equations we do not need to compute the velocity of each species. Using Fick's Law we can write the diffusion velocity in terms of other fields in the model:

$$\mathbf{U}_i = -\mathcal{D}_i \operatorname{grad}(\ln(\mathrm{y}_i)) = -\frac{\mathcal{D}_i}{\mathrm{y}_i} \operatorname{grad} \mathrm{y}_i \tag{1.50}$$

with $\mathcal{D}_i$ the mass diffusion coefficient of species E_i in the mixture. Replacing (1.47) and (1.50) into (1.48) and using (1.41), it yields

$$\frac{\partial (\rho \mathrm{y}_i)}{\partial t} + \operatorname{div}(\rho \mathrm{y}_i \, \mathbf{u}) - \operatorname{div}(\rho \mathcal{D}_i \operatorname{grad} \mathrm{y}_i) = 0 \tag{1.51}$$

which is the mass conservation equation for species E_i in conservative form. Moreover, the integral form used in finite volume methods reads

$$\frac{d}{dt} \int_{\mathcal{R}} \rho \mathrm{y}_i dV + \int_{\partial \mathcal{R}} \rho \mathrm{y}_i \, \mathbf{u} \cdot \boldsymbol{\eta} \, dA - \int_{\partial \mathcal{R}} \rho \mathcal{D}_i \operatorname{grad} \mathrm{y}_i \cdot \boldsymbol{\eta} \, dA = 0. \tag{1.52}$$

1.3.2 Energy equation in terms of specific enthalpy

To deal with the energy conservation equation a new variable is considered.

Definition 1.3.1. We denote by specific enthalpy

$$h = e + \frac{\mathrm{p}}{\rho}.$$

The heat flux vector is decomposed into the heat flux due to radiation effects, $\mathbf{q}_r$, and the heat flux due to convection, $\mathbf{q}_c$. Next, we apply the constitutive law for the convective heat flux which holds

$$\mathbf{q}_c = -k_T \operatorname{grad}\theta - \sum_{i=1}^{N_e} \rho_i \, \mathbf{U}_i \, h_i \tag{1.53}$$

with k_T the diffusion term coefficient, h_i the specific enthalpy of each species verifying

$$h = \sum_{i=1}^{N_e} \mathrm{y}_i h_i. \tag{1.54}$$

Assuming that the mass diffusion coefficient is the same for all the species, that the Lewis number is one, that is, $k_T = \rho \mathcal{D} c_{\mathrm{p}}$, and that the Fick law, (1.50), is verified, we obtain

$$\mathbf{q}_c = -\rho \mathcal{D} \operatorname{grad} h. \tag{1.55}$$

On the other hand, the radiation heat flux and the body forces will be neglected. Hence, the conservative form of the energy equation in terms of enthalpy reads

$$\frac{\partial \rho h}{\partial t} + \operatorname{div}(\rho h \, \mathbf{u}) - \operatorname{div}(\rho \mathcal{D} \operatorname{grad} h) - T \cdot D - \dot{\pi} = 0. \tag{1.56}$$

1.3.3 State law

To close the system of equations defined by the mass, momentum and energy conservation equations we need to define a state equation for the fluid.

Definition 1.3.2. A perfect gas is a fluid for which the following state equation holds:

$$\mathrm{p} = \rho \mathrm{R} \theta \tag{1.57}$$

where $R = \frac{\mathcal{R}}{\mathcal{M}}$, being $\mathcal{R} = 8.314472$ J/mol K the universal constant for perfect gases and $\mathcal{M}$ the molecular mass of the gas.

Proposition 1.3.3. *The specific enthalpy and the specific heat of a perfect gas only depend on temperature.*

Corollary 1.3.4. *For a perfect gas the Mayer equation holds:*

$$c_{\mathrm{p}} = c_v + R. \tag{1.58}$$

Corollary 1.3.5. *The internal enthalpy for a perfect gas is given by*

$$h(\theta) = h_{\theta_0} + \int_{\theta_0}^{\theta} c_\pi(r)dr \tag{1.59}$$

with h_{θ_0} the standard enthalpy formation and θ_0 the temperature of formation.

1.4 Incompressible Newtonian fluids

In order to introduce a new type of material bodies called incompressible Newtonian fluids, we recall the following definition related to thermodynamic processes.

Definition 1.4.1. A thermodynamic process is said to be isochoric if for each $\mathcal{P}_t$

$$\frac{d}{dt}\int_{\mathcal{P}_t} dV = 0.$$

Proposition 1.4.2. *A thermodynamic process is isochoric if and only if*

$$div\,\mathbf{u} = 0.$$

Definition 1.4.3. An incompressible Newtonian fluid is a material body the constitutive class of which consists of all isochoric thermodynamic processes such that there exist mappings

$$\hat{l} : \mathbb{R} \times \mathcal{B} \to \mathcal{L}\left(Lin_0, Sym_0\right), \tag{1.60}$$
$$\hat{e} : \mathbb{R} \times \mathcal{B} \to \mathbb{R}, \tag{1.61}$$
$$\hat{\theta} : \mathbb{R} \times \mathcal{B} \to \mathbb{R}^+, \tag{1.62}$$
$$\hat{\mathbf{q}} : \mathbb{R} \times \mathcal{V} \times \mathcal{B} \to \mathcal{V}, \tag{1.63}$$

satisfying

$$\tau(x,t) = \hat{l}\left(s(x,t),p\right)\left(L(x,t)\right), \tag{1.64}$$
$$e(x,t) = \hat{e}\left(s(x,t),p\right), \tag{1.65}$$
$$\theta(x,t) = \hat{\theta}\left(s(x,t),p\right), \tag{1.66}$$
$$\mathbf{q}(x,t) = \hat{\mathbf{q}}\left(s(x,t), \operatorname{grad}\theta(x,t), p\right). \tag{1.67}$$

Definition 1.4.4. The scalar field p defined by

$$\mathrm{p} = -\frac{1}{3}\operatorname{tr}\left(\mathrm{T}\right) \tag{1.68}$$

is the pressure of the thermodynamic process.

From the former definitions, equation (1.3) becomes

$$\operatorname{div}(\rho\,\mathbf{u}) = 0 \tag{1.69}$$

and equation (1.6) can be expressed as

$$\frac{\partial(\rho\,\mathbf{u})}{\partial t} + \operatorname{div}(\rho\,\mathbf{u}\otimes\mathbf{u}) + \nabla \mathrm{p} = \operatorname{div}\tau + \mathbf{b}. \tag{1.70}$$

Assuming the Principle of Material Frame-Indifference, an analogous result to Proposition 1.2.10 can be proved for incompressible Newtonian fluids.

Proposition 1.4.5. *For any incompressible Newtonian fluid there exists one function*

$$\hat{\mu} : \mathbb{R}^+ \times \mathbb{R} \times \mathcal{B} \to \mathbb{R}, \tag{1.71}$$

such that

$$\tau = 2\hat{\mu}D. \tag{1.72}$$

Corollary 1.4.6. *For an incompressible Newtonian fluid, the motion equation becomes*

$$\frac{\partial(\rho\,\mathbf{u})}{\partial t} + \mathit{div}(\rho\,\mathbf{u}\otimes\mathbf{u}) + \mathit{grad}\,\mathrm{p} = \mathit{div}(2\mu\mathrm{D}) + \mathbf{b}. \tag{1.73}$$

Remark 1.4.1. It is important to realize that, because of the definition of thermodynamic pressure, incompressible Newtonian fluids are not a particular case of fluids.

In the case of a Coleman-Noll material the pressure is identified with the variation of the specific internal energy with respect to ν. If we assume that an incompressible Newtonian fluid is defined as a Coleman-Noll material with constant ν, then, applying equation (1.34), the pressure will always be zero. This conflicts with Definition 1.4.4.

Remark 1.4.2. For incompressible Newtonian fluids the energy conservation equation can be decoupled from the mass and momentum conservation equations.

1.5 Dimensional analysis

In this section, we conduct the dimensional analysis of the conservation equations in order to obtain simplified models for fluids. The case of incompressible Newtonian fluids is analogous.

Gathering together the conservation equations introduced in Sections 1.2 and 1.3, we obtain the following model:

$$\frac{\partial\rho}{\partial t} + \operatorname{div}(\rho\,\mathbf{u}) = 0, \tag{1.74}$$

$$\frac{\partial(\rho\,\mathbf{u})}{\partial t} + \operatorname{div}(\rho\,\mathbf{u}\otimes\mathbf{u}) + \operatorname{grad}\mathrm{p} - \operatorname{div}\left(2\mu\mathrm{D} - \frac{2}{3}\mu\operatorname{div}(\mathbf{u})\,\mathrm{I}\right) = \rho\mathbf{g}, \tag{1.75}$$

$$\frac{\partial(\rho \mathrm{y}_i)}{\partial t} + \operatorname{div}(\rho \mathrm{y}_i\,\mathbf{u}) - \operatorname{div}(\rho\mathcal{D}_i \operatorname{grad}\mathrm{y}_i) = 0, \quad i = 1,\dots,N_e, \tag{1.76}$$

$$\frac{\partial(\rho h)}{\partial t} + \operatorname{div}(\rho h\,\mathbf{u}) - \operatorname{div}(\rho\mathcal{D}\operatorname{grad} h) - T\cdot D - \frac{\partial \pi}{\partial t} = 0, \tag{1.77}$$

$$\mathrm{p} = \rho \mathrm{R}\theta. \tag{1.78}$$

Let us denote with the subindex 0 the characteristic values of the magnitudes of the variables. Then, the Mach number, which is defined as the ratio between the characteristic velocity of the fluid, v_0, and the characteristic velocity of the sound, c_0, reads

$$M = \frac{v_0}{c_0}. \tag{1.79}$$

For a perfect gas it holds

$$c = \sqrt{\gamma R\theta} = \sqrt{\gamma \frac{\mathrm{p}}{\rho}}, \quad \gamma = \frac{c_{\mathrm{p}}}{c_v}. \tag{1.80}$$

Since the flows we will consider are either incompressible or compressible with low Mach number, we can write the pressure as the sum of a spatially constant function, $\overline{\pi}$, and a small perturbation, π,

$$\mathrm{p} = \overline{\pi}(\mathrm{t}) + \pi(\mathrm{x},\mathrm{y},\mathrm{z},\mathrm{t}), \quad \frac{\pi}{\overline{\pi}} = \mathrm{O}(\mathrm{M}^{-2}). \tag{1.81}$$

Furthermore, the perturbation can be neglected in the state equation but it has to be retained in the momentum equation.

To develop the dimensional analysis we consider the following relations

$$x^* = \frac{x}{L_0}, \quad t^* = \frac{t u_0}{L_0}, \quad \rho^* = \frac{\rho}{\rho_0}, \quad \pi^* = \frac{\pi}{\rho_0 u_0^2}, \quad \mathbf{u}^* = u_0^{-1}\,\mathbf{u},$$
$$h^* = \frac{h}{c_{\mathrm{p}\,0}\Delta\theta}, \quad \mu^* = \frac{\mu}{\mu_0}, \quad \mathcal{D}^* = \frac{\mathcal{D} c_{\mathrm{p}\,0}\rho_0}{k_{T\,0}},$$

where $\Delta\theta = \theta_c - \theta_0$ is the gap between the customary temperature of the flux, θ_c, and the reference temperature, θ_0. Then, the mass and momentum conservation equations in dimensionless form read

$$\frac{\partial \rho^*}{\partial t^*} + \operatorname{div}^*(\rho^*\,\mathbf{u}^*) = 0, \tag{1.82}$$

$$\frac{\partial(\rho^*\,\mathbf{u}^*)}{\partial t^*} + \operatorname{div}^*(\rho^*\,\mathbf{u}^*\otimes\mathbf{u}^*) + \operatorname{grad}^*\pi^* - \frac{1}{Re}\operatorname{div}^*\left(2\mu^* D^* - \frac{2}{3}\mu^*\operatorname{div}^*\mathbf{u}^*\, I\right) = \frac{1}{Fr^2}\rho^*\mathbf{e}_3, \tag{1.83}$$

with div^* and grad^* the gradient and divergence with respect to the dimensionless spatial variable, x^*. We have defined two dimensionless groups:

- The Reynolds number,

$$Re = \frac{\rho_0 L_0 u_0}{\mu_0},$$

  which provides the ratio between inertial and viscous terms.

- The Froude number,
$$Fr = \frac{u_0}{\sqrt{gL_0}},$$
that relates inertial and gravitational terms.

By analysing these numbers for each problem we are able to simplify the model. Similarly, for the species transport and energy conservation equations we obtain

$$\frac{\partial \rho^* h^*}{\partial t^*} + \operatorname{div}^* (\rho^* h^* \mathbf{u}^*) - \frac{1}{Pe} \operatorname{div}^* (\rho^* \mathcal{D}^* \operatorname{grad}^* h^*) - \frac{Ec}{Re} T^* \cdot D^* - Ec \frac{\partial \pi^*}{\partial t^*} = 0, \quad (1.84)$$

$$\frac{\partial \rho^* \mathrm{y}_i}{\partial t^*} + \operatorname{div}^* (\rho^* \mathrm{y}_i \mathbf{u}^*) - \frac{1}{Sc\, Re} \operatorname{div}^* (\rho^* \mathcal{D}^* \operatorname{grad}^* \mathrm{y}_i) = 0, \quad (1.85)$$

with

$$Pr = \frac{c_{p0}\mu_0}{k_{T0}}, \quad Pe = Pr\, Re, \quad Sc = \frac{\mu_0}{D_0}, \quad Ec = \frac{u_0^2}{c_{p0}\Delta\theta} \quad (1.86)$$

the Prandtl, Péclet, Schmidt and Eckert numbers, respectively.

Recalling Corollary 1.3.4, we can express the Eckert number as

$$Ec = M^2 (\gamma_0 - 1) \frac{\theta_c}{\Delta\theta}.$$

Since we have assumed that the Mach number is small, then the Eckert number will be small too. Thus, when the Reynolds number is not very small, the term of the heat dissipation due to the viscosity and the contribution of the compressibility heating can be neglected. So, assuming that the Péclet number is not big, the energy equation results

$$\frac{\partial (\rho h)}{\partial t} + \operatorname{div} (\rho h \mathbf{u}) - \operatorname{div} (\rho \mathcal{D} \operatorname{grad} h) = 0. \quad (1.87)$$

Finally, the model to be solved reads

$$\frac{\partial \rho}{\partial t} + \operatorname{div} (\rho \mathbf{u}) = 0, \quad (1.88)$$

$$\frac{\partial (\rho \mathbf{u})}{\partial t} + \operatorname{div} (\rho \mathbf{u} \otimes \mathbf{u}) + \operatorname{grad} \pi - \operatorname{div} \left(2\mu D - \frac{2}{3} \mu \operatorname{div} (\mathbf{u}) I \right) = \rho \mathbf{g}, \quad (1.89)$$

$$\frac{\partial (\rho \mathrm{y}_i)}{\partial t} + \operatorname{div} (\rho \mathrm{y}_i \mathbf{u}) - \operatorname{div} (\rho \mathcal{D}_i \operatorname{grad} \mathrm{y}_i) = 0, \quad i = 1, \ldots, N_e, \quad (1.90)$$

$$\frac{\partial (\rho h)}{\partial t} + \operatorname{div} (\rho h \mathbf{u}) - \operatorname{div} (\rho \mathcal{D} \operatorname{grad} h) = 0, \quad (1.91)$$

$$\overline{\pi} = \rho R \theta. \quad (1.92)$$

Equations (1.88) and (1.89) are called compressible Navier-Stokes equations.

Remark 1.5.1. The dimensional analysis of the model obtained for incompressible Newtonian fluids yields to the incompressible Navier-Stokes equations, namely,

$$\operatorname{div} (\rho \mathbf{u}) = 0, \quad (1.93)$$

$$\frac{\partial (\rho \mathbf{u})}{\partial t} + \operatorname{div} (\rho \mathbf{u} \otimes \mathbf{u}) + \operatorname{grad} \pi - \operatorname{div} (2\mu D) = \rho \mathbf{g}. \quad (1.94)$$

Chapter 2

Turbulence models

We have seen that the Reynolds number relates the inertial and the viscous terms giving an idea about the flow regime. If the Reynolds number is small, then the viscous term plays an important role stabilizing the flow and providing a laminar regime. On the other hand, when the Reynolds number increases, inertial forces prevail over viscous forces. These kind of flows are characterised by having high frequency oscillations which make the flow unstable and rise turbulence. Comprehensive references on turbulent phenomena are, for instance, [Bat53], [Wil88], [MP94] and [CL14].

Turbulent regimes are characterized by being chaotic systems involving a wide range of scales interacting among them. Capturing the fast changes produced on each scale will require for a very fine mesh which increases the computational cost. This is named Direct Numerical Simulation (DNS) and nowadays it is not affordable. Nevertheless, we may not be interested on knowing exactly the flow behaviour of the smallest eddies but the effect they have on the mean flow. So, simplified models to approximate the solutions have been developed. We can classify them into three groups: Reynolds Averaged Navier-Stokes (RANS), Large Eddy Simulation (LES) and Detached Eddy Simulation (DES).

- RANS. They rely on the decomposition of the variables into a mean plus a perturbation. They are focused on solving the averaged Navier-Stokes equations so that the main features of the flow will be captured. To close the system of equations obtained, turbulence models for the perturbation terms are applied.

- LES. In this approach, direct numerical simulation is used in order to resolve the highest scales of the flow. Meanwhile, the smallest ones, called subgrid scales, are modelled. The equations to be solved are computed from the Navier-Stokes equations using a filter.

- DES. It is a combination of RANS and LES approaches. In the neighbouring of walls, where a boundary layer can appear, RANS is applied, whereas LES is used on the remaining region of the fluid.

Despite the great development of computers in the last decades, LES and DES models are still too computational expensive to be broadly used. Only in specific

applications with transitional flow or large separation and for which a high accuracy is required aim to solve these models. On the other hand, since RANS provide a reasonable ratio between accuracy and cost they seem to be a good choice to model turbulence. In the next sections, we will introduce them with great detail following the works on [Wil88], [MP94] and [CL14].

2.1 RANS models

The average of Navier-Stokes equations is done using a temporal filter. Two different options will be used, the Reynolds average and the Favre average. The former is applied for incompressible flows (see [Rey95]). Meanwhile, the second is more suitable for compressible Navier-Stokes equations (see [Fav65]).

Definition 2.1.1. We define the Reynolds average as the statistical time averaging

$$\overline{\phi}(x,t) = \lim_{T\to\infty} \frac{1}{T} \int_{t-t/2}^{T+t/2} \varphi(x,s)ds. \tag{2.1}$$

Its related fluctuation is denoted by

$$\phi' = \phi - \overline{\phi}. \tag{2.2}$$

Definition 2.1.2. The Favre average is a density weighted average given by

$$\widetilde{\phi}(x,t) = \frac{\overline{\rho\phi}}{\overline{\rho}} = \frac{1}{\overline{\rho}} \lim_{T\to\infty} \frac{1}{T} \int_{t-t/2}^{T+t/2} \rho(x,s)\phi(x,s)ds \tag{2.3}$$

with $\overline{\rho}$ the mean density computed in Reynolds average. The corresponding fluctuations read

$$\phi'' = \phi - \widetilde{\phi}. \tag{2.4}$$

The relation between Reynolds and Favre averages is given by

$$\overline{\rho}\widetilde{\phi} = \overline{\rho}\overline{\phi} + \overline{\rho'\phi'}. \tag{2.5}$$

Furthermore, the following properties hold:

$$\overline{\phi + \lambda\psi} = \overline{\phi} + \lambda\overline{\psi}, \tag{2.6}$$
$$\overline{\partial\phi} = \partial\overline{\phi}, \tag{2.7}$$
$$\overline{\overline{\phi}} = \overline{\phi}, \tag{2.8}$$
$$\overline{\phi'} = 0, \tag{2.9}$$
$$\overline{\phi\overline{\psi}} = \overline{\phi\psi}, \widetilde{\phi + \lambda\psi} = \widetilde{\phi} + \lambda\widetilde{\psi}, \tag{2.10}$$
$$\widetilde{\widetilde{\phi}} = 0, \tag{2.11}$$

$$\widetilde{\phi''} = 0, \quad \overline{\phi''} \neq 0, \tag{2.12}$$

$$\widetilde{\rho\phi} = \overline{\rho}\widetilde{\phi}, \tag{2.13}$$

$$\widetilde{\rho\phi''} = 0, \tag{2.14}$$

with $\lambda \in \mathbb{R}$ (see [MP94] and [Wil88] for further information).

Attending to the previous definitions and properties we can average the Navier-Stokes equations. We shall start analysing the incompressible case.

2.2 Averaged incompressible Navier-Stokes equations

Time averaging the incompressible Navier-Stokes equations, (1.93)-(1.94), and replacing $\mathbf{u} = \overline{\mathbf{u}} + \mathbf{u}'$ we get

$$\operatorname{div}(\rho\overline{\mathbf{u}}) = 0, \tag{2.15}$$

$$\frac{\partial(\rho\,\overline{\mathbf{u}})}{\partial t} + \operatorname{div}(\rho\,\overline{\mathbf{u}} \otimes \overline{\mathbf{u}}) + \operatorname{div}\left(\rho\overline{\mathbf{u}' \otimes \mathbf{u}'}\right) + \operatorname{grad}\overline{\pi} - \operatorname{div}\left[\mu\left(\operatorname{grad}\overline{\mathbf{u}} + \operatorname{grad}\overline{\mathbf{u}}^t\right)\right] = \rho\mathbf{g}. \tag{2.16}$$

We observe that a new term related to the fluctuations, the Reynolds stress tensor,

$$\tau^R = -\left(\rho\overline{\mathbf{u}' \otimes \mathbf{u}'}\right), \tag{2.17}$$

has appeared in the averaged momentum equation. As it is a symmetric tensor six new unknowns need to be calculated.

Remark 2.2.1. Lets us notice that the Reynolds stress tensor has been defined following [Ber05].

To compute τ^R, the most straightforward approach seems to be solving a transport equation for each variable (Reynolds Stress Turbulence Models). One of the main problems of this methodology is that it is computationally expensive. Furthermore, developing the system to be solved for τ^R a new unknown tensor of the form $\tau_3^R = -\rho\overline{\mathbf{u}' \otimes \mathbf{u}' \otimes \mathbf{u}'}$ arises. We have arrived to a closure problem. Somewhen, another technique needs to be introduced in order to close the system.

A second approach, which is less accurate but reduces computational costs, relates Reynolds stresses to the mean strain tensor by using Boussinesq assumption.

Hypothesis 2.2.1 (Boussinesq Assumption)**.** *The Reynolds stresses are related with the mean velocity gradients as*

$$\tau^R = -\left(\rho\overline{\mathbf{u}' \otimes \mathbf{u}'}\right) = \mu_t\left(grad\,\overline{\mathbf{u}} + grad\,\overline{\mathbf{u}}^t\right) - \frac{2}{3}\rho k I, \tag{2.18}$$

where μ_t is a nonnegative function called eddy viscosity and

$$k = -\frac{1}{2}\,tr\,\tau^R = \frac{1}{2}\overline{|\mathbf{u}'|^2} \tag{2.19}$$

is the turbulent kinetic energy.

Thus, the system obtained reads

$$\operatorname{div}(\rho\overline{\mathbf{u}}) = 0, \tag{2.20}$$

$$\frac{\partial(\rho\,\overline{\mathbf{u}})}{\partial t} + \operatorname{div}(\rho\,\overline{\mathbf{u}}\otimes\overline{\mathbf{u}}) + \operatorname{grad}\overline{\pi} - \operatorname{div}\left[(\mu+\mu_t)\left(\operatorname{grad}\overline{\mathbf{u}} + \operatorname{grad}\overline{\mathbf{u}}^t\right) - \frac{2}{3}\rho k I\right] = \rho\mathbf{g}. \tag{2.21}$$

It remains to model the eddy viscosity and to provide an equation for k.

2.2.1 Eddy viscosity

Prandtl introduced in [Pra52], the concept of mixing length ℓ, which represents the mean distance travelled by a ball of fluid before disappearing because of the turbulent mixing. This new variable can be used to pose an expression for the eddy viscosity of the form

$$\mu_t = \rho C \ell^2 |D|$$

with C a dimensionless constant to be determined. Furthermore, since k and l are dimensional independent it was also suggested

$$\mu_t = \rho C' \ell \sqrt{k}, \quad C' \in \mathbb{R}. \tag{2.22}$$

Finally, to avoid the computation of ℓ, the $k-\varepsilon$ approach was proposed. Instead of using the mixing length we can employ the mean dissipation of the fluctuation,

$$\varepsilon = 2\mu\overline{|D'|^2}, \quad D' = \frac{1}{2}\left(\operatorname{grad}\mathbf{u}' + \operatorname{grad}\mathbf{u}'^t\right). \tag{2.23}$$

From dimensional analysis it is inferred

$$\ell = \frac{k^{3/2}}{\varepsilon}. \tag{2.24}$$

Thus,

$$\mu_t = \rho C_\mu \frac{k^2}{\varepsilon}, \quad C_\mu \in \mathbb{R} \tag{2.25}$$

and hence, a new equation for ε needs to be derived. Models based on the above definition of the turbulent viscosity are known as $k-\varepsilon$ turbulence models. They have been first put forward by Launder and Spalding in [LS72].

Remark 2.2.2. Another important family of two equation models are the $k-\omega$ turbulence models. They are characterized by giving and expression of the turbulent viscosity depending on the turbulent kinetic energy and on the specific dissipation rate, ω (see [Wil88]).

2.2.2 The turbulent kinetic energy equation

To obtain an equation for the turbulent kinetic energy, k, we will start subtracting Reynolds equation, (2.16), from the momentum equation, (1.94), which leads to

$$\frac{\partial \rho\,\mathbf{u}'}{\partial t} + \operatorname{div}(\rho\,\mathbf{u}'\otimes\mathbf{u}) + \operatorname{div}(\rho\overline{\mathbf{u}}\otimes\mathbf{u}') + \operatorname{div}\left(\rho\overline{\mathbf{u}'\otimes\mathbf{u}'}\right) + \operatorname{grad}\pi' - \operatorname{div}\left[\mu\left(\operatorname{grad}\mathbf{u}' + \operatorname{grad}\mathbf{u}'^{t}\right)\right] = 0. \tag{2.26}$$

The dot product by $\mathbf{u}'$ yields

$$\frac{\partial\left(\rho\frac{|\mathbf{u}'|^2}{2}\right)}{\partial t} + \operatorname{grad}\left(\rho\frac{|\mathbf{u}'|^2}{2}\right)\cdot\mathbf{u} + (\rho\,\mathbf{u}'\otimes\mathbf{u}') :\ \operatorname{grad}(\overline{\mathbf{u}}) + \operatorname{div}\left(\rho\overline{\mathbf{u}'\otimes\mathbf{u}'}\right)\cdot\mathbf{u}' + \operatorname{grad}\pi'\cdot\mathbf{u}' - \operatorname{div}\left[\mu\left(\operatorname{grad}\mathbf{u}' + \operatorname{grad}\mathbf{u}'^{t}\right)\right]\cdot\mathbf{u}' = 0, \tag{2.27}$$

where : denotes the inner product of tensors. Finally, filtering the result and assuming mild homogeneity (see [CL14, Section 4.3.3] for further details), we obtain

$$\frac{\partial\left(\rho\overline{\frac{|\mathbf{u}'|^2}{2}}\right)}{\partial t} + \operatorname{div}\left(\overline{\mathbf{u}}\rho\overline{\frac{|\mathbf{u}'|^2}{2}}\right) + \operatorname{div}\left(\rho\overline{\frac{|\mathbf{u}'|^2}{2}\,\mathbf{u}'}\right) - \left(\rho\overline{\mathbf{u}'\otimes\mathbf{u}'}\right) :\ \operatorname{grad}(\overline{\mathbf{u}}) + \frac{1}{2}\overline{[\mu\left(\operatorname{grad}\mathbf{u}' + \operatorname{grad}\mathbf{u}'^{t}\right)] :\ \left(\operatorname{grad}\mathbf{u}' + \operatorname{grad}\mathbf{u}'^{t}\right)} = 0. \tag{2.28}$$

Taking into account (2.23), the turbulent kinetic energy equation reads

$$\frac{\partial\rho k}{\partial t} + \operatorname{div}(\overline{\mathbf{u}}\rho k) + \operatorname{div}\left(\rho\overline{\frac{|\mathbf{u}'|^2}{2}\,\mathbf{u}'}\right) + \tau^R :\ \operatorname{grad}(\overline{\mathbf{u}}) + \rho\varepsilon = 0. \tag{2.29}$$

2.2.3 The mean dissipation rate equation

As a first step to derive the equation of the mean dissipation rate, ε, we will determine the equation of the vorticity,

$$\boldsymbol{\omega} = \operatorname{curl}\mathbf{u}\,. \tag{2.30}$$

Proposition 2.2.2. *The mean dissipation of the fluctuations is related to the fluctuation of the vorticity by*

$$\varepsilon = 2\frac{\mu}{\rho}\overline{|D'|^2} = \frac{\mu}{\rho}\overline{|\boldsymbol{\omega}'|^2}. \tag{2.31}$$

Since

$$\operatorname{div}(\rho\,\mathbf{u}\otimes\mathbf{u}) = \operatorname{grad}\left(\rho\frac{|\mathbf{u}|^2}{2}\right) + \rho\,\boldsymbol{\omega}\times\mathbf{u},$$

the momentum equation (1.94) can be expressed as

$$\frac{\partial(\rho\,\mathbf{u})}{\partial t} + \rho\,\boldsymbol{\omega}\times\mathbf{u} + \operatorname{grad}\left(\rho\frac{|\mathbf{u}|^2}{2}\right) + \operatorname{grad}\pi - \operatorname{div}(2\mu D) = \rho\mathbf{g}. \tag{2.32}$$

We recall that for any $\mathbf{u}$, $\mathbf{v}$ with free divergence it holds

$$\operatorname{curl}(\mathbf{u}\times\mathbf{v}) = \operatorname{div}(\mathbf{u}\otimes\mathbf{v}) - \operatorname{div}(\mathbf{v}\otimes\mathbf{u}).$$

Then, taking the curl of (2.32) and applying Schwartz theorem, we deduce

$$\frac{\partial\rho\,\boldsymbol{\omega}}{\partial t} + \operatorname{div}(\rho\,\boldsymbol{\omega}\otimes\mathbf{u}) - \operatorname{div}(\mathbf{u}\otimes\rho\,\boldsymbol{\omega}) - \mu\Delta\,\boldsymbol{\omega} = \operatorname{curl}(\rho\mathbf{g}). \tag{2.33}$$

On the other hand, applying the curl operator to the averaged momentum equation, (2.16), we get

$$\frac{\partial\rho\overline{\boldsymbol{\omega}}}{\partial t} + \operatorname{div}(\rho\overline{\boldsymbol{\omega}}\otimes\overline{\mathbf{u}}) - \operatorname{div}(\overline{\mathbf{u}}\otimes\rho\overline{\boldsymbol{\omega}}) - \mu\Delta\overline{\boldsymbol{\omega}} = \operatorname{curl}\left(\operatorname{div}\tau^R\right) + \operatorname{curl}(\rho\mathbf{g}). \tag{2.34}$$

Subtracting (2.34) from (2.33), we obtain the equation of the vorticity

$$\begin{aligned}\frac{\partial\rho\,\boldsymbol{\omega}'}{\partial t} &+ \operatorname{div}(\rho\,\boldsymbol{\omega}'\otimes\mathbf{u}) + \operatorname{div}(\overline{\boldsymbol{\omega}}\otimes\rho\,\mathbf{u}') - \operatorname{div}(\mathbf{u}'\otimes\rho\,\boldsymbol{\omega})\\ &- \operatorname{div}(\rho\overline{\mathbf{u}}\otimes\boldsymbol{\omega}') - \mu\Delta\,\boldsymbol{\omega}' = -\operatorname{curl}\left(\operatorname{div}\tau^R\right).\end{aligned} \tag{2.35}$$

We come now to develop the main steps needed to obtain the equation of the mean dissipation rate following [CL14]. Let us notice that

$$\operatorname{div}(\rho\overline{\boldsymbol{\omega}}\otimes\mathbf{u}') - \operatorname{div}(\mathbf{u}'\otimes\rho\overline{\boldsymbol{\omega}}) = -\operatorname{curl}(\rho\,\mathbf{u}'\times\overline{\boldsymbol{\omega}}), \tag{2.36}$$

$$\operatorname{div}\boldsymbol{\omega}' = 0. \tag{2.37}$$

Moreover, for any $\mathbf{u}$, $\mathbf{v}$ we have

$$\operatorname{div}(\mathbf{u}\otimes\mathbf{v}) = \mathbf{u}\operatorname{div}\mathbf{v} + \operatorname{grad}\mathbf{u}\mathbf{v}, \tag{2.38}$$

$$(\operatorname{grad}\mathbf{u}\,\mathbf{v})\cdot\mathbf{v} = (\mathbf{v}\otimes\mathbf{v}) : \mathbf{u}. \tag{2.39}$$

Therefore, making the dot product of (2.35) with $\boldsymbol{\omega}'$ gives

$$\begin{aligned}\frac{\partial\rho\frac{|\boldsymbol{\omega}'|^2}{2}}{\partial t} &+ \operatorname{div}\left(\rho\frac{|\boldsymbol{\omega}'|^2}{2}\right)\cdot\mathbf{u} - \operatorname{curl}(\rho\,\mathbf{u}'\times\overline{\boldsymbol{\omega}})\cdot\boldsymbol{\omega}' - (\rho\,\boldsymbol{\omega}'\otimes\boldsymbol{\omega}') :\ \operatorname{grad}\overline{\mathbf{u}}\\ &- (\rho\,\boldsymbol{\omega}'\otimes\boldsymbol{\omega}') :\ \operatorname{grad}\mathbf{u}' = \mu\Delta\,\boldsymbol{\omega}'\cdot\boldsymbol{\omega}' - \operatorname{curl}\left(\operatorname{div}\tau^R\right)\cdot\boldsymbol{\omega}'.\end{aligned} \tag{2.40}$$

Taking the product by μ, averaging and applying the mild homogeneity assumption, we conclude

$$\begin{aligned}\frac{\partial\rho\varepsilon}{\partial t} &+ \operatorname{div}(\overline{\mathbf{u}}\rho\overline{\varepsilon}) + \operatorname{div}\left(\overline{\mu\rho\left(|\boldsymbol{\omega}'|^2\right)'\mathbf{u}'}\right) = -2\mu^2\overline{|\operatorname{grad}\boldsymbol{\omega}'|^2}\\ &+2\mu\left(\rho\overline{\boldsymbol{\omega}'\otimes\boldsymbol{\omega}'} :\ \operatorname{grad}\overline{\mathbf{u}} + \rho\overline{\boldsymbol{\omega}'\otimes\boldsymbol{\omega}'} :\ \operatorname{grad}\mathbf{u}'\right).\end{aligned} \tag{2.41}$$

2.2.4 Closure assumptions

Equations (2.29) and (2.41) present terms depending on the fluctuations. To deal with them, we will consider suitable physical assumptions.

Applying Boussinesq assumption 2.2.1 we get

$$\tau^R\colon \operatorname{grad}(\overline{\mathbf{u}}) = -C_\mu \rho \frac{k^2}{2\varepsilon} \left|\operatorname{grad}\overline{\mathbf{u}} + \operatorname{grad}\overline{\mathbf{u}}^t\right|^2, \quad C_\mu \in \mathbb{R}^+, \tag{2.42}$$

$$2\mu\rho\overline{\boldsymbol{\omega}'\otimes\boldsymbol{\omega}'}\colon \operatorname{grad}\overline{\mathbf{u}} = \frac{C_{1\varepsilon}C_\mu}{2}\rho k \left|\operatorname{grad}\overline{\mathbf{u}} + \operatorname{grad}\overline{\mathbf{u}}^t\right|^2, \quad C_{1\varepsilon} \in \mathbb{R}^+. \tag{2.43}$$

For the sake of simplicity we will denote

$$G_k = \frac{\mu_t}{2}\left|\operatorname{grad}\overline{\mathbf{u}} + \operatorname{grad}\overline{\mathbf{u}}^t\right|^2.$$

To approximate the turbulent diffusion terms, we assume there exist μ_{tk}, $\mu_{t\varepsilon} \in \mathbb{R}^+$, such that

$$\operatorname{div}\left(\rho\overline{\frac{|\mathbf{u}'|^2}{2}\mathbf{u}'}\right) = -\operatorname{div}(\mu_{tk}\operatorname{grad}k) = -\operatorname{div}\left(\frac{\mu_t}{\sigma_k}\operatorname{grad}k\right),$$

$$\operatorname{div}\left(\mu\rho\overline{\left(|\boldsymbol{\omega}'|^2\right)'\mathbf{u}'}\right) = -\operatorname{div}(\mu_{t\varepsilon}\operatorname{grad}\varepsilon) = -\operatorname{div}\left(\frac{\mu_t}{\sigma_\varepsilon}\operatorname{grad}\varepsilon\right)$$

with σ_k, $\sigma_\varepsilon \in \mathbb{R}^+$ the Prandtl turbulent numbers (see [MP94]). Moreover, for low Reynolds number flows we will correct the expression of μ_{tk} and $\mu_{t\varepsilon}$ using the laminar viscosity so that we ensure positivity:

$$\operatorname{div}\left(\rho\overline{\frac{|\mathbf{u}'|^2}{2}\mathbf{u}'}\right) = -\operatorname{div}\left[\left(\mu + \frac{\mu_t}{\sigma_k}\right)\operatorname{grad}k\right], \tag{2.44}$$

$$\operatorname{div}\left(\mu\rho\overline{\left(|\boldsymbol{\omega}'|^2\right)'\mathbf{u}'}\right) = -\operatorname{div}\left[\left(\mu + \frac{\mu_t}{\sigma_\varepsilon}\right)\operatorname{grad}\varepsilon\right]. \tag{2.45}$$

Remaining consistent with Boussinesq assumption, the third order correlation term of (2.41) is supposed to be given by

$$2\mu\rho\overline{\boldsymbol{\omega}'\otimes\boldsymbol{\omega}'}\colon \operatorname{grad}\mathbf{u}' = C_{1\gamma}\rho\frac{\varepsilon^2}{k}, \quad C_{1\gamma} \in \mathbb{R}.$$

Besides, using dimensional analysis we obtain

$$-2\mu^2\overline{|\operatorname{grad}\boldsymbol{\omega}'|^2} = -C_{2\gamma}\rho\frac{\varepsilon^2}{k}, \quad C_{2\gamma} \in \mathbb{R}^+.$$

Denoting $C_{2\varepsilon} = C_{2\gamma} - C_{1\gamma}$ it results

$$2\mu\rho\overline{\boldsymbol{\omega}'\otimes\boldsymbol{\omega}'}\colon \operatorname{grad}\mathbf{u}' - 2\mu^2\overline{|\operatorname{grad}\boldsymbol{\omega}'|^2} = -C_{2\varepsilon}\rho\frac{\varepsilon^2}{k}. \tag{2.46}$$

Gathering (2.20), (2.21), (2.25), (2.29), (2.41), (2.42), (2.43), (2.44), (2.45) and (2.46), the system to be solved reads

$$\operatorname{div}(\rho\overline{\mathbf{u}}) = 0, \tag{2.47}$$

$$\frac{\partial(\rho\,\overline{\mathbf{u}})}{\partial t} + \operatorname{div}(\rho\,\overline{\mathbf{u}}\otimes\overline{\mathbf{u}}) + \operatorname{grad}\overline{\pi} - \operatorname{div}\tau^n = \rho\mathbf{g}, \tag{2.48}$$

$$\frac{\partial\rho k}{\partial t} + \operatorname{div}(\overline{\mathbf{u}}\rho k) - \operatorname{div}\left[\left(\mu + \frac{\mu_t}{\sigma_k}\right)\operatorname{grad} k\right] - G_k + \rho\varepsilon = 0, \tag{2.49}$$

$$\frac{\partial\rho\varepsilon}{\partial t} + \operatorname{div}(\overline{\mathbf{u}}\rho\overline{\varepsilon}) - \operatorname{div}\left[\left(\mu + \frac{\mu_t}{\sigma_\varepsilon}\right)\operatorname{grad}\varepsilon\right] = C_{1\varepsilon}\frac{\varepsilon}{k}G_k - C_{2\varepsilon}\rho\frac{\varepsilon^2}{k}, \tag{2.50}$$

$$\tau^n = \left[(\mu+\mu_t)\left(\operatorname{grad}\overline{\mathbf{u}} + \operatorname{grad}\overline{\mathbf{u}}^t\right) + \frac{2}{3}\rho k I\right], \tag{2.51}$$

$$\mu_t = \rho C_\mu \frac{k^2}{\varepsilon}. \tag{2.52}$$

Finally, the dimensionless constants which close the model are fixed from experimental data:

$$C_{1\varepsilon} = 1.44, \quad C_{2\varepsilon} = 1.92, \quad C_\mu = 0.09, \quad \sigma_k = 1.0, \quad \sigma_\varepsilon = 1.3. \tag{2.53}$$

2.3 Averaged compressible Navier-Stokes equations

Using Favre average to decompose the variables,

$$\mathbf{u} = \widetilde{\mathbf{u}} + \mathbf{u}'', \quad Y_i = \widetilde{Y}_i + Y_i'', \quad h = \widetilde{h} + h'',$$

the average of compressible Navier-Stokes equations, (1.88)-(1.92), results

$$\frac{\partial\overline{\rho}}{\partial t} + \operatorname{div}(\overline{\rho}\widetilde{\mathbf{u}}) = 0, \tag{2.54}$$

$$\begin{aligned}\frac{\partial(\overline{\rho}\widetilde{\mathbf{u}})}{\partial t} &+ \operatorname{div}(\overline{\rho}\widetilde{\mathbf{u}}\otimes\widetilde{\mathbf{u}}) + \operatorname{div}\left(\overline{\rho}\widetilde{\mathbf{u}''\otimes\mathbf{u}''}\right) + \operatorname{grad}\overline{\pi} \\ &- \operatorname{div}\left(\mu\left(\operatorname{grad}(\widetilde{\mathbf{u}}) + \operatorname{grad}(\widetilde{\mathbf{u}})^t\right) - \frac{2}{3}\mu\operatorname{div}(\widetilde{\mathbf{v}})I\right) = \overline{\rho}\mathbf{g},\end{aligned} \tag{2.55}$$

$$\frac{\partial(\overline{\rho}\widetilde{y}_i)}{\partial t} + \operatorname{div}(\overline{\rho}\widetilde{y}_i\widetilde{\mathbf{u}}) + \operatorname{div}\left(\overline{\rho}\widetilde{\mathbf{u}''Y_i''}\right) - \operatorname{div}(\overline{\rho}\mathcal{D}\operatorname{grad}\widetilde{y}_i) = 0, \tag{2.56}$$

$$\frac{\partial\left(\overline{\rho}\widetilde{h}\right)}{\partial t} + \operatorname{div}\left(\overline{\rho}\widetilde{h}\widetilde{\mathbf{u}}\right) + \operatorname{div}\left(\overline{\rho}\widetilde{\mathbf{u}''h''}\right) - \operatorname{div}\left(\overline{\rho}\mathcal{D}\operatorname{grad}\widetilde{h}\right) = 0, \tag{2.57}$$

$$\pi_0 = \overline{\rho}R\widetilde{\theta}, \tag{2.58}$$

where

$$\pi_0 = \lim_{T\to\infty}\frac{1}{T}\int_{t-T/2}^{t+T/2}\left(\frac{1}{\operatorname{vol}(B_s)}\int_{B_s}\pi(x,s)dx\right)ds. \tag{2.59}$$

The terms related to the fluctuations are called Favre stresses. As for incompressible flows they introduce in the momentum equation up to six new unknowns that will be approached considering Boussinesq assumption:

$$\tau^F = -\left(\overline{\rho}\widetilde{\mathbf{u}'\otimes\mathbf{u}'}\right) = \mu_t\left(\operatorname{grad}\widetilde{\mathbf{u}} + \operatorname{grad}\widetilde{\mathbf{u}}^t\right) - \frac{2}{3}\mu_t \operatorname{div}\widetilde{\mathbf{u}} - \frac{2}{3}\overline{\rho}kI. \tag{2.60}$$

Moreover, since the use of the $k-\varepsilon$ turbulence model gives a good compromise between numerical accuracy and computational cost, it will be applied to compute the turbulent viscosity.

2.4 The $k-\varepsilon$ model for compressible flows

The $k-\varepsilon$ model for compressible flows is obtained likewise for incompressible flows (see [Van83], [Wil88], [MP94] and [Saa11]). The main differences are the addition of terms which account for the compressibility and the definition of the mean energy dissipation rate.

Definition 2.4.1. The mass rate of turbulent energy dissipation is given by

$$\overline{\rho}\varepsilon = \frac{\mu}{2}\overline{|\operatorname{grad}\mathbf{u}'' + \operatorname{grad}\mathbf{u}''^t|^2} - \frac{2}{3}\mu\overline{|\operatorname{div}\mathbf{u}''|^2}. \tag{2.61}$$

The reduced model for compressible flows reads

$$\frac{\partial\overline{\rho}}{\partial t} + \operatorname{div}\left(\overline{\rho}\widetilde{\mathbf{u}}\right) = 0, \tag{2.62}$$

$$\begin{aligned}\frac{\partial\left(\overline{\rho}\widetilde{\mathbf{u}}\right)}{\partial t} &+ \operatorname{div}\left(\overline{\rho}\widetilde{\mathbf{u}}\otimes\widetilde{\mathbf{u}}\right) + \operatorname{grad}\overline{\pi} - \operatorname{div}\left[\left(\mu+\mu_t\right)\left(\operatorname{grad}(\widetilde{\mathbf{u}})\right.\right.\\ &\left.\left.+\operatorname{grad}(\widetilde{\mathbf{u}})^t\right) - \frac{2}{3}\left(\mu+\mu_t\right)\operatorname{div}(\widetilde{\mathbf{u}})I - \frac{2}{3}\overline{\rho}kI\right] = \overline{\rho}\mathbf{g},\end{aligned} \tag{2.63}$$

$$\frac{\partial\left(\overline{\rho}\widetilde{\mathrm{y}_i}\right)}{\partial t} + \operatorname{div}\left(\overline{\rho}\widetilde{\mathrm{y}_i}\widetilde{\mathbf{u}}\right) - \operatorname{div}\left[\left(\overline{\rho}\mathcal{D} + \frac{\mu_t}{Sc_t}\right)\operatorname{grad}\widetilde{\mathrm{y}_i}\right] = 0, \tag{2.64}$$

$$\frac{\partial\left(\overline{\rho}\widetilde{h}\right)}{\partial t} + \operatorname{div}\left(\overline{\rho}\widetilde{h}\widetilde{\mathbf{u}}\right) - \operatorname{div}\left[\left(\overline{\rho}\mathcal{D} + \frac{\mu_t}{Sc_t}\right)\operatorname{grad}\widetilde{h}\right] = 0, \tag{2.65}$$

$$\frac{\partial\overline{\rho}k}{\partial t} + \operatorname{div}\left(\widetilde{\mathbf{u}}\overline{\rho}k\right) - \operatorname{div}\left[\left(\mu + \frac{\mu_t}{\sigma_k}\right)\operatorname{grad}k\right] - G_k + \rho\varepsilon = 0, \tag{2.66}$$

$$\frac{\partial\overline{\rho}\varepsilon}{\partial t} + \operatorname{div}\left(\widetilde{\mathbf{u}}\overline{\rho}\varepsilon\right) - \operatorname{div}\left[\left(\mu + \frac{\mu_t}{\sigma_\varepsilon}\right)\operatorname{grad}\varepsilon\right] = C_{1\varepsilon}\frac{\varepsilon}{k}G_k - C_{2\varepsilon}\rho\frac{\varepsilon^2}{k}, \tag{2.67}$$

$$\pi_0 = \overline{\rho}\mathcal{R}\widetilde{\theta}, \tag{2.68}$$

$$\mu_t = \overline{\rho}C_\mu\frac{k^2}{\varepsilon}. \tag{2.69}$$

The Schmidt turbulent number, Sc_t, is taken to be 0.07. The remaining closure coefficients are given by (2.53).

Remark 2.4.1. From now on, we will use the same notation for the mean variables than for the complete variables in systems (2.47)-(2.52) and (2.62)-(2.69).

USC
UNIVERSIDADE
DE SANTIAGO
DE COMPOSTELA

Conclusions

The main goal of this part was the review of the mathematical models for laminar and turbulent incompressible and compressible low Mach number flows.

We started by recalling some basic definitions of fluid dynamics. The notions of thermodynamic process, material body and Coleman-Noll materials were presented. Moreover, we have detailed the laws of mass, momentum and energy conservation. To close the system of equations defined we used the state equation. Regarding Coleman-Noll mixtures the equation of transport of species was derived. Finally, a dimensional analysis of the resulting systems has led to the introduction of turbulence.

The different approaches available in the literature to capture turbulent effects were studied. The election of the RANS $k - \varepsilon$ model was justified by means of the computational cost. The related equations were derived and the global systems which model turbulent incompressible flows and turbulent compressible low Mach number flows were recovered.

USC
UNIVERSIDADE
DE SANTIAGO
DE COMPOSTELA

Part II

Numerical analysis of the unidimensional advection-diffusion-reaction equation

USC
UNIVERSIDADE
DE SANTIAGO
DE COMPOSTELA

Contents

Introduction

Advection-diffusion-reaction equations are present in a wide variety of physical and biological problems. Navier-Stokes equations are a prominent example, which constitute a major focus for the development of numerical methods of practical use to the scientific community. A classical and successful approach for solving the aforementioned and related equations are finite volume methods (see, e.g., [Tor09], [BFSVC14], [GR96], [LeV02] and references herein).

A motivation of this part concerns the simulation of incompressible flows in a turbulent regime. As we have seen in Part I, these phenomena can be represented by the Navier-Stokes equations coupled to a RANS $k - \varepsilon$ turbulent model (see [BBC$^+$15]). The approach introduces turbulent viscosity, which is typically computed by solving an additional pair of advection-diffusion-reaction equations, that is, equations for the turbulent kinetic energy and the dissipation rate. One issue here is the time dependency of the viscous term. This requires the use of methods that are at least second-order accurate in space and time for all terms involved. In practice, it is often the case that the numerical methods used are of low order of accuracy. Typically, methods may be of second-order in space but only first-order in time, or may be second-order in both space and time but only for some of the terms in the equations. For diffusion equations a popular choice is the second-order Crank-Nicolson method (see [SO88]). The accuracy for reaction terms, coupled to the remaining terms of the equations, is usually sacrificed, resulting in overall low order of accuracy.

For advection equations, several approaches for constructing high-order methods have been put forward. A classical example is the Lax-Wendroff scheme [LW60], [Lax57]. Nonetheless, this scheme is linear in the sense of Godunov [God59] and thus oscillatory, according to Godunov's theorem [God59]. We note that the oscillatory nature remains so even when (physical) viscous terms are added. A major step forward in this direction was the work of Kolgan [Kol11], who introduced, for the first time, a method that circumvents Godunov's theorem, via the construction of a non-linear scheme using non-linear reconstructions (limited slopes). Since then, many more works have appeared in the literature, reporting schemes, such as the CVC Kolgan-type method, Total Variation Diminishing methods (TVD) and Flux Limiter methods (see, for instance, [CVC12], [vL84], [vL97] and [Swe84]). Comprehensive reviews are found in [Tor09] and [LeV02], for example.

More advanced non-linear methods for advection dominated problems include the semi-discrete ENO and WENO approaches (see [HEOC87], [SO88], [Shu98] and [LOC94]).

We also found the method of Harten and collaborators [HEOC87], which is a fully discrete high-order scheme. In [CT08], this scheme was called the HEOC scheme, and was re-interpreted in terms of the solution of a generalised Riemann problem, solved in a particular way. If fact, it is easily shown that the HEOC scheme is a generalisation of the MUSCL-Hancock method (see [vL84] and [Ber06]).

The ADER approach, first put forward in [TMN01], is also a fully discrete approach that relies on non-linear reconstructions and the solution of the generalised Riemann problem, to any order of accuracy. The resulting schemes are arbitrarily accurate in both space and time in the sense that they have no theoretical accuracy barrier. An introduction to ADER schemes is found in Chapters 19 and 20 of [Tor09]. Further developments and applications are found, for example, in [DM05], [Tit05], [TT05a], [TT05c], [TT05b], [TDTK06], [TT06a], [TT06b], [Tak06], [TT07], [DET08], [DBTM08], [Zah08], [Dum10], [HD11],[MT14], [BD14], [BDL16].

Another motivation of this part comes from solving compressible Navier-Stokes equations. Incompressible flows have constant density so that the flux depends on the spatial variable through the velocities. Therefore, to get an stable scheme we only add an artificial viscosity related to the Jacobian of the flux. However, for compressible flows, the flux also counts for the spatial variable via the density. We have observed that this fact makes necessary to introduce some extra artificial viscosity to the numerical flux (see [BLVC17a]). Otherwise, the resulting numerical scheme can produce spurious oscillations on the solutions due to a lack of upwind.

The development and the theoretical analysis of high-order finite volume schemes results highly complicated in three-dimensions. Consequently, in this part, we set a scalar simplified problem which retains the main difficulties of Navier-Stokes equations. For turbulent incompressible flows, the advection-diffusion-reaction equation with variable diffusion coefficient results appropriate. On the other hand, the density variation on compressible flows motivate the presence of a time and space dependent advection coefficient. Therefore, the aim of this part is to develop finite volume schemes of second-order of accuracy to solve the advection-diffusion-reaction equation, admitting time and space dependent advection and diffusion coefficients.

As first approach we recall Kolgan and CVC Kolgan-type schemes (see [Kol11] and [CVC12]). Then, we follow ADER and MUSCL-Hancock methodologies and compare both approaches. Finally, a modification on ADER is proposed providing a new method called Local ADER (LADER). The features of the new methodology will prove useful when extending it to the three-dimensional case. Detailed analysis, such as linear stability and accuracy in the sense of local truncation error is lacking for these methodologies applied to advection-diffusion-reaction equations. One of the leading objectives of this part is precisely to carry out detailed stability and accuracy analysis of these methods. Moreover, to determine the stability region a new graphical methodology is introduced.

The outline of this part is as follows. In Chapter 3 the advection-diffusion-reaction equation is introduced. Diverse numerical schemes to solve the advection equation are presented. The development of a numerical scheme for the advection-diffusion-

reaction equation with time and space dependent advection and diffusion coefficients is detailed. The ADER approach is adopted to approximate linear advection-reaction equations and is modified to account for a diffusion term with variable coefficient. The methodology developed for the ADER scheme to treat source-term like terms is applied to the MUSCL-Hancock method. Next, the modification on ADER is introduced obtaining LADER scheme. The new methodology is extended to solve the advection-diffusion-reaction equation with variable advection coefficient. Besides, we detect that the time and space dependency of the advection coefficient demands a new numerical viscosity term. A detailed description of it is provided. In Chapter 4, we conduct the stability and accuracy analysis of the aforementioned schemes. Finally, Chapter 5 is devoted to the study of empirical convergence rates of the schemes. The test problems introduced are used to compare the main features of the diverse methods.

USC
UNIVERSIDADE
DE SANTIAGO
DE COMPOSTELA

Chapter 3

High-order schemes

In this chapter four different methodologies to solve the scalar advection equation are introduced. Moreover, two of them are extended to solve the advection-diffusion-reaction equation. Finally, a new numerical methodology is proposed and applied to solve the advection-diffusion-reaction equation with time and space dependent advection and diffusion coefficients.

We start by recalling the advection-diffusion-reaction equation and we derive its integral form. Next, the Kolgan scheme, [Kol11], and the CVC Kolgan-type scheme, [CVC12], are presented for the resolution of the advection equation. A detailed description of the different branches for both schemes is included. Aiming to increase the order of accuracy, the MUSCL-Hancock, [vL84], and ADER, [TMN01], methodologies are extended to solve the advection-diffusion-reaction equation with a space and time dependent diffusion coefficient, [BTVC16]. The developed method is modified in order to ease its extension to the three-dimensional case. Among its advantages we highlight the reduction of the stencil of the resulting scheme and the possibility of computing the gradients involved using a Galerkin approach. In what follows, we will refer to this new method as LADER. The last section is devoted to the advection-diffusion-reaction equation with time and space dependent advection coefficient. This dependency entails new difficulties on the design of the numerical schemes. Moreover, we introduce an extra artificial viscosity term derived from the variation of the advection coefficient. Finally, LADER methodology is extended to account for the variable advection coefficient.

3.1 The advection-diffusion-reaction equation

The advection-diffusion-reaction equation reads

$$\partial_t q(x,t) + \lambda \partial_x q(x,t) = \partial_x \left(\alpha \partial_x q\right)(x,t) + \beta q(x,t), \tag{3.1}$$

where $q(x,t)$ is the conservative variable; x, t are the spatial and temporal independent variables; λ is the characteristic speed; $\alpha(x,t)$ is the diffusion coefficient, a prescribed

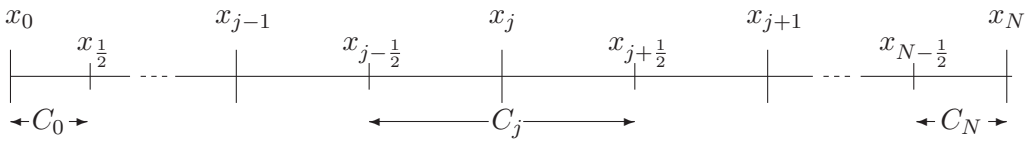

Figure 3.1: Finite volume grid: interior finite volume C_j. Boundary finite volumes C_0 and C_N.

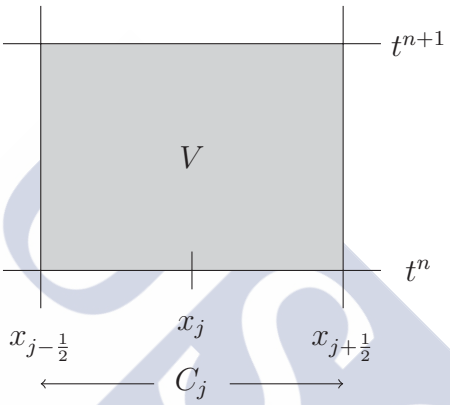

Figure 3.2: Control volume $V = C_j \times [t^n, t^{n+1}]$.

function; and β is the coefficient of the reaction term (source term).

In order to solve equation (3.1) we work in the finite volume framework (see [Tor09] and [VC15]). To start with, the spatial domain $[a, b]$ is discretized using an arbitrary grid $\mathcal{C}_{\Delta x}$. We denote $\{x_j,\, j = 0, \ldots, N\}$ the set of nodes of the grid, verifying $x_0 = a$ and $x_N = b$, and

$$\Delta x = \max_{x_{j-1}, x_j \in \mathcal{C}_{\Delta x}} |x_j - x_{j-1}| \tag{3.2}$$

is the norm of the grid. Moreover, interior cells are defined by

$$C_j = \left(x_{j-\frac{1}{2}}, x_{j+\frac{1}{2}}\right) = \left(x_j - \frac{x_j - x_{j-1}}{2}, x_j + \frac{x_{j+1} - x_j}{2}\right) \tag{3.3}$$

while the boundary cells are

$$C_0 = \left(x_0, x_{\frac{1}{2}}\right), \quad C_N = \left(x_{N-\frac{1}{2}}, x_N\right) \tag{3.4}$$

(see Figure 3.1). For simplicity, we assume a constant distance between nodes. Since we are interested on solving equation (3.1) over time, we also consider a discretization in time with time step $\Delta t = t^{n+1} - t^n$. Next, we define the control volume $V = [x_{j-\frac{1}{2}}, x_{j+\frac{1}{2}}] \times [t^n, t^{n+1}]$ in the $x - t$ plane (see Figure 3.2).

Then, the exact integration of equation (3.1) in the control volume V gives

$$\int_{x_{j-\frac{1}{2}}}^{x_{j+\frac{1}{2}}}\Big[q(x,t^{n+1})-q(x,t^n)\Big]\,dx+\int_{t^n}^{t^{n+1}}\Big[f(q(x_{j+\frac{1}{2}},t))-f(q(x_{j-\frac{1}{2}},t))\Big]\,dt$$
$$=\int_{x_{j-\frac{1}{2}}}^{x_{j+\frac{1}{2}}}\left[\int_{t^n}^{t^{n+1}}\partial_x\left(\alpha\partial_x q\right)(x,t)\;dt\right]dx+\int_{x_{j-\frac{1}{2}}}^{x_{j+\frac{1}{2}}}\left[\int_{t^n}^{t^{n+1}}\beta q(x,t)\,dt\right]dx, \tag{3.5}$$

where

$$f(q(x,t))=\lambda q\left(x,t\right). \tag{3.6}$$

Introducing the notation

$$q_j^{n+1}=\frac{1}{\Delta x}\int_{x_{j-\frac{1}{2}}}^{x_{j+\frac{1}{2}}}q(x,t^{n+1})\,dx,\quad q_j^{n}=\frac{1}{\Delta x}\int_{x_{j-\frac{1}{2}}}^{x_{j+\frac{1}{2}}}q(x,t^{n})\,dx,$$

$$f_{j+\frac{1}{2}}^n=\frac{1}{\Delta t}\int_{t^n}^{t^{n+1}}f(q(x_{j+\frac{1}{2}},t))\,dt,\quad f_{j-\frac{1}{2}}^n=\frac{1}{\Delta t}\int_{t^n}^{t^{n+1}}f(q(x_{j-\frac{1}{2}},t))\,dt,$$

$$g_j^n=\frac{1}{\Delta t\Delta x}\int_{x_{j-\frac{1}{2}}}^{x_{j+\frac{1}{2}}}\left[\int_{t^n}^{t^{n+1}}\partial_x\left(\alpha\partial_x q\right)(x,t)\,dt\right]dx,$$

$$s_j^n=\frac{1}{\Delta t\Delta x}\int_{x_{j-\frac{1}{2}}}^{x_{j+\frac{1}{2}}}\left[\int_{t^n}^{t^{n+1}}\beta q(x,t)\,dt\right]dx,$$

we arrive at the exact relation

$$q_j^{n+1}=q_j^n-\frac{\Delta t}{\Delta x}\left(f_{j+\frac{1}{2}}^n-f_{j-\frac{1}{2}}^n\right)+\Delta t g_j^n+\Delta t s_j^n. \tag{3.7}$$

Thus, we can construct a numerical method to find the solution of (3.1) at time t^{n+1} by interpreting (3.7) in an approximate manner, that is by approximating the integrals in (3.7). We analyse five different approaches for computing them: Kolgan, CVC Kolgan-type, ADER, MUSCL-Hancock and LADER methodologies. For the sake of simplicity, we will use the same notation for the approximate values than for the exact values of the integrals in (3.7). It is appropriate to remark that the integral g_j^n could be further integrated to yield corresponding expressions for viscous numerical fluxes.

3.2 Rusanov flux

The approximation of the physical flux in (3.7) is performed by means of the numerical flux,

$$f_{j+\frac{1}{2}}^n\simeq\phi(q_{j-l_1}^n,\ldots,q_{j+l_2}^n),\quad f_{j-\frac{1}{2}}^n\simeq\phi(q_{j-l_1-1}^n,\ldots,q_{j+l_2-1}^n) \tag{3.8}$$

with l_1, l_2 two non-negative integers. Assuming a piecewise constant solution, the computation of the numerical flux states a Riemann problem at each of the finite

volume boundaries. Depending on the choice of the discrete flux function different conservative schemes are obtained. A review on the discrete flux functions can be found in [HLvL83], [LeV92], [Tor09] and [VC15].

In this thesis, we will consider Rusanov scheme, [Rus62]. This choice lies on the results presented in [BFSVC14] for the **Q**-scheme of van Leer and the Rusanov scheme. Let us denote u, v two nearby states and $\lambda(u)$, $\lambda(v)$ the eigenvalues corresponding to the jacobian matrix of a non-linear flux at each state. The Rusanov numerical flux function for the scalar equation with a non-linear advection term reads

$$\phi(u,v) = \frac{f(u)+f(v)}{2} - \frac{1}{2}\alpha_{RS}(u,v)(v-u) \tag{3.9}$$

where

$$\alpha_{RS}(u,v) = \max\left\{|\lambda(u)|, |\lambda(v)|\right\} \tag{3.10}$$

is called the Rusanov coefficient. For the scalar advection-diffusion-reaction equation with linear advection, (3.1), it is verified

$$\alpha_{RS}(u,v) = |\lambda|. \tag{3.11}$$

Remark 3.2.1. This scheme can be extended to non-linear systems by taking α_{RS} as the maximum of the absolute eigenvalues of the Jacobian matrix of the flux at each side of the face. Furthermore, it can be seen as a regularization of the **Q**-schemes by means of the absolute value matrix of **Q**,

$$\phi(u,v) = \frac{f(u)+f(v)}{2} - \frac{1}{2}|\mathbf{Q}(u,v)|\,(v-u). \tag{3.12}$$

We recall that the absolute value matrix of **Q**, $|\mathbf{Q}|$, is the matrix whose eigenvalues are the absolute values of the eigenvalues of **Q**,

$$|\mathbf{Q}| = \mathbf{P}\,|\Lambda|\,\mathbf{P}, \tag{3.13}$$

being $|\Lambda|$ the diagonal matrix defined by $|\Lambda|_{ii} = |\lambda_{ii}|$, $i = 1, \ldots, p$. For equation (3.1), $|\mathbf{Q}(u,v)| = |\lambda|$ and so, the **Q**-schemes match Rusanov scheme.

3.3 Kolgan-type schemes

The development of high-order methods to solve the advection equation has been broadly studied in the literature. As a result, several linear schemes like the presented by Lax-Wendrof ([LW60]), Fromm ([Fro68]) or Warming-Beam ([WB76]) were developed. However, for solutions involving high gradients these methods produce spurious oscillations. On the other hand, linear monotone schemes avoid these phenomena but, as counterpart, they have a limited accuracy. The previous conclusions have been theoretically proved in Godunov's theorem, [God59]:

Theorem 3.3.1 (Godunov's theorem)**.** *There are no monotone, linear schemes for the advection equation of second or higher order of accuracy.*

Kolgan, [Kol11], introduced for the first time a non linear high-order scheme that circumvents Godunov's theorem. In order to do that, he proposed the use of limited slopes in the reconstruction of the conservative values needed to build the flux function.

For the scalar advection equation, Kolgan scheme written in conservative form reads

$$q_j^{n+1} = q_j^n - \frac{\Delta t}{\Delta x}\left[\phi\left(q^n_{L\,j+\frac{1}{2}}, q^n_{R\,j+\frac{1}{2}}\right) - \phi\left(q^n_{L\,j-\frac{1}{2}}, q^n_{R\,j-\frac{1}{2}}\right)\right], \tag{3.14}$$

being $q^n_{L\,j+\frac{1}{2}}, q^n_{R\,j+\frac{1}{2}}, q^n_{L\,j-\frac{1}{2}}$ and $q^n_{R\,j-\frac{1}{2}}$ the data reconstruction of the conservative variables at the two boundaries of the finite volume cell, namely, $x_{j-\frac{1}{2}}$ and $x_{j+\frac{1}{2}}$, which are obtained by means of linear interpolation:

$$q^n_{L\,j-\frac{1}{2}} = q^n_{j-1} + \frac{1}{2}\Delta_{j-1}^{n\,L_*}, \qquad q^n_{R\,j-\frac{1}{2}} = q^n_j + \frac{1}{2}\Delta_j^{n\,R_*}, \tag{3.15}$$

$$q^n_{L\,j+\frac{1}{2}} = q^n_j + \frac{1}{2}\Delta_j^{n\,L_*}, \qquad q^n_{R\,j+\frac{1}{2}} = q^n_{j+1} + \frac{1}{2}\Delta_{j+1}^{n\,R_*}. \tag{3.16}$$

Where $\Delta_j^{L_*}$ and $\Delta_j^{R_*}$ denote the left and right slopes, related to de conservative variable, at node x_j. To minimize this gradients inside the cell, the slopes are chosen using the minmod-type limiter (see [Kol11]):

$$\Delta_j^{n\,L_*} = \begin{cases} \max\left[0, \min\left[q_j^n - q_{j-1}^n, q_{j+1}^n - q_j^n\right]\right], & \text{if } q_{j+1}^n - q_j^n > 0, \\ \min\left[0, \max\left[q_j^n - q_{j-1}^n, q_{j+1}^n - q_j^n\right]\right], & \text{if } q_{j+1}^n - q_j^n < 0, \end{cases} \tag{3.17}$$

$$\Delta_j^{n\,R_*} = \begin{cases} \max\left[0, \min\left[-q_j^n + q_{j-1}^n, -q_{j+1}^n + q_j^n\right]\right], & \text{if } q_{j-1}^n - q_j^n > 0, \\ \min\left[0, \max\left[-q_j^n + q_{j-1}^n, -q_{j+1}^n + q_j^n\right]\right], & \text{if } q_{j-1}^n - q_j^n < 0. \end{cases} \tag{3.18}$$

Denoting

$$\Delta_j^n = q_{j+1}^n - q_j^n, \tag{3.19}$$

relations (3.17) and (3.18) can be rewritten as

$$\Delta_j^{n\,L_*} = \begin{cases} \Delta_{j-1}^n, & \text{if } \left|\Delta_{j-1}^n\right| < \left|\Delta_j^n\right|,\ \Delta_{j-1}^n\Delta_j^n > 0, & (3.20) \\ \Delta_j^n, & \text{if } \left|\Delta_{j-1}^n\right| > \left|\Delta_j^n\right|,\ \Delta_{j-1}^n\Delta_j^n > 0, & (3.21) \\ 0, & \text{if } \Delta_{j-1}^n\Delta_j^n < 0, & (3.22) \end{cases}$$

$$\Delta_j^{n\,R_*} = \begin{cases} -\Delta_{j-1}^n, & \text{if } \left|\Delta_{j-1}^n\right| < \left|\Delta_j^n\right|,\ \Delta_{j-1}^n\Delta_j^n > 0, \quad (3.23)\\ -\Delta_j^n, & \text{if } \left|\Delta_{j-1}^n\right| > \left|\Delta_j^n\right|,\ \Delta_{j-1}^n\Delta_j^n > 0, \quad (3.24)\\ 0, & \text{if } \Delta_{j-1}^n\Delta_j^n < 0. \quad (3.25) \end{cases}$$

Assuming, without loss of generality, that $\lambda > 0$ and substituting (3.20)-(3.22) on (3.14), the derived scheme has four branches:

$$q_j^{n+1} = q_j^n - \frac{\lambda\Delta t}{2\Delta x}\left(\Delta_{j-1}^n + \Delta_j^n\right), \quad \text{if } \left|\Delta_{j-2}^n\right| \geq \left|\Delta_{j-1}^n\right| \geq \left|\Delta_j^n\right|, \quad (3.26)$$

$$q_j^{n+1} = q_j^n + \frac{\lambda\Delta t}{2\Delta x}\left(\Delta_{j-2}^n - 3\Delta_{j-1}^n\right), \quad \text{if } \left|\Delta_{j-2}^n\right| \leq \left|\Delta_{j-1}^n\right| \leq \left|\Delta_j^n\right|, \quad (3.27)$$

$$q_j^{n+1} = q_j^n - \frac{\lambda\Delta t}{\Delta x}\Delta_{j-1}^n, \quad \text{if } \left|\Delta_{j-2}^n\right| \geq \left|\Delta_{j-1}^n\right| \leq \left|\Delta_j^n\right|, \quad (3.28)$$

$$q_j^{n+1} = q_j^n + \frac{\lambda\Delta t}{2\Delta x}\left(\Delta_{j-2}^n - 2\Delta_{j-1}^n - \Delta_j^n\right), \quad \text{if } \left|\Delta_{j-2}^n\right| \leq \left|\Delta_{j-1}^n\right| \geq \left|\Delta_j^n\right|. \quad (3.29)$$

Taking into account (3.19) we obtain

$$q_j^{n+1} = q_j^n + \frac{\lambda\Delta t}{2\Delta x}\left(q_{j-1}^n - q_{j+1}^n\right), \quad \text{if } \left|\Delta_{j-2}^n\right| \geq \left|\Delta_{j-1}^n\right| \geq \left|\Delta_j^n\right|, \quad (3.30)$$

$$q_j^{n+1} = q_j^n + \frac{\lambda\Delta t}{2\Delta x}\left(-q_{j-2}^n + 4q_{j-1}^n - 3q_j^n\right), \quad \text{if } \left|\Delta_{j-2}^n\right| \leq \left|\Delta_{j-1}^n\right| \leq \left|\Delta_j^n\right|, \quad (3.31)$$

$$q_j^{n+1} = q_j^n + \frac{\lambda\Delta t}{\Delta x}\left(q_{j-1}^n - q_j^n\right), \quad \text{if } \left|\Delta_{j-2}^n\right| \geq \left|\Delta_{j-1}^n\right| \leq \left|\Delta_j^n\right|, \quad (3.32)$$

$$q_j^{n+1} = q_j^n + \frac{\lambda\Delta t}{2\Delta x}\left(-q_{j-2}^n + 3q_{j-1}^n - q_j^n - q_{j+1}^n\right), \quad \text{if } \left|\Delta_{j-2}^n\right| \leq \left|\Delta_{j-1}^n\right| \geq \left|\Delta_j^n\right|. \quad (3.33)$$

The limited slopes are the point of Kolgan's landmark contribution as they provide a non-linear, monotone, second-order in space scheme which circunvents Godunov's theorem.

Considering the case in which no limiters are needed, Kolgan scheme reduces to its second branch, (3.31),

$$q_j^{n+1} = q_j^n + \frac{c}{2}\left(-q_{j-2}^n + 4q_{j-1}^n - 3q_j^n\right), \quad (3.34)$$

where $c = \dfrac{\lambda\Delta t}{\Delta x}$ is the, so called, Courant or CFL number (see [CFL28]).

3.3.1 The CVC Kolgan-type scheme

Following the work of Kolgan, the CVC Kolgan-type scheme was introduced in [CVC10] and [CVC12] for the shallow water equations. This scheme considers the slopes and limiters introduced for the Kolgan scheme, (3.15)-(3.18), but it chooses a non-linear modification of the Q-schemes for the computation of the numerical flux.

The data reconstruction of the variables at the cell faces, q_L^n and q_R^n, is used only for the viscosity part of the numerical flux whereas the original values are retained in the centred part:

$$\phi(q_j^n, q_{j+1}^n, q_{L\,j+\frac{1}{2}}^n, q_{R\,j+\frac{1}{2}}^n) = \frac{f(q_j^n) + f(q_{j+1}^n)}{2} - \frac{1}{2}\,|\lambda|\,(q_{R\,j+\frac{1}{2}}^n - q_{L\,j+\frac{1}{2}}^n). \tag{3.35}$$

The nine feasible branches obtained from the different elections of the slopes and limiters considering $\lambda > 0$ are depicted in Table 3.1. Assuming that flux limiters are not needed, the scheme for the linear advection equation reads

$$q_j^{n+1} = q_j^n - \frac{c}{2}\left(\frac{1}{2}q_{j-2}^n - 3q_{j-1}^n + 3q_j^n - q_{j+1}^n + \frac{1}{2}q_{j+2}^n\right). \tag{3.36}$$

Remark 3.3.1. When limiters are used, scheme (3.36) is not a doable branch.

Option	$\Delta_{j-1}^{n\,L_*}$	$\Delta_j^{n\,L_*}$	$\Delta_j^{n\,R_*}$	$\Delta_{j+1}^{n\,R_*}$	Scheme
1	(3.20)	(3.20)	(3.23)	(3.23)	$q_j^{n+1} = q_j^n - \frac{c}{4}\left(-\Delta_{j-2}^n + 4\Delta_{j-1}^n + \Delta_j^n\right)$ $= -\frac{c}{4}q_{j-2}^n + \frac{5c}{4}q_{j-1}^n + \left(1 - \frac{3c}{4}\right)q_j^n - \frac{c}{4}q_{j+1}^n.$ (3.37)
2	(3.20)	(3.21)	(3.24)	(3.23)	
3	(3.20)	(3.20)	(3.23)	(3.24)	$q_j^{n+1} = q_j^n - \frac{c}{4}\left(-\Delta_{j-2}^n + 4\Delta_{j-1}^n + \Delta_{j+1}^n\right)$ $= \frac{-c}{4}q_{j-2}^n + \frac{5c}{4}q_{j-1}^n + (1-c)q_j^n + \frac{c}{4}q_{j+1}^n - \frac{c}{4}q_{j+2}^n.$ (3.38)
4	(3.20)	(3.21)	(3.24)	(3.24)	
5	(3.20)	(3.20)	(3.23)	(3.25)	$q_j^{n+1} = q_j^n - \frac{c}{4}\left(-\Delta_{j-2}^n + 4\Delta_{j-1}^n\right)$ $= -\frac{c}{4}q_{j-2}^n + \frac{5c}{4}q_{j-1}^n + (1-c)\,q_j^n.$ (3.39)
6	(3.20)	(3.21)	(3.24)	(3.25)	

Option	$\Delta_{j-1}^{n\,L_*}$	$\Delta_j^{n\,L_*}$	$\Delta_j^{n\,R_*}$	$\Delta_{j+1}^{n\,R_*}$	Scheme
7	(3.21)	(3.20)	(3.23)	(3.23)	$q_j^{n+1} = q_j^n - \frac{c}{4}\left(3\Delta_{j-1}^n + \Delta_j^n\right)$ $= \frac{3c}{4}q_{j-1}^n + \left(1 - \frac{c}{2}\right)q_j^n - \frac{c}{4}q_{j+1}^n.$ (3.40)
8	(3.21)	(3.21)	(3.24)	(3.23)	
9	(3.21)	(3.22)	(3.25)	(3.23)	
10	(3.21)	(3.20)	(3.23)	(3.24)	$q_j^{n+1} = q_j^n - \frac{c}{4}\left(-3\Delta_{j-1}^n + \Delta_{j+1}^n\right)$ $= \frac{3c}{4}q_{j-1}^n + \left(1 - \frac{3c}{4}\right)q_j^n + \frac{c}{4}q_{j+1}^n - \frac{c}{4}q_{j+2}^n.$ (3.41)
11	(3.21)	(3.21)	(3.24)	(3.24)	
12	(3.21)	(3.22)	(3.25)	(3.24)	
13	(3.21)	(3.20)	(3.23)	(3.25)	$q_j^{n+1} = q_j^n - \frac{3c}{4}\Delta_{j-1}^n$ $= \frac{3c}{4}q_{j-1}^n + \left(1 - \frac{3c}{4}\right)q_j^n.$ (3.42)
14	(3.21)	(3.21)	(3.24)	(3.25)	
15	(3.21)	(3.22)	(3.25)	(3.25)	
16	(3.22)	(3.20)	(3.23)	(3.23)	$q_j^{n+1} = q_j^n - \frac{c}{4}\left(4\Delta_{j-1}^n + \Delta_j^n\right)$ $= cq_{j-1}^n + \left(1 - \frac{3c}{4}\right)q_j^n - \frac{c}{4}q_{j+1}^n.$ (3.43)
17	(3.22)	(3.21)	(3.24)	(3.23)	
18	(3.22)	(3.22)	(3.25)	(3.23)	
19	(3.22)	(3.20)	(3.23)	(3.24)	$q_j^{n+1} = q_j^n - \frac{c}{4}\left(4\Delta_{j-1}^n + \Delta_{j+1}^n\right)$ $= \frac{c}{4}q_{j-1}^n + (1-c)\,q_j^n + \frac{c}{4}q_{j+1}^n - \frac{c}{4}q_{j+2}^n.$ (3.44)
20	(3.22)	(3.21)	(3.24)	(3.24)	
21	(3.22)	(3.22)	(3.25)	(3.24)	
22	(3.22)	(3.20)	(3.23)	(3.25)	$q_j^{n+1} = q_j^n - \frac{c}{2}\Delta_{j-1}^n$ $= \frac{c}{2}q_{j-1}^n + \left(1 - \frac{c}{2}\right)q_j^n.$ (3.45)
23	(3.22)	(3.21)	(3.24)	(3.25)	
24	(3.22)	(3.22)	(3.25)	(3.25)	

Table 3.1: Branches of the CVC Kolgan-type scheme for $\lambda > 0$. Each option refers to a feasible combination of slopes, (3.17)-(3.18), detailed in columns two to five. The diverse branches of the scheme can be attained by two or three different elections of the slopes.

3.4 ADER approach

The Arbitrary high-order DErivative Riemann problem (ADER) approach was first put forward in [TMN01] for the linear advection equation in one and three space dimensions. In this section, we introduce a modification of ADER approach to solve the advection-diffusion-reaction equation. The proposed method includes the following steps:

Step 1. Polynomial reconstruction.

Following [TMN01], we consider a reconstruction of the data in terms of first-degree polynomials of the form

$$p_j(x) = q_j^n + \Delta_j^n (x - x_j), \tag{3.46}$$

where Δ_j^n denotes the spatial derivative of $q(x,t)$ at time t^n in volume C_j (or an approximation) for $j = 1, 2, \ldots, M$, with M the total number of finite volumes. Initially, we consider centred slopes, that is

$$\Delta_j^n = \frac{q_{j+1}^n - q_{j-1}^n}{2\Delta x}, \tag{3.47}$$

which, as proved in Section 4.4, will provide a scheme of second-order accuracy in space and time. We note however that the resulting schemes will be linear and hence oscillatory in the presence of large spatial gradients.

To circumvent Godunov's theorem we consider a non-linear reconstruction of the slopes. More precisely, the ENO (Essentially Non-Oscillatory) interpolation method is used (see [SO88], [Shu98] and [Tor09]). Applying ENO methodology within the polynomial reconstruction step, the slopes are adaptively chosen as follows:

$$\Delta_j^n = \begin{cases} \Delta_{j\,C}^n = \dfrac{q_{j+1}^n - q_{j-1}^n}{2\Delta x}, & \text{if } \left|\Delta_{j\,C}^n\right| = \min\left\{\left|\Delta_{j\,C}^n\right|, \left|\Delta_{j\,U}^n\right|, \left|\Delta_{j\,D}^n\right|\right\}, \\ \Delta_{j\,U}^n = \dfrac{q_{j+1}^n - q_j^n}{\Delta x}, & \text{if } \left|\Delta_{j\,U}^n\right| = \min\left\{\left|\Delta_{j\,C}^n\right|, \left|\Delta_{j\,U}^n\right|, \left|\Delta_{j\,D}^n\right|\right\}, \\ \Delta_{j\,D}^n = \dfrac{q_j^n - q_{j-1}^n}{\Delta x}, & \text{if } \left|\Delta_{j\,D}^n\right| = \min\left\{\left|\Delta_{j\,C}^n\right|, \left|\Delta_{j\,U}^n\right|, \left|\Delta_{j\,D}^n\right|\right\}. \end{cases} \tag{3.48}$$

Step 2. Solution of the generalized Riemann problem (GRP).

To construct the numerical flux the following generalizations of the Classical Riemann Problem are made. On the one hand, the initial condition is assumed to be a piecewise first-degree polynomial. On the other hand, the partial differential

equation accounts for diffusion and reaction terms. That leads to the problem

$$\begin{cases} \partial_t q\,(x,t) + \lambda \partial_x q\,(x,t) = \partial_x\left(\alpha \partial_x q\right)(x,t) + \beta q\,(x,t)\,, \\ q(x,0) = \begin{cases} p_j(x) & \text{if } x < 0, \\ p_{j+1}(x) & \text{if } x > 0, \end{cases} \end{cases} \tag{3.49}$$

where we have considered a local coordinates system setting the origin at the fixed interface position, $x_{j+\frac{1}{2}}$, and at time t^n.

Step 3. Reaction and diffusion terms.

These terms are computed by approximating the integrals by the mid-point rule in both space and time.

In the following sections we will develop the last two steps.

3.4.1 Step 2. Solution of the generalized Riemann problem

For ease of presentation, two different cases for the diffusion term will be considered: zero diffusion term and a space and time dependent diffusion coefficient.

Numerical flux without diffusion

Expressing the solution of the GRP at the interface as a Taylor series expansion in time and setting a new coordinate system with the origin on $\left(x_{j+\frac{1}{2}}, t^n\right)$, we have

$$\overline{q^n_{j+\frac{1}{2}}} = q(0,0_+) + \tau \partial_t q(0,0_+)\,. \tag{3.50}$$

We find the solution of (3.49) as given by two terms. One being the solution of a classical Riemann problem, $q(0,0_+)$, and the other as given by the high-order term, $\tau \partial_t q(0,0_+)$.

The classical Riemann problem related to $q(0,0_+)$ reads

$$\begin{cases} \partial_t q\,(x,t) + \lambda \partial_x q\,(x,t) = 0, \\ q(x,0) = \begin{cases} q^n_j + \frac{1}{2}\Delta x \Delta^n_j, & \text{if } x < 0, \\ q^n_{j+1} - \frac{1}{2}\Delta x \Delta^n_{j+1}, & \text{if } x > 0. \end{cases} \end{cases} \tag{3.51}$$

Its similarity solution, $d^{(0)}_{j+\frac{1}{2}}(x/t)$, is

$$d^{(0)}_{j+\frac{1}{2}}(x/t) = \begin{cases} q^n_j + \dfrac{1}{2}\Delta x \Delta^n_j, & \text{if } \dfrac{x}{t} < \lambda, \\ q^n_{j+1} - \dfrac{1}{2}\Delta x \Delta^n_{j+1}, & \text{if } \dfrac{x}{t} > \lambda. \end{cases} \tag{3.52}$$

Hence, the leading term is the Godunov state ($\frac{x}{t}=0$)

$$q(0,0_+)=d^{(0)}_{j+\frac{1}{2}}(0)=\begin{cases} q^n_j+\dfrac{1}{2}\Delta x\Delta^n_j, & \text{if } \lambda>0,\\ q^n_{j+1}-\dfrac{1}{2}\Delta x\Delta^n_{j+1}, & \text{if } \lambda<0. \end{cases} \tag{3.53}$$

On the other hand, considering Cauchy-Kovalevskaya procedure (see [Tor09]) and assuming a zero diffusion term, it is verified

$$\partial_t q\left(x,t\right)=-\lambda\partial_x q\left(x,t\right)+\beta q\left(x,t\right), \tag{3.54}$$

thus, we can express (3.50) in terms of spatial derivatives

$$\overline{q^n_{j+\frac{1}{2}}}=q(0,0_+)+\tau\left[-\lambda\partial_x q(0,0_+)+\beta q(0,0_+)\right]. \tag{3.55}$$

It is easy to show that the following evolution equation for the spatial derivative of the conservative variable is valid

$$\partial_t(\partial_x q(x,t))+\lambda\partial^{(2)}_x q(x,t)=\beta\partial_x q(x,t)\ . \tag{3.56}$$

Neglecting the source term, a new classical Riemann problem can be set for the spatial gradient

$$\begin{cases} \partial_t(\partial_x q(x,t))+\lambda\partial^{(2)}_x q(x,t)=0,\\ \partial_x q(x,0)=\begin{cases} \Delta^n_j, & \text{if } x<0,\\ \Delta^n_{j+1}, & \text{if } x>0. \end{cases} \end{cases} \tag{3.57}$$

Its similarity solution, $d^{(1)}_{j+\frac{1}{2}}\left(\dfrac{x}{t}\right)$, is given by

$$d^{(1)}_{j+\frac{1}{2}}\left(\frac{x}{t}\right)=\begin{cases} \Delta^n_j, & \text{if } \dfrac{x}{t}<\lambda,\\ \Delta^n_{j+1}, & \text{if } \dfrac{x}{t}>\lambda, \end{cases} \tag{3.58}$$

and the solution at $\dfrac{x}{t}=0$ results

$$\partial_x q(0,0_+)=d^{(1)}_{j+\frac{1}{2}}\left(0\right)=\begin{cases} \Delta^n_j, & \text{if } \lambda>0,\\ \Delta^n_{j+1}, & \text{if } \lambda<0. \end{cases} \tag{3.59}$$

Then, from (3.53) and (3.59), the sought complete solution reads

$\overline{q^n_{j+\frac{1}{2}}}=q(0,0_+)+\tau\partial_t q(0,0_+)$

$$= \begin{cases} q_j^n + \frac{1}{2}\Delta x \Delta_j^n + \tau\left[-\lambda\Delta_j^n + \beta\left(q_j^n + \frac{1}{2}\Delta x\Delta_j^n\right)\right], & \text{if } \lambda > 0, \\ q_{j+1}^n - \frac{1}{2}\Delta x \Delta_{j+1}^n + \tau\left[-\lambda\Delta_{j+1}^n + \beta\left(q_{j+1}^n - \frac{1}{2}\Delta x\Delta_{j+1}^n\right)\right], & \text{if } \lambda < 0. \end{cases} \tag{3.60}$$

Performing exact integration, or equivalently applying the mid-point rule with $\tau = \frac{1}{2}\Delta t$, we obtain the numerical flux,

$$f_{j+\frac{1}{2}}^n = \begin{cases} \lambda\left\{q_j^n + \frac{1}{2}\Delta x\Delta_j^n + \frac{\Delta t}{2}\left[-\lambda\Delta_j^n + \beta\left(q_j^n + \frac{1}{2}\Delta x\Delta_j^n\right)\right]\right\}, & \text{if } \lambda > 0, \\ \lambda\left\{q_{j+1}^n - \frac{1}{2}\Delta x\Delta_{j+1}^n + \frac{\Delta t}{2}\left[-\lambda\Delta_{j+1}^n + \beta\left(q_{j+1}^n - \frac{1}{2}\Delta x\Delta_{j+1}^n\right)\right]\right\}, & \text{if } \lambda < 0. \end{cases} \tag{3.61}$$

Numerical flux with diffusion

In order to treat the diffusion term we adopt the following strategy. The term is regarded as a source term but is introduced in the Cauchy-Kovalevskaya procedure and is evaluated in an upwind fashion. The upwinding of the diffusion term can be justified because in the case of constant diffusion coefficient α, the second derivative of the solution $q(x, y)$ of the linear advection equation, in fact any order derivative, obeys identically the same linear advection equation. Hence we can pose and solve a classical Riemann problem for these spatial derivatives leading effectively to *upwinding the diffusion term.*

The Cauchy-Kovalevskaya procedure used in the Taylor series expansion in time for the solution of the GRP,

$$\overline{q_{j+\frac{1}{2}}^n} = q(0, 0_+) + \tau\partial_t q(0, 0_+), \tag{3.62}$$

gives

$$\overline{q_{j+\frac{1}{2}}^n} = q(0, 0_+) + \tau\left[-\lambda\partial_x q(0, 0_+) + \partial_x\left(\alpha\partial_x q\right)(0, 0_+) + \beta q(0, 0_+)\right]. \tag{3.63}$$

As anticipated previously, the term $\partial_x\left(\alpha\partial_x q_j\right)(0, 0_+)$ is approximated in a central difference fashion as follows

$$\partial_x\left(\alpha\partial_x q\right)(0, 0_+) = \frac{1}{\Delta x^2}\left[\alpha_{j+\frac{1}{2}}\left(q_{j+1}^n - q_j^n\right) - \alpha_{j-\frac{1}{2}}\left(q_j^n - q_{j-1}^n\right)\right]. \tag{3.64}$$

The choice made for approximating the diffusion term in this manner is motivated by the fact that in the three-dimensional Navier-Stokes code developed, VolFEM3D, this term will be computed by solving a pair of advection-diffusion-reaction equations.

For notational convenience we set $\left(\Delta\alpha\Delta\right)_j^n = \partial_x\left(\alpha\partial_x q\right)(0, 0_+)$. Integrating, the

numerical flux results

$$f^n_{j+\frac{1}{2}} = \begin{cases} \lambda \left\{ q^n_j + \frac{1}{2}\Delta x \Delta^n_j + \frac{\Delta t}{2}\left[-\lambda \Delta^n_j \right. \right. \\ \qquad \left. \left. + \beta \left(q^n_j + \frac{1}{2}\Delta x \Delta^n_j \right) + (\Delta \alpha \Delta)^n_j \right] \right\}, & \text{if } \lambda > 0, \\ \lambda \left\{ q^n_{j+1} - \frac{1}{2}\Delta x \Delta^n_{j+1} + \frac{\Delta t}{2}\left[-\lambda \Delta^n_{j+1} \right. \right. \\ \qquad \left. \left. + \beta \left(q^n_{j+1} - \frac{1}{2}\Delta x \Delta^n_{j+1} \right) + (\Delta \alpha \Delta)^n_{j+1} \right] \right\}, & \text{if } \lambda < 0. \end{cases} \tag{3.65}$$

Remark 3.4.1. From now on, we will focus on the development and analysis of the schemes for $\lambda > 0$. The results for $\lambda < 0$ can be similarly obtained.

Remark 3.4.2. The whole scheme can be derived from the finite volume framework, resulting in an intercell numerical flux with two terms, one for the advection and one for the diffusion (see [TT01] and [TH09]). However, it is worth mentioning that through an appropriated choice of the approximation for the slopes it will result in the same numerical scheme than the one proposed in this thesis.

Furthermore, our motivation is to couple the numerical method developed to the methodology used to solve the three-dimensional Navier-Stokes equations, see Part III. To this end, the approach proposed here turns out to be very convenient and achieves the order of accuracy sought.

3.4.2 Step 3. Approximation of diffusion and reaction terms

Let us recall that second-order approximations to the integrals defining the finite volume method can be obtained via the mid-point rule approximation (see [Tor09]). This requires an approximation at the centre of the volume at the half time, which is achieved by a Taylor expansion and the use of the Cauchy-Kovalevskaya procedure, namely

$$\overline{q^n_j} = q^n_j + \tau \left(-\lambda \Delta_j + (\Delta \alpha \Delta)_j + \beta q^n_j \right). \tag{3.66}$$

Step 3.1. Diffusion term

Denoting

$$\Delta^n_{j+\frac{1}{2}} = \frac{1}{\Delta x}\left(q^n_{j+1} - q^n_j \right), \tag{3.67}$$

the approximation of the diffusion term becomes

$$\overline{(\Delta \alpha \Delta)^n_j} = \frac{\overline{\alpha^n_{j+\frac{1}{2}}}\,\overline{\Delta^n_{j+\frac{1}{2}}} - \overline{\alpha^n_{j-\frac{1}{2}}}\,\overline{\Delta^n_{j-\frac{1}{2}}}}{\Delta x} = \frac{1}{\Delta x^2}\left[\overline{\alpha^n_{j+\frac{1}{2}}}\left(\overline{q^n_{j+1}} - \overline{q^n_j} \right) - \overline{\alpha^n_{j-\frac{1}{2}}}\left(\overline{q^n_j} - \overline{q^n_{j-1}} \right) \right], \tag{3.68}$$

that is

$$\begin{aligned}\overline{(\Delta\alpha\Delta)_j^n} =& \frac{1}{\Delta x^2}\left\{\left[\alpha_{j+\frac{1}{2}}^n + \frac{\Delta t}{2}\partial_t\alpha_{j+\frac{1}{2}}^n\right]\left[q_{j+1}^n - q_j^n + \frac{\Delta t}{2}\left(-\lambda\left(\Delta_{j+1}^n - \Delta_j^n\right)\right.\right.\right.\\ &\left.\left.\left. + \ (\Delta\alpha\Delta)_{j+1}^n - (\Delta\alpha\Delta)_j^n + \beta\left(q_{j+1}^n - q_j^n\right)\right)\right]\\ &+ \left[\alpha_{j-\frac{1}{2}}^n + \frac{\Delta t}{2}\partial_t\alpha_{j-\frac{1}{2}}^n\right]\left[q_{j-1}^n - q_j^n + \frac{\Delta t}{2}\left(-\lambda\left(\Delta_{j-1}^n - \Delta_j^n\right)\right.\right.\\ &\left.\left. + \ (\Delta\alpha\Delta)_{j-1}^n - (\Delta\alpha\Delta)_j^n + \beta\left(q_{j-1}^n - q_j^n\right)\right)\right]\Bigg\},\end{aligned} \tag{3.69}$$

where the time derivative of the viscous coefficient can be computed as

$$\partial_t\alpha_{j+\frac{1}{2}}^n \approx \frac{1}{2}\left(\frac{\alpha_{j+1}^n - \alpha_{j+1}^{n-1}}{\Delta t} + \frac{\alpha_j^n - \alpha_j^{n-1}}{\Delta t}\right). \tag{3.70}$$

If α is a function depending on conservative variables (which would be the case, for example, of the viscous term for turbulent Navier-Stokes equations), we can also apply Cauchy-Kovalevskaya procedure.

Step 3.2. Numerical source

Lumping together the contributions of the reactive and diffusion terms we get a numerical source term as follows

$$s_j^n = \beta\overline{q_j^n} = \beta\left[q_j^n + \frac{\Delta t}{2}\left(-\lambda\Delta_j^n + (\Delta\alpha\Delta)_j^n + \beta q_j^n\right)\right]. \tag{3.71}$$

Gathering (3.65), (3.69) and (3.71), the numerical scheme for the advection-diffusion-reaction equation, with $\lambda > 0$, reads

$$\begin{aligned}q_j^{n+1} =& q_j^n - \frac{\lambda\Delta t}{\Delta x}\left\{q_j^n + \frac{1}{2}\Delta x\Delta_j^n + \frac{\Delta t}{2}\left[-\lambda\Delta_j^n + \beta\left(q_j^n + \frac{1}{2}\Delta x\Delta_j^n\right) + (\Delta\alpha\Delta)_j^n\right]\right.\\ &\left. - \ q_{j-1}^n - \frac{1}{2}\Delta x\Delta_{j-1}^n - \frac{\Delta t}{2}\left[-\lambda\Delta_{j-1}^n + \beta\left(q_{j-1}^n + \frac{1}{2}\Delta x\Delta_{j-1}^n\right) + (\Delta\alpha\Delta)_{j-1}^n\right]\right\}\\ &+ \frac{\Delta t}{\Delta x^2}\left\{\left[\alpha_{j+\frac{1}{2}}^n + \frac{\Delta t}{2}\partial_t\alpha_{j+\frac{1}{2}}^n\right]\left[q_{j+1}^n - q_j^n + \frac{\Delta t}{2}\left(-\lambda\left(\Delta_{j+1}^n - \Delta_j^n\right)\right.\right.\right.\\ &\left.\left.\left. + \ (\Delta\alpha\Delta)_{j+1}^n - (\Delta\alpha\Delta)_j^n + \beta\left(q_{j+1}^n - q_j^n\right)\right)\right]\\ &+ \left[\alpha_{j-\frac{1}{2}}^n + \frac{\Delta t}{2}\partial_t\alpha_{j-\frac{1}{2}}^n\right]\left[q_{j-1}^n - q_j^n + \frac{\Delta t}{2}\left(-\lambda\left(\Delta_{j-1}^n - \Delta_j^n\right)\right.\right.\\ &\left.\left. + \ (\Delta\alpha\Delta)_{j-1}^n - (\Delta\alpha\Delta)_j^n + \beta\left(q_{j-1}^n - q_j^n\right)\right)\right]\Bigg\}\end{aligned}$$

$$+\beta\Delta t\left[q_j^n+\frac{\Delta t}{2}\left(-\lambda\Delta_j^n+(\Delta\alpha\Delta)_j^n+\beta q_j^n\right)\right]. \tag{3.72}$$

Finally, taking into account the centred approach of the slopes, (3.47) and (3.64), one obtains

$$\begin{aligned}
q_j^{n+1} =& q_j^n - c\left\{\frac{2+r}{2}\left(q_j^n-q_{j-1}^n\right)+\frac{2-2c+r}{8}\left(q_{j+1}^n-q_j^n-q_{j-1}^n+q_{j-2}^n\right)\right.\\
&\left.+\frac{\Delta t}{2\Delta x^2}\left[\alpha_{j+\frac12}^n\left(q_{j+1}^n-q_j^n\right)-2\alpha_{j-\frac12}^n\left(q_j^n-q_{j-1}^n\right)+\alpha_{j-\frac32}^n\left(q_{j-1}^n-q_{j-2}^n\right)\right]\right\}\\
&+\frac{\Delta t}{\Delta x^2}\left\{\left[\alpha_{j+\frac12}^n+\frac{\Delta t}{2}\partial_t\alpha_{j+\frac12}^n\right]\left[\frac{2+r}{2}\left(q_{j+1}^n-q_j^n\right)-\frac{c}{4}\left(q_{j+2}^n-q_{j+1}^n\right.\right.\right.\\
&\left.-\ q_j^n+q_{j-1}^n\right)+\frac{\Delta t}{2\Delta x^2}\left(\alpha_{j+\frac32}^n\left(q_{j+2}^n-q_{j+1}^n\right)-2\alpha_{j+\frac12}^n\left(q_{j+1}^n-q_j^n\right)\right.\\
&\left.+\ \alpha_{j-\frac12}^n\left(q_j^n-q_{j-1}^n\right)\right)\Big]+\left[\alpha_{j-\frac12}^n+\frac{\Delta t}{2}\partial_t\alpha_{j-\frac12}^n\right]\left[\frac{2+r}{2}\left(q_{j-1}^n-q_j^n\right)\right.\\
&-\ \frac{c}{4}\left(q_j^n-q_{j-2}^n-q_{j+1}^n+q_{j-1}^n\right)+\frac{\Delta t}{2\Delta x^2}\left[2\alpha_{j-\frac12}^n\left(q_j^n-q_{j-1}^n\right)\right.\\
&\left.\left.\left.-\ \alpha_{j-\frac32}^n\left(q_{j-1}^n-q_{j-2}^n\right)-\alpha_{j+\frac12}^n\left(q_{j+1}^n-q_j^n\right)\right]\right]\right\}\\
&+r\left\{q_j^n+\left[-\frac{c}{4}\left(q_{j+1}^n-q_{j-1}^n\right)+\frac{\Delta t}{2\Delta x^2}\left[\alpha_{j+\frac12}^n\left(q_{j+1}^n-q_j^n\right)\right.\right.\right.\\
&\left.\left.\left.-\ \alpha_{j-\frac12}^n\left(q_j^n-q_{j-1}^n\right)\right]+\frac{r}{2}q_j^n\right]\right\}
\end{aligned} \tag{3.73}$$

where $r=\beta\Delta t$ is called reaction number.

Remark 3.4.3 (Constant diffusion coefficient). If we consider a constant diffusion coefficient and denote $\alpha\Delta_j^{(2)}=(\Delta\alpha\Delta)_j$, scheme (3.72) reads

$$\begin{aligned}
q_j^{n+1} =& q_j^n-\frac{\lambda\Delta t}{\Delta x}\left\{q_j^n+\frac12\Delta x\Delta_j^n+\frac{\Delta t}{2}\left[-\lambda\Delta_j^n+\beta\left(q_j^n+\frac12\Delta x\Delta_j^n\right)+\alpha\Delta_j^{(2)\,n}\right]\right.\\
&\left.-\ q_{j-1}^n+\frac12\Delta x\Delta_{j-1}^n-\frac{\Delta t}{2}\left[-\lambda\Delta_{j-1}^n+\beta\left(q_{j-1}^n-\frac12\Delta x\Delta_{j-1}^n\right)+\alpha\Delta_{j-1}^{(2)\,n}\right]\right\}\\
&+\frac{\alpha\Delta t}{\Delta x^2}\left\{\left(q_{j+1}^n-2q_j^n+q_{j-1}^n\right)+\frac{\Delta t}{2}\left[-\lambda\left(\Delta_{j+1}^n-2\Delta_j^n+\Delta_{j-1}^n\right)\right.\right.\\
&\left.\left.+\ \alpha\left(\Delta_{j+1}^{(2)\,n}-2\Delta_j^{(2)\,n}+\Delta_{j-1}^{(2)\,n}\right)+\beta\left(q_{j+1}^n-2q_j^n+q_{j-1}^n\right)\right]\right\}\\
&+\beta\Delta t\left[q_j^n+\frac{\Delta t}{2}\left(-\lambda\Delta_j^n+\alpha\Delta_j^{(2)\,n}+\beta q_j^n\right)\right].
\end{aligned} \tag{3.74}$$

Hence, the scheme for the advection-diffusion-reaction equation with constant diffusion

coefficient becomes

$$\begin{aligned} q_j^{n+1} =& q_j^n - c\left[\frac{2+r}{2}\left(q_j^n - q_{j-1}^n\right) + \frac{2-2c+r}{8}\left(q_{j+1}^n - q_{j-1}^n - q_j^n + q_{j-2}^n\right)\right. \\ &\left. + \frac{d}{2}\left(q_{j+1}^n - 3q_j^n + 3q_{j-1}^n - q_{j-2}^n\right)\right] \\ &+ d\left[q_{j+1}^n - 2q_j^n + q_{j-1}^n - \frac{c}{4}\left(q_{j+2}^n - 2q_{j+1}^n + 2q_{j-1}^n - q_{j-2}^n\right)\right. \\ &\left. + \frac{d}{2}\left(q_{j+2}^n - 4q_{j+1}^n + 6q_j^n - 4q_{j-1}^n + q_{j-2}^n\right) + \frac{r}{2}\left(q_{j+1}^n - 2q_j^n + q_{j-1}^n\right)\right] \\ &+ r\left[q_j^n - \frac{c}{4}\left(q_{j+1}^n - q_{j-1}^n\right) + \frac{d}{2}\left(q_{j+1}^n - 2q_j^n + q_{j-1}^n\right) + \frac{r}{2}q_j^n\right] \end{aligned} \tag{3.75}$$

where $d = \dfrac{\alpha\Delta t}{\Delta x^2}$.

Remark 3.4.4 (Advection-reaction equation). Assuming zero diffusivity, the scheme for the linear advection-reaction equation is recovered from (3.72),

$$\begin{aligned} q_j^{n+1} =& q_j^n - \frac{\lambda\Delta t}{\Delta x}\left\{q_j^n + \frac{1}{2}\Delta x\Delta_j^n + \frac{\Delta t}{2}\left[-\lambda\Delta_j^n + \beta\left(q_j^n + \frac{1}{2}\Delta x\Delta_j^n\right)\right]\right. \\ &\left. - q_{j-1}^n + \frac{1}{2}\Delta x\Delta_{j-1}^n - \frac{\Delta t}{2}\left[-\lambda\Delta_{j-1}^n + \beta\left(q_{j-1}^n - \frac{1}{2}\Delta x\Delta_{j-1}^n\right)\right]\right\} \\ &+ \beta\Delta t\left[q_j^n + \frac{\Delta t}{2}\left(-\lambda\Delta_j^n + \beta q_j^n\right)\right]. \end{aligned} \tag{3.76}$$

Furthermore, using centred slopes we get

$$\begin{aligned} q_j^{n+1} =& q_j^n - c\left[\frac{2+r}{2}\left(q_j^n - q_{j-1}^n\right) + \frac{2-2c+r}{8}\left(q_{j+1}^n - q_j^n - q_{j-1}^n + q_{j-2}^n\right)\right] \\ &+ r\left[q_j^n - \frac{c}{4}\left(q_{j+1}^n - q_{j-1}^n\right) + \frac{r}{2}q_j^n\right]. \end{aligned} \tag{3.77}$$

Remark 3.4.5. In case the reconstruction done in Step 1 is performed with constant polynomials and the half in time evolution of the variables given by the Taylor series expansion is neglected, the resulting scheme reduces to

$$q_j^{n+1} = q_j^n - c\left(q_j^n - q_{j-1}^n\right) - \frac{\Delta t}{\Delta x^2}\left[\alpha_{j+\frac{1}{2}}^n\left(q_{j+1}^n - q_j^n\right) + \alpha_{j-\frac{1}{2}}^n\left(q_{j-1}^n - q_j^n\right)\right] + rq_j^n \tag{3.78}$$

which is a first-order in time and space scheme for the advection-diffusion-reaction equation (3.1).

Remark 3.4.6 (Linear advection equation). Neglecting the source term ADER scheme for the linear advection equation is derived:

$$q_j^{n+1} = q_j^n - c\left[\frac{2+r}{2}\left(q_j^n - q_{j-1}^n\right) + \frac{2-2c}{8}\left(q_{j+1}^n - q_j^n - q_{j-1}^n + q_{j-2}^n\right)\right]. \tag{3.79}$$

3.5 MUSCL-Hancock

The MUSCL-Hancock method, originally credited to Hancock in [vL97], is extended here to account for the source and diffusion terms. The extension is motivated by the ADER framework introduced earlier. First recall that the MUSCL-Hancock method for the homogeneous linear advection equation has the following steps:

Step 1. Data reconstruction.

A first-degree polynomial for a cell C_j is used, namely

$$p_j(x) = q_j^n + \Delta_j^n (x - x_j) \tag{3.80}$$

with Δ_j^n the centred slope defined in (3.47).

Step 2. Computation of boundary extrapolated values.

Cell boundary values are computed by simply evaluating the polynomials appropriately

$$q_j^{n\,L} = p_j(x_{j-\frac{1}{2}}) = q_j^n - \frac{1}{2}\Delta x \Delta_j^n, \tag{3.81}$$

$$q_j^{n\,R} = p_j(x_{j+\frac{1}{2}}) = q_j^n + \frac{1}{2}\Delta x \Delta_j^n. \tag{3.82}$$

Step 3. Evolution of boundary extrapolated values.

Boundary-extrapolated values are evolved by half a time step,

$$\overline{q_j^{n\,R}} = q_j^{n\,R} - \frac{\Delta t}{2\Delta x}\left(f\left(q_j^{n\,R}\right) - f\left(q_j^{n\,L}\right)\right), \tag{3.83}$$

$$\overline{q_j^{n\,L}} = q_j^{n\,L} - \frac{\Delta t}{2\Delta x}\left(f\left(q_j^{n\,R}\right) - f\left(q_j^{n\,L}\right)\right). \tag{3.84}$$

Step 4. Solution of the Riemann problem and numerical flux.

The evolved boundary-extrapolated values are used to define a classical Riemann problem at each intercell boundary,

$$\begin{cases} \partial_t q\,(x,t) + \lambda \partial_x q\,(x,t) = 0, \\ q(x,0) = \begin{cases} \overline{q_j^{n\,R}}, & \text{if } x < 0, \\ \overline{q_{j+1}^{n\,L}}, & \text{if } x > 0, \end{cases} \end{cases} \tag{3.85}$$

the solution of which is

$$q(x,t) = \begin{cases} \overline{q_j^{n\,R}}, & \text{if } \dfrac{x}{t} < \lambda, \\ \overline{q_{j+1}^{n\,L}}, & \text{if } \dfrac{x}{t} > \lambda. \end{cases} \tag{3.86}$$

Hence, the sought intercell flux is given by

$$f_{j+\frac{1}{2}}^{n\,MH} = \begin{cases} \lambda\overline{q_j^{n\,R}} = \lambda\left(q_j^n + \dfrac{1-c}{2}\Delta x\Delta_j^n\right), & \text{if } \lambda > 0, \\ \lambda\overline{q_{j+1}^{n\,L}} = \lambda\left(q_{j+1}^n - \dfrac{1+c}{2}\Delta x\Delta_{j+1}^n\right), & \text{if } \lambda < 0. \end{cases} \tag{3.87}$$

Note that if no reconstruction is performed, the MUSCL-Hancock method reduces to the Godunov first-order method, with the particular numerical flux employed in the last step.

By choosing centred slopes, as already done for ADER, and assuming $\lambda > 0$ (the discussion of the case $\lambda < 0$ is analogous) we obtain the MUSCL-Hancock scheme for the linear advection equation:

$$q_j^{n+1} = q_j^n - c\left[q_j^n - q_{j-1}^n + \frac{1-c}{4}\left(q_{j+1}^n - q_j^n - q_{j-1}^n + q_{j-2}^n\right)\right]. \tag{3.88}$$

3.5.1 Source and diffusion terms

The inclusion of reaction and diffusion terms is accomplished by modifying Step 3, in which such terms at the half time are added to the evolution of boundary extrapolated values. Thus we obtain:

$$\begin{aligned} \overline{q_j^{n\,R}} =& q_j^{n\,R} - \frac{\Delta t}{2}\left\{\frac{1}{\Delta x}\left[f\left(q_j^{n\,R}\right) - f\left(q_j^{n\,L}\right)\right]\right. \\ & \left. - \frac{1}{\Delta x^2} g\left((\alpha\Delta q)_j^{n\,R}, (\alpha\Delta q)_j^{n\,L}\right) - s\left(q_j^{n\,R}\right)\right\}, \end{aligned} \tag{3.89}$$

$$\begin{aligned} \overline{q_{j+1}^{n\,L}} =& q_{j+1}^{n\,L} - \frac{\Delta t}{2}\left\{\frac{1}{\Delta x}\left[f\left(q_{j+1}^{n\,R}\right) - f\left(q_{j+1}^{n\,L}\right)\right]\right. \\ & \left. - \frac{1}{\Delta x^2} g\left((\alpha\Delta q)_{j+1}^{n\,R}, (\alpha\Delta q)_{j+1}^{n\,L}\right) - s\left(q_{j+1}^{n\,L}\right)\right\}, \end{aligned} \tag{3.90}$$

where

$$\begin{aligned} (\alpha\Delta q)_j^{n\,R} &= \alpha_{j+\frac{1}{2}}^n\left(q_{j+1}^n - q_j^n\right), \\ (\alpha\Delta q)_j^{n\,L} &= \alpha_{j-\frac{1}{2}}^n\left(q_j^n - q_{j-1}^n\right), \\ g\left((\alpha\Delta q)_j^{n\,R}, (\alpha\Delta q)_j^{n\,L}\right) &= (\alpha\Delta q)_j^{n\,R} - (\alpha\Delta q)_j^{n\,L}. \end{aligned}$$

The final step is as before, that is, the numerical flux is computed by solving the Riemann problem for the linear advection equation with evolved boundary-extrapolated values as initial conditions. Just as ADER, the numerical flux includes the contribution due to diffusion and source terms. Additional contributions to the scheme resulting from diffusion and reaction are accounted for by following the ADER approach introduced in Section 3.4.

Remark 3.5.1. The schemes obtained for the advection-diffusion-reaction equation (3.1), constructed from the ADER and MUSCL-Hancock approaches, are algebraically identical.

3.6 LADER methodology

ADER methodology was successfully extended in Section 3.4 to solve advection-diffusion-reaction equations. Despite this method would be easily programmed for the one dimensional code, the computation of the fluxes focusing on a particular finite volume at each time is not suitable for the mesh structure we will have in the three-dimensional code VolFEM3D. In this case, we would like to take profit from the loop on the faces of the finite volumes and reduce the computational cost. To do that, LADER method, which preserves the stability and the accuracy of the aforementioned ADER methodology, was developed. Three relevant issues must be taken into account:

1. The advection term depends on the diffusion term. That is, within the computation of the flux we will use Cauchy-Kovalevskaya procedure to obtain evolved values for the variables which contain information from both terms.

2. The evolved variables obtained for computing the diffusion term neglect the presence of the advection term.

3. As a consecuence of items 1 and 2, advection and diffusion terms need to be computed using the proper evolved variables, which will be different for each of them.

The proposed method includes the following steps:

Step 1. Polynomial reconstruction.

We consider a reconstruction of the data in terms of piecewise first-degree polynomials of the form

$$p_j(x) = \begin{cases} p_{j\,L}(x) = q_j^n + \Delta_{j\,L}^n (x - x_j), & \text{if } x \in \left(x_{j-\frac{1}{2}}, x_j\right], \\ \\ p_{j\,R}(x) = q_j^n + \Delta_{j\,R}^n (x - x_j), & \text{if } x \in \left[x_j, x_{j+\frac{1}{2}}\right), \end{cases} \tag{3.91}$$

where $\Delta_{j\,L}^n$, $\Delta_{j\,R}^n$ denote the approximations of the spatial derivatives of $q(x,t)$ at time t^n related to two auxiliary elements of volume $\mathcal{C}_j = \left[x_{j-\frac{1}{2}}, x_{j+\frac{1}{2}}\right]$:

$$T_{j-1i\,L} = [x_j, x_{j+1}], \qquad T_{ji+1\,R} = [x_{j-1}, x_j] \tag{3.92}$$

(see Figure 3.3).

To avoid the spurious oscillations generated by the linearity of the scheme, an ENO approach can be considered. Thus, the slopes involved in $p_{j\,L}$ and $p_{j\,R}$ are adaptively chosen between $\Delta_{j\,L}^n$ and $\Delta_{j\,R}^n$.

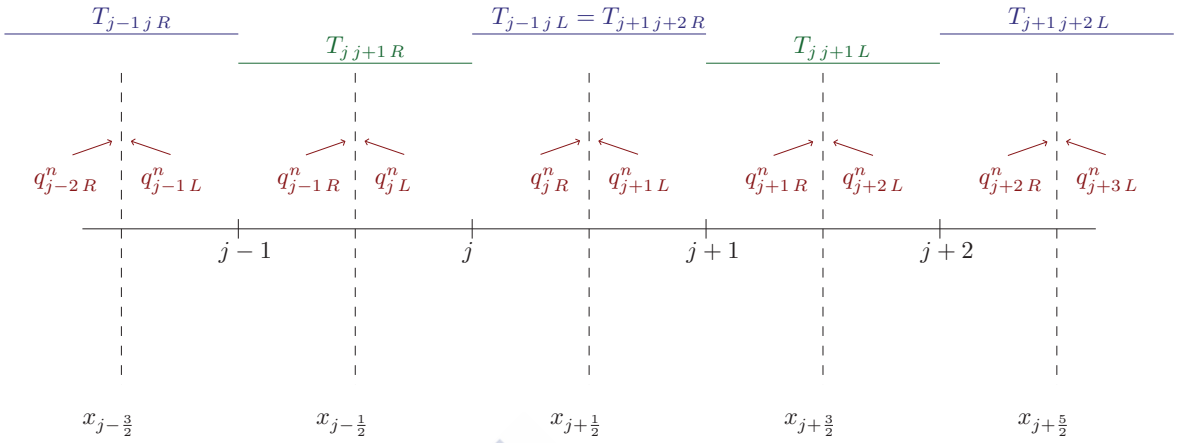

Figure 3.3: Mesh and nomenclature.

Step 2. Solution of the generalized Riemann problem.

$$\begin{cases} \partial_t q\,(x,t) + \lambda \partial_x q\,(x,t) = \partial_x\left(\alpha \partial_x q\right)(x,t) + \beta q\,(x,t)\,, \\ q(x,0) = \begin{cases} p_{j\,R}(x), & \text{if } x < 0, \\ p_{j+1\,L}(x), & \text{if } x > 0. \end{cases} \end{cases} \tag{3.93}$$

Step 3. Diffusion and reaction terms.

These terms are computed by approximating the integrals by the mid-point rule in both space and time.

The solution of the GRP at the interface $x_{j+\frac{1}{2}}$, set in Step 2, is expressed as a Taylor series expansion in time, namely,

$$\overline{q^n_{j+\frac{1}{2}}} = q(0,0_+) + \tau \partial_t q(0,0_+). \tag{3.94}$$

The first term of the above equation is computed as the solution of the classical Riemann problem

$$\begin{cases} \partial_t q\,(x,t) + \lambda \partial_x q\,(x,t) = 0, \\ q(x,0) = \begin{cases} q^n_{j\,R}, & \text{if } x < 0, \\ q^n_{j+1\,L}, & \text{if } x > 0, \end{cases} \end{cases} \tag{3.95}$$

where

$$q^n_{j\,R} = q^n_j + \frac{\Delta x}{2}\Delta^n_{j\,R} = q^n_j + \frac{q^n_j - q^n_{j-1}}{2} = \frac{1}{2}\left(3q^n_j - q^n_{j-1}\right), \tag{3.96}$$

$$q^n_{j+1\,L} = q^n_{j+1} - \frac{\Delta x}{2}\Delta^n_{j+1\,L} = q^n_{j+1} - \frac{q^n_{j+2} - q^n_{j+1}}{2} = \frac{1}{2}\left(3q^n_{j+1} - q^n_{j+2}\right). \tag{3.97}$$

Then, the sought solution is

$$q\left(0, 0_+\right) = \begin{cases} q^n_{j\,R}, & \text{if } \lambda > 0, \\ q^n_{j+1\,L}, & \text{if } \lambda < 0. \end{cases}$$

The second term is computed following the Cauchy-Kovalevskaya procedure which allows us to express the time derivative of the conservative variable as a combination of the spatial derivatives,

$$\partial_t q(x,t) = -\lambda \partial_x q(x,t) + \partial_x\left(\alpha \partial_x q\right)(x,t) + \beta q\left(x,t\right), \tag{3.98}$$

so,

$$\overline{q^n_{j+\frac{1}{2}}} = q(0,0_+) + \tau\left[-\lambda \partial_x q(0,0_+) + \partial_x\left(\alpha \partial_x q\right)(0,0_+) + \beta q(0,0_+)\right]. \tag{3.99}$$

From now on, we will focus on the scheme for $\lambda > 0$ (the case $\lambda < 0$ is analogous). Approximating

$$\partial_x q(0,0_+) = \Delta^n_{j+\frac{1}{2}} \approx \frac{1}{\Delta x}\left(q^n_{j+1} - q^n_j\right), \tag{3.100}$$

$$\partial_x\left(\alpha \partial_x q\right)(0,0_+) = \left(\Delta\alpha\Delta\right)^n_{j+\frac{1}{2}} \approx \frac{1}{\Delta x^2}\left[\alpha^n_{j+1}\left(q^n_{j+2} - q^n_{j+1}\right) - \alpha^n_j\left(q^n_j - q^n_{j-1}\right)\right] \tag{3.101}$$

and performing exact integration, the numerical flux becomes

$$\begin{aligned} f^n_{j+\frac{1}{2}} &= \lambda\overline{q^n_{j+\frac{1}{2}}} = \lambda\left\{q^n_{j\,R} + \frac{\Delta t}{2}\left[-\lambda\Delta^n_{j+\frac{1}{2}} + \left(\Delta\alpha\Delta\right)^n_{j+\frac{1}{2}} + \beta q^n_j\right]\right\} \\ &= \lambda\left\{q^n_j + \frac{1}{2}\left(q^n_j - q^n_{j-1}\right) - \frac{\lambda\Delta t}{2\Delta x}\left(q^n_{j+1} - q^n_j\right)\right. \\ &\quad \left. + \frac{\Delta t}{2\Delta x^2}\left[\alpha^n_{j+1}\left(q^n_{j+2} - q^n_{j+1}\right) - \alpha^n_j\left(q^n_j - q^n_{j-1}\right)\right] + \beta\frac{\Delta t}{2}q^n_j\right\}. \end{aligned} \tag{3.102}$$

For the diffusion term computation we build new evolved variables depending on the diffusion and reaction terms:

$$\begin{aligned} \overline{\left(\Delta\alpha\Delta\right)^n_j} &= \frac{\overline{\alpha^n_{j+\frac{1}{2}}}\,\overline{\Delta^n_{j+\frac{1}{2}}} - \overline{\alpha^n_{j-\frac{1}{2}}}\,\overline{\Delta^n_{j-\frac{1}{2}}}}{\Delta x} \\ &= \frac{1}{\Delta x^2}\left[\overline{\alpha^n_{j+\frac{1}{2}}}\left(\overline{q^n_{j+1}} - \overline{q^n_j}\right) - \overline{\alpha^n_{j-\frac{1}{2}}}\left(\overline{q^n_j} - \overline{q^n_{j-1}}\right)\right] \\ &= \frac{1}{\Delta x^2}\left\{\left[\alpha^n_{j+\frac{1}{2}} + \frac{\Delta t}{2}\partial_t\alpha^n_{j+\frac{1}{2}}\right]\left[q^n_{j+1} - q^n_j\right.\right. \\ &\quad \left.\left. + \frac{\Delta t}{2}\left[\left(\Delta\alpha\Delta\right)^n_{j+1} - \left(\Delta\alpha\Delta\right)^n_j + \beta\left(q^n_{j+1} - q^n_j\right)\right]\right] \end{aligned}$$

$$+\left[\alpha^n_{j-\frac{1}{2}}+\frac{\Delta t}{2}\partial_t\alpha^n_{j-\frac{1}{2}}\right]\left[q^n_{j-1}-q^n_j\right.$$
$$\left.+\frac{\Delta t}{2}\left[(\Delta\alpha\Delta)^n_{j-1}-(\Delta\alpha\Delta)^n_j+\beta\left(q^n_{j-1}-q^n_j\right)\right]\right]\Bigg\}. \tag{3.103}$$

Within the above approximation centred slopes were considered (see equations (3.47) and (3.64)). Moreover, the partial derivatives of the diffusion coefficient, $\partial_t\alpha^n_{j+\frac{1}{2}}$ and $\partial_t\alpha^n_{j-\frac{1}{2}}$, were computed following (3.70). The reaction term is calculated like for ADER scheme,

$$\beta\overline{q^n_j}=\beta\left[q^n_j+\frac{\Delta t}{2}\left(-\lambda\Delta^n_j+(\Delta\alpha\Delta)^n_j+\beta q^n_j\right)\right]. \tag{3.104}$$

Finally, denoting $c=\dfrac{\lambda\Delta t}{\Delta x}$ the Courant number and $r=\beta\Delta t$ the reaction number, the finite volume scheme for the advection-diffusion-reaction equation results

$$\begin{aligned}
q^{n+1}_j=&q^n_j-c\Bigg\{q^n_j+\frac{1}{2}\left(q^n_j-q^n_{j-1}\right)-\frac{c}{2}\left(q^n_{j+1}-q^n_j\right)\\
&+\frac{\Delta t}{2\Delta x^2}\left[\alpha^n_{j+1}\left(q^n_{j+2}-q^n_{j+1}\right)-\alpha^n_j\left(q^n_j-q^n_{j-1}\right)\right]+\frac{r}{2}q^n_j\\
&-q^n_{j-1}-\frac{1}{2}\left(q^n_{j-1}-q^n_{j-2}\right)+\frac{c}{2}\left(q^n_j-q^n_{j-1}\right)\\
&-\frac{\Delta t}{2\Delta x^2}\left[\alpha^n_j\left(q^n_{j+1}-q^n_j\right)-\alpha^n_{j-1}\left(q^n_{j-1}-q^n_{j-2}\right)\right]-\frac{r}{2}q^n_{j-1}\Bigg\}\\
&+\frac{\Delta t}{\Delta x^2}\Bigg\{\left[\alpha^n_{j+\frac{1}{2}}+\frac{\Delta t}{2}\partial_t\alpha^n_{j+\frac{1}{2}}\right]\left[q^n_{j+1}-q^n_j\right.\\
&+\frac{\Delta t}{2\Delta x^2}\left(\alpha^n_{j+\frac{3}{2}}\left(q^n_{j+2}-q^n_{j+1}\right)-2\alpha^n_{j+\frac{1}{2}}\left(q^n_{j+1}-q^n_j\right)+\alpha^n_{j-\frac{1}{2}}\left(q^n_j-q^n_{j-1}\right)\right)\\
&\left.+\frac{r}{2}\left(q^n_{j+1}-q^n_j\right)\right]+\left[\alpha^n_{j-\frac{1}{2}}+\frac{\Delta t}{2}\partial_t\alpha^n_{j-\frac{1}{2}}\right]\left[q^n_{j-1}-q^n_j\right.\\
&+\frac{\Delta t}{2\Delta x^2}\left(-\alpha^n_{j+\frac{1}{2}}\left(q^n_{j+1}-q^n_j\right)+2\alpha^n_{j-\frac{1}{2}}\left(q^n_j-q^n_{j-1}\right)-\alpha^n_{j-\frac{3}{2}}\left(q^n_{j-1}-q^n_{j-2}\right)\right)\\
&\left.+\frac{r}{2}\left(q^n_{j-1}-q^n_j\right)\right]\Bigg\}+r\Bigg\{q^n_j-\frac{c}{4}\left(q^n_{j+1}-q^n_{j-1}\right)\\
&+\frac{\Delta t}{2\Delta x^2}\left[\alpha^n_{j+\frac{1}{2}}\left(q^n_{j+1}-q^n_j\right)-\alpha^n_{j-\frac{1}{2}}\left(q^n_j-q^n_{j-1}\right)\right]+\frac{r}{2}q^n_j\Bigg\}.
\end{aligned} \tag{3.105}$$

Remark 3.6.1 (Constant diffusion coefficient). The scheme for the advection-diffusion-reaction equation with constant diffusion coefficient reads

$$\begin{aligned}
q^{n+1}_j=&q^n_j-c\Bigg[q^n_j-q^n_{j-1}+\frac{1}{2}\left(q^n_j-2q^n_{j-1}+q^n_{j-2}\right)-\frac{c}{2}\left(q^n_{j+1}-2q^n_j+q^n_{j-1}\right)\\
&+\frac{d}{2}\left(q^n_{j+2}-2q^n_{j+1}+2q^n_{j-1}-q^n_{j-2}\right)+\frac{r}{2}\left(q^n_j-q^n_{j-1}\right)\Bigg]
\end{aligned}$$

$$
\begin{aligned}
&+ d\left[q_{j+1}^n - 2q_j^n + q_{j-1}^n + \frac{d}{2}\left(q_{j+2}^n - 4q_{j+1}^n + 6q_j^n - 4q_{j-1}^n + q_{j-2}^n\right)\right.\\
&\left.+ \frac{r}{2}\left(q_{j+1}^n - 2q_j^n + q_{j-1}^n\right)\right]\\
&+ r\left[q_j^n - \frac{c}{4}\left(q_{j+1}^n - q_{j-1}^n\right) + \frac{d}{2}\left(q_{j+1}^n - 2q_j^n + q_{j-1}^n\right) + \frac{r}{2}q_j^n\right], \qquad (3.106)
\end{aligned}
$$

where $d = \dfrac{\alpha\Delta t}{\Delta x^2}$.

Remark 3.6.2 (Advection-reaction equation). Assuming zero diffusivity we deduce the scheme for the linear advection-reaction equation

$$
\begin{aligned}
q_j^{n+1} =& q_j^n - c\left\{q_j^n - q_{j-1}^n + \frac{1}{2}\left(q_j^n - 2q_{j-1}^n + q_{j-2}^n\right) - \frac{c}{2}\left(q_{j+1}^n - 2q_j^n + q_{j-1}^n\right)\right.\\
&\left.+\frac{r}{2}\left(q_j^n - q_{j-1}^n\right)\right\} + r\left[q_j^n - \frac{c}{4}\left(q_{j+1}^n - q_{j-1}^n\right) + \frac{r}{2}q_j^n\right]. \qquad (3.107)
\end{aligned}
$$

Furthermore, neglecting also the source term the LADER scheme for the linear advection equation reduces to

$$
q_j^{n+1} = q_j^n - c\left[q_j^n - q_{j-1}^n + \frac{1}{2}\left(q_j^n - 2q_{j-1}^n + q_{j-2}^n\right) - \frac{c}{2}\left(q_{j+1}^n - 2q_j^n + q_{j-1}^n\right)\right]. \qquad (3.108)
$$

3.7 Advection-diffusion-reaction equation with variable advection coefficient

As we have already mentioned, the numerical analysis of high-order finite volume schemes is too complex in three dimensions. Consequently, we have set a scalar simplified problem, (3.1), which retains the main difficulties of incompressible Navier-Stokes equations. Nevertheless, the equations modelling compressible low Mach number flows entail a new challenge due to the time and space dependency of the density. This fact can be conveyed to the scalar equation by assuming a variable advection coefficient. Moreover, an arbitrary source term can be introduced. As a result we obtain the advection-diffusion-reaction equation with variable coefficients,

$$
\partial_t q(x,t) + \partial_x\left(\lambda q\right)(x,t) = \partial_x\left(\alpha\partial_x q\right)(x,t) + s(x,t). \qquad (3.109)
$$

To ease the theoretical analysis of advection equations with variable advection coefficient, we focus on the following scalar advection equation

$$
\partial_t q(x,t) + \partial_x\left(\lambda q\right)(x,t) = 0. \qquad (3.110)
$$

Two main issues must be taken into account with respect to the advection equation with constant coefficient:

- A new numerical viscosity related to the spatial derivative of $\lambda(x,t)$ should be included. The main difficulties introduced due to the time and space dependency of the advection coefficient have been put forward in [BLVC17a] for the multi-component Euler equations. In this thesis, we follow the methodology already proposed to solve the non-linear advection equation.
- To build a second-order in time and space scheme using LADER methodology, the extrapolation and the half in time evolution of $\lambda(x,t)$ need to be performed.

In what follows, we will further develop the points above.

3.7.1 Advection term with time and space dependent coefficient

The use of Rusanov scheme to approximate the numerical flux function may not work properly. Let us remark that Rusanov flux is divided into two terms:

$$\phi(q_j^n, q_{j+1}^n, \lambda_j^n, \lambda_{j+1}^n) = \frac{1}{2}\left(\lambda_j^n q_j^n + \lambda_{j+1}^n q_{j+1}^n\right) - \frac{1}{2}\alpha_{RS}\left(q_j^n, q_{j+1}^n, \lambda_j^n, \lambda_{j+1}^n\right)\left(q_{j+1}^n - q_j^n\right). \tag{3.111}$$

The first one corresponds to a centred approximation of the flux. The second one is supposed to introduce the numerical viscosity needed for the stability of the scheme. However, splitting the spatial derivative of the flux into two terms,

$$\partial_x\left(\lambda q\right)(x,t) = \lambda(x,t)\partial_x q(x,t) + q(x,t)\partial_x\lambda(x,t), \tag{3.112}$$

we notice that Rusanov flux only adds the artificial viscosity related to the first one. Therefore, spurious oscillations may be produced. To correct this lack of upwind, we propose to introduce a new artificial viscosity term, namely,

$$-\left[\partial_\lambda\left(\lambda q\right)\Delta\lambda\right]_{\Big|_{j+\frac{1}{2}}} \approx -\frac{1}{2}\text{sign}\left(\breve{\alpha}_{RS}\right) q_{j+\frac{1}{2}}^n\left(\lambda_{j+1}^n - \lambda_j^n\right) \tag{3.113}$$

with $\breve{\alpha}_{RS}$ the value of the eigenvalue used to compute α_{RS}. Then, the numerical flux on the boundary $x_{j+\frac{1}{2}}$ reads,

$$\begin{aligned}\phi(q_j^n, q_{j+1}^n, \lambda_j^n, \lambda_{j+1}^n) =& \frac{1}{2}\left(\lambda_j^n q_j^n + \lambda_{j+1}^n q_{j+1}^n\right) - \frac{1}{2}\alpha_{RS}\left(q_j^n, q_{j+1}^n, \lambda_j^n, \lambda_{j+1}^n\right)\left(q_{j+1}^n - q_j^n\right) \\ &- \frac{1}{2}\text{sign}\left(\breve{\alpha}_{RS}\left(q_j^n, q_{j+1}^n, \lambda_j^n, \lambda_{j+1}^n\right)\right) q_{j+\frac{1}{2}}^n\left(\lambda_{j+1}^n - \lambda_j^n\right).\end{aligned} \tag{3.114}$$

3.7.2 LADER scheme for the advection equation with time and space dependent advection coefficient

To attain a second-order of accuracy scheme for equation (3.110) we apply LADER methodology. Initially, the polynomial reconstruction is performed on the conservative variable obtaining the following extrapolated values at the neighbouring of the

boundaries of a cell C_j:

$$q^n_{j-1R} = q^n_j + \frac{1}{2}\left(q^n_{j-1} - q^n_{j-2}\right), \tag{3.115}$$

$$q^n_{jL} = q^n_j - \frac{1}{2}\left(q^n_{j+1} - q^n_j\right), \tag{3.116}$$

$$q^n_{jR} = q^n_j + \frac{1}{2}\left(q^n_j - q^n_{j-1}\right), \tag{3.117}$$

$$q^n_{j+1L} = q^n_j - \frac{1}{2}\left(q^n_{j+2} - q^n_{j+1}\right). \tag{3.118}$$

Next, the resolution of the generalized Riemann problem entails the computation of the half in time evolved values,

$$\overline{q^n_{j-1R}} = q^n_{j-1R} - \frac{\Delta t}{2\Delta x}\left(\lambda^n_j q^n_j - \lambda^n_{j-1} q^n_{j-1}\right), \tag{3.119}$$

$$\overline{q^n_{jL}} = q^n_{jL} - \frac{\Delta t}{2\Delta x}\left(\lambda^n_j q^n_j - \lambda^n_{j-1} q^n_{j-1}\right), \tag{3.120}$$

$$\overline{q^n_{jR}} = q^n_{jR} - \frac{\Delta t}{2\Delta x}\left(\lambda^n_{j+1} q^n_{j+1} - \lambda^n_j q^n_j\right), \tag{3.121}$$

$$\overline{q^n_{j+1L}} = q^n_{j+1L} - \frac{\Delta t}{2\Delta x}\left(\lambda^n_{j+1} q^n_{j+1} - \lambda^n_j q^n_j\right). \tag{3.122}$$

Furthermore, extrapolating the advection coefficient and calculating its half in time evolution, we get

$$\overline{\lambda^n_{j-1R}} = \lambda^n_{j-1R} + \frac{\Delta t}{2}\partial_t \lambda^n_{j-\frac{1}{2}} = \lambda^n_j + \frac{1}{2}\left(\lambda^n_{j-1} - \lambda^n_{j-2}\right) + \frac{\Delta t}{2}\partial_t \lambda^n_{j-\frac{1}{2}}, \tag{3.123}$$

$$\overline{\lambda^n_{jL}} = \lambda^n_{jL} + \frac{\Delta t}{2}\partial_t \lambda^n_{j-\frac{1}{2}} = \lambda^n_j - \frac{1}{2}\left(\lambda^n_{j+1} - \lambda^n_j\right) + \frac{\Delta t}{2}\partial_t \lambda^n_{j-\frac{1}{2}}, \tag{3.124}$$

$$\overline{\lambda^n_{jR}} = \lambda^n_{jR} + \frac{\Delta t}{2}\partial_t \lambda^n_{j+\frac{1}{2}} = \lambda^n_j + \frac{1}{2}\left(\lambda^n_j - \lambda^n_{j-1}\right) + \frac{\Delta t}{2}\partial_t \lambda^n_{j+\frac{1}{2}}, \tag{3.125}$$

$$\overline{\lambda^n_{j+1L}} = \lambda^n_{j+1L} + \frac{\Delta t}{2}\partial_t \lambda^n_{j+\frac{1}{2}} = \lambda^n_j - \frac{1}{2}\left(\lambda^n_{j+2} - \lambda^n_{j+1}\right) + \frac{\Delta t}{2}\partial_t \lambda^n_{j+\frac{1}{2}}. \tag{3.126}$$

Substituting (3.119)-(3.126) on the numerical flux function (3.114), LADER scheme for the advection equation, (3.110), reads

$$\begin{aligned} q^{n+1}_j = & q^n_j - \frac{\Delta t}{2\Delta x}\left\{\left[\left(\overline{\lambda^n_{jR}}\,\overline{q^n_{jR}} + \overline{\lambda^n_{j+1L}}\,\overline{q^n_{j+1L}}\right) - \overline{\alpha^n_{RS,\,i+\frac{1}{2}}}\left(\overline{q^n_{j+1L}} - \overline{q^n_{jR}}\right)\right.\right. \\ & \left. - \text{sign}\left(\breve{\overline{\alpha^n_{RS,\,i+\frac{1}{2}}}}\right)\overline{q^n_{j+\frac{1}{2}}}\left(\overline{\lambda^n_{j+1L}} - \overline{\lambda^n_{jR}}\right)\right] - \left[\left(\overline{\lambda^n_{j-1R}}\,\overline{q^n_{j-1R}} + \overline{\lambda^n_{jL}}\,\overline{q^n_{jL}}\right)\right. \\ & \left.\left. - \overline{\alpha^n_{RS,\,i-\frac{1}{2}}}\left(\overline{q^n_{jL}} - \overline{q^n_{j-1R}}\right) - \text{sign}\left(\breve{\overline{\alpha^n_{RS,\,i-\frac{1}{2}}}}\right)\overline{q^n_{j-\frac{1}{2}}}\left(\overline{\lambda^n_{jL}} - \overline{\lambda^n_{j-1R}}\right)\right]\right\} \end{aligned} \tag{3.127}$$

where

$$\overline{\alpha^n_{RS,\,i-\frac{1}{2}}} = \max\left\{\left|\overline{\lambda^n_{j-1R}}\right|, \left|\overline{\lambda^n_{jL}}\right|\right\},$$

$$\overline{\alpha^n_{RS,\,i+\frac{1}{2}}} = \max\left\{\left|\overline{\lambda^n_{jR}}\right|, \left|\overline{\lambda^n_{j+1L}}\right|\right\}.$$

3.7.3 LADER scheme for the advection-diffusion-reaction equation with time and space dependent advection coefficient

The construction of a numerical scheme to solve the advection-diffusion-reaction equation with time and space dependent advection and diffusion coefficients requires for a modification of the generalized Riemann problem to be solved. As a result, the approximation of the evolved variables (3.119)-(3.122) accounts for the diffusion and reaction terms,

$$\begin{aligned}
\overline{q^n_{j-1R}} =& q^n_{j-1R} - \frac{\Delta t}{2\Delta x}\left(\lambda^n_j q^n_j - \lambda^n_{j-1} q^n_{j-1}\right) \\
&+ \frac{\Delta t}{2\Delta x^2}\left[\alpha^n_j\left(q^n_{j+1} - q^n_j\right) - \alpha^n_{j-1}\left(q^n_{j-1} - q^n_{j-2}\right)\right] + \frac{\Delta t}{2} s^n_{j-\frac{1}{2}}, \qquad (3.128)\\
\overline{q^n_{jL}} =& q^n_{jL} - \frac{\Delta t}{2\Delta x}\left(\lambda^n_j q^n_j - \lambda^n_{j-1} q^n_{j-1}\right) \\
&+ \frac{\Delta t}{2\Delta x^2}\left[\alpha^n_j\left(q^n_{j+1} - q^n_j\right) - \alpha^n_{j-1}\left(q^n_{j-1} - q^n_{j-2}\right)\right] + \frac{\Delta t}{2} s^n_{j-\frac{1}{2}}, \qquad (3.129)\\
\overline{q^n_{jR}} =& q^n_{jR} - \frac{\Delta t}{2\Delta x}\left(\lambda^n_{j+1} q^n_{j+1} - \lambda^n_j q^n_j\right) \\
&+ \frac{\Delta t}{2\Delta x^2}\left[\alpha^n_{j+1}\left(q^n_{j+2} - q^n_{j+1}\right) - \alpha^n_j\left(q^n_j - q^n_{j-1}\right)\right] + \frac{\Delta t}{2} s^n_{j+\frac{1}{2}}, \qquad (3.130)\\
\overline{q^n_{j+1L}} =& q^n_{j+1L} - \frac{\Delta t}{2\Delta x}\left(\lambda^n_{j+1} q^n_{j+1} - \lambda^n_j q^n_j\right) \\
&+ \frac{\Delta t}{2\Delta x^2}\left[\alpha^n_{j+1}\left(q^n_{j+2} - q^n_{j+1}\right) - \alpha^n_j\left(q^n_j - q^n_{j-1}\right)\right] + \frac{\Delta t}{2} s^n_{j+\frac{1}{2}}, \qquad (3.131)
\end{aligned}$$

where $s^n_{j+\frac{1}{2}} = s\left(\frac{1}{2}(x_j + x_{j+1}), t^n\right)$, $s^n_{j-\frac{1}{2}} = s\left(\frac{1}{2}(x_{j-1} + x_j), t^n\right)$. These new approximations are substituted on the flux function (3.114) providing the expression of the numerical flux. Likewise in Section 3.6, the diffusion and reaction terms are computed by the mid-point rule. Finally, LADER scheme for equation (3.109) reads

$$\begin{aligned}
q^{n+1}_j =& q^n_j - \frac{\Delta t}{2\Delta x}\left\{\left[\left(\overline{\lambda^n_{jR} q^n_{jR}} + \overline{\lambda^n_{j+1L} q^n_{j+1L}}\right) - \overline{\alpha^n_{RS,\,i+\frac{1}{2}}}\left(\overline{q^n_{j+1L}} - \overline{q^n_{jR}}\right)\right.\right. \\
&\left. -\text{sign}\left(\overline{\alpha^n_{RS,\,i+\frac{1}{2}}}\right)\overline{q^n_{j+\frac{1}{2}}}\left(\overline{\lambda^n_{j+1L}} - \overline{\lambda^n_{jR}}\right)\right] - \left[\left(\overline{\lambda^n_{j-1R} q^n_{j-1R}} + \overline{\lambda^n_{jL} q^n_{jL}}\right)\right. \\
&\left.\left. -\overline{\alpha^n_{RS,\,i-\frac{1}{2}}}\left(\overline{q^n_{jL}} - \overline{q^n_{j-1R}}\right) - \text{sign}\left(\overline{\alpha^n_{RS,\,i-\frac{1}{2}}}\right)\overline{q^n_{j-\frac{1}{2}}}\left(\overline{\lambda^n_{jL}} - \overline{\lambda^n_{j-1R}}\right)\right]\right\} \\
&+ \frac{\Delta t}{\Delta x^2}\left\{\left[\alpha^n_{j+\frac{1}{2}} + \frac{\Delta t}{2}\partial_t \alpha^n_{j+\frac{1}{2}}\right]\left[q^n_{j+1} - q^n_j + \frac{\Delta t}{2\Delta x^2}\left(\alpha^n_{j+\frac{3}{2}}\left(q^n_{j+2} - q^n_{j+1}\right)\right.\right.\right. \\
&\left.\left. -2\alpha^n_{j+\frac{1}{2}}\left(q^n_{j+1} - q^n_j\right) + \alpha^n_{j-\frac{1}{2}}\left(q^n_j - q^n_{j-1}\right)\right) + \frac{\Delta t}{2}\left(s^n_{j+1} - s^n_j\right)\right] \\
&+ \left[\alpha^n_{j-\frac{1}{2}} + \frac{\Delta t}{2}\partial_t \alpha^n_{j-\frac{1}{2}}\right]\left[q^n_{j-1} - q^n_j + \frac{\Delta t}{2\Delta x^2}\left(-\alpha^n_{j+\frac{1}{2}}\left(q^n_{j+1} - q^n_j\right)\right.\right.
\end{aligned}$$

$$+2\alpha^n_{j-\frac{1}{2}}\left(q^n_j - q^n_{j-1}\right) - \alpha^n_{j-\frac{3}{2}}\left(q^n_{j-1} - q^n_{j-2}\right)\Big) + \frac{\Delta t}{2}\left(s^n_{j-1} - s^n_j\right)\Big]\Big\}$$
$$+ s_j^{n+\frac{1}{2}} \tag{3.132}$$

with $s^n_j = s\left(x_j, t^n\right)$ and $s_j^{n+\frac{1}{2}} = s\left(x_j, t^n + \frac{\Delta t}{2}\right)$.

Remark 3.7.1. In this section, we have focused on LADER methodology due to its advantages when adapting it to solve the three-dimensional Navier-Stokes equations. However, the extrapolation of ADER methodology to solve the advection-diffusion-reaction equation with variable advection and diffusion coefficients can be similarly performed.

USC
UNIVERSIDADE
DE SANTIAGO
DE COMPOSTELA

Chapter 4

Stability and accuracy

This chapter is intended to provide the stability and accuracy analysis of the schemes presented in Chapter 3.

Within the first section, a detailed linear stability analysis of the advection equation is performed for Kolgan and CVC Kolgan-type schemes. In Section 4.2, von Neumann stability analysis is conducted for ADER and LADER schemes considering the linear advection-diffusion-reaction equation. The accuracy analysis of the proposed schemes is accomplished in Section 4.4.

4.1 Stability analysis of Kolgan-type schemes

Stability analysis of linear models is done following von Neumann stability analysis procedure (see [CN96], [CFVN50], [Str04] and [VC15]). To investigate the stability of Kolgan scheme we start by applying von Neumann stability analysis to its second branch, (3.34).

Proposition 4.1.1. *Scheme* (3.34) *is unconditionally unstable in von Neumann sense.*

Proof. Let us consider the trial function

$$q_j^n = A^n e^{i\theta j}, \tag{4.1}$$

where $A \in \mathbb{C}$ represents an amplitude, i denotes the complex unity, and $\theta = P\Delta x$ is an angle with P the wave number in the x-direction. Then, (3.34) yields to

$$A^{n+1}e^{i\theta j} = A^n e^{i\theta j} - \frac{c}{2}\left(A^n e^{i\theta(j-2)} - 4A^n e^{i\theta(j-1)} + 3A^n e^{i\theta j}\right). \tag{4.2}$$

So that, the amplification factor is given by

$$\begin{aligned} A =& 1 - \frac{c}{2}\left(e^{-2i\theta} - 4e^{-i\theta} + 3\right) \\ =& 1 - \frac{c}{2}\left(\cos^2\theta - \sin^2\theta - 4\cos\theta + 3\right) + ic\left(\sin\theta\cos\theta - 2\sin\theta\right) \end{aligned} \tag{4.3}$$

and thus,

$$\begin{aligned}|A|^2 =& 3c^2\cos^2\theta - 2c + 4c\cos\theta + 5c^2 - 2c\cos\theta + 5c^2 - 2c\cos^2\theta - 8c^2\cos\theta + 1\\ =& (\cos\theta - 1)\left[c^2(3\cos\theta - 5) - c(\cos\theta - 1)\right] + 1.\end{aligned} \tag{4.4}$$

Since $\theta \in [-\pi, \pi]$, we can choose for any value of c a value of θ_c such that $\cos\theta_c = 1-\varepsilon$, $0 < \varepsilon \ll 1$. Then, we obtain

$$0 > c(\cos\theta_c - 1) = -\varepsilon c \tag{4.5}$$

and

$$0 > c^2(3\cos\theta_c - 5) = -2c^2 - 3\varepsilon c^2. \tag{4.6}$$

Substituting θ_c in the right-hand side of (4.4) and assuming $\varepsilon < c$, the following restriction holds:

$$\begin{aligned}|A|^2 &= (\cos\theta_c - 1)\left[c^2(3\cos\theta_c - 5) - c(\cos\theta_c - 1)\right] + 1\\ &= -\varepsilon\left[c^2(-2 - 3\varepsilon) + c\varepsilon\right] + 1 > 1.\end{aligned} \tag{4.7}$$

Therefore, we conclude that for any c there exists $\theta_c \in [-\pi, \pi]$ such that $|A| > 1$. □

We note that the usual method of analysis is not valid for the complete Kolgan scheme due to its variable coefficients. However, we can proof its stability by considering some inequalities.

Lemma 4.1.2. *For* $\dfrac{\Delta t}{\Delta x} \leq \dfrac{1}{2}$, *if* $\Delta^n_{j-1} \geq 0$ *then* $q^n_{j-1} \leq q^{n+1}_j \leq q^n_j$, *otherwise* $q^n_{j-1} \geq q^{n+1}_j \geq q^n_j$.

Proof. For easy of presentation, we will assume that $\Delta^n_{j-1} \geq 0$, $\Delta^n_{j-1} \leq 0$ can be done similarly. We prove the result for each branch of the scheme after another:

- Branch (3.30):

  As $\left|\Delta^n_{j-1}\right| \geq \left|\Delta^n_j\right|$ and $\Delta^n_{j-1} \geq 0$, then $\Delta^n_{j-1} \geq \Delta^n_j \geq -\Delta^n_{j-1}$. Hence, taking into account (3.30),

  $$q^{n+1}_j - q^n_j = -\frac{\lambda\Delta t}{2\Delta x}\left(\Delta^n_{j-1} + \Delta^n_j\right) \leq 0 \tag{4.8}$$

  and we conclude $q^{n+1}_j \leq q^n_j$. On the other hand, adding and subtracting q^n_{i-1} from (3.30) and considering $\dfrac{\lambda\Delta t}{\Delta x} \leq 1$, we get

  $$q^{n+1}_j - q^n_{j-1} = q^n_j - q^n_{j-1} - \frac{\lambda\Delta t}{2\Delta x}\left(\Delta^n_{j-1} + \Delta^n_j\right) \geq \left(1 - \frac{\lambda\Delta t}{\Delta x}\right)\Delta^n_{j-1} \geq 0 \tag{4.9}$$

  which implies that $q^{n+1}_j \geq q^n_{j-1}$.

- Branch (3.31):
  Since $\left|\Delta_{j-1}^n\right| \geq \left|\Delta_{j-2}^n\right|$ it is verified

$$q_j^{n+1} - q_j^n = \frac{\lambda\Delta t}{2\Delta x}\left(\Delta_{j-2}^n - 3\Delta_{j-1}^n\right) \leq 0 \tag{4.10}$$

  thus $q_j^{n+1} \leq q_j^n$. Assuming $\dfrac{\lambda\Delta t}{\Delta x} \leq \dfrac{1}{2}$, we obtain

$$q_j^{n+1} - q_{j-1}^n = \Delta_{j-1}^n + \frac{\lambda\Delta t}{2\Delta x}\left(\Delta_{j-2}^n - 3\Delta_{j-1}^n\right) \geq \left(1 - \frac{2\lambda\Delta t}{\Delta x}\right)\Delta_{j-1}^n \geq 0 \tag{4.11}$$

  so $q_j^{n+1} \geq q_{j-1}^n$.

- Branch (3.32):
  If $\dfrac{\lambda\Delta t}{\Delta x} \leq 1$, we can show that

$$q_j^{n+1} - q_j^n = -\frac{\lambda\Delta t}{\Delta x}\Delta_{j-1}^n \leq 0 \tag{4.12}$$

  and

$$q_j^{n+1} - q_{j-1}^n = \Delta_{j-1}^n - \frac{\lambda\Delta t}{\Delta x}\Delta_{j-1}^n \geq 0. \tag{4.13}$$

  Consequently, $q_{j-1}^n \leq q_j^{n+1} \leq q_j^n$.

- Branch (3.33):
  For $\left|\Delta_{j-1}^n\right| \geq \left|\Delta_j^n\right|$, $\left|\Delta_{j-1}^n\right| \geq \left|\Delta_{j-2}^n\right|$, $\Delta_{j-1}^n \geq 0$ and $\dfrac{\lambda\Delta t}{\Delta x} \leq \dfrac{1}{2}$, we have

$$q_j^{n+1} - q_j^n = \frac{\lambda\Delta t}{2\Delta x}\left(\Delta_{j-2}^n - 2\Delta_{j-1}^n - \Delta_j^n\right) \leq 0 \tag{4.14}$$

  and

$$q_j^{n+1} - q_{j-1}^n = \Delta_{j-1}^n + \frac{\lambda\Delta t}{2\Delta x}\left(\Delta_{j-2}^n - 2\Delta_{j-1}^n - \Delta_j^n\right) \geq \left(1 - \frac{2\lambda\Delta t}{\Delta x}\right)\Delta_{j-1}^n \geq 0. \tag{4.15}$$

  Hence, $q_{j-1}^n \leq q_j^{n+1} \leq q_j^n$.

□

Corollary 4.1.3. *Kolgan scheme is stable for* $\dfrac{\lambda\Delta t}{\Delta x} \leq \dfrac{1}{2}$.

Proof. We already know from the previous lemma that

$$\left|q_j^{n+1}\right| \leq \max\left\{\left|q_{j-1}^n\right|, \left|q_j^n\right|\right\} \leq \max_j\left\{\left|q_j^n\right|\right\}.$$

Therefore, assuming that there exists $M \in \mathbb{R}^+$ such that $\max_j \left\{\left|q_j^n\right|\right\} \leq M$, we deduce

$$\left|q_j^{n+1}\right| \leq \max_j \left\{\left|q_j^n\right|\right\} \leq M, \quad \forall j.$$

Thus,

$$\max_j \left\{\left|q_j^{n+1}\right|\right\} \leq M.$$

□

Corollary 4.1.4. *Kolgan scheme is monotone for* $\dfrac{\lambda \Delta t}{\Delta x} \leq \dfrac{1}{2}$.

Proof. Let us consider $\Delta_j^n \geq 0$ for all j. Then, from Lemma 4.1.2, we obtain

$$q_{j-1}^{n-1} \leq q_j^n \leq q_j^{n-1}, \qquad q_j^{n-1} \leq q_j^{n+1} \leq q_{j+1}^{n-1} \tag{4.16}$$

which leads to

$$q_j^n \leq q_j^{n+1}. \tag{4.17}$$

Analogously, if $\Delta_j^n \leq 0$ for all j,

$$q_{j-1}^{n-1} \geq q_j^n \geq q_j^{n-1}, \qquad q_j^{n-1} \geq q_j^{n+1} \geq q_{j+1}^{n-1} \tag{4.18}$$

We conclude

$$q_j^n \geq q_j^{n+1}. \tag{4.19}$$

□

4.1.1 CVC Kolgan stability analysis

Like for Kolgan scheme, we start by performing a von Neumann stability analysis of the non limited CVC Kolgan-type scheme, (3.36).

Proposition 4.1.5. *The CVC Kolgan-type scheme* (3.36) *is unconditionally unstable in von Neumann sense.*

Proof. Considering the trial function (4.1), we obtain

$$\begin{aligned} A^{n+1} e^{i\theta j} = A^n e^{i\theta j} - \frac{\lambda \Delta t}{2\Delta x} \Big(& \frac{1}{2} A^n e^{i\theta(j-2)} - 3A^n e^{i\theta(j-1)} + 3A^n e^{i\theta j} \\ & - A^n e^{i\theta(j+1)} + \frac{1}{2} A^n e^{i\theta(j+2)} \Big) \end{aligned} \tag{4.20}$$

thus,

$$\begin{aligned} A &= 1 - \frac{\lambda \Delta t}{2\Delta x} \left(\frac{1}{2} e^{-2i\theta} - 3e^{-i\theta} + 3 - e^{i\theta} + \frac{1}{2} e^{2i\theta} \right) \\ &= 1 - c \left(\cos\theta - 1\right)^2 + ci \sin\theta. \end{aligned} \tag{4.21}$$

This leads to

$$|A|^2 = 1 + c^2\left[(1-\cos\theta)^4 + \left(1-\cos^2\theta\right)\right] - 2c\,(1-\cos\theta)^2\,. \tag{4.22}$$

Assuming that the scheme is stable, then

$$c^2\left[(1-\cos\theta)^4 + \left(1-\cos^2\theta\right)\right] - 2c\,(1-\cos\theta)^2 \leq 0 \tag{4.23}$$

which is true if and only if

$$c \in \left[0, \frac{2\,(1-\cos\theta)^2}{(1-\cos\theta)^4 + (1-\cos^2\theta)}\right]. \tag{4.24}$$

However, as $\theta \in [-\pi, \pi]$ then a value for θ_c can be chosen such that θ_c is as near to zero as we want and, hence, we arrive to an inconsistency. □

Next, we analyse the stability properties of the complete CVC Kolgan-type scheme using inequalities. As we have seen in Corollary 4.1.3 for Kolgan scheme, stability is guaranteed if $\left|q_j^{n+1}\right| \leq \max_j\left\{\left|q_j^n\right|\right\}$. Thus, we will analyse the diverse options of the scheme:

- Option 1.

  Let us assume $\Delta_{j-1}^n > 0$ then, $\Delta_{j-2}^n > 0$, $\Delta_j^n > 0$, $\Delta_{j+1}^n > 0$, $\Delta_{j+2}^n > 0$. Furthermore, denoting $M = \sup_j\left\{\left|q_j^n\right|\right\}$, $k > 3$, and choosing $\epsilon > 0$, $q_{j-2}^n = -M$, $q_{j-1}^n = -M+\epsilon$, $q_j^n = -M+3\epsilon$, $q_{j+1}^n = -M+(k+3)\,\epsilon$ and $q_{j+2}^n = -M+2\,(k+3)\,\epsilon$, we obtain that

  - $\Delta_{j-2}^n = q_{j-1}^n - q_{j-2}^n = -M+\epsilon+M = \epsilon > 0$,
  - $\Delta_{j-1}^n = q_j^n - q_{j-1}^n = -M+3\epsilon+M-\varepsilon = 2\epsilon > 0$,
  - $\Delta_j^n = q_{j+1}^n - q_j^n = -M+(k+3)\,\epsilon+M-3\varepsilon = k\epsilon > 0$,
  - $\Delta_{j+1}^n = q_{j+2}^n - q_{j+1}^n = -M+2\,(k+3)\,\epsilon+M-(k+3)\,\varepsilon = (k+3)\,\epsilon > 0$,
  - $\Delta_{j-2}^n = \epsilon < 2\epsilon = \Delta_{j-1}^n$,
  - $\Delta_{j-1}^n = 2\epsilon < k\epsilon = \Delta_j^n$,
  - $\Delta_j^n = k\epsilon < (k+3)\,\epsilon = \Delta_{j+1}^n$.

  Thus, we fall into Option 1 and so,

$$\begin{aligned} q_j^{n+1} - q_{j-2}^n &= \Delta_{j-2}^n + \Delta_{j-1}^n - \frac{c}{4}\left(-\Delta_{j-2}^n + 4\Delta_{j-1}^n + \Delta_j^n\right) \\ &< 2\Delta_{j-1}^n - \frac{c}{4}\left(3\Delta_{j-1}^n + \Delta_j^n\right) \\ &< 2\Delta_{j-1}^n - \frac{c}{4}\Delta_j. \end{aligned} \tag{4.25}$$

  If $k > \frac{8}{c}$ then $2\Delta_{j-1}^n - \frac{c}{4}\Delta_j^n < 0$ and so, $q_j^{n+1} < q_{j-2}^n = -M$. Therefore, branch (3.37) of CVC Kolgan-type scheme obtained following Option 1 is unstable.

- Option 2.

  Considering $\Delta_{j-1}^n > 0$ (for $\Delta_{j-1}^n < 0$ the derivation is analogous) we get

  $$q_j^{n+1} - q_j^n = -\frac{c}{4}\left(-\Delta_{j-2}^n + 4\Delta_{j-1}^n + \Delta_j^n\right) < -\frac{c}{4}\left(3\Delta_{j-1}^n\right) < 0. \tag{4.26}$$

  On the other hand, adding and subtracting q_{j-1}^n it follows

  $$q_j^{n+1} - q_{j-1}^n = \Delta_{j-1}^n - \frac{c}{4}\left(-\Delta_{j-2}^n + 4\Delta_{j-1}^n + \Delta_j^n\right) > \left(1 - \frac{5c}{4}\right)\Delta_{j-1}^n \tag{4.27}$$

  which will be greater than zero if $c < \frac{4}{5}$. From (4.26) and (4.27) we conclude $q_{j-1}^n < q_j^{n+1} < q_j^n$ and thus Option 2 is stable.

- Option 3.

  Let us assume $\Delta_{j-1}^n > 0$, $M = \sup_j \left\{\left|q_j^n\right|\right\}$, $1 > \epsilon > 0$, $k > 3$ and $q_{j-2}^n = -M$, $q_{j-1}^n = -M+\epsilon$, $q_j^n = -M+3\epsilon$, $q_{j+1}^n = -M+(k+4)\epsilon$ and $q_{j+2}^n = -M+(2k+4)\epsilon$, we have

  - $\Delta_{j-2}^n = q_{j-1}^n - q_{j-2}^n = -M + \epsilon + M = \epsilon > 0$,
  - $\Delta_{j-1}^n = q_j^n - q_{j-1}^n = -M + 3\epsilon + M - \varepsilon = 2\epsilon > 0$,
  - $\Delta_j^n = q_{j+1}^n - q_j^n = -M + (k+4)\epsilon + M - 3\varepsilon = (k+1)\epsilon > 0$,
  - $\Delta_{j+1}^n = q_{j+2}^n - q_{j+1}^n = -M + (2k+4)\epsilon + M - (k+4)\varepsilon = k\epsilon > 0$,
  - $\Delta_{j-2}^n = \epsilon < 2\epsilon = \Delta_{j-1}^n$,
  - $\Delta_{j-1}^n = 2\epsilon < (k+1)\epsilon = \Delta_j^n$,
  - $\Delta_j^n = (k+1)\epsilon > k\epsilon = \Delta_{j+1}^n$.

  Hence, the hypothesis over the slopes of Option 3 are verified. Taking

  $$k > \max\left\{\left(\frac{16}{c} - 3\right), 3\right\}$$

  on equation (3.38), it results

  $$\begin{aligned} q_j^{n+1} - q_{j-2}^n &= \Delta_{j-2}^n + \Delta_{j-1}^n - \frac{c}{4}\left(-\Delta_{j-2}^n + 4\Delta_{j-1}^n + \Delta_{j+1}^n\right) \\ &< 2\Delta_{j-1}^n - \frac{c}{4}\left(3\Delta_{j-1}^n + \Delta_{j+1}^n\right) \\ &< 2\Delta_{j-1}^n - \frac{c}{4}\Delta_{j+1}^n < 4\epsilon - \frac{c}{4}k\epsilon < 0. \end{aligned} \tag{4.28}$$

  Consequently, $q_j^{n+1} < q_{j-2}^n = -M$ so Option 3 is unstable.

- Option 4.

  Assuming $\Delta_{j-1}^n > 0$ and $c < \frac{4}{5}$ we obtain

  $$q_j^{n+1} - q_j^n = \frac{c}{4}\left(\Delta_{j-2}^n - 4\Delta_{j-1}^n - \Delta_{j+1}^n\right) < -\frac{c}{4}\left(3\Delta_{j-1}^n + \Delta_{j+1}^n\right) < 0 \tag{4.29}$$

  and

  $$q_j^{n+1} - q_{j-1}^n = \Delta_{j-1}^n - \frac{c}{4}\left(-\Delta_{j-2}^n + 4\Delta_{j-1}^n + \Delta_{j+1}^n\right) > \left(1 - \frac{5c}{4}\right)\Delta_{j-1}^n. \tag{4.30}$$

  Hence $q_{j-1}^n < q_j^{n+1} < q_j^n$. That is, Option 4 is stable.

- Option 5 and 6.

  Suppose $\Delta_{j-1}^n > 0$ and $c < 1$, then

  $$q_j^{n+1} - q_j^n = \frac{c}{4}\left(\Delta_{j-2}^n - 4\Delta_{j-1}^n\right) < -\frac{3c}{4}\Delta_{j-1}^n < 0 \tag{4.31}$$

  and

  $$q_j^{n+1} - q_{j-1}^n = \Delta_{j-1}^n - \frac{c}{4}\left(-\Delta_{j-2}^n + 4\Delta_{j-1}^n\right) > (1-c)\,\Delta_{j-1}^n > 0. \tag{4.32}$$

  Consequently $q_{j-1}^n < q_j^{n+1} < q_j^n$ and thus, Options 5 and 6 are stable.

- Option 7.

  In case that $M = \sup_j\left\{\left|q_j^n\right|\right\}$, $\epsilon > 0$, $k > 3$, $q_{j-2}^n = -M$, $q_{j-1}^n = -M + 2\epsilon$, $q_j^n = -M + 3\epsilon$, $q_{j+1}^n = -M + k\epsilon$ and $q_{j+2}^n = -M + 2k\epsilon$, it results

  - $\Delta_{j-2}^n = q_{j-1}^n - q_{j-2}^n = -M + 2\epsilon + M = 2\epsilon > 0$,
  - $\Delta_{j-1}^n = q_j^n - q_{j-1}^n = -M + 3\epsilon + M - 2\epsilon = \epsilon > 0$,
  - $\Delta_j^n = q_{j+1}^n - q_j^n = -M + k\epsilon + M - 3\varepsilon = (k-3)\,\epsilon > 0$,
  - $\Delta_{j+1}^n = q_{j+2}^n - q_{j+1}^n = -M + 2k\epsilon + M - k\varepsilon = k\epsilon > 0$,
  - $\Delta_{j-2}^n = 2\epsilon > \epsilon = \Delta_{j-1}^n$,
  - $\Delta_{j-1}^n = \epsilon < (k-3)\,\epsilon = \Delta_j^n$,
  - $\Delta_j^n = (k-3)\,\epsilon < k\epsilon = \Delta_{j+1}^n$.

  Moreover,

  $$q_j^{n+1} - q_{j-2}^n = \Delta_{j-2}^n + \Delta_{j-1}^n - \frac{c}{4}\left(3\Delta_{j-1}^n + \Delta_j^n\right) = 3\epsilon - \frac{c}{4}k\epsilon. \tag{4.33}$$

  So, for any $c > 0$ taking $k > \max\left\{3, \frac{12}{c}\right\}$ we observe that Option 7 is unstable.

- Option 8.

  Let us consider $\Delta_{j-1}^n > 0$ and $c < 1$, then

  $$q_j^{n+1} - q_j^n = -\frac{c}{4}\left(3\Delta_{j-1}^n + \Delta_j^n\right) < 0 \tag{4.34}$$

  and

  $$q_j^{n+1} - q_{j-1}^n = \Delta_{j-1}^n - \frac{c}{4}\left(3\Delta_{j-1}^n + \Delta_j^n\right) > (1-c)\,\Delta_{j-1}^n > 0. \tag{4.35}$$

  Hence, $q_{j-1}^n < q_j^{n+1} < q_j^n$ which leads to the stability of Option 8.

- Option 9.

  Denoting $M = \sup_j \left\{\left|q_j^n\right|\right\}$ and assuming $q_{j-2}^n = \frac{M}{9}$, $q_{j-1}^n = \frac{8M}{9}$, $q_j^n = M$, $q_{j+1}^n = \frac{M}{2}$ and $q_{j+2}^n = -\frac{M}{2}$ we get

  - $\Delta_{j-2}^n = q_{j-1}^n - q_{j-2}^n = \frac{8M}{9} - \frac{M}{9} = \frac{7M}{9} > 0$,
  - $\Delta_{j-1}^n = q_j^n - q_{j-1}^n = M - \frac{8M}{9} = \frac{M}{9} > 0$,
  - $\Delta_j^n = q_{j+1}^n - q_j^n = \frac{M}{2} - M = -\frac{M}{2} < 0$,
  - $\Delta_{j+1}^n = q_{j+2}^n - q_{j+1}^n = -\frac{M}{2} - \frac{M}{2} = -M < 0$,
  - $\Delta_{j-2}^n = \frac{7M}{9} > \frac{M}{9} = \Delta_{j-1}^n$,
  - $\left|\Delta_j^n\right| = \frac{M}{2} < M = \left|\Delta_{j+1}^n\right|$,
  - $3\Delta_{j-1}^n + \Delta_j^n = -\frac{M}{6} < 0$.

  Using these inequalities in (3.40) arises $q_j^{n+1} > q_j^n = M$. Therefore, Option 9 is unstable.

- Option 10.

  Suppose $\Delta_{j-1}^n > 0$, $M = \sup_j \left\{\left|q_j^n\right|\right\}$, $\epsilon > 0$, $k > 3$, $q_{j-2}^n = -M$, $q_{j-1}^n = -M + 2\epsilon$, $q_j^n = -M + 3\epsilon$, $q_{j+1}^n = -M + (k+4)\,\epsilon$ and $q_{j+2}^n = -M + (2k+4)\,\epsilon$, then

  - $\Delta_{j-2}^n = q_{j-1}^n - q_{j-2}^n = -M + 2\epsilon + M = 2\epsilon > 0$,
  - $\Delta_{j-1}^n = q_j^n - q_{j-1}^n = -M + 3\epsilon + M - 2\epsilon = \epsilon > 0$,
  - $\Delta_j^n = q_{j+1}^n - q_j^n = -M + (k+4)\,\epsilon + M - 3\epsilon = (k+1)\,\epsilon > 0$,
  - $\Delta_{j+1}^n = q_{j+2}^n - q_{j+1}^n = -M + (2k+4)\,\epsilon + M - (k+4)\,\epsilon = k\epsilon > 0$,
  - $\Delta_{j-2}^n = 2\epsilon > \epsilon = \Delta_{j-1}^n$,
  - $\Delta_{j-1}^n = \epsilon < (k+1)\,\epsilon = \Delta_j^n$,
  - $\Delta_j^n = (k+1)\,\epsilon > k\epsilon = \Delta_{j+1}^n$.

Furthermore,

$$q_j^{n+1} - q_{j-2}^n = \Delta_{j-2}^n + \Delta_{j-1}^n + \frac{c}{4}\left(3\Delta_{j-1}^n - \Delta_{j+1}^n\right) = 3\epsilon\left(1 + \frac{c}{4}\right) - \frac{c}{4}k\epsilon. \quad (4.36)$$

Since for any c we can find $k > 3$ such that $12 + 3c < ck$, we have proven that Option 10 is unstable.

- Option 11.

  Using $\Delta_{j-1}^n > 0$ in equation (3.3.1) gives

  $$q_j^{n+1} - q_j^n = \frac{c}{4}\left(3\Delta_{j-1}^n - \Delta_{j+1}^n\right) > 0 \quad (4.37)$$

  and

  $$q_j^{n+1} - q_{j+2}^n = -\Delta_{j+1}^n - \Delta_j^n - \frac{c}{4}\left(3\Delta_{j-1}^n - \Delta_{j+1}^n\right) < \left(-1 - \frac{1}{2}c\right)\Delta_{j-1}^n < 0. \quad (4.38)$$

  So $q_j^n < q_j^{n+1} < q_{j+2}^n$ which asses the stability of Option 11.

- Option 12.

  Being $M = \sup_j \left\{\left|q_j^n\right|\right\}$, and supposing $q_{j-2}^n = \frac{M}{4}$, $q_{j-1}^n = \frac{3M}{4}$, $q_j^n = M$, $q_{j+1}^n = -\frac{M}{2}$ and $q_{j+2}^n = -\frac{3M}{4}$, we have

  - $\Delta_{j-2}^n = q_{j-1}^n - q_{j-2}^n = \frac{M}{2} > 0$,
  - $\Delta_{j-1}^n = q_j^n - q_{j-1}^n = \frac{M}{4} > 0$,
  - $\Delta_j^n = q_{j+1}^n - q_j^n = -\frac{3M}{2} < 0$,
  - $\Delta_{j+1}^n = q_{j+2}^n - q_{j+1}^n = -\frac{M}{4} < 0$,
  - $\Delta_{j-2}^n = \frac{M}{2} > \frac{M}{4} = \Delta_{j-1}^n$,
  - $\left|\Delta_j^n\right| = \frac{3M}{2} > \frac{M}{4} = \left|\Delta_{j+1}^n\right|$.

  From the previous inequalities we conclude that Option 12 is unstable:

  $$q_j^{n+1} = q_j^n + \frac{c}{4}\left(3\Delta_{j-1}^n - \Delta_{j+1}^n\right) = q_j^n + \frac{c}{4}M > q_j^n = M. \quad (4.39)$$

- Option 13, Option 14 and Option 15.

  Assuming $\Delta_{j-1}^n > 0$ in (3.42) and $c < \frac{4}{3}$, we get

  $$q_j^{n+1} - q_j^n = -\frac{3c}{4}\Delta_{j-1}^n < 0 \quad (4.40)$$

  and

  $$q_j^{n+1} - q_{j-1}^n = \left(1 - \frac{3}{4}c\right)\Delta_{j-1}^n > 0. \quad (4.41)$$

  Therefore, $q_{j-1}^n < q_j^{n+1} < q_j^n$ which proves that Options 13, 14 and 15 are stable.

- Option 16.

  We define $M = \sup_j \left\{\left|q_j^n\right|\right\}$. If $\epsilon > 0$, $k > 1$, $q_{j-1}^n = -M$, $q_j^n = -M + \epsilon$, $q_{j+1}^n = -M + (k+1)\,\epsilon$ and $q_{j+2}^n = -M + (2k+2)\,\epsilon$, we obtain

  - $\Delta_{j-2}^n = q_{j-1}^n - q_{j-2}^n = -M - q_{j-2}^n < 0$,
  - $\Delta_{j-1}^n = q_j^n - q_{j-1}^n = -M + \epsilon + M = \epsilon > 0$,
  - $\Delta_j^n = q_{j+1}^n - q_j^n = -M + (k+1)\epsilon + M - \epsilon = k\epsilon > 0$,
  - $\Delta_{j+1}^n = q_{j+2}^n - q_{j+1}^n = -M + (2k+2)\epsilon + M - (k+1)\epsilon = (k+1)\epsilon > 0$,
  - $\Delta_{j-1}^n = \epsilon < k\epsilon = \Delta_j^n$,
  - $\Delta_j^n = k\epsilon < (k+1)\epsilon = \Delta_{j+1}^n$.

  Hence,

  $$q_j^{n+1} - q_{j-1}^n = \Delta_{j-1}^n - \frac{c}{4}\left(4\Delta_{j-1}^n + \Delta_j^n\right) = \epsilon - \frac{c}{4}\left(4\epsilon + k\epsilon\right). \tag{4.42}$$

  Furthermore, given $c>0$ we can define $k = \max\left\{1, \frac{4}{c}\right\}$ such that $q_j^{n+1} < q_{j-1}^n = -M$. Herein, Option 16 is unstable.

- Option 17.

  We consider $\Delta_{j-1}^n > 0$ and $c < \frac{4}{5}$, then

  $$q_j^{n+1} - q_j^n = -\frac{c}{4}\left(4\Delta_{j-1}^n + \Delta_j^n\right) < 0 \tag{4.43}$$

  and

  $$q_j^{n+1} - q_{j-1}^n > \left(1 - \frac{5}{4}c\right)\Delta_{j-1}^n > 0. \tag{4.44}$$

  Consequently, $q_{j-1}^n < q_j^{n+1} < q_j^n$. Thus, Option 17 is stable.

- Option Option 18.

  Assuming $M = \sup_j \left\{\left|q_j^n\right|\right\}$, $q_{j-2}^n = \frac{31M}{32}$, $q_{j-1}^n = \frac{15M}{16}$, $q_j^n = M$, $q_{j+1}^n = \frac{M}{2}$ and $q_{j+2}^n = -\frac{M}{4}$, we have

  - $\Delta_{j-2}^n = q_{j-1}^n - q_{j-2}^n = -\frac{M}{32} < 0$,
  - $\Delta_{j-1}^n = q_j^n - q_{j-1}^n = \frac{M}{16} > 0$,
  - $\Delta_j^n = q_{j+1}^n - q_j^n = -\frac{M}{2} < 0$,
  - $\Delta_{j+1}^n = q_{j+2}^n - q_{j+1}^n = -\frac{3M}{4} < 0$,
  - $\left|\Delta_j^n\right| = \frac{M}{2} < \frac{3M}{4} = \left|\Delta_{j+1}^n\right|$.

Substituting in (3.43) we obtain

$$q_j^{n+1} - q_j^n = -\frac{c}{4}\left(4\Delta_{j-1}^n + \Delta_{j+1}^n\right) > \frac{1}{8}Mc > 0. \tag{4.45}$$

Hence, Option 18 is unstable.

- Option 19.
  Let $M = \sup_j \left\{\left|q_j^n\right|\right\}$, $k > 1$, $q_{j-1}^n = -M$, $q_j^n = -M + \epsilon$, $q_{j+1}^n = -M + (2k+1)\,\epsilon$ and $q_{j+2}^n = -M + (3k+1)\,\epsilon$, then
  - $\Delta_{j-2}^n = q_{j-1}^n - q_{j-2}^n < 0$,
  - $\Delta_{j-1}^n = q_j^n - q_{j-1}^n = \epsilon > 0$,
  - $\Delta_j^n = q_{j+1}^n - q_j^n = 2k\epsilon > 0$,
  - $\Delta_{j+1}^n = q_{j+2}^n - q_{j+1}^n = k\epsilon > 0$,
  - $\Delta_{j-1}^n = \epsilon < 2k\epsilon = \Delta_j^n$,
  - $\Delta_j^n = 2k\epsilon > k\epsilon = \Delta_{j+1}^n$.

  Consequently,

$$q_j^{n+1} - q_{j-1}^n = \Delta_{j-1}^n - \frac{c}{4}\left(4\Delta_{j-1}^n + \Delta_{j+1}^n\right) = \epsilon - \frac{c}{4}\,(4+k)\,\epsilon. \tag{4.46}$$

  Given c we can chose $k > \frac{4}{c} - 4$ such that $q_j^{n+1} < q_{j-1}^n = -M$. Herein, Option 19 is unstable.

- Option 20.
  Let us assume $\Delta_{j-1} > 0$ and $c < \frac{4}{5}$, then

$$q_j^{n+1} - q_j^n = -\frac{c}{4}\left(4\Delta_{j-1}^n + \Delta_{j+1}^n\right) < 0 \tag{4.47}$$

  and

$$q_j^{n+1} - q_{j-1}^n > \left(1 - \frac{5}{4}c\right)\Delta_{j-1}^n > 0. \tag{4.48}$$

  Since $q_{j-1}^n < q_j^{n+1} < q_j^n$, Option 20 is stable.

- Option 21.
  If $M = \sup_j \left\{\left|q_j^n\right|\right\}$, $q_{i-2}^n = \frac{63M}{64}$, $q_{j-1}^n = \frac{31M}{32}$, $q_j^n = M$, $q_{j+1}^n = \frac{M}{2}$ and $q_{j+2}^n = \frac{M}{4}$, then
  - $\Delta_{j-2}^n = q_{j-1}^n - q_{j-2}^n = -\frac{M}{64} < 0$,
  - $\Delta_{j-1}^n = q_j^n - q_{j-1}^n = \frac{M}{32} > 0$,
  - $\Delta_j^n = q_{j+1}^n - q_j^n = -\frac{M}{2} < 0$,

- $\Delta^n_{j+1} = q^n_{j+2} - q^n_{j+1} = -\frac{M}{4} < 0$,
- $\left|\Delta^n_j\right| = \frac{M}{2} > \frac{M}{4} = \left|\Delta^n_{j+1}\right|$.

Substituting in equation(3.44), we get

$$q^{n+1}_j - q^n_j = -\frac{c}{4}\left(4\Delta^n_{j-1} + \Delta^n_{j+1}\right) = c\frac{M}{32} > 0. \tag{4.49}$$

Thus, Option 21 is unstable.

- Option 22, 23 and 24.

  We suppose $\Delta^n_{j-1} > 0$ and $c < 2$, thus

$$q^{n+1}_j - q^n_j = -\frac{c}{2}\Delta^n_{j-1} < 0 \tag{4.50}$$

and

$$q^{n+1}_j - q^n_{j-1} = \left(1 - \frac{c}{2}\right)\Delta^n_{j-1} > 0. \tag{4.51}$$

So, $q^n_{j-1} < q^{n+1}_j < q^n_j$. Finally, Options 22, 23 and 24 are stable.

Remark 4.1.1. Within the previous analysis, we state that an option is unstable if we can not determine a fixed value for c such that the related branch is stable. Nevertheless, for a particular problem we might be able to select c ensuring a stable solution.

4.2 Stability analysis of ADER schemes

The stability analysis of the schemes obtained applying ADER and MUSCL-Hancock methodologies is divided into two cases. On the one hand, linear advection equation allows for an easy computation of the stability region. On the other hand, advection-diffusion-reaction equation with constant diffusion coefficient will be analysed thanks to graphical representation.

4.2.1 Advection equation

Stability analysis of linear models is done following von Neumann stability analysis procedure.

Proposition 4.2.1. *ADER scheme for the advection equation with* $\lambda > 0$, (3.88), *is conditionally stable with stability condition*

$$0 \leq c \leq 1. \tag{4.52}$$

Proof. Let us consider the trial function (4.1). Then, (3.88) yields to

$$A^{n+1}e^{i\theta j} = A^n e^{i\theta j} - c\left[A^n e^{i\theta j} - A^n e^{i\theta(j-1)} + \frac{1-c}{4}\left(A^n e^{i\theta(j+1)} - A^n e^{i\theta j} - A^n e^{i\theta(j-1)} + A^n e^{i\theta(j-2)}\right)\right]. \tag{4.53}$$

Simplifying,

$$A = 1 - c\left[1 - e^{-i\theta} + \frac{1-c}{4}\left(e^{i\theta} - 1 - e^{-i\theta} + e^{-2i\theta}\right)\right] \tag{4.54}$$

and hence,

$$|A|^2 = c\,(c-1)\,(\cos\theta - 1)^2\left[\frac{1}{2}c\,(c-1)\,(\cos\theta + 1) + 1\right] + 1. \tag{4.55}$$

The stability condition, $|A|^2 \leq 1$, is verified if and only if

$$c\,(c-1)\,(\cos\theta - 1)^2\left[\frac{1}{2}c\,(c-1)\,(\cos\theta + 1) + 1\right] \leq 0, \tag{4.56}$$

that is,

$$c\,(c-1)\,(\cos\theta + 1) \geq -2 \text{ and } c \leq 1. \tag{4.57}$$

From which it follows that the scheme is stable if the Courant number, c, lies between zero and unity. Therefore, it is conditionally stable with stability condition

$$0 \leq c \leq 1. \tag{4.58}$$

□

Remark 4.2.1. If $\lambda < 0$ it can be proved that the corresponding ADER scheme for the advection equation is stable for $-1 \leq c \leq 0$.

Sometimes the amplification factor is a difficult expression to deal with. In order to make it easier, we can represent the value of the function of the binomial expression of the amplification factor,

$$\begin{array}{rcl} A : [-\pi, \pi] \times \mathbb{R} & \longrightarrow & \mathbb{C} \\ (\theta, c) & \rightsquigarrow & A(\theta, c), \end{array} \tag{4.59}$$

for different values of c (see [Hof89]). In Figure 4.1, we can observe that the functions whose image is completely contained in the square $[-1,1] \times [-1,1] \subset \mathbb{C}$ are defined for $c \in [0,1]$. This agrees with the analytical results already obtained.

On the other hand, we can plot the function defined by the square of the modulus of the amplification factor, $|A(\theta, c)|^2 \in \mathbb{R}$. As A depends on two variables, θ and c, the plot, Figure 4.2a, is a surface in $\mathbb{R}^3$. Drawing the contour lines we can confirm that the stability condition is verified if and only if $0 \leq c \leq 1$. In Figure 4.2b we consider $c \in [0, 1.2]$ to remark that for any chosen $c_0 > 1$ there exist $\theta_{c_0} \in [-\pi, \pi]$ such that the values of $|A(\theta_{c_0}, c_0)|^2$ are larger than one.

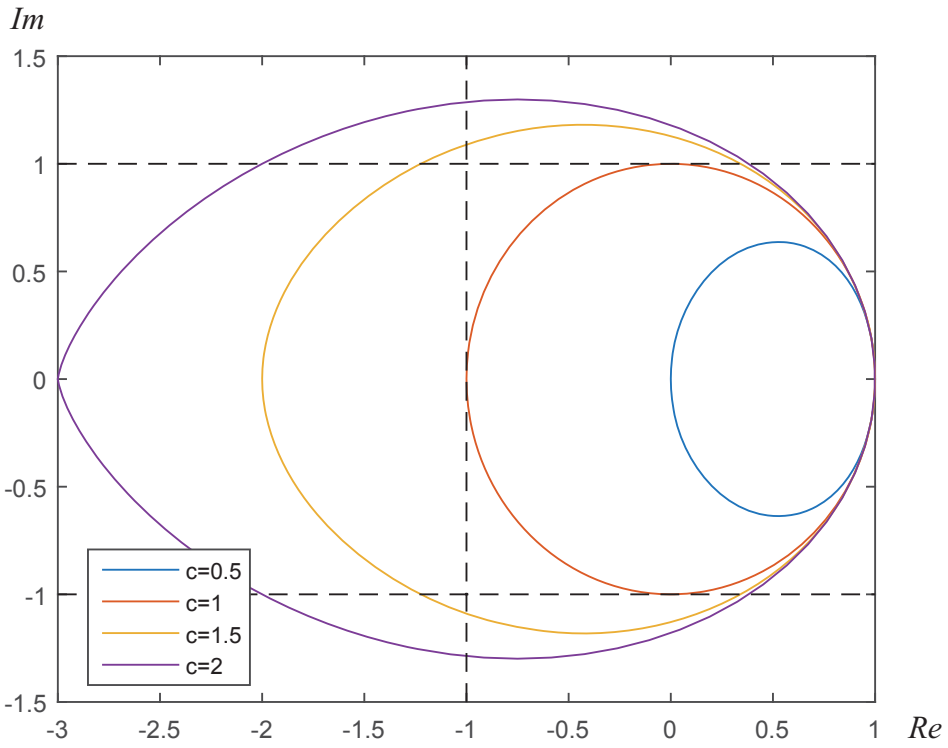

Figure 4.1: ADER scheme (3.88). Representation in the complex plane of the amplification factor for several values of c with $\theta \in [-\pi, \pi]$. It can be observed that c is bounded above by 1 when $|A|$ is bounded by 1.

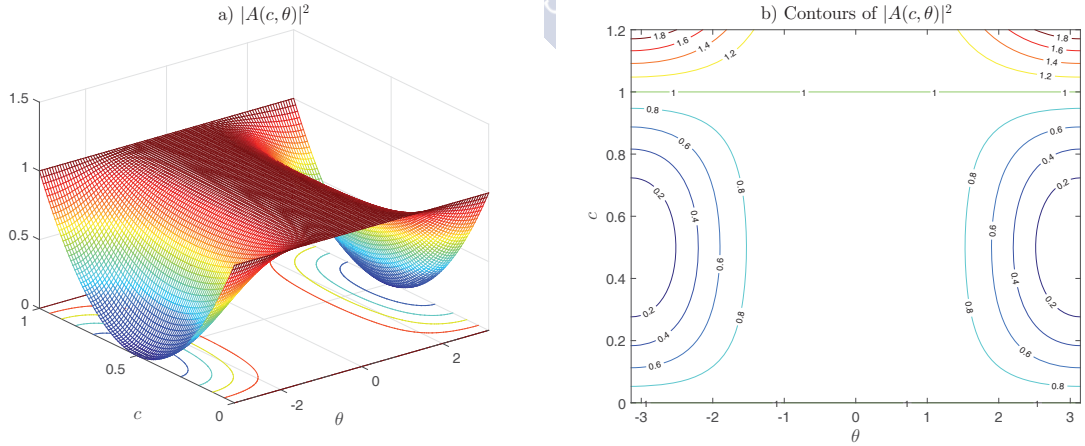

Figure 4.2: ADER scheme (3.88). Graph and contour lines of $|A(\theta, c)|^2$. The stability region is clearly determined for $0 \leq c \leq 1$.

4.2.2 Advection-diffusion-reaction equation

The amplification factor of scheme (3.74), which depends on the angle θ and on the parameters $c = \frac{\lambda \Delta t}{\Delta x}$, $d = \frac{\alpha \Delta t}{\Delta x^2}$ and $r = \beta \Delta t$, is computed using von Neumann procedure obtaining

$$\begin{aligned} A =& 1 - c \left\{ 1 - \cos\theta + i \sin\theta + \frac{1-c}{4} \left(2i \sin\theta - 1 + \cos 2\theta - i \sin 2\theta \right) \right. \\ & + \frac{r}{2} \left[1 - \cos\theta + i \sin\theta + \frac{1}{4} \left(2i \sin\theta - 1 + \cos 2\theta - i \sin 2\theta \right) \right] \\ & \left. + \frac{d}{2} \left(4 \cos\theta - 2i \sin\theta - 3 - \cos 2\theta - i \sin 2\theta \right) \right\} \\ & + d \left\{ 2 \cos\theta - 2 - \frac{c}{4} \left(2i \sin 2\theta - 6i \sin\theta \right) + \frac{d}{2} \left(2 \cos 2\theta - 8 \cos\theta + 6 \right) \right. \\ & \left. + \frac{r}{2} \left(2 \cos\theta - 2 \right) \right\} + r \left\{ 1 - \frac{c}{2} i \sin\theta + d \left(\cos\theta - 1 \right) + \frac{r}{2} \right\}. \end{aligned} \tag{4.60}$$

As the bounds of c, d and r in order to limit the amplification factor are interdependent, the computation of the constraints will produce complicated expressions. Still, a graphical representation provides us with a good approach to determine the stability region.

Advection-reaction equation

The function related with the amplification factor of the linear advection-reaction equation with constant coefficients results

$$\begin{array}{rcl} |A|^2 : [-\pi, \pi] \times \mathbb{R} \times \mathbb{R} & \longrightarrow & \mathbb{R} \\ (\theta, c, r) & \longrightarrow & |A(\theta, c, r)|^2 . \end{array} \tag{4.61}$$

Its graph is embedded in $\mathbb{R}^4$, therefore, instead of plotting contour lines, we represent the isosurface of level one which splits $\mathbb{R}^3$ in two domains (see Figure 4.3). One of them, which contains the point $(\theta, c, r) = (0, 0, 0)$, is the stability region of the scheme. Inside the other domain the scheme is unconditionally unstable. Furthermore, the orthogonal planes to the r-axis, that is, the planes resulting for a fixed value of r, provide the contour plots of level one for the linear advection-reaction equation related to the set r (see the two-dimensional subplots of Figure 4.3 where S denotes the stability region of the scheme).

For instance, assuming $r = -1$ the value $c = 1.1$ guarantees the stability. However, we must carefully analyse these results. For a specific problem, with a given mesh, setting $r = -1$ does not imply that Δt is such that $c = 1.1$ and vice versa. A particular example will help us to better understand the situation. We consider the linear advection-reaction equation

$$\partial_t q(x,t) + \lambda_0 \partial_x q(x,t) = \beta_0 q(x,t) \tag{4.62}$$

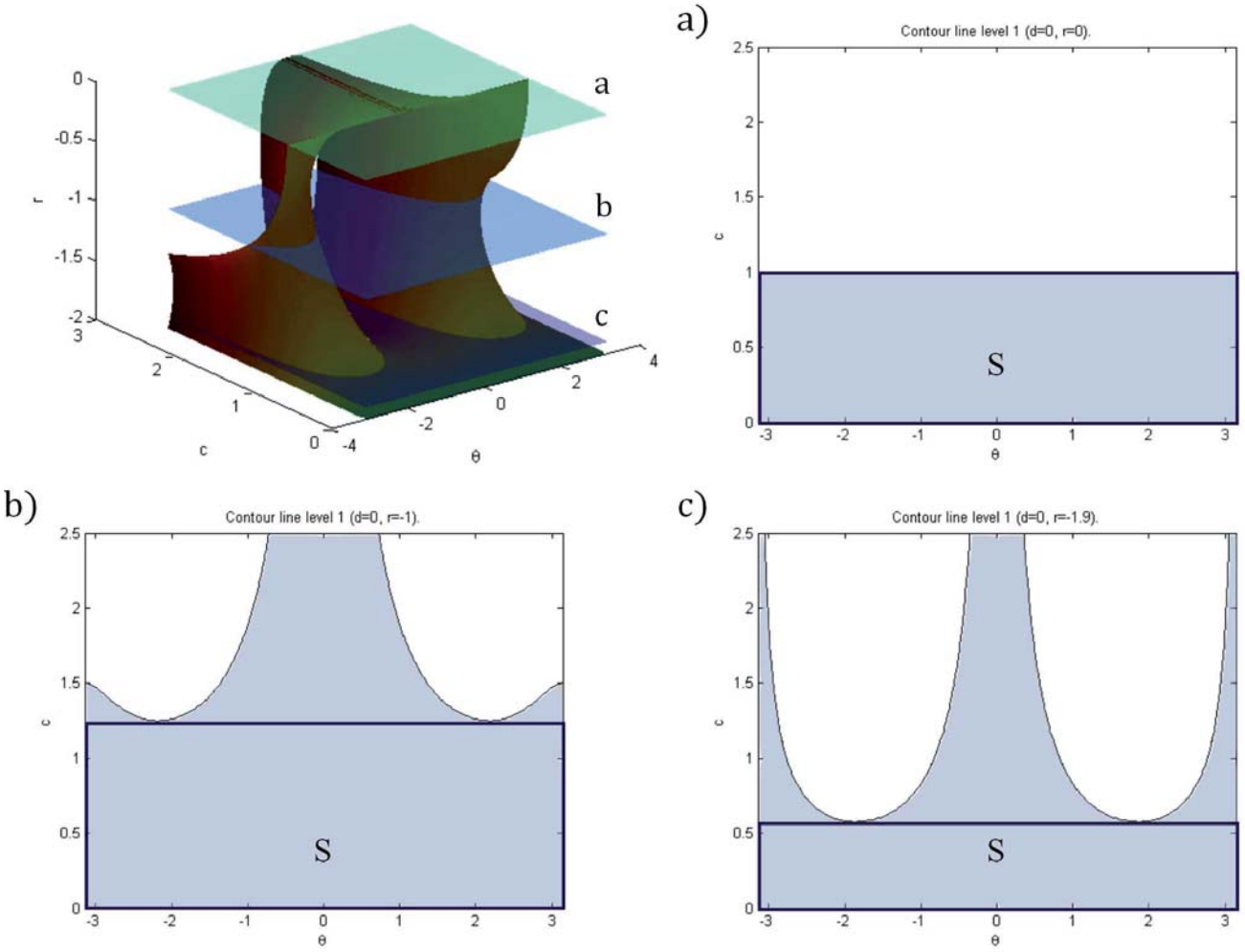

Figure 4.3: ADER scheme (3.74). Stability region for the linear advection-reaction equation. The isosurface of level one splits $\mathbb{R}^3$ into the stability region, containing the origin, and the unstable region. Subplots a), b), c) represent the contour plots of level one for the fixed values of $r = 0$, $r = -1$ and $r = -1.9$, respectively. The shaded regions correspond to the stability region. The blue rectangles identified as S are the admissible regions of stability.

with fixed $\lambda_0 \in \mathbb{R}^+$ and $\beta_0 \in \mathbb{R}^-$. If the mesh size is $\Delta x = \Delta x_0$, then it is verified

$$\begin{cases} r = \beta_0 \Delta t, \\ c = \dfrac{\lambda_0 \Delta t}{\Delta x_0}. \end{cases} \tag{4.63}$$

So, if Δt is computed from $r = r_0$ fixed, then

$$c = \frac{\lambda_0 r_0}{\beta_0 \Delta x_0} \tag{4.64}$$

is determined. Similarly, given $c = c_0$ the value of Δt is resolved and

$$r = \frac{\beta_0 c_0 \Delta x_0}{\lambda_0}. \tag{4.65}$$

Hence, for $r = -1$ the value of c is determined and can be different from the expected value, $c = 1.1$. In case it is bigger, we would have fallen into the unstable region.

To avoid the previous trouble, we define rectangular cuboids

$$O_{c_M, r_m} = \left\{ (\theta, c, r) \mid \theta \in [-\pi, \pi],\ c \in [0, c_M],\ r \in [r_m, 0],\ c_M \in \mathbb{R}^+,\ r_m \in \mathbb{R}^- \right\} \tag{4.66}$$

embedded in the stability region. Selecting $c_M = 1$, the upper bound of c, and $r_m = -1$, the lower bound of of r, the resulting scheme is stable.

Advection-diffusion equation

The previous procedure can also be applied for the linear advection-diffusion equation with constant coefficient. Hence, we consider

$$\begin{array}{rcl} |A|^2 : [-\pi, \pi] \times \mathbb{R} \times \mathbb{R} & \longrightarrow & \mathbb{R} \\ (\theta, c, d) & \longrightarrow & |A(\theta, c, d)|^2 \end{array} \tag{4.67}$$

and

$$O_{c_M, d_M} = \left\{ (\theta, c, d) \mid \theta \in [-\pi, \pi],\ c \in [0, c_M],\ d \in [0, d_M],\ c_M,\ d_M \in \mathbb{R}^+ \right\}. \tag{4.68}$$

In Figure 4.4, we can observe that $c_M = 1$ and $d_M = 0.5$ generate an admissible cuboid.

Advection-diffusion-reaction equation

As last step, we study the stability for the linear advection-diffusion-reaction equation with constant coefficients. The amplification factor function reads

$$\begin{array}{rcl} |A|^2 : [-\pi, \pi] \times \mathbb{R} \times \mathbb{R} \times \mathbb{R} & \longrightarrow & \mathbb{R} \\ (\theta, c, d, r) & \longrightarrow & |A(\theta, c, d, r)|^2 \end{array} \tag{4.69}$$

so its graph belongs to $\mathbb{R}^5$ and the isosurfaces are embedded in $\mathbb{R}^4$. Admissible regions can be established through 4-orthotopes,

$$O_{c_M,d_M,r_m} = \Big\{(\theta,c,r,d) \mid \theta\in[-\pi,\pi],\ c\in[0,c_M],\ d\in[0,d_M],\ r\in[r_m,0], \\ c_M,\ d_M\in\mathbb{R}^+,\ r_m\in\mathbb{R}^-\Big\}. \quad (4.70)$$

To get an idea of the shape of the stability region, we can picture an evolutionary problem where one of the variables, for instance r, plays the role of time and the remaining ones are considered as spacial variables. Therefore, the stability region is determined by the intersection of the stability regions for the different snapshots of r. Figures 4.4-4.6 show the graphs obtained for fixed values of r. We can conclude that $c_M = 1$, $d_M = \frac{1}{4}$ and $r_m = -\frac{1}{2}$ define a 4-orthotope embedded in the stability region.

A new alternative way to depict the stability region is to plot the isosurface of level one of the function defined by

$$m_\theta(c,d,r) = \max_{\theta\in[-\pi,\pi]} |A(\theta,c,d,r)|^2 . \quad (4.71)$$

Figure 4.7 confirms that the 4-orthotope defined above, $O_{1,\frac{1}{4},-\frac{1}{2}}$, is embedded in the stability region.

4.3 Stability analysis of LADER schemes

As done for ADER schemes, we will divide the stability analysis of LADER schemes into the study of the linear advection equation and of the linear advection-diffusion-reaction equation.

Advection equation

Proposition 4.3.1. *LADER scheme for the advection equation with positive advection coefficient,* (3.108)*, is conditionally stable with stability condition*

$$0 \le c \le -1+\sqrt{2}.$$

Proof. Performing von Neumann stability analysis we get

$$A^{n+1}e^{i\theta j} = A^n e^{i\theta j} - c\Big[A^n e^{i\theta j} - A^n e^{i\theta(j-1)} + \frac{1}{2}\Big(A^n e^{i\theta j} - 2A^n e^{i\theta(j-1)} \\ + A^n e^{i\theta(j-2)}\Big) - \frac{c}{2}\Big(A^n e^{i\theta(j+1)} - 2A^n e^{i\theta j} + A^n e^{i\theta(j-1)}\Big)\Big]. \quad (4.72)$$

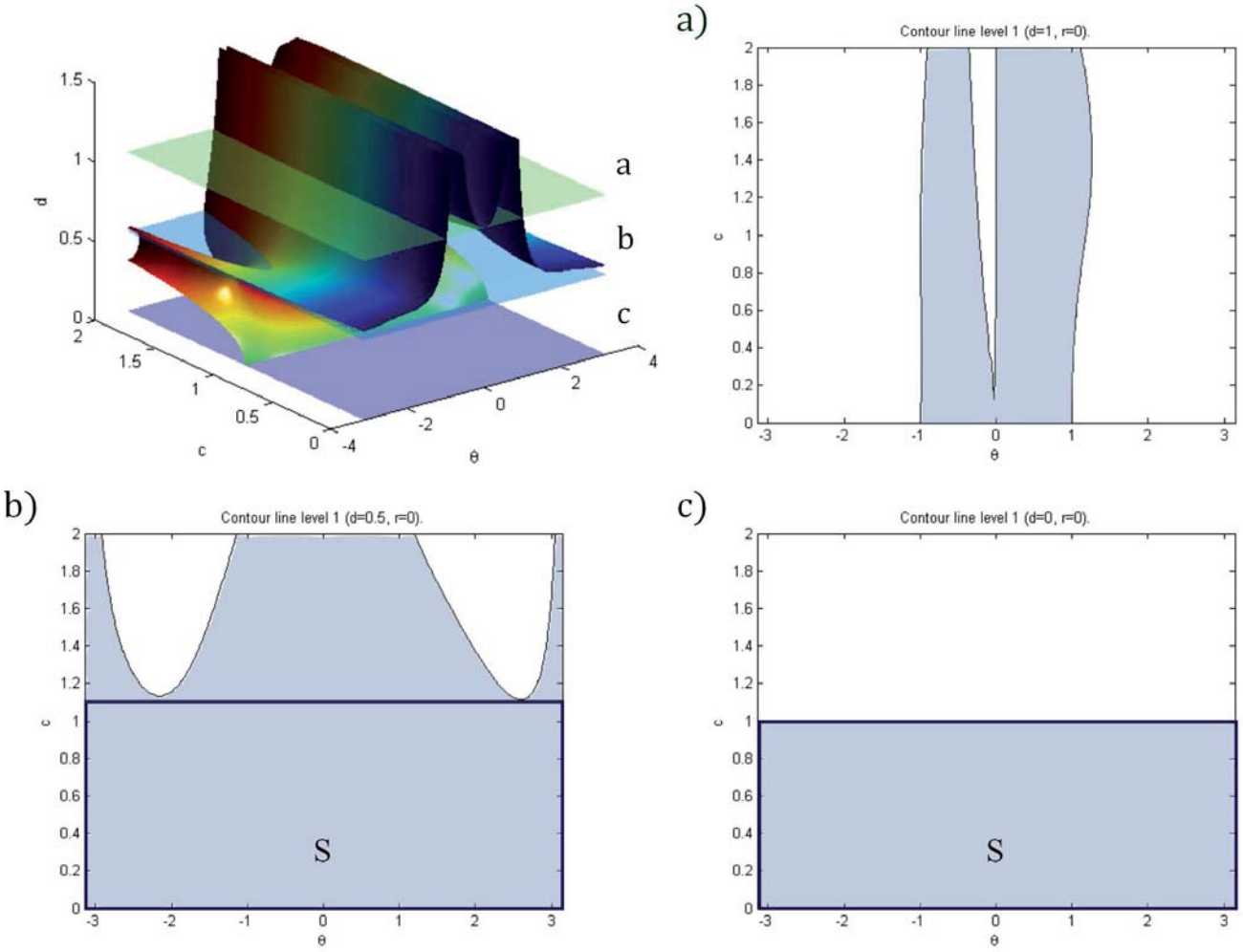

Figure 4.4: ADER scheme (3.74). Stability region for the linear advection-diffusion equation. The isosurface of level one splits $\mathbb{R}^3$ into the stability region, containing the origin, and the unstable region. Subplots a), b), c) represent the contour plots of level one for the fixed values of $d = 1$, $d = 0.5$ and $d = 0$, respectively. The shaded regions correspond to the stability region. The blue rectangles identified as S are the admissible regions of stability.

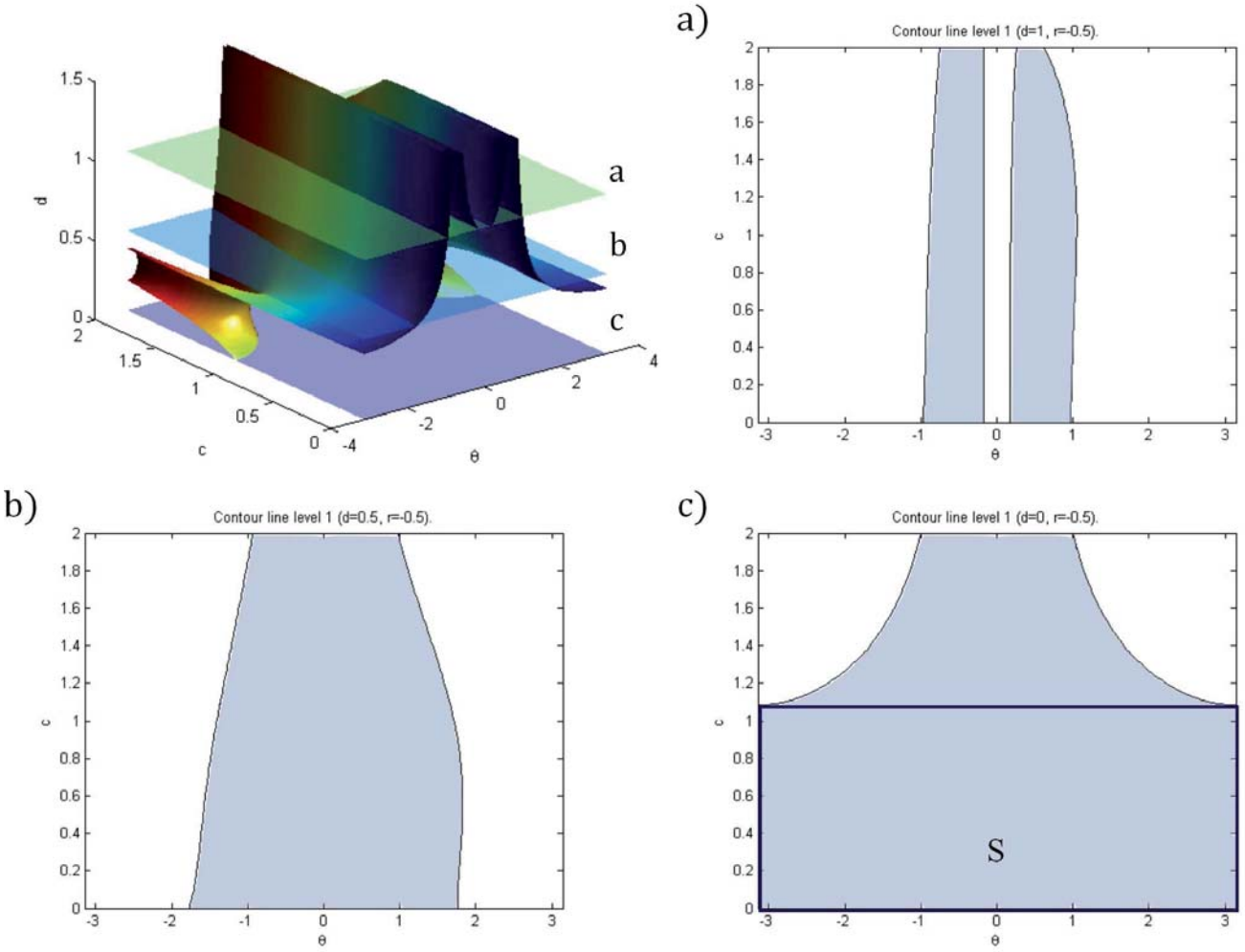

Figure 4.5: ADER scheme (3.74). Stability region for the linear advection-diffusion-reaction equation with fixed reaction number $r = -0.5$. The isosurface of level one splits $\mathbb{R}^3$ into the stability region, containing the origin, and the unstable region. Subplots a), b), c) represent the contour plots of level one for the fixed values of $d = 1$, $d = 0.5$ and $d = 0$, respectively. The shaded regions correspond to the stability region. The blue rectangles identified as S are the admissible regions of stability.

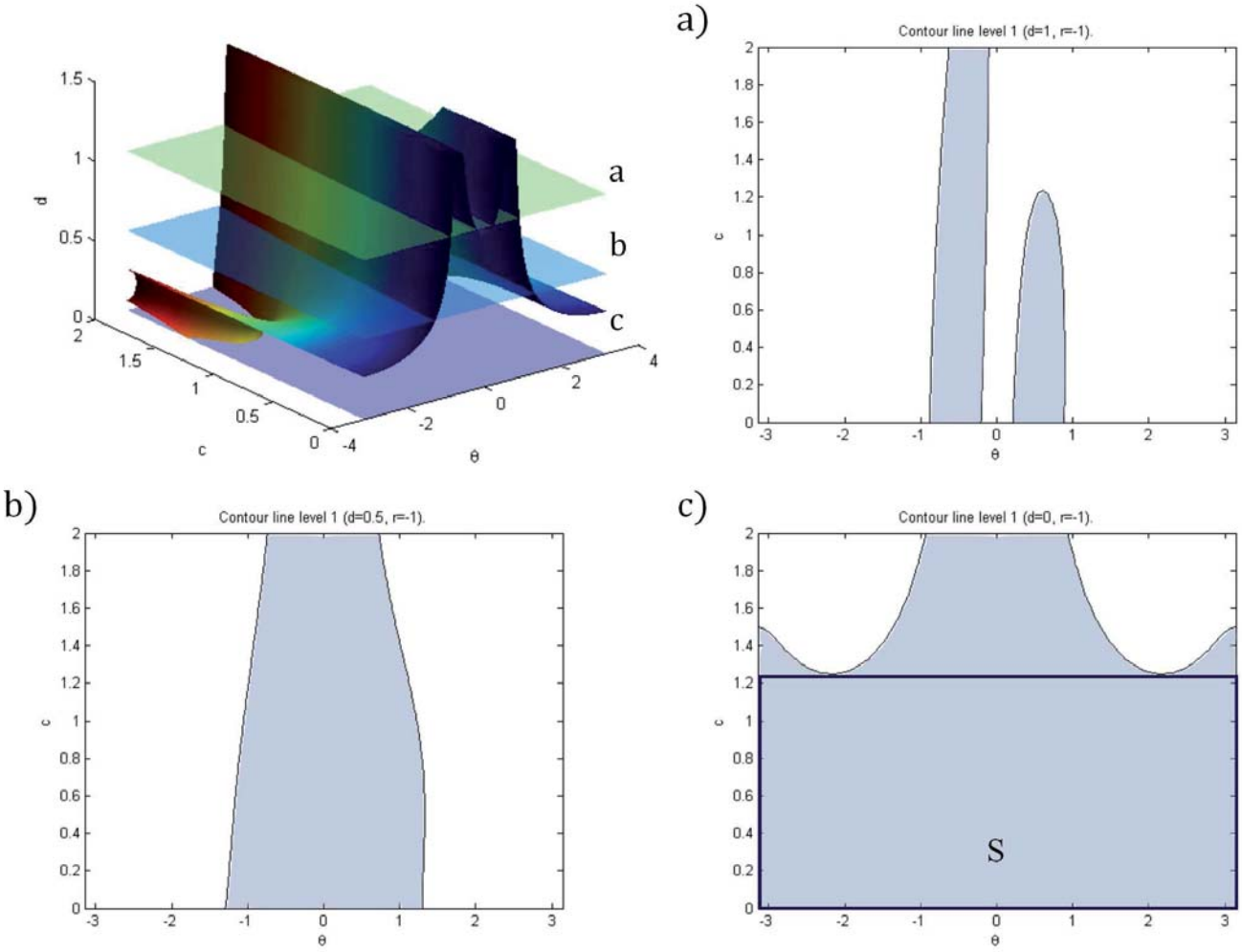

Figure 4.6: ADER scheme (3.74). Stability region for the linear advection-diffusion-reaction equation with fixed reaction number $r = -1$. The isosurface of level one splits $\mathbb{R}^3$ into the stability region, containing the origin, and the unstable region. Subplots a), b), c) represent the contour plots of level one for the fixed values of $d = 1$, $d = 0.5$ and $d = 0$, respectively. The shaded regions correspond to the stability region. The blue rectangles identified as S are the admissible regions of stability.

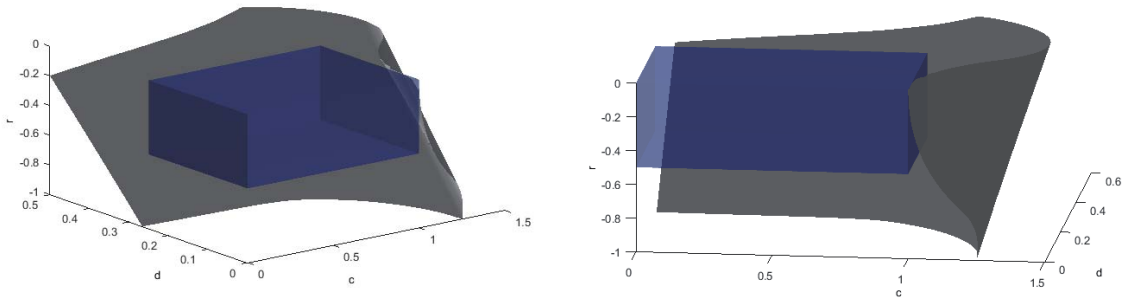

Figure 4.7: ADER scheme (3.74). Two different views of the isosurface of level one of function $m_{\theta,\,\mathrm{ADER}}$, (4.71), (grey) and the 4-orthotope of stability $O_{1,\frac{1}{4},-\frac{1}{2}}$ for the linear advection-diffusion-reaction equation (blue).

Furthermore, we deduce an expression for the square of the modulus of the amplification factor of the form

$$|A|^2 = 4c^4 \sin^4\left(\frac{\theta}{2}\right) + 16c^3 \sin^6\left(\frac{\theta}{2}\right) + 12c^2 \sin^4\left(\frac{\theta}{2}\right) - 8c \sin^4\left(\frac{\theta}{2}\right) + 1. \tag{4.73}$$

According to the above, the amplification factor is lower or equal to one if and only if

$$c^3 + 4c^2 \sin^2\left(\frac{\theta}{2}\right) + 3c - 2 \leq 0. \tag{4.74}$$

Taking into account that $\sin^2\left(\frac{\theta}{2}\right) \in [0,1]$ and factoring, we get

$$(c+2)\left(c-1+\sqrt{2}\right)\left(c-1-\sqrt{2}\right) \leq 0. \tag{4.75}$$

Herein,

$$c \leq -1+\sqrt{2} \tag{4.76}$$

is the stability condition of scheme (3.108). □

Remark 4.3.1. LADER scheme for the advection equation with $\lambda < 0$ is stable for $1-\sqrt{2} \leq c \leq 0$.

Advection-diffusion-reaction equation

The stability analysis of scheme (3.106) is investigated through graphical representation. We start computing the amplification factor of the scheme:

$$\begin{aligned} A =& 1 - c\Big[1 - \cos\theta + i\sin\theta + \frac{1}{2}\left(1 - 2\cos\theta + 2i\sin\theta + \cos 2\theta - i\sin 2\theta\right) \\ & - \frac{c}{2}\left(2\cos\theta - 2 + \cos\theta\right) + \frac{r}{2}\left(1 - \cos\theta + i\sin\theta\right) + d\left(i\sin 2\theta - 2i\sin\theta\right)\Big] \end{aligned}$$

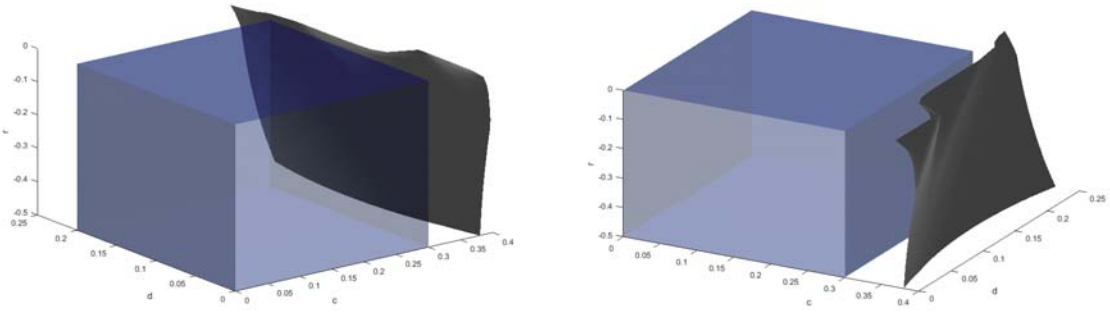

Figure 4.8: LADER scheme (3.106). Two different views of the isosurface of level one of function $m_{\theta,\,\mathrm{LADER}}$, (4.71), (grey) and the 4-orthotope of stability $O_{0.3,0.2,-0.5}$ for the linear advection-diffusion-reaction equation (blue).

$$+ d\left[2\cos\theta - 2 + d\left(\cos 2\theta - 4\cos\theta + 3\right) + r\left(\cos\theta - 1\right)\right]$$
$$+ r\left[1 - \frac{c}{2}i\sin\theta + d\left(\cos\theta - 1\right) + \frac{r}{2}\right]. \tag{4.77}$$

As done in Section 4.2, stability regions for fixed values of c, d or r can be determined by the analysis of the related isosurfaces of level one. Furthermore, considering (4.77) we can plot the isosurface of level one of the function introduced in (4.71) to determine a feasible 4-orthotope of stability.

Proposition 4.3.2. *There exist c_M, d_M, $r_m \in \mathbb{R}$ such that LADER scheme,* (3.106)*, is stable in the 4-orthotopes*

$$O_{c_M,d_M,r_m} = \Big\{(\theta, c, r, d) \mid \theta \in [-\pi, \pi],\ c \in [0, c_M],\ d \in [0, d_M],$$
$$r \in [r_m, 0],\ c_M,\ d_M \in \mathbb{R}^+,\ r_m \in \mathbb{R}^-\Big\}. \tag{4.78}$$

In Figure 4.8 we can observe that the 4-orthotope defined by $c_M = 0.3$, $d_M = 0.2$ and $r_m = -0.5$ is embedded in the stability region.

4.4 Accuracy analysis

In this section, we will quantify the accuracy of the presented schemes by the form of the leading term in its local truncation error. Appropriate definitions and techniques to analyse the accuracy of a scheme are found, for instance, in [Hir07] and [Hof89].

4.4.1 Accuracy analysis of Kolgan-type schemes

Proposition 4.4.1. *Kolgan scheme* (3.34) *is second-order in space and first-order in time accurate.*

Proof. Computing the truncation error of this scheme we can see that it is second-order in space and first-order in time:

$$\begin{aligned}
\tau_j^n &= \frac{1}{\Delta t}\left(q(x_j,t^{n+1})-q(x_j,t^n)\right)-\frac{\lambda}{2\Delta x}\left(q(x_{j-2},t^n)-4q(x_{j-1},t^n)+3q(x_j,t^n)\right)\\
&= \frac{1}{\Delta t}\left[q(x_j,t^n)+\partial_t q(x_j,t^n)\Delta t+\frac{1}{2}\partial_t^{(2)}q(x_j,t^n)\Delta t^2+\mathcal{O}\left(\Delta t^3\right)-q(x_j,t^n)\right]\\
&\quad -\frac{\lambda}{2\Delta x}\left[\, q(x_j,t^n)-2\partial_x q(x_j,t^n)\Delta x+2\partial_x^{(2)}q(x_j,t^n)\Delta x^2-4q(x_j,t^n)\right.\\
&\quad \left.+4\partial_x q(x_j,t^n)\Delta x-2\partial_x^{(2)}q(x_j,t^n)\Delta x^2+3q(x_j,t^n)+\mathcal{O}\left(\Delta x^3\right)\right]\\
&= \partial_t q(x_j,t^n)+\frac{1}{2}\partial_t^{(2)}q(x_j,t^n)\Delta t+\mathcal{O}\left(\Delta t^2\right)+\lambda\delta_x q(x_j,t^n)+\mathcal{O}\left(\Delta x^2\right)\\
&= \frac{1}{2}\partial_t^{(2)}q(x_j,t^n)\Delta t+\mathcal{O}\left(\Delta t^2\right)+\mathcal{O}\left(\Delta x^2\right)\\
&= \mathcal{O}\left(\Delta t\right)+\mathcal{O}\left(\Delta x^2\right). \qquad (4.79)
\end{aligned}$$

□

Proposition 4.4.2. *The CVC Kolgan-type scheme* (3.36) *is second-order in space and first-order in time.*

Proof. We compute the truncation error of scheme (3.36):

$$\begin{aligned}
\tau_j^n &= \frac{1}{\Delta t}\left(q(x_j,t^{n+1})-q(x_j,t^n)\right)-\frac{\lambda}{2\Delta x}\left(\frac{1}{2}q(x_{j-2},t^n)-3q(x_{j-1},t^n)\right.\\
&\quad \left.+3q(x_j,t^n)-q(x_{j+1},t^n)+\frac{1}{2}q(x_{j+2},t^n)\right)\\
&= \frac{1}{\Delta t}\left(q(x_j,t^n)+\partial_t q(x_j,t^n)\Delta t+\frac{1}{2}\partial_t^{(2)}q(x_j,t^n)\Delta t^2+\mathcal{O}(\Delta t^3)-q(x_j,t^n)\right)\\
&\quad -\frac{\lambda}{2\Delta x}\left[\frac{1}{2}\left(q(x_j,t^n)-\partial_x q(x_j,t^n)\,(2\Delta x)+\frac{1}{2}\partial_x^{(2)}q(x_j,t^n)\,(2\Delta x)^2+\mathcal{O}(\Delta x^3)\right)\right.\\
&\quad -3\left(q(x_j,t^n)-\partial_x q(x_j,t^n)\Delta x+\frac{1}{2}\partial_x^{(2)}q(x_j,t^n)\Delta x^2+\mathcal{O}(\Delta x^3)\right)+3q(x_j,t^n)\\
&\quad -\left(q(x_j,t^n)+\partial_x q(x_j,t^n)\Delta x+\frac{1}{2}\partial_x^{(2)}q(x_j,t^n)\Delta x^2+\mathcal{O}(\Delta x^3)\right)\\
&\quad \left.+\frac{1}{2}\left(q(x_j,t^n)+\partial_x q(x_j,t^n)\,(2\Delta x)+\frac{1}{2}\partial_x^{(2)}q(x_j,t^n)\,(2\Delta x)^2+\mathcal{O}(\Delta x^3)\right)\right]\\
&= \partial_t q(x_j,t^n)+\frac{1}{2}\partial_t^{(2)}q(x_j,t^n)\Delta t+\mathcal{O}(\Delta t^2)-\lambda\partial_x q(x_j,t^n)+\mathcal{O}(\Delta x^2)\\
&= \frac{1}{2}\partial_t^{(2)}q(x_j,t^n)\Delta t+\mathcal{O}(\Delta t^2)+\mathcal{O}(\Delta x^2)\\
&= \mathcal{O}(\Delta t)+\mathcal{O}(\Delta x^2). \qquad (4.80)
\end{aligned}$$

□

Remark 4.4.1. Propositions 4.4.1 and 4.4.2 report the accuracy of branches of Kolgan and CVC Kolgan schemes where no limiters are used. However, each one of the branches has a different order of error. A detailed analysis on the remaining branches is included in Appendix A.

4.4.2 Accuracy analysis of ADER schemes

In this section, the order of accuracy of ADER schemes is analysed. Two distinct cases are studied: the linear advection-reaction equation with constant advection coefficient and the advection-diffusion-reaction equation with time and space dependent diffusion coefficient.

Proposition 4.4.3 (Truncation error of the linear advection-reaction equation)**.** *ADER scheme* (3.77) *is second-order in space and time.*

Proof. Using Taylor series expansion, second-order in space and time can be proved for scheme (3.76) with centred slopes, (3.77):

$$
\begin{aligned}
\tau_j^n \;=\;& \frac{1}{\Delta t}\Big(q(x_j,t^{n+1})-q(x_j,t^n)\Big)+\frac{\lambda}{\Delta x}\Bigg\{\Big(q(x_j,t^n)-q(x_{j-1},t^n)\Big)\\
&+\frac{1}{4}\Big(q(x_{j+1},t^n)-q(x_j,t^n)-q(x_{j-1},t^n)+q(x_{j-2},t^n)\Big)\\
&+\frac{\Delta t}{2}\Bigg[-\frac{\lambda}{2\Delta x}\Big(q(x_{j+1},t^n)-q(x_j,t^n)-q(x_{j-1},t^n)+q(x_{j-2},t^n)\Big)\\
&+\beta\Bigg(\Big(q(x_j,t^n)-q(x_{j-1},t^n)\Big)\\
&+\frac{1}{4}\Big(q(x_{j+1},t^n)-q(x_j,t^n)-q(x_{j-1},t^n)+q(x_{j-2},t^n)\Big)\Bigg)\Bigg]\Bigg\}\\
&-\beta\left[q(x_j,t^n)+\frac{\Delta t}{2}\left(-\frac{\lambda}{2\Delta x}\left(q(x_{j+1},t^n)-q(x_{j-1},t^n)\right)+\beta q(x_j,t^n)\right)\right]\\
=\;& \partial_t q(x_j,t^n)+\lambda\partial_x q(x_j,t^n)-\beta q(x_j,t^n)\\
&+\lambda\left[-\frac{1}{2}\partial_x^{(2)}q(x_j,t^n)\Delta x+\frac{1}{6}\partial_x^{(3)}q(x_j,t^n)\Delta x^2\right.\\
&\left.+\frac{1}{4}\Big(2\partial_x^{(2)}q(x_j,t^n)\Delta x-\partial_x^{(3)}q(x_j,t^n)\Delta x^2\Big)\right]\\
&+\Delta t\left\{\frac{1}{2}\partial_t^{(2)}q(x_j,t^n)+\frac{\lambda}{2}\left[-\frac{\lambda}{2}\Big(2\partial_x^{(2)}q(x_j,t^n)-\partial_x^{(3)}q(x_j,t^n)\Delta x\Big)\right.\right.\\
&+\beta\Big(\partial_x q(x_j,t^n)-\frac{1}{2}\partial_x^{(2)}q(x_j,t^n)\Delta x+\frac{1}{6}\partial_x^{(3)}q(x_j,t^n)\Delta x^2\\
&\left.\left.+\frac{1}{4}\Big(2\partial_x^{(2)}q(x_j,t^n)\Delta x-\partial_x^{(3)}q(x_j,t^n)\Delta x^2\Big)\Big)\right]\\
&-\frac{\beta}{2}\left[-\frac{\lambda}{2\Delta x}\left(2\partial_x q(x_j,t^n)\Delta x+\frac{1}{3}\partial_x^{(3)}q(x_j,t^n)\Delta x^3\right)+\beta q(x_j,t^n)\right]\Bigg\}
\end{aligned}
$$

$$
\begin{aligned}
& +\mathcal{O}\left(\Delta t^2\right)+\mathcal{O}\left(\Delta x^2\right)+\mathcal{O}\left(\Delta x \Delta t\right) \\
= & \frac{\Delta t}{2}\left(\partial_t^{(2)} q(x_j,t^n)-\lambda^2\partial_x^{(2)} q(x_j,t^n)+2\lambda\beta\partial_x q(x_j,t^n)-\beta^2 q(x_j,t^n)\right) \\
& +\mathcal{O}\left(\Delta t^2\right)+\mathcal{O}\left(\Delta x^2\right)+\mathcal{O}(\Delta x \Delta t) \\
= & \mathcal{O}\left(\Delta t^2\right)+\mathcal{O}\left(\Delta x^2\right)+\mathcal{O}(\Delta x \Delta t). \qquad (4.81)
\end{aligned}
$$

The last equality arises from

$$
\partial_t^{(2)} q(x_j,t^n)-\lambda^2\partial_x^{(2)} q(x_j,t^n)+\lambda\beta\partial_x q(x_j,t^n)=-\lambda\beta\partial_x q(x_j,t^n)-\beta^2 q(x_j,t^n) \qquad (4.82)
$$

which is obtained following the Cauchy-Kovalevskaya procedure. □

Corollary 4.4.4 (Truncation error of the linear advection equation)**.** *ADER scheme for the linear advection equation,* (3.79)*, is second-order in space and time.*

Proposition 4.4.5 (Truncation error of the advection-diffusion-reaction equation)**.** *ADER scheme* (3.73) *is second-order in space and time.*

Proof. The truncation error of the scheme for the advection-diffusion-reaction equation with time and space dependent diffusion coefficient is given by

$$
\begin{aligned}
\tau_j^n = & \frac{1}{\Delta t}\left(q(x_j,t^{n+1})-q(x_j,t^n)\right)+\frac{\lambda}{\Delta x}\Bigg\{\left(q(x_j,t^n)-q(x_{j-1},t^n)\right) \\
& +\frac{1}{4}\left(q(x_{j+1},t^n)-q(x_j,t^n)-q(x_{j-1},t^n)+q(x_{j-2},t^n)\right) \\
& +\frac{\Delta t}{2}\Bigg[-\frac{\lambda}{2\Delta x}\left(q(x_{j+1},t^n)-q(x_j,t^n)-q(x_{j-1},t^n)+q(x_{j-2},t^n)\right) \\
& +\frac{1}{\Delta x}\Bigg[\left(\alpha(x_{j+\frac{1}{2}},t^n)\frac{q(x_{j+1},t^n)-q(x_j,t^n)}{\Delta x}-\alpha(x_{j-\frac{1}{2}},t^n)\frac{q(x_j,t^n)-q(x_{j-1},t^n)}{\Delta x}\right) \\
& -\left(\alpha(x_{j-\frac{1}{2}},t^n)\frac{q(x_j,t^n)-q(x_{j-1},t^n)}{\Delta x}-\alpha(x_{j-\frac{3}{2}},t^n)\frac{q(x_{j-1},t^n)-q(x_{j-2},t^n)}{\Delta x}\right)\Bigg] \\
& +\beta\Bigg(\Big(q(x_j,t^n)-q(x_{j-1},t^n)\Big)+\frac{1}{4}\Big(q(x_{j+1},t^n)-q(x_j,t^n) \\
& -q(x_{j-1},t^n)+q(x_{j-2},t^n)\Big)\Bigg)\Bigg]\Bigg\}-\frac{1}{\Delta x^2}\Bigg\{\overline{\alpha}(x_{j+\frac{1}{2}},t^n)\Bigg[q(x_{j+1},t^n)-q(x_j,t^n) \\
& +\frac{\Delta t}{2}\Bigg(-\lambda\left(q(x_{j+2},t^n)-2q(x_{j+1},t^n)+q(x_j,t^n)\right)+\frac{1}{\Delta x^2}\alpha(x_{j+\frac{3}{2}},t^n) \\
& \left(q(x_{j+2},t^n)-q(x_{j+1},t^n)\right)-\frac{1}{\Delta x^2}\alpha(x_{j+\frac{1}{2}},t^n)\left(2q(x_{j+1},t^n)-2q(x_j,t^n)\right) \\
& +\frac{1}{\Delta x^2}\alpha(x_{j-\frac{1}{2}},t^n)\left(q(x_j,t^n)-q(x_{j-1},t^n)\right)+\beta\left(q(x_{j+1},t^n)-q(x_j,t^n)\right)\Bigg)\Bigg]
\end{aligned}
$$

$$
\begin{aligned}
&+ \overline{\alpha}(x_{j-\frac{1}{2}}, t^n)\left[q(x_{j-1}, t^n) - q(x_j, t^n) + \frac{\Delta t}{2}\left(- \lambda\left(-q(x_{j+1}, t^n) + 2q(x_j, t^n)\right.\right.\right.\\
&- \left.\left.\left. q(x_{j-1}, t^n)\right) - \frac{1}{\Delta x^2}\alpha(x_{j+\frac{1}{2}}, t^n)\left(q(x_{j+1}, t^n) - q(x_j, t^n)\right)\right.\right.\\
&+ \left.\left.\frac{1}{\Delta x^2}\alpha(x_{j-\frac{1}{2}}, t^n)\left(2q(x_j, t^n) - 2q(x_{j-1}, t^n)\right) - \frac{1}{\Delta x^2}\alpha(x_{j-\frac{3}{2}}, t^n)\left(q(x_{j-1}, t^n)\right.\right.\right.\\
&- \left.\left.\left. q(x_{j-2}, t^n)\right) + \beta\left(q(x_{j-1}, t^n) - q(x_j, t^n)\right)\right)\right]\Bigg\}\\
&-\beta\left\{q(x_j, t^n) + \frac{\Delta t}{2}\left[-\frac{\lambda}{2\Delta x}\left(q(x_{j+1}, t^n) - q(x_{j-1}, t^n)\right)\right.\right.\\
&+ \frac{1}{\Delta x^2}\left(\alpha(x_{j+\frac{1}{2}}, t^n)\left(q(x_{j+1}, t^n) - q(x_j, t^n)\right)\right.\\
&- \left.\left.\left.\alpha(x_{j-\frac{1}{2}}, t^n)\left(q(x_j, t^n) - q(x_{j-1}, t^n)\right)\right) + \frac{\beta}{2}q(x_j, t^n)\right]\right\},
\end{aligned}
\tag{4.83}
$$

where

$$
\overline{\alpha}(x_{j+\frac{1}{2}}, t^n) = \alpha(x_{j+\frac{1}{2}}, t^n) + \frac{\Delta t}{2}\partial_t\alpha(x_{j+\frac{1}{2}}, t^n), \tag{4.84}
$$

$$
\overline{\alpha}(x_{j-\frac{1}{2}}, t^n) = \alpha(x_{j-\frac{1}{2}}, t^n) + \frac{\Delta t}{2}\partial_t\alpha(x_{j-\frac{1}{2}}, t^n). \tag{4.85}
$$

Then, we can proceed analysing the terms that depend on the diffusion term one by one:

- Local truncation error contribution of the diffusion term to the flux term:

$$
\begin{aligned}
&\frac{\lambda\Delta t}{2\Delta x^2}\left\{\left[\alpha(x_{j+\frac{1}{2}}, t^n)\frac{q(x_{j+1}, t^n) - q(x_j, t^n)}{\Delta x} - \alpha(x_{j-\frac{1}{2}}, t^n)\frac{q(x_j, t^n) - q(x_{j-1}, t^n)}{\Delta x}\right]\right.\\
&\left. - \left[\alpha(x_{j-\frac{1}{2}}, t^n)\frac{q(x_j, t^n) - q(x_{j-1}, t^n)}{\Delta x} - \alpha(x_{j-\frac{3}{2}}, t^n)\frac{q(x_{j-1}, t^n) - q(x_{j-2}, t^n)}{\Delta x}\right]\right\}\\
= \;& \frac{\lambda\Delta t}{2\Delta x^3}\left\{\left[\alpha(x_{j+\frac{1}{2}}, t^n)\left(q(x_j, t^n) + \partial_x q(x_j, t^n)\Delta x + \frac{1}{2}\partial^{(2)}q(x_j, t^n)\Delta x^2\right.\right.\right.\\
&+ \left.\left.\left.\frac{1}{6}\partial^{(3)}q(x_j, t^n)\Delta x^3 + \mathcal{O}(\Delta x^4) - q(x_j, t^n)\right) - \alpha(x_{j-\frac{1}{2}}, t^n)\left(q(x_j, t^n) - q(x_j, t^n)\right.\right.\right.\\
&+ \left.\left.\left.\partial_x q(x_j, t^n)\Delta x - \frac{1}{2}\partial^{(2)}q(x_j, t^n)\Delta x^2 + \frac{1}{6}\partial^{(3)}q(x_j, t^n)\Delta x^3 + \mathcal{O}(\Delta x^4)\right)\right]\right.\\
&- \left[\alpha(x_{j-\frac{1}{2}}, t^n)\left(q(x_j, t^n) - q(x_j, t^n) + \partial_x q(x_j, t^n)\Delta x - \frac{1}{2}\partial^{(2)}q(x_j, t^n)\Delta x^2\right.\right.\\
&+ \left.\left.\frac{1}{6}\partial^{(3)}q(x_j, t^n)\Delta x^3 + \mathcal{O}(\Delta x^4)\right) - \alpha(x_{j-\frac{3}{2}}, t^n)\left(q(x_j, t^n) - \partial_x q(x_j, t^n)\Delta x\right.\right.\\
&+ \left.\left.\frac{1}{2}\partial^{(2)}q(x_j, t^n)\Delta x^2 - \frac{1}{6}\partial^{(3)}q(x_j, t^n)\Delta x^3 + \mathcal{O}(\Delta x^4) - q(x_j, t^n)\right.\right.\\
&+ \left.\left.\left.2\partial_x q(x_j, t^n)\Delta x - 2\partial^{(2)}q(x_j, t^n)\Delta x^2 + \frac{4}{3}\partial^{(3)}q(x_j, t^n)\Delta x^3 + \mathcal{O}(\Delta x^4)\right)\right]\right\}
\end{aligned}
$$

$$
\begin{aligned}
&= \frac{\lambda\Delta t}{2\Delta x^2}\Big\{\partial_x q(x_j,t^n)\left[\alpha(x_{j+\frac{1}{2}},t^n)-2\alpha(x_{j-\frac{1}{2}},t^n)+\alpha(x_{j-\frac{3}{2}},t^n)\right]\\
&\quad+\frac{1}{2}\partial_x^{(2)}q(x_j,t^n)\Delta x\left[\alpha(x_{j+\frac{1}{2}},t^n)+2\alpha(x_{j-\frac{1}{2}},t^n)-3\alpha(x_{j-\frac{3}{2}},t^n)\right]\\
&\quad+\frac{1}{6}\partial_x^{(3)}q(x_j,t^n)\Delta x^2\left[\alpha(x_{j+\frac{1}{2}},t^n)-2\alpha(x_{j-\frac{1}{2}},t^n)+7\alpha(x_{j-\frac{3}{2}},t^n)\right]+\mathcal{O}(\Delta x^4)\Big\}\\
&= \frac{\lambda\Delta t}{2}\Big[\partial_x q(x_j,t^n)\partial_x^{(2)}\alpha(x_j,t^n)+2\partial_x^{(2)}q(x_j,t^n)\partial_x\alpha(x_j,t^n)\\
&\quad+\partial_x^{(3)}q(x_j,t^n)\alpha(x_j,t^n)+\mathcal{O}(\Delta x)\Big]\\
&= \frac{\lambda\Delta t}{2}\partial_x\left[\partial_x\left(\alpha(x_j,t^n)\partial_x q(x_j,t^n)\right)\right]+\mathcal{O}(\Delta x\Delta t). \qquad (4.86)
\end{aligned}
$$

- Local truncation error contribution of the diffusion term:

$$
\begin{aligned}
&-\frac{1}{\Delta x^2}\Big\{\overline{\alpha}(x_{j+\frac{1}{2}},t^n)\Big[q(x_{j+1},t^n)-q(x_j,t^n)\\
&+\frac{\Delta t}{2}\Big(-\lambda\Big(q(x_{j+2},t^n)-2q(x_{j+1},t^n)+q(x_j,t^n)\Big)\\
&+\frac{1}{\Delta x^2}\alpha(x_{j+\frac{3}{2}},t^n)\Big(q(x_{j+2},t^n)-q(x_{j+1},t^n)\Big)\\
&-\frac{1}{\Delta x^2}\alpha(x_{j+\frac{1}{2}},t^n)\Big(2q(x_{j+1},t^n)-2q(x_j,t^n)\Big)\\
&+\frac{1}{\Delta x^2}\alpha(x_{j-\frac{1}{2}},t^n)\Big(q(x_j,t^n)-q(x_{j-1},t^n)\Big)+\beta\Big(q(x_{j+1},t^n)-q(x_j,t^n)\Big)\Big)\Big]\\
&+\overline{\alpha}(x_{j-\frac{1}{2}},t^n)\Big[q(x_{j-1},t^n)-q(x_j,t^n)\\
&+\frac{\Delta t}{2}\Big(-\lambda\Big(-q(x_{j+1},t^n)+2q(x_j,t^n)-q(x_{j-1},t^n)\Big)\\
&-\frac{1}{\Delta x^2}\alpha(x_{j+\frac{1}{2}},t^n)\Big(q(x_{j+1},t^n)-q(x_j,t^n)\Big)\\
&+\frac{1}{\Delta x^2}\alpha(x_{j-\frac{1}{2}},t^n)\Big(2q(x_j,t^n)-2q(x_{j-1},t^n)\Big)\\
&-\frac{1}{\Delta x^2}\alpha(x_{j-\frac{3}{2}},t^n)\Big(q(x_{j-1},t^n)-q(x_{j-2},t^n)\Big)+\beta\Big(q(x_{j-1},t^n)-q(x_j,t^n)\Big)\Big)\Big]\Big\}\\
&= -\left[\partial_x\overline{\alpha}(x_j,t^n)\right)\left(\partial_x q(x_j,t^n)\right]-\frac{\overline{\alpha}(x_{j+1},t^n)+\overline{\alpha}(x_{j-1},t^n)}{2}\partial_x^{(2)}q(x_j,t^n)\\
&-\lambda\frac{\Delta t}{2}\left(\partial_x\overline{\alpha}(x_j,t^n)\right)\left(\partial_x^{(2)}q(x_j,t^n)\right)+\lambda\frac{\Delta t}{2}\overline{\alpha}(x_j,t^n)\left(\partial_x^{(3)}q(x_j,t^n)\right)\\
&-\frac{\Delta t}{2}\Big[\left(\partial_x q(x_j,t^n)\right)\left(\partial_x^{(2)}\alpha(x_j,t^n)\right)\left(\partial_x\overline{\alpha}(x_j,t^n)\right)\\
&+\overline{\alpha}(x_j,t^n)\left(\partial_x q(x_j,t^n)\right)\left(\partial_x^{(3)}\alpha(x_j,t^n)\right)\\
&+2\left(\partial_x\overline{\alpha}(x_j,t^n)\right)\left(\partial_x^{(2)}q(x_j,t^n)\right)\left(\partial_x\alpha(x_j,t^n)\right)
\end{aligned}
$$

$$
\begin{aligned}
&+ 3\overline{\alpha}(x_j,t^n)\left(\partial_x^{(2)}q(x_j,t^n)\right)\left(\partial_x^{(2)}\alpha(x_j,t^n)\right)\\
&+ \left(\partial_x\overline{\alpha}(x_j,t^n)\right)\left(\partial_x^{(3)}q(x_j,t^n)\right)\alpha(x_j,t^n)\\
&+ 3\overline{\alpha}(x_j,t^n)\left(\partial_x^{(3)}q(x_j,t^n)\right)\left(\partial_x\alpha(x_j,t^n)\right)\\
&+ \overline{\alpha}(x_j,t^n)\left(\partial_x^{(4)}q(x_j,t^n)\right)\alpha(x_j,t^n)\Big] - \beta\frac{\Delta t}{2}\Big[\left(\partial_x\overline{\alpha}(x_j,t^n)\right)\left(\partial_x q(x_j,t^n)\right)\\
&+ \overline{\alpha}(x_j,t^n)\left(\partial_x^{(2)}q(x_j,t^n)\right)\Big] + \mathcal{O}(\Delta x^2) + \mathcal{O}(\Delta x\Delta t)\\
= \;& -\partial_x\left(\alpha(x_j,t^n)\partial_x q(x_j,t^n)\right) + \frac{\Delta t}{2}\Big\{\partial_x\left(\partial_t\alpha(x_j,t^n)\partial_x q(x_j,t^n)\right)\\
&- \lambda\partial_x\left(\alpha(x_j,t^n)\partial_x^{(2)}q(x_j,t^n)\right) + \partial_x\left[\alpha(x_j,t^n)\partial_x^{(2)}\left(\alpha(x_j,t^n)\partial_x q(x_j,t^n)\right)\right]\\
&+ \beta\partial_x\left(\alpha(x_j,t^n)\partial_x q(x_j,t^n)\right)\Big\} + \mathcal{O}(\Delta x^2) + \mathcal{O}(\Delta x\Delta t). \qquad (4.87)
\end{aligned}
$$

- Local truncation error contribution of the diffusion term to the source term:

$$
\begin{aligned}
&-\frac{\beta\Delta t}{2\Delta x^2}\left\{\alpha(x_{j+\frac{1}{2}},t^n)\left[q(x_{j+1},t^n)-q(x_j,t^n)\right] - \alpha(x_{j-\frac{1}{2}},t^n)\left[q(x_j,t^n)-q(x_{j-1},t^n)\right]\right\}\\
= \;& -\frac{\beta\Delta t}{2\Delta x^2}\Big[\alpha(x_{j+\frac{1}{2}},t^n)\Big(q(x_j,t^n)+\partial_x q(x_j,t^n)\Delta x + \frac{1}{2}\partial^{(2)}q(x_j,t^n)\Delta x^2\\
&+ \frac{1}{6}\partial^{(3)}q(x_j,t^n)\Delta x^3 + \mathcal{O}(\Delta x^4) - q(x_j,t^n)\Big) - \alpha(x_{j-\frac{1}{2}},t^n)\Big(q(x_j,t^n) - q(x_j,t^n)\\
&- \partial_x q(x_j,t^n)\Delta x + \frac{1}{2}\partial^{(2)}q(x_j,t^n)\Delta x^2 - \frac{1}{6}\partial^{(3)}q(x_j,t^n)\Delta x^3 + \mathcal{O}(\Delta x^4)\Big)\Big]\\
= \;& -\frac{\beta\Delta t}{2\Delta x}\Big[\partial_x q(x_j,t^n)\left(\alpha(x_{j+\frac{1}{2}},t^n) - \alpha(x_{j-\frac{1}{2}},t^n)\right)\\
&+ \frac{1}{2}\partial_x^{(2)}q(x_j,t^n)\Delta x\left(\alpha(x_{j+\frac{1}{2}},t^n) + \alpha(x_{j-\frac{1}{2}},t^n)\right)\\
&+ \frac{1}{6}\partial_x^{(3)}q(x_j,t^n)\Delta x^2\left(\alpha(x_{j+\frac{1}{2}},t^n) - \alpha(x_{j-\frac{1}{2}},t^n)\right) + \mathcal{O}(\Delta x^3)\Big]\\
= \;& -\frac{\beta\Delta t}{2}\partial_x\left(\alpha(x_j,t^n)\partial_x q(x_j,t^n)\right) + \mathcal{O}(\Delta x^2) + \mathcal{O}(\Delta x\Delta t). \qquad (4.88)
\end{aligned}
$$

Gathering together the previous terms and the already obtained for the linear advection-reaction equation (4.4.2), we get

$$
\begin{aligned}
\tau^n \;=\;& \partial_t q(x_j,t^n) + \lambda\partial_x q(x_j,t^n) - \partial_x\left[\alpha(x_j,t^n)\partial_x q(x_j,t^n)\right] - \beta q(x_j,t^n)\\
&+\frac{\Delta t}{2}\Big[\partial_t^{(2)}q(x_j,t^n) + \lambda\partial_x\left[-\lambda\partial_x q(x_j,t^n) + \beta q(x_j,t^n)\right]\\
&- \beta\left[-\lambda\partial_x q(x_j,t^n) + \beta q(x_j,t^n)\right]\Big] - \frac{\Delta t}{2}\Big\{\partial_x\left[\partial_t\alpha(x_j,t^n)\partial_x q(x_j,t^n)\right]
\end{aligned}
$$

$$
\begin{aligned}
&- \lambda\partial_x\left[\alpha(x_j,t^n)\partial_x^{(2)}q(x_j,t^n)\right] + \partial_x\left\{\alpha(x_j,t^n)\partial_x^{(2)}\left[\alpha(x_j,t^n)\partial_x q(x_j,t^n)\right]\right\} \\
&+ \beta\partial_x\left[\alpha(x_j,t^n)\partial_x q(x_j,t^n)\right]\Bigg\} - \frac{\beta\Delta t}{2}\partial_x\left[\alpha(x_j,t^n)\partial_x q(x_j,t^n)\right] \\
&+\frac{\Delta t}{2}\partial_x^{(2)}\left[\alpha(x_j,t^n)\partial_x q(x_j,t^n)\right] + \mathcal{O}\left(\Delta t^2\right) + \mathcal{O}\left(\Delta x^2\right) + \mathcal{O}\left(\Delta x\Delta t\right) \\
= \;& \mathcal{O}\left(\Delta t^2\right) + \mathcal{O}\left(\Delta x^2\right) + \mathcal{O}(\Delta x\Delta t), \qquad (4.89)
\end{aligned}
$$

where we have taken into account that, following Cauchy-Kovalevskaya,

$$
\begin{aligned}
\partial_t^{(2)}q - \lambda^2\partial_x^{(2)}q - \partial_x\left[\alpha\partial_x^{(2)}\left(\alpha\partial_x q\right)\right] - \beta^2 q + 2\lambda\beta\partial_x q - 2\beta\partial_x\left(\alpha\partial_x q\right) \\
-\partial_x\left[\left(\partial_t\alpha\right)\left(\partial_x q\right)\right] + \lambda\partial_x^{(2)}\left(\alpha\partial_x q\right) + \lambda\partial_x\left(\alpha\partial_x^{(2)}q\right) = 0. \qquad (4.90)
\end{aligned}
$$

Thus, we conclude that the scheme is second-order in space and time.

□

4.4.3 Accuracy analysis of LADER schemes

The last schemes to be analysed are the attained using LADER methodology.

Proposition 4.4.6. *LADER scheme,* (3.105)*, is second-order in space and time.*

Proof. To prove the accuracy of Scheme (3.105), we take into account the analysis carried out for the ADER scheme introduced in the previous section and we detail the terms which have changed:

- Local truncation error contribution of the flux term neglecting the diffusion term contribution:

$$
\begin{aligned}
&\frac{\lambda}{\Delta x}\Bigg[q(x_j,t^n) - (x_{j-1},t^n) + \frac{1}{2}\left(q(x_j,t^n) - 2q(x_{j-1},t^n) + q(x_{j-2},t^n)\right) \\
&- \frac{c}{2}\left(q(x_{j+1},t^n) - 2q(x_j,t^n) + q(x_{j-1},t^n)\right)\Bigg] \\
= \;& \frac{\lambda}{\Delta x}\Bigg\{\partial_x q(x_j,t^n)\Delta x - \frac{1}{2}\partial_x^{(2)}q(x_j,t^n)\Delta x^2 + \frac{1}{6}\partial_x^{(3)}q(x_j,t^n)\Delta x^3 + \mathcal{O}\left(\Delta x^4\right) \\
&+ \frac{1}{2}\left[\partial_x^{(2)}q(x_j,t^n)\Delta x^2 - \partial_x^{(3)}q(x_j,t^n)\Delta x^3 + \mathcal{O}\left(\Delta x^4\right)\right] \\
&- \frac{c}{2}\left[\partial_x^{(2)}q(x_j,t^n)\Delta x^2 - \frac{1}{12}\partial_x^{(4)}q(x_j,t^n)\Delta x^4 + \mathcal{O}\left(\Delta x^5\right)\right]\Bigg\} \\
= \;& \lambda\partial_x q(x_j,t^n) - \frac{\lambda^2\Delta t}{2}\partial_x^{(2)}q(x_j,t^n) + \mathcal{O}\left(\Delta x^2\right). \qquad (4.91)
\end{aligned}
$$

- Local truncation error contribution of the diffusion term to the flux term:

$$
\begin{aligned}
&\frac{\lambda\Delta t}{2\Delta x^2}\left\{\left[\alpha(x_{j+1},t^n)\frac{q(x_{j+2},t^n)-q(x_{j+1},t^n)}{\Delta x}-\alpha(x_j,t^n)\frac{q(x_j,t^n)-q(x_{j-1},t^n)}{\Delta x}\right]\right.\\
&\left.-\left[\alpha(x_j,t^n)\frac{q(x_{j+1},t^n)-q(x_j,t^n)}{\Delta x}-\alpha(x_{j-1},t^n)\frac{q(x_{j-1},t^n)-q(x_{j-2},t^n)}{\Delta x}\right]\right\}\\
=\;&\frac{\lambda\Delta t}{2\Delta x^3}\left\{\alpha(x_{j+1},t^n)\left[\partial_x q(x_j,t^n)\Delta x+\frac{3}{2}\partial_x^{(2)}q(x_j,t^n)\Delta x^2\right.\right.\\
&\left.+\frac{7}{6}\partial_x^{(3)}q(x_j,t^n)\Delta x^3+\mathcal{O}(\Delta x^4)\right]-\alpha(x_j,t^n)\left[2\partial_x q(x_j,t^n)\Delta x\right.\\
&\left.\left.+\frac{1}{3}\partial_x^{(3)}q(x_j,t^n)\Delta x^3+\mathcal{O}(\Delta x^4)\right)\right]+\alpha(x_{j-1},t^n)\left[\partial_x q(x_j,t^n)\Delta x\right.\\
&\left.-\frac{3}{2}\partial^{(2)}q(x_j,t^n)\Delta x^2+\frac{7}{6}\partial^{(3)}q(x_j,t^n)\Delta x^3+\mathcal{O}(\Delta x^4)\right]\\
=\;&\frac{\lambda\Delta t}{2\Delta x^3}\left[\partial_x^{(2)}\alpha(x_j,t^n)\partial_x q(x_j,t^n)\Delta x^3+3\partial_x\alpha_i^n\partial_x^{(2)}q(x_j,t^n)\Delta x^3\right.\\
&\left.+2\alpha_i^n\partial_x^{(3)}q(x_j,t^n)\Delta x^3+\mathcal{O}\left(\Delta x^4\right)\right]\\
=\;&\frac{\lambda\Delta t}{2}\left[\partial_x^{(2)}\left(\alpha(x_j,t^n)\partial_x q(x_j,t^n)\right)+\partial_x\left(\alpha(x_j,t^n)\partial_x^{(2)}q(x_j,t^n)\right)\right]+\mathcal{O}(\Delta x\Delta t). \quad (4.92)
\end{aligned}
$$

- Local truncation error contribution of the diffusion term:

$$
\begin{aligned}
&-\frac{1}{\Delta x^2}\left\{\overline{\alpha}(x_{j+\frac{1}{2}},t^n)\left[q(x_{j+1},t^n)-q(x_j,t^n)+\frac{\Delta t}{2}\left(\frac{1}{\Delta x^2}\alpha(x_{j+\frac{3}{2}},t^n)\right.\right.\right.\\
&\left[q(x_{j+2},t^n)-q(x_{j+1},t^n)\right]-\frac{1}{\Delta x^2}\alpha(x_{j+\frac{1}{2}},t^n)\left[2q(x_{j+1},t^n)-2q(x_j,t^n)\right]\\
&\left.\left.+\frac{1}{\Delta x^2}\alpha(x_{j-\frac{1}{2}},t^n)\left[q(x_j,t^n)-q(x_{j-1},t^n)\right]+\beta\left[q(x_{j+1},t^n)-q(x_j,t^n)\right]\right)\right]\\
&+\overline{\alpha}(x_{j-\frac{1}{2}},t^n)\left[\;q(x_{j-1},t^n)-q(x_j,t^n)+\frac{\Delta t}{2}\left(-\frac{1}{\Delta x^2}\alpha(x_{j+\frac{1}{2}},t^n)\right.\right.\\
&\left[q(x_{j+1},t^n)-q(x_j,t^n)\right]+\frac{1}{\Delta x^2}\alpha(x_{j-\frac{1}{2}},t^n)\left[2q(x_j,t^n)-2q(x_{j-1},t^n)\right]\\
&\left.\left.\left.-\frac{1}{\Delta x^2}\alpha(x_{j-\frac{3}{2}},t^n)\left[q(x_{j-1},t^n)-q(x_{j-2},t^n)\right]+\beta\left[q(x_{j-1},t^n)-q(x_j,t^n)\right]\right)\right]\right\}\\
=\;&-\partial_x\left(\alpha(x_j,t^n)\partial_x q(x_j,t^n)\right)+\frac{\Delta t}{2}\left\{\partial_x\left(\partial_t\alpha(x_j,t^n)\partial_x q(x_j,t^n)\right)\right.\\
&+\partial_x\left[\alpha(x_j,t^n)\partial_x^{(2)}\left(\alpha(x_j,t^n)\partial_x q(x_j,t^n)\right)\right]\\
&\left.+\beta\partial_x\left(\alpha(x_j,t^n)\partial_x q(x_j,t^n)\right)\right\}+\mathcal{O}(\Delta x^2)+\mathcal{O}(\Delta x\Delta t). \quad (4.93)
\end{aligned}
$$

Finally, taking into account the truncation error of the remaining terms of the scheme and Cauchy-Kovalevskaya equality, we get

$$
\tau_j^n = \partial_t q(x_j,t^n)+\lambda\partial_x q(x_j,t^n)-\partial_x\left[\alpha(x_j,t^n)\partial_x q(x_j,t^n)\right]-\beta q(x_j,t^n)
$$

$$
\begin{aligned}
&+\frac{\Delta t}{2}\Big\{\partial_t^{(2)}q(x_j,t^n)+\lambda\partial_x\left[-\lambda\partial_x q(x_j,t^n)+\beta q(x_j,t^n)\right]\\
&-\beta\left[-\lambda\partial_x q(x_j,t^n)+\beta q(x_j,t^n)\right]-\partial_x\left[\partial_t\alpha(x_j,t^n)\partial_x q(x_j,t^n)\right]\\
&+\lambda\partial_x\left[\alpha(x_j,t^n)\partial_x^{(2)}q(x_j,t^n)\right]-\partial_x\left\{\alpha(x_j,t^n)\partial_x^{(2)}\left[\alpha(x_j,t^n)\partial_x q(x_j,t^n)\right]\right\}\\
&-\beta\partial_x\left[\alpha(x_j,t^n)\partial_x q(x_j,t^n)\right]-\beta\partial_x\left[\alpha(x_j,t^n)\partial_x q(x_j,t^n)\right]\\
&+\partial_x^{(2)}\left[\alpha(x_j,t^n)\partial_x q(x_j,t^n)\right]\Big\}+\mathcal{O}\left(\Delta t^2\right)+\mathcal{O}\left(\Delta x^2\right)+\mathcal{O}\left(\Delta x\Delta t\right)\\
=\;&\mathcal{O}\left(\Delta t^2\right)+\mathcal{O}\left(\Delta x^2\right)+\mathcal{O}(\Delta x\Delta t). \qquad (4.94)
\end{aligned}
$$

□

Corollary 4.4.7. *LADER scheme for the linear advection-reaction equation,* (3.107)*, is second-order in space and time.*

Corollary 4.4.8. *LADER scheme for the linear advection equation,* (3.108)*, is second-order in space and time.*

Proposition 4.4.9. *LADER scheme for the advection equation with time and space dependent advection coefficient,* (3.127)*, is of second-order in space and time.*

Proof. We start by computing the local truncation error related to $\overline{\lambda_{jR}^n}\overline{q_{jR}^n}+\overline{\lambda_{j+1L}^n}\overline{q_{j+1L}^n}$;

$$
\begin{aligned}
&2\lambda(x_j,t^n)q(x_j,t^n)+\partial_x\left(\lambda(x_j,t^n)q(x_j,t^n)\right)\Delta x\\
&+\frac{(\Delta x)^2}{2}\left(-\lambda(x_j,t^n)\partial_x^2 q(x_j,t^n)-q(x_j,t^n)\partial_x^2\lambda(x_j,t^n)+\partial_x\lambda(x_j,t^n)\partial_x q(x_j,t^n)\right)\\
&-\Delta t\left[\lambda(x_j,t^n)\partial_x\left(\lambda(x_j,t^n)q(x_j,t^n)\right)-q(x_j,t^n)\partial_t\lambda(x_{j+\frac{1}{2}},t^n)\right]\\
&-\frac{\Delta t\Delta x}{2}\left[\lambda(x_j,t^n)\partial_x^{(2)}\left(\lambda(x_j,t^n)q(x_j,t^n)\right)+\partial_x\lambda(x_j,t^n)\partial_x\left(\lambda(x_j,t^n)q(x_j,t^n)\right)\right.\\
&\left.-\partial_t\lambda(x_{j+\frac{1}{2}},t^n)\partial_x q(x_j,t^n)\right]-\frac{(\Delta t)^2}{2}\partial_t\lambda(x_{j+\frac{1}{2}},t^n)\partial_x\left(\lambda(x_j,t^n)q(x_j,t^n)\right)+\mathcal{O}(\Delta x^3).
\end{aligned}
$$

Similarly, the local truncation error of $\overline{\lambda_{j-1R}^n}\overline{q_{j-1R}^n}+\overline{\lambda_{jL}^n}\overline{q_{jL}^n}$ results

$$
\begin{aligned}
&2\lambda(x_j,t^n)q(x_j,t^n)-\partial_x\left(\lambda(x_j,t^n)q(x_j,t^n)\right)\Delta x\\
&+\frac{(\Delta x)^2}{2}\left(-\lambda(x_j,t^n)\partial_x^2 q(x_j,t^n)-q(x_j,t^n)\partial_x^2\lambda(x_j,t^n)+\partial_x\lambda(x_j,t^n)\partial_x q(x_j,t^n)\right)\\
&-\Delta t\left[\lambda(x_j,t^n)\partial_x\left(\lambda(x_j,t^n)q(x_j,t^n)\right)-q(x_j,t^n)\partial_t\lambda(x_{j-\frac{1}{2}},t^n)\right]\\
&+\frac{\Delta t\Delta x}{2}\left[\lambda(x_j,t^n)\partial_x^{(2)}\left(\lambda(x_j,t^n)q(x_j,t^n)\right)+\partial_x\lambda(x_j,t^n)\partial_x\left(\lambda(x_j,t^n)q(x_j,t^n)\right)\right.\\
&\left.-\partial_t\lambda(x_{j-\frac{1}{2}},t^n)\partial_x q(x_j,t^n)\right]-\frac{(\Delta t)^2}{2}\partial_t\lambda(x_{j-\frac{1}{2}},t^n)\partial_x\left(\lambda(x_j,t^n)q(x_j,t^n)\right)+\mathcal{O}(\Delta x^3).
\end{aligned}
$$

Finally, it is verified that $\alpha^n_{RS,\,i+\frac{1}{2}}\left(\overline{q^n_{j+1L}}-\overline{q^n_{jR}}\right)$, $\alpha^n_{RS,\,i-\frac{1}{2}}\left(\overline{q^n_{jL}}-\overline{q^n_{j-1R}}\right)$, $\overline{q^n_{j+\frac{1}{2}}}\left(\overline{\lambda^n_{j+1L}}-\overline{\lambda^n_{jR}}\right)$ and $\overline{q^n_{j-\frac{1}{2}}}\left(\overline{\lambda^n_{jL}}-\overline{\lambda^n_{j-1R}}\right)$ have a local truncation error of $\mathcal{O}(\Delta x^3)$. Then,

$$\begin{aligned}\tau^n =& \partial_t q(x_j,t^n)+\partial_x\left(q(x_j,t^n)\lambda(x_j,t^n)\right)+\frac{\Delta t}{2\Delta x}q(x_j,t^n)\left(\partial_t\lambda(x_{j+\frac{1}{2}},t^n)-\partial_t\lambda(x_{j-\frac{1}{2}},t^n)\right)\\ &+\frac{\Delta t}{2}\partial_t^{(2)}q(x_j,t^n)+\frac{\Delta t}{4}\left(\partial_t\lambda(x_{j+\frac{1}{2}},t^n)+\partial_t\lambda(x_{j-\frac{1}{2}},t^n)\right)\partial_x q(x_j,t^n)\\ &-\frac{\Delta t}{2}\left[\lambda(x_j,t^n)\partial_x^{(2)}\left(\lambda(x_j,t^n)q(x_j,t^n)\right)+\partial_x\lambda(x_j,t^n)\partial_x\left(\lambda(x_j,t^n)q(x_j,t^n)\right)\right]\\ &+\mathcal{O}\left(\Delta x^2\right)+\mathcal{O}\left(\Delta t^2\right)+\mathcal{O}\left(\Delta t\Delta x\right). \end{aligned} \tag{4.95}$$

Moreover, applying the Taylor series expansion in space of $\lambda(x_{j+\frac{1}{2}},t^n)$ and $\lambda(x_{j-\frac{1}{2}},t^n)$ we obtain

$$\begin{aligned}&\frac{\Delta t}{2\Delta x}q(x_j,t^n)\left(\partial_t\lambda(x_{j+\frac{1}{2}},t^n)-\partial_t\lambda(x_{j-\frac{1}{2}},t^n)\right)=\frac{\Delta t}{2}q(x_j,t^n)\partial_t\left(\partial_x\lambda(x_j,t^n)\right)+\mathcal{O}\left(\Delta x\Delta t\right),\\ &\frac{\Delta t}{4}\left(\partial_t\lambda(x_{j+\frac{1}{2}},t^n)+\partial_t\lambda(x_{j-\frac{1}{2}},t^n)\right)\partial_x q(x_j,t^n)=\frac{\Delta t}{2}\partial_t\lambda(x_j,t^n)\partial_x q(x_j,t^n)+\mathcal{O}\left(\Delta x\Delta t\right).\end{aligned}$$

Therefore,

$$\begin{aligned}\tau^n =& \partial_t q(x_j,t^n)+\partial_x\left(q(x_j,t^n)\lambda(x_j,t^n)\right)+\frac{\Delta t}{2}\partial_t^{(2)}q(x_j,t^n)\\ &+\frac{\Delta t}{2}q(x_j,t^n)\partial_t\left(\partial_x\lambda(x_j,t^n)\right)+\frac{\Delta t}{2}\partial_t\lambda(x_j,t^n)\partial_x q(x_j,t^n)\\ &-\frac{\Delta t}{2}\left[\lambda(x_j,t^n)\partial_x^{(2)}\left(\lambda(x_j,t^n)q(x_j,t^n)\right)+\partial_x\lambda(x_j,t^n)\partial_x\left(\lambda(x_j,t^n)q(x_j,t^n)\right)\right]\\ &+\mathcal{O}\left(\Delta x^2\right)+\mathcal{O}\left(\Delta t^2\right)+\mathcal{O}\left(\Delta t\Delta x\right)\\ =&\mathcal{O}\left(\Delta x^2\right)+\mathcal{O}\left(\Delta t^2\right)+\mathcal{O}\left(\Delta t\Delta x\right),\end{aligned} \tag{4.96}$$

where we have taken into account that the time derivative equation (3.110) reads

$$\partial_t^{(2)}q+\partial_x q\partial_t\lambda+q\partial_t\left(\partial_x\lambda\right)-\partial_x\lambda\partial_x\left(\lambda q\right)-\lambda\partial_x^{(2)}\left(\lambda q\right)=0. \tag{4.97}$$

□

Remark 4.4.2. Let us remark that, when applying LADER methodology to the advection equation with space and time dependent advection coefficient, we must consider the extrapolated and evolved values for the two variables involved in equation (3.110), λ and q. Otherwise, the order of the resulting scheme is lower than two.

USC
UNIVERSIDADE
DE SANTIAGO
DE COMPOSTELA

Chapter 5

Numerical results

This chapter is devoted to the empirical convergence rate studies of the numerical methods introduced in Chapter 3.

The error is analysed by computing the norms

$$\mathrm{Err}_{\mathcal{L}^1} = \|q - \hat{q}\|_{l^\infty(\mathcal{L}^1(\Omega))}\,,\ \mathrm{Err}_{\mathcal{L}^2} = \|q - \hat{q}\|_{l^\infty(\mathcal{L}^2(\Omega))}\,,\ \mathrm{Err}_{\mathcal{L}^\infty} = \|q - \hat{q}\|_{l^\infty(\mathcal{L}^\infty(\Omega))},$$

where $\hat{q}$ denotes the numerical solution and q is whether the exact solution or a reference solution computed for a refined mesh if the problem does not have an analytical solution.

The outline of this chapter is as follows. We start by analysing two different test problems for the advection-reaction equation. Kolgan, CVC Kolgan-type, ADER, ADER-ENO, LADER and LADER-ENO methodologies are compared. Next, another two tests are posed for the advection-diffusion-reaction equation and the results for ADER and LADER schemes are presented. Indeed, a diffusion problem with a time and space dependent diffusion coefficient is studied using ADER and LADER. Finally, LADER methodology is proven useful to solve the advection-reaction equation with variable advection coefficients and the advection-diffusion-reaction equation with time and space dependent advection and diffusion coefficients.

5.1 Test 1. Advection-reaction equation

Here we asses the performance of the developed methods for the advection-reaction equation. Two test cases are presented, both considering Dirichlet boundary conditions. The exact solution is imposed at the boundary nodes and for the computation of the numerical flux at the first node we use a forward approximation of the slope, namely,

$$\Delta_1^n = \frac{q_2^n - q_1^n}{\Delta x}. \tag{5.1}$$

An analogous procedure is considered for the last node.

5.1.1 Test 1.1.

The first test problem studied is given by

$$\partial_t q(x,t) + \partial_x q(x,t) = -q(x,t), \quad q(x,0) = e^{-2x^2}, \tag{5.2}$$

with exact solution

$$q(x,t) = e^{-2(x-\lambda t)^2+\beta t}. \tag{5.3}$$

To run the simulation, seven structured meshes were built in the computational domain $\Omega = [0,2]$. The time interval is set to $[0,1]$.

We first analyse the results obtained for Kolgan and CVC Kolgan-type schemes. To determine the time step we have considered $c_M = 0.5$, $r_m = -1$ for the Kolgan scheme and $c_M = 0.25$, $r_m = -1$ for the CVC Kolgan-type scheme. The errors and orders obtained are reported in Tables 5.1 and 5.2. We observe that the errors made when using the CVC Kolgan-type scheme are lower than the ones of Kolgan scheme. Whereas, the order of CVC seems to be a little bit lower than that of Kolgan. In both cases first-order is reached. Despite a higher order can be initially expected, the time dependency of the solution jointly with the need of limiters justify a decrease on the accuracy.

Cells	$\mathrm{Err}_{\mathcal{L}^1}$	$\mathcal{O}_{\mathcal{L}^1}$	$\mathrm{Err}_{\mathcal{L}^2}$	$\mathcal{O}_{\mathcal{L}^2}$	$\mathrm{Err}_{\mathcal{L}^\infty}$	$\mathcal{O}_{\mathcal{L}^\infty}$
8	$2.45e-02$		$3.34e-02$		$6.28e-02$	
16	$2.87e-02$	-0.23	$3.48e-02$	-0.06	$7.23e-02$	-0.20
32	$1.71e-02$	0.74	$1.92e-02$	0.86	$4.37e-02$	0.73
64	$8.73e-03$	0.97	$9.10e-03$	1.08	$2.14e-02$	1.03
128	$4.26e-03$	1.03	$4.31e-03$	1.08	$1.02e-02$	1.06
256	$2.12e-03$	1.01	$2.06e-03$	1.06	$4.82e-03$	1.09
512	$1.06e-03$	0.99	$1.00e-03$	1.04	$2.29e-03$	1.08

Table 5.1: Test 1.1. Errors and convergence rates obtained using Kolgan scheme. $r = -\Delta t$. $\Omega = [0,2]$, $t_{\text{end}} = 1$, $c = c_M = 0.5$.

When looking for a better approximation of the exact solution ADER and LADER methods are applied. The time step is determined to guarantee that c and r belong to the rectangular cuboid (4.78) defined by $c_M = 1$, $r_m = -1$. Since the time step condition imposed by c_M is lower than the defined by r_m, the values of r are computed following (4.65). The obtained r, errors and order for ADER and LADER schemes are depicted in Tables 5.3 and 5.4, respectively. The attained second-order was theoretically expected. Results also report an important decrease of the errors compared with

the obtained using Kolgan-type schemes. The approximated solutions using the mesh of 32 nodes are portrayed in Figure 5.1.

Cells	$\text{Err}_{\mathcal{L}^1}$	$\mathcal{O}_{\mathcal{L}^1}$	$\text{Err}_{\mathcal{L}^2}$	$\mathcal{O}_{\mathcal{L}^2}$	$\text{Err}_{\mathcal{L}^\infty}$	$\mathcal{O}_{\mathcal{L}^\infty}$
8	$1.12e-02$		$1.38e-02$		$2.32e-02$	
16	$9.70e-03$	0.20	$1.05e-02$	0.39	$1.86e-02$	0.32
32	$7.06e-03$	0.46	$7.45e-03$	0.50	$1.44e-02$	0.37
64	$3.89e-03$	0.86	$3.85e-03$	0.95	$7.78e-03$	0.89
128	$2.02e-03$	0.95	$1.96e-03$	0.98	$4.30e-03$	0.85
256	$1.06e-03$	0.94	$9.90e-04$	0.98	$1.87e-03$	1.20
512	$5.91e-04$	0.84	$5.45e-04$	0.86	$1.13e-03$	0.73

Table 5.2: Test 1.1. Errors and convergence rates obtained using CVC Kolgan-type scheme. $r = -\Delta t$. $\Omega = [0, 2]$, $t_{\text{end}} = 1$, $c = c_M = 0.25$.

Cells	$\text{Err}_{\mathcal{L}^1}$	$\mathcal{O}_{\mathcal{L}^1}$	$\text{Err}_{\mathcal{L}^2}$	$\mathcal{O}_{\mathcal{L}^2}$	$\text{Err}_{\mathcal{L}^\infty}$	$\mathcal{O}_{\mathcal{L}^\infty}$	r
8	$2.15E-2$		$2.17E-02$		$2.95E-02$		$-\frac{1}{8}$
16	$7.10E-3$	1.6	$6.97E-3$	1.64	$1.03E-2$	1.52	$-\frac{1}{16}$
32	$1.95E-3$	1.87	$1.86E-3$	1.91	$2.77E-3$	1.9	$-\frac{1}{32}$
64	$5.02E-4$	1.96	$4.73E-4$	1.98	$7.00E-4$	1.99	$-\frac{1}{64}$
128	$1.27E-4$	1.99	$1.18E-4$	2.0	$1.74E-4$	2.01	$-\frac{1}{128}$
256	$3.19E-5$	2.0	$2.96E-5$	2.0	$4.33E-5$	2.01	$-\frac{1}{256}$
512	$7.98E-6$	2.0	$7.40E-6$	2.0	$1.08E-5$	2.0	$-\frac{1}{512}$

Table 5.3: Test 1.1. Columns from second to seventh show the errors and convergence rates obtained using ADER scheme. The last column depicts the values obtained for $r = -\Delta t$. $\Omega = [0, 2]$, $t_{\text{end}} = 1$, $c = c_M = 1$.

Cells	$\text{Err}_{\mathcal{L}^1}$	$\mathcal{O}_{\mathcal{L}^1}$	$\text{Err}_{\mathcal{L}^2}$	$\mathcal{O}_{\mathcal{L}^2}$	$\text{Err}_{\mathcal{L}^\infty}$	$\mathcal{O}_{\mathcal{L}^\infty}$	r
8	$1.82e-02$		$1.79e-02$		$2.54e-02$		$-\frac{1}{8}$
16	$4.68e-03$	1.96	$4.54e-03$	1.98	$6.71e-03$	1.92	$-\frac{1}{16}$
32	$1.16e-03$	2.01	$1.09e-03$	2.05	$1.59e-03$	2.07	$-\frac{1}{32}$
64	$2.87e-04$	2.02	$2.66e-04$	2.04	$3.79e-04$	2.07	$-\frac{1}{64}$
128	$7.12e-05$	2.01	$6.53e-05$	2.03	$9.23e-05$	2.04	$-\frac{1}{128}$
256	$1.77e-05$	2.01	$1.62e-05$	2.01	$2.27e-05$	2.02	$-\frac{1}{256}$
512	$4.42e-06$	2.0	$4.02e-06$	2.01	$5.65e-06$	2.01	$-\frac{1}{512}$

Table 5.4: Test 1.1. Columns from second to seventh show the errors and convergence rates obtained using LADER scheme. The last column depicts the values obtained for $r = -\Delta t$. $\Omega = [0, 2]$, $t_{\text{end}} = 1$, $c = c_M = 1$.

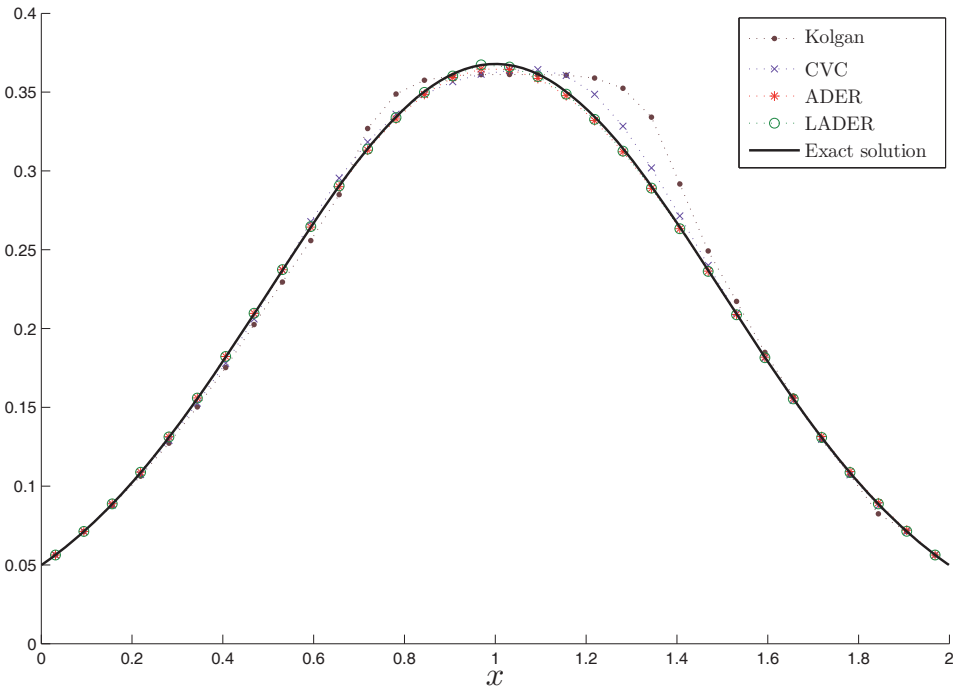

Figure 5.1: Test 1.1. Exact solution and numerical results obtained applying Kolgan, CVC Kolgan-type, ADER and LADER schemes. $\Omega = [0, 2]$, $t_{\text{end}} = 1$, $N_{\text{nodes}} = 32$.

It is important to notice that neither of the chosen values for c_M and r_m are the optimal in the case of an advection-reaction equation. That is, within this test the

exact solution is not expected to be reached.

5.1.2 Test 1.2.

The second test analysed presents a propagation velocity of 0.5 and considers a square wave as initial condition:

$$\partial_t q(x,t) + \frac{1}{2}\partial_x q(x,t) = -q(x,t),$$

$$q(x,0) = \begin{cases} 1, & \text{if } x \in \left[\frac{1}{8}, \frac{1}{2}\right], \\ 0, & \text{if } x \in \left[0, \frac{1}{8}\right) \cup \left(\frac{1}{2}, \frac{3}{2}\right]. \end{cases} \tag{5.4}$$

Its exact solution reads

$$q(x,t) = \begin{cases} 1, & \text{if } x - \frac{1}{2}t \in \left[\frac{1}{8}, \frac{1}{2}\right], \\ 0, & \text{if } x - \frac{1}{2}t \in \left[0, \frac{1}{8}\right) \cup \left(\frac{1}{2}, \frac{3}{2}\right]. \end{cases} \tag{5.5}$$

This test is very useful in assessing the monotonicity of a scheme. As shown in Figure 5.2, Kolgan scheme provides a smooth approximation of the solution but clips the peak value. This is related with the use of limiters which allow us to change between first and second-order in space schemes so that monotonicity is ensured but it provides more diffusive results than a full second-order method. The CVC Kolgan-type method reduces the smearing at the cost of producing overshoots and undershoots in the vicinity of discontinuities (see Figure 5.3). These spurious oscillations are due to the non-monotonicity of some branches of the method.

On the other hand, ADER and LADER schemes provide more accurate results than those of Kolgan-type schemes. Nevertheless, in Figures 5.4-5.6, we can observe that the loss of monotonicity of the schemes produces oscillations near the discontinuity. This problem arises from considering centred slopes, (3.47), which provide a linear scheme. Indeed, we need to circumvent Godunov's theorem to obtain a monotone scheme. This can be done by including non-linear slopes. We will consider an ENO-based reconstruction in both methods, ADER and LADER. A zoom on the numerical results obtained in a vicinity of the left discontinuity are shown in Figure 5.7. Other approaches can be used like WENO or WAF which have already been studied in the literature combined with ADER providing good results.

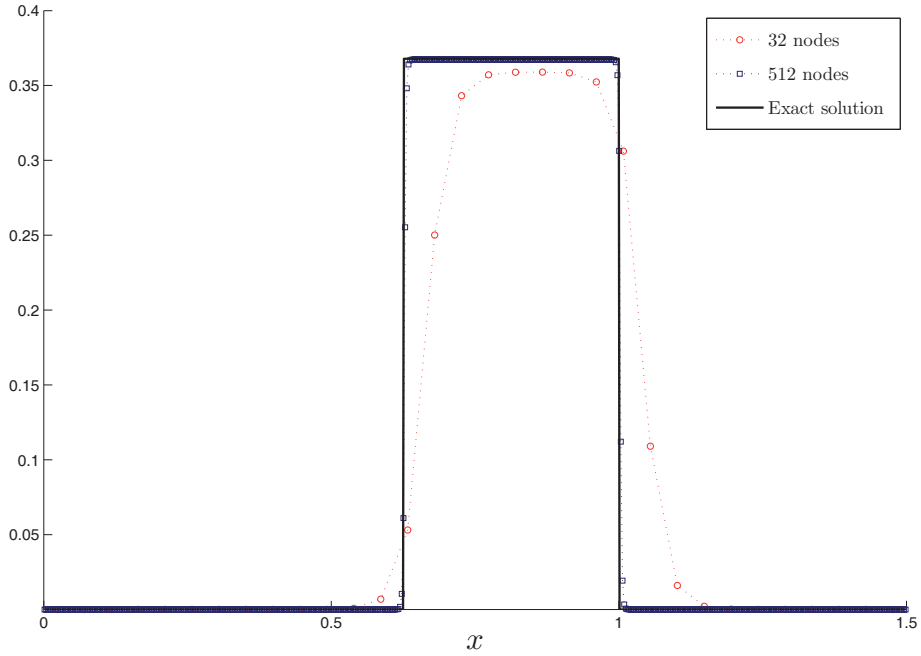

Figure 5.2: Test 1.2. Exact solution and numerical results obtained using Kolgan scheme. $\Omega = [0, 1.5]$, $t_{\text{end}} = 1$, $c_M = 0.5$, $r_m = -1$.

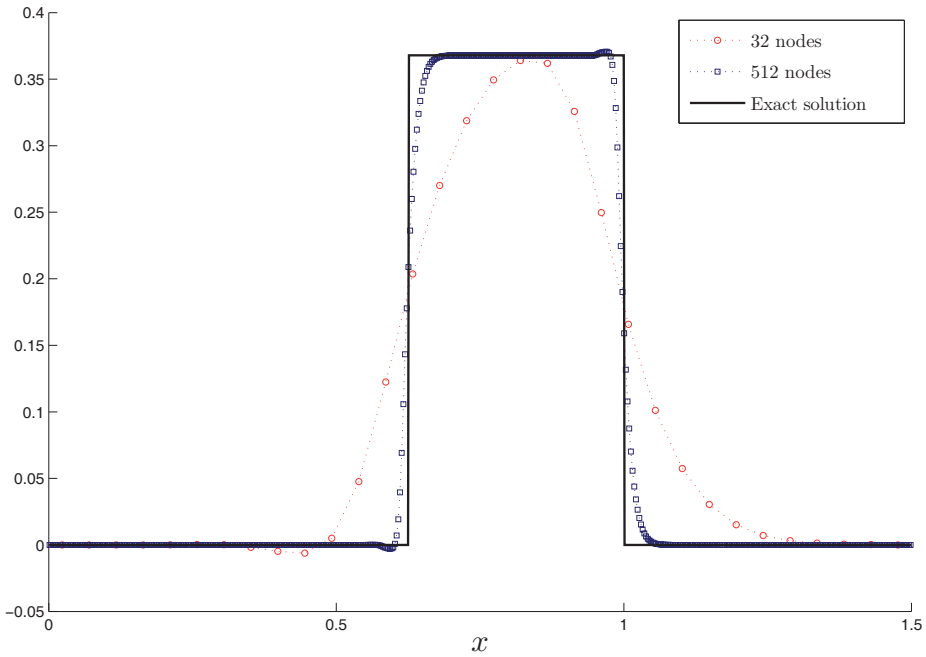

Figure 5.3: Test 1.2. Exact solution and numerical results obtained using CVC Kolgan-type scheme. $\Omega = [0, 1.5]$, $t_{\text{end}} = 1$, $c_M = 0.05$, $r_m = -1$.

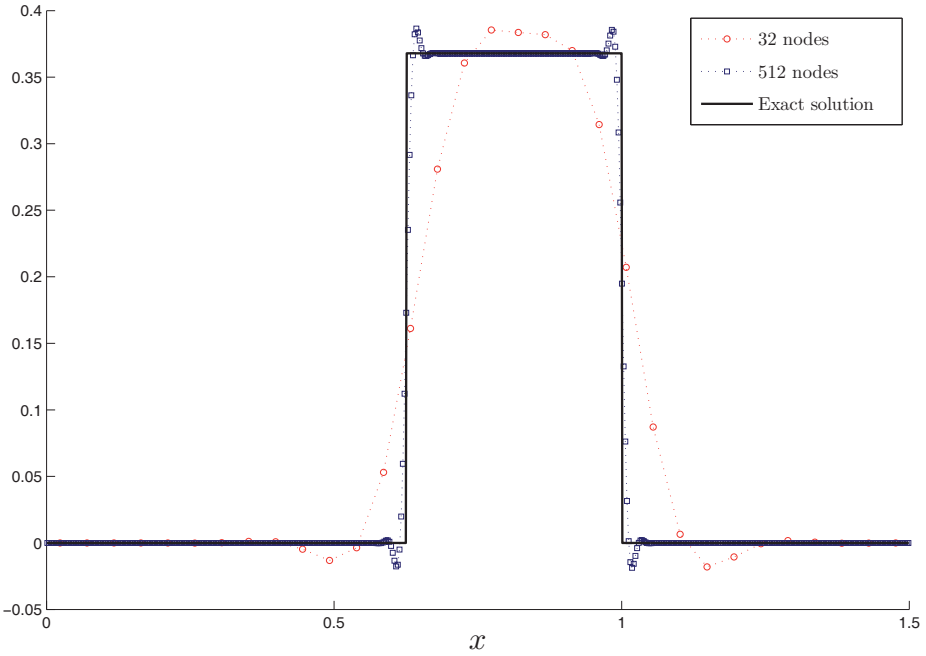

Figure 5.4: Test 1.2. Exact solution and numerical results obtained using ADER scheme. $\Omega = [0, 1.5]$, $t_{\text{end}} = 1$, $c_M = 1$, $r_m = -1$.

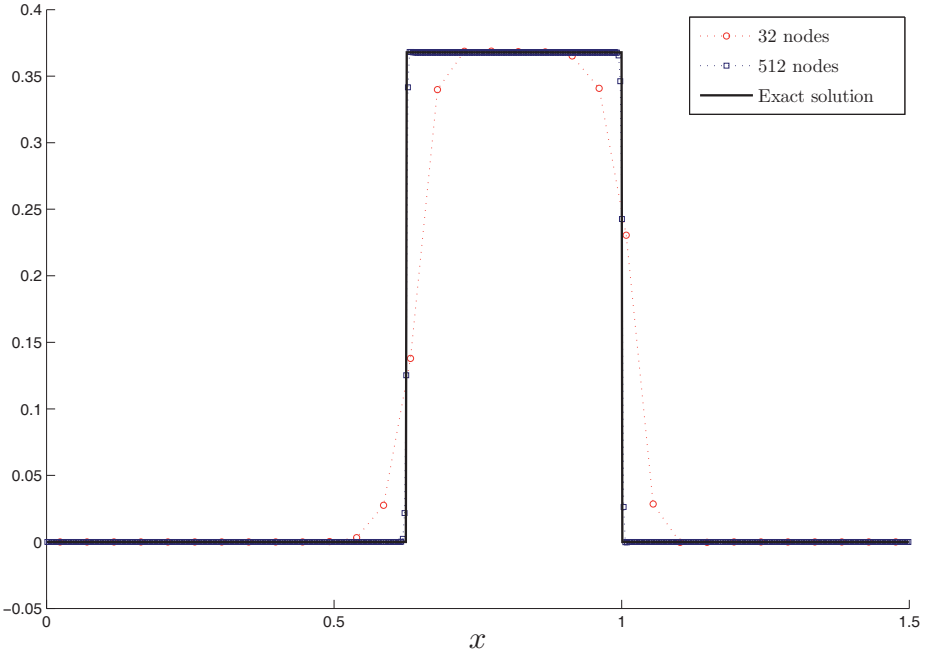

Figure 5.5: Test 1.2. Exact solution and numerical results obtained using LADER scheme. $\Omega = [0, 1.5]$, $t_{\text{end}} = 1$, $c_M = 1$, $r_m = -1$.

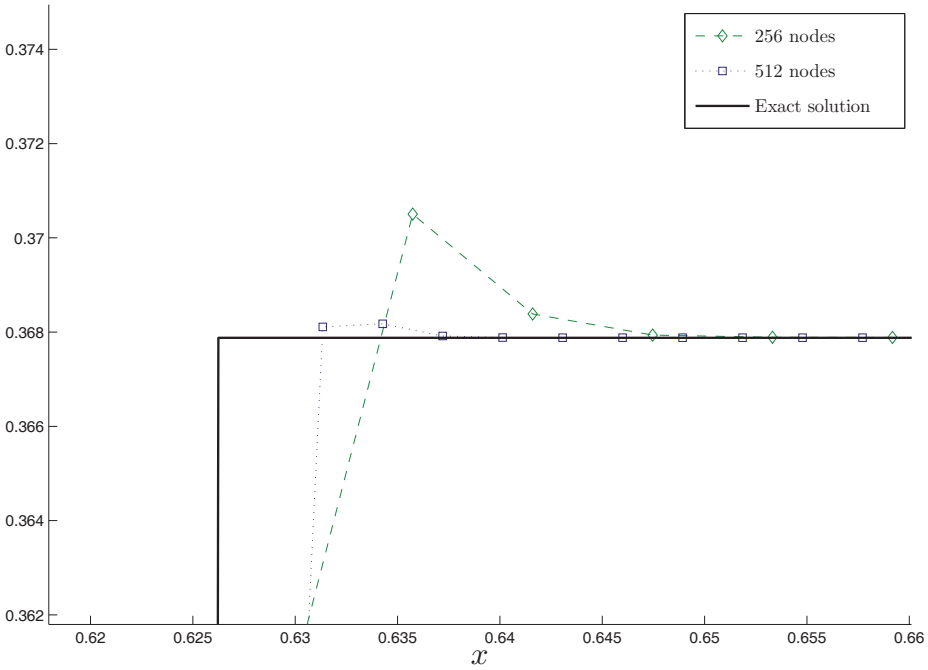

Figure 5.6: Test 1.2. Exact solution and numerical results obtained in the vicinity of the left discontinuity using LADER scheme. $\Omega = [0, 1.5]$, $t_{\text{end}} = 1$, $c_M = 1$, $r_m = -1$.

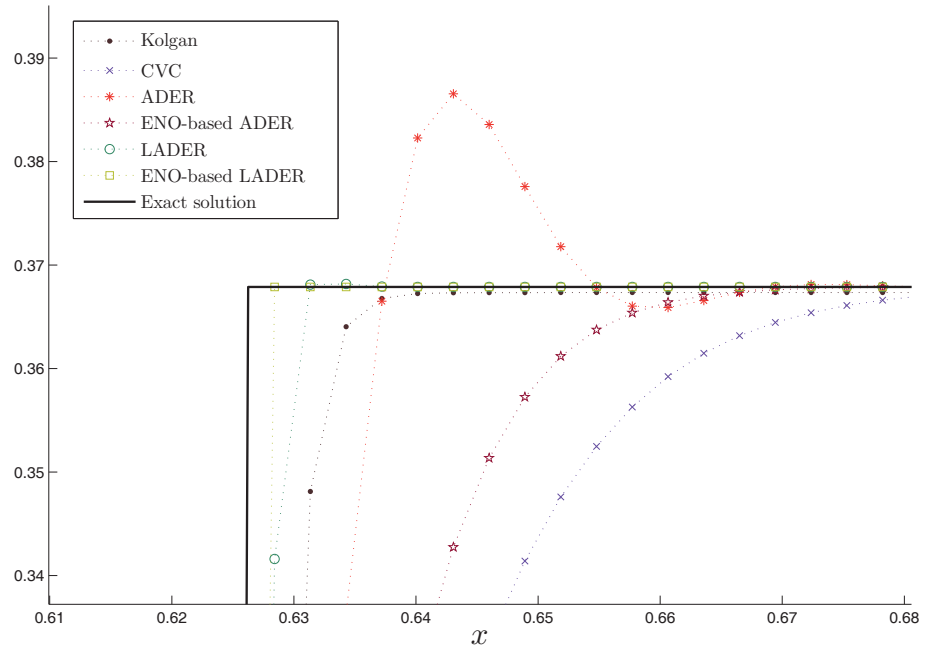

Figure 5.7: Test 1.2. Comparison of the exact solution and numerical results obtained in the vicinity of the left discontinuity. $t_{\text{end}} = 1$, 512 nodes.

5.2 Test 2. Advection-diffusion-reaction equation

Next, we consider two initial value problems for the advection-diffusion-reaction equation.

5.2.1 Test 2.1.

Following [TM14], we set a problem with constant diffusion coefficient:

$$\partial_t q(x,t) + 10\partial_x q(x,t) - 10^{-5}\partial_x^{(2)} q(x,t) = -5q(x,t),$$
$$q(x,0) = \sin(\pi x), \tag{5.6}$$

in the computational domain $\Omega \times T = [-1,1]\times[0,1]$ with Dirichlet boundary conditions. The exact solution reads

$$q(x,t) = e^{(-\alpha\pi^2+\beta)t}\sin(\pi(x-\lambda t)). \tag{5.7}$$

The numerical results obtained using ADER and LADER schemes are detailed in Tables 5.5 and 5.6. The expected second-order is attained. The lose of accuracy for the finer mesh is due to the boundary condition approach.

Cells	$\text{Err}_{\mathcal{L}^1}$	$\mathcal{O}_{\mathcal{L}^1}$	$\text{Err}_{\mathcal{L}^2}$	$\mathcal{O}_{\mathcal{L}^2}$	$\text{Err}_{\mathcal{L}^\infty}$	$\mathcal{O}_{\mathcal{L}^\infty}$
8	$4.52E-03$		$6.80E-03$		$1.53E-02$	
16	$1.45E-03$	1.64	$2.01E-03$	1.76	$4.64E-03$	1.72
32	$4.03E-04$	1.85	$5.38E-04$	1.90	$1.25E-03$	1.89
64	$1.06E-04$	1.93	$1.39E-04$	1.95	$3.23E-04$	1.95
128	$2.74E-05$	1.95	$3.55E-05$	1.97	$8.24E-05$	1.97
256	$7.75E-06$	1.82	$1.00E-05$	1.83	$2.09E-05$	1.98
512	$4.24E-06$	0.87	$5.29E-06$	0.92	$1.31E-05$	0.67

Table 5.5: Test 2.1. Relative errors and convergence rates obtained using ADER. $\Omega = [-1,1]$, $t_{\text{end}} = 1$, $c_M = 0.1$, $d_M = 0.25$, $r_m = -0.25$.

Cells	$\text{Err}_{\mathcal{L}^1}$	$\mathcal{O}_{\mathcal{L}^1}$	$\text{Err}_{\mathcal{L}^2}$	$\mathcal{O}_{\mathcal{L}^2}$	$\text{Err}_{\mathcal{L}^\infty}$	$\mathcal{O}_{\mathcal{L}^\infty}$
8	$1.74E-02$		$2.51E-02$		$4.99E-02$	
16	$6.52E-03$	1.41	$8.80E-03$	1.51	$1.70E-02$	1.56
32	$1.88E-03$	1.79	$2.49E-03$	1.82	$4.76E-03$	1.83
64	$5.01E-04$	1.91	$6.53E-04$	1.93	$1.25E-03$	1.93
128	$1.29E-04$	1.96	$1.67E-04$	1.97	$3.19E-04$	1.97
256	$3.27E-05$	1.98	$4.22E-05$	1.98	$8.12E-05$	1.97
512	$8.91E-06$	1.88	$1.15E-05$	1.88	$2.55E-05$	1.67

Table 5.6: Test 2.1. Relative errors and convergence rates obtained using LADER. $\Omega = [-1, 1]$, $t_{\text{end}} = 1$, $c_M = 0.1$, $d_M = 0.25$, $r_m = -0.25$.

5.2.2 Test 2.2.

We consider the computational domain $\Omega \times T = [0, 2\pi] \times [0, 1]$ and the initial value problem with a time and space dependent diffusion coefficient given by

$$\partial_t q(x,t) + 10\partial_x q(x,t) - 10^{-5}\partial_x \left[e^{x(t-1)^2}\partial_x q(x,t)\right] = -5q(x,t),$$
$$q(x,0) = e^{2\sin(x)}, \tag{5.8}$$

with periodic boundary conditions. The exact solution for this problem is unknown. Therefore, in order to obtain the error and the order of accuracy, we compare the obtained solutions with a reference solution computed for a finer mesh (512 cells).

The obtained results, confirming second-order of accuracy for ADER and LADER schemes, are depicted in Tables 5.7 and 5.8 and in Figures 5.8 and 5.9. Moreover, the values of the parameters c, d and r used for each mesh are detailed in Table 5.9. It is important to remark that d is obtained by neglecting the space and time dependent part of α coefficient assuming a constant value of 10^{-5}. Thus, the computed c, d and r coincide for ADER and LADER schemes.

Cells	$\text{Err}_{\mathcal{L}^1}$	$\mathcal{O}_{\mathcal{L}^1}$	$\text{Err}_{\mathcal{L}^2}$	$\mathcal{O}_{\mathcal{L}^2}$	$\text{Err}_{\mathcal{L}^\infty}$	$\mathcal{O}_{\mathcal{L}^\infty}$
8	$1.39E+00$		$7.18E-01$		$6.90E-01$	
16	$3.48E-01$	1.99	$2.00E-01$	1.84	$2.16E-01$	1.68
32	$6.98E-02$	2.32	$4.26E-02$	2.24	$4.81E-02$	2.16
64	$1.41E-02$	2.31	$8.45E-03$	2.33	$9.55E-03$	2.33
128	$2.94E-03$	2.26	$1.73E-03$	2.29	$1.91E-03$	2.32
256	$5.50E-04$	2.42	$3.19E-04$	2.44	$3.46E-04$	2.47

Table 5.7: Test 2.2. ADER. Errors and convergence rates obtained. $\Omega = [0, 2\pi]$, $t_{\text{end}} = 1$, $c_M = 0.5$, $d_M = 0.25$, $r_m = -0.5$.

Cells	$\text{Err}_{\mathcal{L}^1}$	$\mathcal{O}_{\mathcal{L}^1}$	$\text{Err}_{\mathcal{L}^2}$	$\mathcal{O}_{\mathcal{L}^2}$	$\text{Err}_{\mathcal{L}^\infty}$	$\mathcal{O}_{\mathcal{L}^\infty}$
8	$2.20E+00$		$1.06E+00$		$8.46E-01$	
16	$7.03E-01$	1.65	$3.88E-01$	1.46	$3.51E-01$	1.27
32	$1.90E-01$	1.89	$1.10E-01$	1.82	$1.07E-01$	1.71
64	$4.63E-02$	2.03	$2.75E-02$	2.00	$2.78E-02$	1.95
128	$1.09E-02$	2.09	$6.49E-03$	2.08	$6.66E-03$	2.06
256	$2.16E-03$	2.33	$1.29E-03$	2.33	$1.32E-03$	2.33

Table 5.8: Test 2.2. LADER. Errors and convergence rates obtained. $\Omega = [0, 2\pi]$, $t_{\text{end}} = 1$, $c_M = 0.5$, $d_M = 0.25$, $r_m = -0.5$.

5.3 Test 3. Diffusion equation

As third example, we consider the non-linear diffusion problem proposed in [TH09]:

$$\begin{aligned} \partial_t q(x,t) &= \partial_x \left[(q(x,t))^{-1} \partial_x q(x,t) \right], \\ q(x,0) &= \frac{\sinh(2)}{\cosh(2) - \sin\left(\sqrt{2}\,(x-1)\right)}, \end{aligned} \tag{5.9}$$

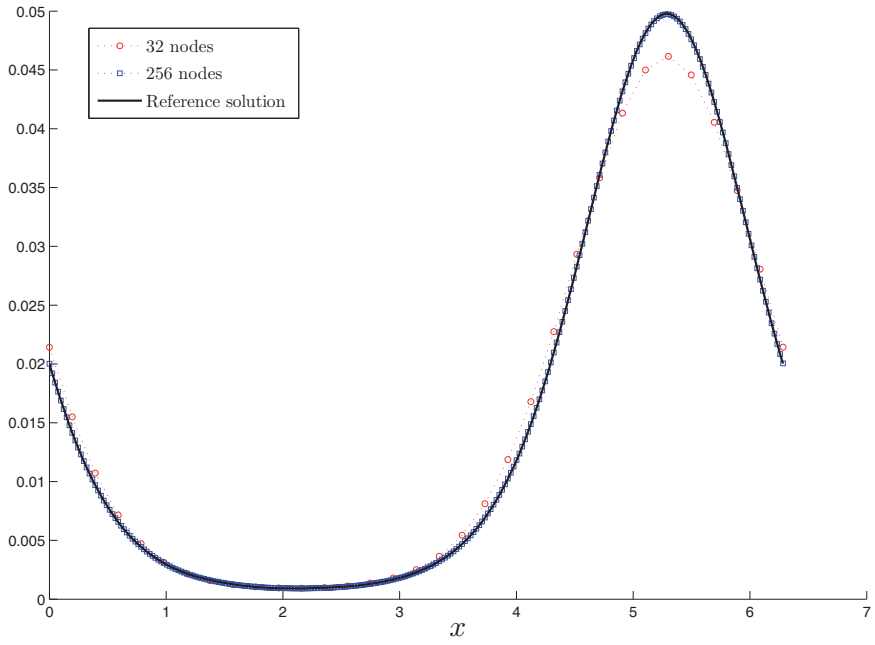

Figure 5.8: Test 2.2. Exact solution and numerical results obtained using ADER. $\Omega = [0, 2\pi]$, $t_{\text{end}} = 1$, $c_M = 0.5$, $d_M = 0.25$, $r_m = -0.5$.

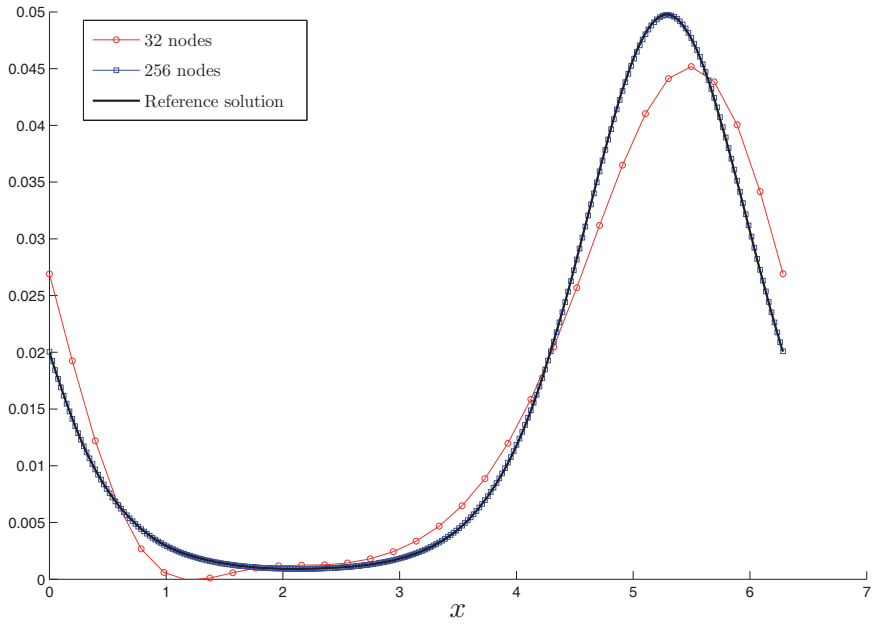

Figure 5.9: Test 2.2. Exact solution and numerical results obtained using LADER. $\Omega = [0, 2\pi]$, $t_{\text{end}} = 1$, $c_M = 0.5$, $d_M = 0.25$, $r_m = -0.5$.

Cells	c	d	r
8	0.5	$6.37E-7$	$-1.96E-1$
16	0.5	$1.27E-6$	$-9.82E-2$
32	0.5	$2.55E-6$	$-4.92E-2$
64	0.5	$5.09E-6$	$-2.45E-2$
128	0.5	$1.02E-5$	$-1.23E-2$
256	0.5	$2.04E-5$	$-6.14E-3$

Table 5.9: Test 2.2. Values of the parameters c, d and r at the final time for ADER and LADER schemes. $\Omega = [0, 2\pi]$, $t_{\text{end}} = 1$, $c_M = 0.5$, $d_M = 0.25$, $r_m = -0.5$.

with periodic boundary conditions in the computational domain $\Omega = [-\sqrt{2}\pi, \sqrt{2}\pi]$. Its exact solution reads

$$q(x,t) = \frac{\sinh(2t+2)}{\cosh(2t+2) - \sin\left(\sqrt{2}\,(x-1)\right)}. \tag{5.10}$$

The numerical results presented in Table 5.10 confirm second-order of accuracy of ADER scheme. Here, it is important to notice that ADER and LADER methodologies provide the same scheme when solving a diffusion equation. Figure 5.10 shows good agreement between the exact solution and the computed solution for two different meshes (32 and 512 nodes).

Cells	$\text{Err}_{\mathcal{L}^1}$	$\mathcal{O}_{\mathcal{L}^1}$	$\text{Err}_{\mathcal{L}^2}$	$\mathcal{O}_{\mathcal{L}^2}$	$\text{Err}_{\mathcal{L}^\infty}$	$\mathcal{O}_{\mathcal{L}^\infty}$
8	$2.33E-01$		$9.19E-02$		$5.30E-02$	
16	$5.10E-02$	2.19	$1.88E-02$	2.29	$1.07E-02$	2.31
32	$1.19E-02$	2.10	$4.48E-03$	2.07	$2.47E-03$	2.12
64	$2.93E-03$	2.02	$1.10E-03$	2.03	$6.17E-04$	2.00
128	$7.26E-04$	2.01	$2.72E-04$	2.01	$1.53E-04$	2.01
256	$1.81E-04$	2.01	$6.77E-05$	2.01	$3.83E-05$	2.00
512	$4.51E-05$	2.00	$1.69E-05$	2.00	$9.58E-06$	2.00

Table 5.10: Test 3. Errors and convergence rates obtained using ADER. $\Omega = [-\sqrt{2}\pi, \sqrt{2}\pi]$, $t_{\text{end}} = 1$, $d_M = 0.25$.

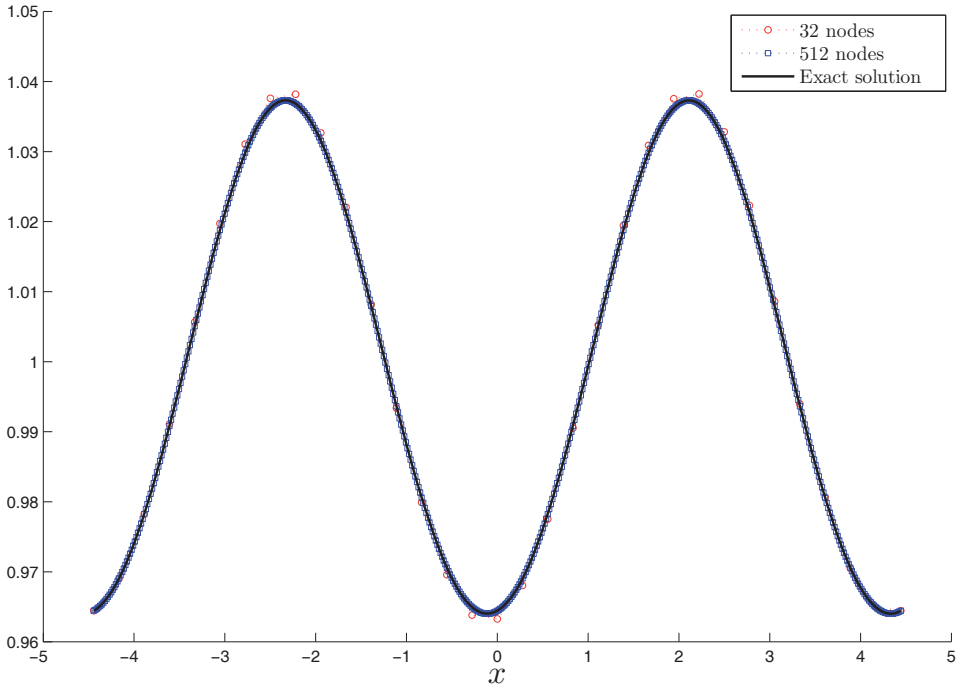

Figure 5.10: Test 3. Exact solution and numerical results obtained using ADER. $\Omega = [-\sqrt{2}\pi, \sqrt{2}\pi]$, $t_{\text{end}} = 1$, $d_M = 0.25$.

5.4 Test 4. Advection equation with time and space dependent advection coefficient

To asses the accuracy of LADER scheme (3.127), we slightly modify Test 1.1 including space and time dependent advection coefficients. Indeed, the method of manufactured solutions is applied in order to obtain a generalized source term assuming a given expression for the exact solution. The two test cases are run considering Dirichlet boundary conditions.

5.4.1 Test 4.1.

We assume a space dependent advection coefficient of the form $\lambda(x,t) = x + 2$ and we define $q(x,t) = e^{-2(x-t)^2-t}$. Applying the method of manufactured solutions to compute the source term for the corresponding advection equation, the problem to be solved reads

$$\partial_t q(x,t) + \partial_x \left[\lambda(x,t) q\left(x,t\right)\right] = s(x,t),$$

$$q(x,0) = e^{-2x^2}, \tag{5.11}$$

with

$$s(x,t) = 4(x-t)(-1+x)e^{-2(x-t)^2-t}. \tag{5.12}$$

The simulations are run considering seven uniform meshes. Tables 5.11 and 5.12 report the errors and convergence rates obtained using a first-order scheme and LADER method, respectively. The orders attained match the theoretically expected.

Cells	$\text{Err}_{\mathcal{L}^1}$	$\mathcal{O}_{\mathcal{L}^1}$	$\text{Err}_{\mathcal{L}^2}$	$\mathcal{O}_{\mathcal{L}^2}$	$\text{Err}_{\mathcal{L}^\infty}$	$\mathcal{O}_{\mathcal{L}^\infty}$
8	$8.87E-02$		$8.71E-02$		$1.13E-01$	
16	$5.36E-02$	0.73	$5.26E-02$	0.73	$6.98E-02$	0.69
32	$2.95E-02$	0.86	$2.88E-02$	0.87	$3.87E-02$	0.85
64	$1.55E-02$	0.93	$1.50E-02$	0.94	$2.03E-02$	0.93
128	$7.98E-03$	0.96	$7.69E-03$	0.97	$1.04E-02$	0.96
256	$4.04E-03$	0.98	$3.89E-03$	0.98	$5.28E-03$	0.98
512	$2.03E-03$	0.99	$1.96E-03$	0.99	$2.65E-03$	0.99

Table 5.11: Test 4.1. Errors and convergence rates obtained using the first-order scheme. $\Omega = [0,2]$, $t_{\text{end}} = 1$, $c = c_M = 0.5$.

Cells	$\text{Err}_{\mathcal{L}^1}$	$\mathcal{O}_{\mathcal{L}^1}$	$\text{Err}_{\mathcal{L}^2}$	$\mathcal{O}_{\mathcal{L}^2}$	$\text{Err}_{\mathcal{L}^\infty}$	$\mathcal{O}_{\mathcal{L}^\infty}$
8	$5.05E-02$		$5.59E-02$		$8.69E-02$	
16	$1.73E-02$	1.55	$1.93E-02$	1.53	$3.43E-02$	1.34
32	$5.17E-03$	1.74	$5.93E-03$	1.71	$1.17E-02$	1.55
64	$1.27E-03$	2.02	$1.54E-03$	1.94	$3.48E-03$	1.75
128	$3.16E-04$	2.01	$3.90E-04$	1.98	$9.63E-04$	1.85
256	$7.88E-05$	2.00	$9.86E-05$	1.99	$2.57E-04$	1.91
512	$1.97E-05$	2.00	$2.48E-05$	1.99	$6.63E-05$	1.95

Table 5.12: Test 4.1. Errors and convergence rates obtained using LADER scheme. $\Omega = [0,2]$, $t_{\text{end}} = 1$, $c = c_M = 0.5$.

The need of introducing the new artificial viscosity term related to the advection coefficient is evidenced in Table 5.13. Neglecting the new upwind term on the numerical flux function, LADER methodology does not achieve second-order of accuracy.

Moreover, spurious oscillations arise. However, the errors obtained using the first-order scheme, Table 5.14, are not highly affected by the lack of the upwind term. This may be due to the fact that the error committed not considering it is masked by the error caused by the remaining terms of the scheme.

Cells	$\text{Err}_{\mathcal{L}^1}$	$\mathcal{O}_{\mathcal{L}^1}$	$\text{Err}_{\mathcal{L}^2}$	$\mathcal{O}_{\mathcal{L}^2}$	$\text{Err}_{\mathcal{L}^\infty}$	$\mathcal{O}_{\mathcal{L}^\infty}$
8	$5.73E-02$		$5.80E-02$		$8.73E-02$	
16	$2.10E-02$	1.45	$2.02E-02$	1.52	$3.54E-02$	1.30
32	$6.58E-03$	1.67	$6.42E-03$	1.66	$1.20E-02$	1.56
64	$2.57E-03$	1.36	$2.61E-03$	1.30	$8.93E-03$	0.43
128	$1.44E-03$	0.83	$1.55E-03$	0.75	$8.08E-03$	0.14
256	$7.62E-04$	0.92	$9.26E-04$	0.74	$7.71E-03$	0.07
512	$3.92E-04$	0.96	$5.74E-04$	0.69	$7.54E-03$	0.03

Table 5.13: Test 4.1. Errors and convergence rates obtained using LADER scheme without the new numerical viscosity term. $\Omega = [0, 2]$, $t_{\text{end}} = 1$, $c = c_M = 0.5$.

Cells	$\text{Err}_{\mathcal{L}^1}$	$\mathcal{O}_{\mathcal{L}^1}$	$\text{Err}_{\mathcal{L}^2}$	$\mathcal{O}_{\mathcal{L}^2}$	$\text{Err}_{\mathcal{L}^\infty}$	$\mathcal{O}_{\mathcal{L}^\infty}$
8	$8.34E-02$		$8.20E-02$		$1.07E-01$	
16	$5.13E-02$	0.70	$5.03E-02$	0.71	$6.65E-02$	0.68
32	$2.88E-02$	0.83	$2.79E-02$	0.85	$3.73E-02$	0.83
64	$1.53E-02$	0.91	$1.47E-02$	0.92	$1.98E-02$	0.92
128	$7.92E-03$	0.95	$7.55E-03$	0.96	$1.02E-02$	0.96
256	$4.02E-03$	0.98	$3.83E-03$	0.98	$5.17E-03$	0.98
512	$2.03E-03$	0.99	$1.93E-03$	0.99	$2.60E-03$	0.99

Table 5.14: Test 4.1. Errors and convergence rates obtained using the first-order scheme without the new numerical viscosity term. $\Omega = [0, 2]$, $t_{\text{end}} = 1$, $c = c_M = 0.5$.

Finally, the results presented in Table 5.15 confirm that second-order can not be reached if we do not perform step one, that is, the polynomial extrapolation, when applying LADER methodology. Furthermore, instability occurs.

Cells	$\mathrm{Err}_{\mathcal{L}^1}$	$\mathcal{O}_{\mathcal{L}^1}$	$\mathrm{Err}_{\mathcal{L}^2}$	$\mathcal{O}_{\mathcal{L}^2}$	$\mathrm{Err}_{\mathcal{L}^\infty}$	$\mathcal{O}_{\mathcal{L}^\infty}$
8	$2.71E-01$		$3.03E-01$		$4.28E-01$	
16	$6.00E-01$	-1.15	$1.09E+00$	-1.84	$2.98E+00$	-2.80
32	$4.90E-01$	0.29	$1.30E+00$	-0.26	$5.15E+00$	-0.79
64	$3.11E-01$	0.66	$1.12E+00$	0.22	$6.28E+00$	-0.28
128	$1.71E-01$	0.86	$8.57E-01$	0.38	$6.81E+00$	-0.12
256	$8.91E-02$	0.94	$6.28E-01$	0.45	$7.06E+00$	-0.05
512	$4.56E-02$	0.97	$4.51E-01$	0.48	$7.18E+00$	-0.02

Table 5.15: Test 4.1. Errors and convergence rates obtained using LADER scheme without extrapolating the variables. $\Omega = [0, 2]$, $t_{\text{end}} = 1$, $c = c_M = 0.5$.

5.4.2 Test 4.2.

The second test proposed with a variable advection coefficient reads

$$\partial_t q(x,t) + \partial_x \left[\lambda\left(x,t\right) q\left(x,t\right)\right] = s(x,y),$$
$$q(x,0) = e^{-2x^2}, \tag{5.13}$$

where

$$\lambda(x,t) = x + t^2 + 2, s(x,y) = 4(x-t)\left(-1-x-t^2\right)e^{-2(x-t)^2-t}. \tag{5.14}$$
$$\tag{5.15}$$

Let us notice that the advection coefficient considered is time and space dependent. Furthermore, we have included a generalized source term so that the exact solution is

$$q\left(x,t\right) = e^{-2(x-t)^2-t}. \tag{5.16}$$

The results obtained using the first-order scheme are depicted in Table 5.16. Regarding LADER scheme, this test case requires for ENO reconstruction on the conservative variable to avoid instabilities. Moreover, the test case is set to push the capabilities of the numerical scheme to the limit. This leads to a decrease on the order of accuracy attained (see Table 5.17).

Cells	$\text{Err}_{\mathcal{L}^1}$	$\mathcal{O}_{\mathcal{L}^1}$	$\text{Err}_{\mathcal{L}^2}$	$\mathcal{O}_{\mathcal{L}^2}$	$\text{Err}_{\mathcal{L}^\infty}$	$\mathcal{O}_{\mathcal{L}^\infty}$
8	$1.23E-01$		$1.20E-01$		$1.44E-01$	
16	$8.35E-02$	0.56	$7.47E-02$	0.68	$8.62E-02$	0.74
32	$4.77E-02$	0.81	$4.14E-02$	0.85	$4.74E-02$	0.86
64	$2.55E-02$	0.91	$2.18E-02$	0.93	$2.49E-02$	0.93
128	$1.32E-02$	0.95	$1.12E-02$	0.96	$1.27E-02$	0.97
256	$6.71E-03$	0.97	$5.66E-03$	0.98	$6.45E-03$	0.98
512	$3.38E-03$	0.99	$2.85E-03$	0.99	$3.24E-03$	0.99

Table 5.16: Test 4.2. Errors and convergence rates obtained using a first-order scheme. $\Omega = [0, 2]$, $t_{\text{end}} = 1$, $c = c_M = 0.5$.

Cells	$\text{Err}_{\mathcal{L}^1}$	$\mathcal{O}_{\mathcal{L}^1}$	$\text{Err}_{\mathcal{L}^2}$	$\mathcal{O}_{\mathcal{L}^2}$	$\text{Err}_{\mathcal{L}^\infty}$	$\mathcal{O}_{\mathcal{L}^\infty}$
8	$6.82E-02$		$6.66E-02$		$9.31E-02$	
16	$2.44E-02$	1.48	$2.27E-02$	1.55	$3.62E-02$	1.36
32	$6.59E-03$	1.89	$6.56E-03$	1.79	$1.20E-02$	1.59
64	$1.83E-03$	1.85	$1.67E-03$	1.97	$3.50E-03$	1.78
128	$6.23E-04$	1.56	$5.11E-04$	1.71	$9.66E-04$	1.86
256	$2.39E-04$	1.38	$2.02E-04$	1.34	$2.82E-04$	1.78
512	$1.06E-04$	1.17	$8.90E-05$	1.18	$1.18E-04$	1.26

Table 5.17: Test 4.2. Errors and convergence rates obtained using LADER scheme with an ENO-based reconstruction. $\Omega = [0, 2]$, $t_{\text{end}} = 1$, $c = c_M = 0.5$.

5.5 Test 5. Advection-diffusion-reaction equation with variable coefficients

As last test we propose the following initial value problem on the advection-diffusion-reaction equation with variable advection and diffusion coefficients

$$\partial_t q(x,t) + \partial_x \left[\lambda(x,t) q\,(x,t)\right] + \partial_x \left[\alpha(x,t)\partial_x q(x,t)\right] = s(x,t), \qquad q(x,0) = e^{-2x^2}, \tag{5.17}$$

where

$$\lambda(x,t) = 2 + x + t^2, \tag{5.18}$$

$$\alpha(x,t) = 10^{-5} e^{x(t-1)^2}, \tag{5.19}$$

$$\begin{aligned} s(x,t) = &- e^{-2(x-t)^2-t} + 4e^{-2(x-t)^2-t}(x-t)(-1-x-t^2) + e^{-2(x-t)^2-t} \\ &+ 10^{-5}(t-1)^2 e^{x(t-1)^2}(-4(x-t)e^{-2(x-t)^2-t}) \\ &+ 10^{-5} e^{x(t-1)^2}(-4+16(x-t)^2)e^{-2(x-t)^2-t}. \end{aligned} \tag{5.20}$$

Herein, the exact solution reads

$$q\,(x,t) = e^{-2(x-t)^2-t}. \tag{5.21}$$

The results obtained using the first-order scheme and LADER methodology with ENO reconstruction are shown in Tables 5.18 and 5.19. They reinforce the conclusions already got for the previous tests. In Table 5.20 we present the errors and order obtained for LADER methodology when neglecting the artificial viscosity term related to the gradient of the advection coefficient. We can resolve that spurious oscillation arise if this term is not included. Moreover, to avoid instabilities, an ENO-based reconstruction needs to be performed resulting on a decrease of the order of accuracy attained. Though, the magnitude of the errors obtained is lower than for the first-order scheme.

Cells	$\text{Err}_{\mathcal{L}^1}$	$\mathcal{O}_{\mathcal{L}^1}$	$\text{Err}_{\mathcal{L}^2}$	$\mathcal{O}_{\mathcal{L}^2}$	$\text{Err}_{\mathcal{L}^\infty}$	$\mathcal{O}_{\mathcal{L}^\infty}$
8	$1.40E-01$		$1.35E-01$		$1.61E-01$	
16	$9.46E-02$	0.56	$8.43E-02$	0.67	$9.65E-02$	0.74
32	$5.37E-02$	0.82	$4.64E-02$	0.86	$5.28E-02$	0.87
64	$2.86E-02$	0.91	$2.43E-02$	0.93	$2.76E-02$	0.94
128	$1.47E-02$	0.95	$1.24E-02$	0.97	$1.41E-02$	0.97
256	$7.50E-03$	0.98	$6.30E-03$	0.98	$7.14E-03$	0.98

Table 5.18: Test 5. Errors and convergence rates obtained using the first-order scheme. $\Omega = [0,2]$, $t_{\text{end}} = 1$, $c = c_M = 0.5$.

Cells	$\text{Err}_{\mathcal{L}^1}$	$\mathcal{O}_{\mathcal{L}^1}$	$\text{Err}_{\mathcal{L}^2}$	$\mathcal{O}_{\mathcal{L}^2}$	$\text{Err}_{\mathcal{L}^\infty}$	$\mathcal{O}_{\mathcal{L}^\infty}$
8	$6.86E-02$		$6.67E-02$		$9.31E-02$	
16	$2.44E-02$	1.49	$2.27E-02$	1.56	$3.62E-02$	1.36
32	$6.57E-03$	1.89	$6.56E-03$	1.79	$1.20E-02$	1.59
64	$1.83E-03$	1.84	$1.67E-03$	1.97	$3.50E-03$	1.78
128	$6.23E-04$	1.56	$5.11E-04$	1.71	$9.66E-04$	1.86
256	$2.38E-04$	1.38	$2.02E-04$	1.34	$3.48E-04$	1.47

Table 5.19: Test 5. Errors and convergence rates obtained using LADER scheme with an ENO-base reconstruction. $\Omega = [0, 2]$, $t_{\text{end}} = 1$, $c = c_M = 0.5$.

Cells	$\text{Err}_{\mathcal{L}^1}$	$\mathcal{O}_{\mathcal{L}^1}$	$\text{Err}_{\mathcal{L}^2}$	$\mathcal{O}_{\mathcal{L}^2}$	$\text{Err}_{\mathcal{L}^\infty}$	$\mathcal{O}_{\mathcal{L}^\infty}$
8	$7.80E-02$		$7.49E-02$		$9.51E-02$	
16	$3.18E-02$	1.30	$2.68E-02$	1.48	$3.88E-02$	1.29
32	$1.12E-02$	1.50	$9.57E-03$	1.48	$1.59E-02$	1.28
64	$5.29E-03$	1.08	$4.25E-03$	1.17	$7.00E-03$	1.19
128	$2.59E-03$	1.03	$2.15E-03$	0.99	$3.22E-03$	1.12
256	$1.30E-03$	1.00	$1.09E-03$	0.98	$1.53E-03$	1.07

Table 5.20: Test 5. Errors and convergence rates obtained using LADER scheme without the new numerical viscosity term. $\Omega = [0, 2]$, $t_{\text{end}} = 1$, $c = c_M = 0.5$.

Conclusions

In this part we have constructed numerical schemes of second-order of accuracy in both space and time, for solving advection-diffusion-reaction partial differential equations. As first step, we have analysed the Kolgan and CVC Kolgan-type schemes applied to the advection-reaction equation. Next, we have adopted ADER and MUSCL-Hancock approaches to solve the advection-diffusion-reaction equation with variable diffusion coefficient. A modification of ADER methodology, LADER, was also developed and extended to account for a time and space dependent advection coefficient. Second-order of accuracy is ensured by appropriately approximating the integrals that arise in the finite volume framework. For the model equation we have performed a detailed linear stability analysis as well as an accuracy analysis in terms of local truncation error. Empirical convergence rate studies confirm the expected theoretical accuracy analysis. The numerical schemes presented will prove useful in solving systems of time-dependent advection-diffusion-reaction equations for realist applications.

USC
UNIVERSIDADE
DE SANTIAGO
DE COMPOSTELA

Part III

The projection hybrid finite volume-finite element method for Navier-Stokes equations

USC
UNIVERSIDADE
DE SANTIAGO
DE COMPOSTELA

Contents

Introduction

Finite volume methods combined with approximate Riemann solvers have been successfully developed for different kinds of flows in the 1980's (see [Tor09] and the references therein). Focusing on the incompressible case, pressure results in a Lagrange multiplier that adapts itself to ensure the incompressibility condition of the velocities. In order to handle this situation, the typical explicit stage of finite volume methods has to be complemented with the so-called projection stage where a pressure correction is computed to get a divergence-free velocity. Many papers exist in the literature devoted to introduce and analyse projection finite volume methods for the incompressible Navier-Stokes equations (see, for instance, [BDA$^+$02] or [PAB$^+$95]). In order to get stability, staggered grids have been used to discretize velocity and pressure. While this can be done straightforwardly in the context of structured meshes, the adaptation to unstructured meshes is more challenging (see [BDDVC98], [GGHL08], [GLL12], [PBH04], [TA07] and [TAPW09]).

On the other hand, projection methods have also been used in combination with finite element discretizations (see [GMS06]). Within this approach, the divergence-free condition for the velocity is replaced by an equation prescribing the divergence of the linear momentum density which is a conservative variable.

The scope of this part is to extend the hybrid finite volume - finite element projection method introduced in [BFSVC14] for both laminar and turbulent incompressible flows considering also transport of species. Moreover, the needed modifications to solve compressible low Mach number flows are proposed. Finally, new methods to increase the accuracy of the methodology are developed.

Starting from a 3D tetrahedral finite element mesh of the computational domain, the equations of the transport-diffusion stage are discretized by a finite volume method associated with a dual finite volume mesh where the nodes of the volumes are the barycenter of the faces of the initial tetrahedra. These volumes, which allow us for an easy implementation of flux boundary conditions, have already been used, among others, for the 2D shallow water equation (see [BDDVC98]), for solving conservative and non conservative systems in 2D and 3D (see [THD09] and [DHC$^+$10]) and for DG schemes employed to solve compressible Navier-Stokes equations (see [TD17]). For the time discretization we use the explicit Euler scheme. The convective term is upwinded using Rusanov scheme (see [Tor09] and [VC15]). Concerning the projection stage, the pressure correction is computed by continuous piecewise linear finite elements associated with the initial tetrahedral mesh. The use of the above "staggered" meshes

together with a simple specific way of passing the information from the transport-diffusion stage to the projection one and vice versa leads to a stable scheme. The former is done by redefining the conservative variable (i.e. the momentum density) constant per tetrahedron. Conversely, the finite element pressure correction is redefined to constant values on the faces of the finite volumes and then used in the transport-diffusion stage.

The coupling of Navier-Stokes equations and the turbulence model introduces turbulent viscosity which is typically computed by solving an additional pair of advection-diffusion-reaction equations, that is equations for the turbulent kinetic energy and the dissipation rate. One issue here is the time dependency of the viscous terms. This requires the use of methods that are at least second-order accurate in space and time for all terms involved (see [CFVC06] and [Saa11]).

In the present thesis, the CVC Kolgan-type scheme is analysed and implemented at the transport-diffusion stage for the convective terms of the considered conservation laws: momentum conservation, transport equations and k-ε model. The obtained scheme, second-order in space and first-order in time is combined with a Galerkin approach of the gradients involved in the viscous term. An alternative option will be the decomposition of the diffusion term into its orthogonal and non-orthogonal parts as introduced in [BFSVC14].

Seeking for a second-order in space and time methodology, LADER method was extended to the three-dimensional case. It profits from the dual mesh to reduce the stencil and, herein, the computational cost. Moreover, an ENO-based reconstruction is considered in order to prevent spurious oscillations.

Regarding low Mach number flows, a new source term of the system solved at the projection stage appears. To compute it, we introduce a pre-projection stage in which the temperature and the mass fractions of the species are used to approximate the time derivative of the density. Besides, the space dependency of the density leads to a modification on the approximation of the numerical flux of momentum equations. More precisely, to avoid spurious oscillations on the solution, a new artificial viscosity term is added.

To asses the performance of the methodology, different manufactured solution tests are introduced and the numerical results obtained are shown. Furthermore, several classical test problems from fluid mechanics are presented and some results are compared with experimental data (see [Saa11] and [BFSVC14]).

This part is organized as follows. In Chapter 6, we develop the above described methodology in order to solve incompressible flows. We start by introducing the overall algorithm and the staggered mesh used. Then, the transport diffusion stage is described focusing on the development of second-order accuracy methods. Next, we recall the projection stage and we present the boundary conditions considered. The performance of the methodology is assessed through diverse tests. Moreover, realistic problems are analysed. On the other hand, Chapter 7 is devoted to the extension of the former methodology to solve compressible low Mach number flows. At the pre-projection stage, the data of the temperature and the composition of the mixture are used to

compute the time derivative of the density employed as source term in the projection stage. The time and space dependency of the density will produce spurious oscillations on the solutions if we just compute the flux term like for incompressible flows. A detailed analysis of these terms is performed and a correction consistent in adding a new artificial viscosity term is proposed.

USC
UNIVERSIDADE
DE SANTIAGO
DE COMPOSTELA

Chapter 6

Incompressible flows

In Part I, we have introduced a system, (2.47)-(2.52), which provides a model for turbulent incompressible flows. To solve it, the methodologies proposed in Part II will be extended to the three-dimensional case. Furthermore, finite volume methods are combined with a finite element method through a projection method which decouples the pressure and velocity computations.

The outline of this chapter is as follows. The mathematical model for turbulent incompressible flows is recalled in the first section. Then, the numerical discretization is detailed. Special attention is paid to the description of the finite volume algorithm. Aiming to achieve a high-order scheme, two different methodologies for the flux terms are developed: the CVC Kolgan-type method, second-order in space and first-order in time, and LADER methodology, second-order in space and time. The needed modifications, on the approximation of the remaining terms of the equations, to achieve a high-order scheme are also presented. A Galerkin approach to compute the diffusion terms is introduced. Finally, some of the numerical results obtained with the developed code are shown. On the one hand, the order of convergence of the method is studied using the method of manufactured solutions. On the other hand, several classical test problems are analysed.

6.1 Governing equations

We are aiming to solve the problem defined by (2.47)-(2.52). Moreover, species transport, (2.64) is also included in the former system. To this end, we start by defining the vector of conservative variables $\mathbf{w} = (\mathbf{w_u}, \widehat{\mathbf{w}})^T$, with $\mathbf{w_u} = \rho\mathbf{u}$ the conservative variable related to the velocities and $\widehat{\mathbf{w}}$ the vector of the conservative variables connected to turbulence and species, i.e., $\widehat{\mathbf{w}} = (w_k, w_\varepsilon, \mathbf{w_y})^T$, $w_k = \rho k$, $w_\varepsilon = \rho\varepsilon$ and $\mathbf{w_y} = \rho\mathbf{y}$. Then, rewriting the complete system in terms of the new variables we get

$$\mathrm{div}\mathbf{w_u} = 0, \tag{6.1}$$

$$\frac{\partial \mathbf{w_u}}{\partial t} + \mathrm{div}\mathcal{F}^{\mathbf{w_u}}(\mathbf{w_u}) + \mathrm{grad}\,\pi - \mathrm{div}\,\tau = \mathbf{f_u}, \tag{6.2}$$

$$\frac{\partial w_k}{\partial t} + \mathrm{div}\mathcal{F}^{w_k}\left(w_k, \mathbf{u}\right) - \mathrm{div}\left[\left(\mu + \frac{\mu_t}{\sigma_k}\right)\mathrm{grad}\left(\frac{w_k}{\rho}\right)\right] + w_\varepsilon = G_k + f_k, \tag{6.3}$$

$$\frac{\partial w_\varepsilon}{\partial t} + \mathrm{div}\mathcal{F}^{w_\varepsilon}(w_\varepsilon, \mathbf{u}) - \mathrm{div}\left[\left(\mu + \frac{\mu_t}{\sigma_\varepsilon}\right)\mathrm{grad}\left(\frac{w_\varepsilon}{\rho}\right)\right] + C_{2\varepsilon}\frac{w_\varepsilon^2}{w_k} = C_{1\varepsilon}\frac{w_\varepsilon}{w_k}G_k + f_\varepsilon, \tag{6.4}$$

$$\frac{\partial \mathbf{w_y}}{\partial t} + \mathrm{div}\mathcal{F}^{\mathbf{w_y}}\left(\mathbf{w_y}, \mathbf{u}\right) - \mathrm{div}\left[\left(\rho\mathcal{D} + \frac{\mu_t}{Sc_t}\right)\mathrm{grad}\left(\frac{1}{\rho}\mathbf{w_y}\right)\right] = \mathbf{f_y}, \tag{6.5}$$

where

$$\mathcal{F}(\mathbf{w}) = \left(\mathcal{F}^{\mathbf{w_u}}\left(\mathbf{w_u}\right), \mathcal{F}^{w_k}\left(w_k, \mathbf{u}\right), \mathcal{F}^{w_\varepsilon}\left(w_\varepsilon, \mathbf{u}\right), \mathcal{F}^{\mathbf{w_y}}\left(\mathbf{w_y}, \mathbf{u}\right)\right)^T \tag{6.6}$$

is the complete flux tensor whose three components read

$$\mathcal{F} = \left(\mathcal{F}_1 | \mathcal{F}_2 | \mathcal{F}_3\right)_{(3+2+N_e+1)\times 3}, \quad \mathcal{F}_i\left(\mathbf{w}\right) = u_i\mathbf{w}, \quad i = 1, 2, 3. \tag{6.7}$$

Equations (6.2)-(6.5) include the additional terms $\mathbf{f_u}$, f_k, f_ε and $\mathbf{f_y}$ which correspond to the generic source terms needed, for example, for the manufactured test problems.

6.2 Numerical discretization

The numerical discretization of the complete system is performed by extending the projection method first put forward in [BFSVC14]. The developed numerical method solves, at each time step, equations (6.2)-(6.5) with a finite volume method (FVM) and, so, an approximation of $\mathbf{w}$ is obtained. The next step is to apply projection to system (6.1)-(6.2). The pressure correction is provided by a piecewise linear finite element method (FEM). At the post-projection stage, an approximation of $\mathbf{w_u}$ verifying the divergence condition, (6.1), is obtained. Furthermore, the production terms of the turbulence equations are also computed in this stage to account for the corrected velocities. The reaction terms are treated via a semi-implicit method.

We start by considering a two-stage in time discretization scheme: in order to get the solution at time t^{n+1}, we use the previously obtained approximations $\mathbf{W}^n$ of the conservative variables $\mathbf{w}(x, y, z, t^n)$, $\mathbf{U}^n$ of the velocity $\mathbf{u}(x, y, z, t^n)$ and π^n of the pressure perturbation $\pi(x, y, z, t^n)$, and compute $\mathbf{W}^{n+1}$ and π^{n+1} from the following system of equations:

$$\frac{1}{\Delta t}\left(\widetilde{\mathbf{W}}_{\mathbf{u}}^{n+1} - \mathbf{W}_{\mathbf{u}}^n\right) + \mathrm{div}\mathcal{F}^{\mathbf{w_u}}(\mathbf{W}_{\mathbf{u}}^n) + \mathrm{grad}\,\pi^n - \mathrm{div}\,\tau^n = \mathbf{f}_{\mathbf{u}}^n, \tag{6.8}$$

$$\frac{1}{\Delta t}\left(\mathbf{W}_{\mathbf{u}}^{n+1} - \widetilde{\mathbf{W}}_{\mathbf{u}}^{n+1}\right) + \mathrm{grad}(\pi^{n+1} - \pi^n) = 0, \tag{6.9}$$

$$\mathrm{div}\mathbf{W}_{\mathbf{u}}^{n+1} = 0, \tag{6.10}$$

$$\frac{1}{\Delta t}\left(\widetilde{W}_k^{n+1} - W_k^n\right) + \mathrm{div}\mathcal{F}^{w_k}\left(W_k^n, \mathbf{U}^n\right) - \mathrm{div}\left[\left(\mu + \frac{\mu_t}{\sigma_k}\right)\mathrm{grad}\,\frac{W_k^n}{\rho}\right] = 0, \tag{6.11}$$

$$\frac{1}{\Delta t}\left(W_k^{n+1} - \widetilde{W}_k^{n+1}\right) + W_\varepsilon^n - G_k^{n+1} = f_k^n, \tag{6.12}$$

$$\frac{1}{\Delta t}\left(\widetilde{W}_{\varepsilon}^{n+1}-W_{\varepsilon}^{n}\right)+\mathrm{div}\mathcal{F}^{w_{\varepsilon}}\left(W_{\varepsilon}^{n},\mathbf{U}^{n}\right)-\mathrm{div}\left[\left(\mu+\frac{\mu_{t}^{n}}{\sigma_{\varepsilon}}\right)\mathrm{grad}\,\frac{W_{\varepsilon}^{n}}{\rho}\right]=0, \tag{6.13}$$

$$\frac{1}{\Delta t}\left(W_{\varepsilon}^{n+1}-\widetilde{W}_{\varepsilon}^{n+1}\right)+C_{2\varepsilon}\frac{W_{\varepsilon}^{n+1}W_{\varepsilon}^{n}}{W_{k}^{n}}-C_{1\varepsilon}\frac{W_{\varepsilon}^{n}}{W_{k}^{n}}G_{k}^{n+1}=f_{\varepsilon}^{n}. \tag{6.14}$$

$$\frac{1}{\Delta t}\left(\widetilde{\mathbf{W}}_{\mathbf{y}}^{n+1}-\mathbf{W}_{\mathbf{y}}^{n}\right)+\mathrm{div}\mathcal{F}^{\mathbf{w_y}}\left(\mathbf{W}_{\mathbf{y}}^{n},\mathbf{U}^{n}\right)-\mathrm{div}\left[\left(\rho\mathcal{D}+\frac{\mu_{t}^{n}}{Sc_{t}}\right)\mathrm{grad}\left(\frac{1}{\rho}\mathbf{W}_{\mathbf{y}}^{n}\right)\right]=0, \tag{6.15}$$

$$\frac{1}{\Delta t}\left(\mathbf{W}_{\mathbf{y}}^{n+1}-\widetilde{\mathbf{W}}_{\mathbf{y}}^{n+1}\right)=\mathbf{f}_{\mathbf{y}}^{n}. \tag{6.16}$$

Concerning the discretization of mass conservation and momentum equations, by adding equations (6.8)-(6.9), we easily see that the scheme is actually implicit for the pressure term. However, the writing above shows that the pressure and the velocity can be solved in three uncoupled stages. The first of them corresponds to equation (6.8) and will be called the transport-diffusion stage; it is explicit and allows us to compute the intermediate approximation of the conservative variables $\widetilde{\mathbf{W}}_{\mathbf{u}}^{n+1}$ (we notice that, in general, this approximation does not satisfy the divergence condition (6.10)). The second one, to be called the projection stage, is implicit; it consists of solving the coupled equations (6.9) and (6.10) with a finite element method to obtain the pressure correction $\delta^{n+1} := \pi^{n+1} - \pi^{n}$. The last one is the post-projection stage; the intermediate approximation for the velocity conservative variables is updated with the pressure correction providing the final approximations $\mathbf{W}_{\mathbf{u}}^{n+1}$ and π^{n+1} (see [BFSVC14] for further details).

As a novelty, for the remaining conservation laws the approximation of the conservative variables is obtained in two steps. At the transport-diffusion stage we compute an approximation of the conservative variables, $\widetilde{W}_{k}^{n+1}$, $\widetilde{W}_{\varepsilon}^{n+1}$ and $\widetilde{\mathbf{W}}_{\mathbf{y}}^{n+1}$, taking into account the corresponding flux and diffusion terms. Let us remark that at this stage the update of the approximations involves all the neighbouring nodes of the finite volume C_i. On the other hand, the discretization of the source terms related to manufactured solutions or other production terms in equations (6.12), (6.14) and (6.16) involves pointwise evaluations at cell C_i which will be computed at the post-projection stage. Furthermore, the production terms of the turbulence equations are computed taking into account the updated velocities and the reaction terms are treated via a semi-implicit method. As a result, we obtain the updated conservative variables W_{k}^{n+1}, W_{ε}^{n+1} and $\mathbf{W}_{\mathbf{y}}^{n+1}$.

Summarizing, the overall method consists of:

- *Transport-diffusion stage:* equations (6.8), (6.11), (6.13) and (6.15) are solved by a FVM.
- *Projection stage:* the pressure correction $\delta^{n+1} := \pi^{n+1} - \pi^{n}$ is obtained by solving equations (6.9) and (6.10) with a FEM.
- *Post-projection stage:* the $\widetilde{\mathbf{W}}_{\mathbf{u}}^{n+1}$ computed at the first stage is updated by using δ^{n+1} in order to obtain another approximation $\mathbf{W}_{\mathbf{u}}^{n+1}$, satisfying the divergence

condition (6.10). Next, the turbulence and species variables are updated from equations (6.12), (6.14) and (6.16), respectively.

In what follows, we will detail each one of the above defined stages. However, we will start by describing the staggered unstructured mesh to be used.

6.3 A dual finite volume mesh

Despite structured meshes are simpler and, thus, more suitable to develop high-order methods they are not always able to capture the features of a complex domain. Hence, the spatial discretization of three-dimensional irregular geometries requires the use of unstructured meshes.

We start by considering a three-dimensional unstructured tetrahedral finite element mesh $\{T_k,\, i = 1, \ldots, nel\}$ from which we build a dual finite volume mesh. At this point, two main approaches can be considered.

Firstly, we can define a co-located grid. By placing the cell nodes in the barycenter of the tetrahedra, we can assume that the new mesh coincides with the original triangulation. The resulting volumes are known of tetrahedra-type. The main inconvenient of these meshes is that a careful treatment needs to be applied to avoid checker-board pressure solutions (see, for instance, [ZZB14]).

As second approach, two different types of staggered grids can be introduced. On the one hand, we can set the vertex of the original tetrahedra as the nodes. Then, the volume obtained is delimited by the medians of the original tetrahedra. These vertex-type volumes have as disadvantage the impossibility of determining the number of finite elements related to each new finite volume. Furthermore, as pointed out in [DD92], in irregular domains a boundary node may have associated two different normal vectors.

Another staggered mesh can be built using the so called face-type volumes. They were proposed in [BDDVC98] and [BFSVC14] in order to get a mesh such that each boundary node has associated only one normal vector. The main feature of this discretization is that the nodes are taken to be the baricentres of the faces of the original tetrahedra. Thus, each interior finite volume is related to two finite elements whereas the boundary volumes belong only to one finite element and has its node on the boundary of the domain. Consequently, they permit an easy implementation of Dirichlet boundary conditions (see [Cea05]).

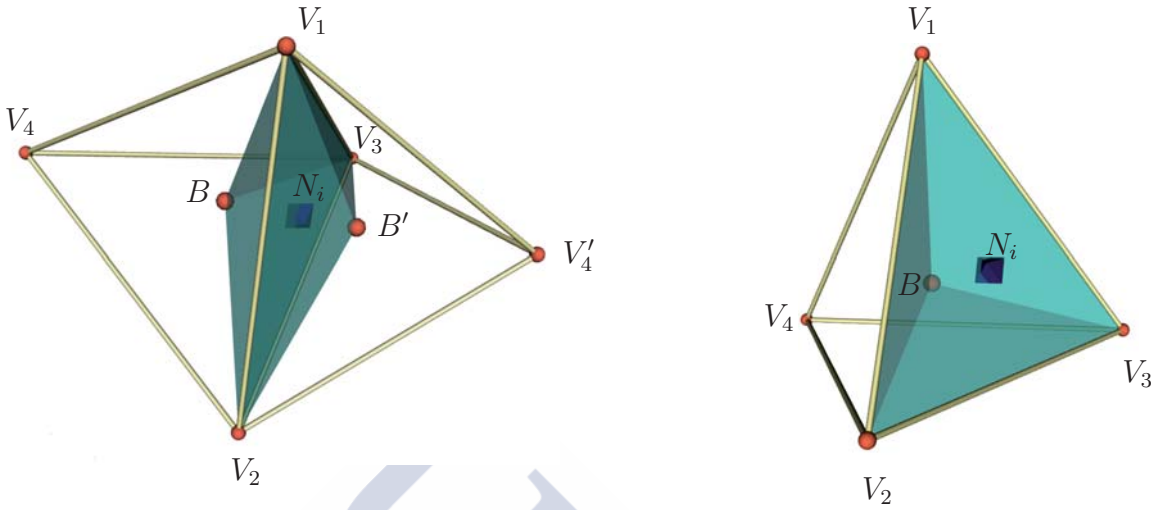

Figure 6.1: Interior (left) and boundary (right) finite volumes of the face-type.

Since the last approach is the one chosen in this thesis, we will further detail it:

- We consider the barycenters $\{B_k, k = 1, \ldots, nel\}$ of the tetrahedra of the initial mesh.
- Every tetrahedron T_k is subdivided into four sub-tetrahedra connecting its barycenter to the three vertices of each face.
- Let us consider the barycenters of the faces of the initial mesh,

$$\{N_i,\, i = 1, \ldots, nnodes\}\,.$$

  - If a barycenter N_i is an interior point of the domain, it belongs to two of the sub-tetrahedra defined in the previous step. The finite volume C_i is then defined to be the union of these two sub-tetrahedra. Its node N_i is the above barycenter. In Figure 6.1-left the five points that define the faces Γ_{ij} of cell C_i are the three vertices V_1, V_2 and V_3, and the barycenters B and B'.
  - If node N_i belongs to the boundary, then the finite volume C_i is equal to the unique sub-tetrahedron containing N_i. In Figure 6.1-right the four points that define the faces Γ_{ij} of cell C_i are the three vertices V_1, V_2 and V_3, and the barycenter B.

- Each interior node N_i has as neighboring nodes the set $\mathcal{K}_i$ consisting of the barycenters of the faces of the two tetrahedra of the initial mesh to which it belongs. Therefore it always has six neighboring nodes. On the contrary, if the node is at the boundary, then it only has three neighboring nodes.

- The face Γ_{ij} is the interface between cells C_i and C_j. The boundary of C_i is denoted by $\Gamma_i = \bigcup_{N_j \in \mathcal{K}_i} \Gamma_{ij}$.

- Finally, $\widetilde{\boldsymbol{\eta}}_{ij}$ denotes the outward unit normal vector to Γ_{ij}. Moreover we define $\boldsymbol{\eta_{ij}} := \widetilde{\boldsymbol{\eta}}_{\boldsymbol{ij}} ||\boldsymbol{\eta_{ij}}||$, where $||\boldsymbol{\eta_{ij}}|| := \text{Area}(\Gamma_{ij})$.

The former method to obtain staggered grids has proven useful for diverse numerical methods as finite volumes schemes and discontinuous-Galerkin methods (see [Cea05], [CFVC06], [CCM15], [CCML17], [THD09], [DHC+10], [TD14], [TD15], [TD16], [TD17] and references therein).

6.4 Transport-diffusion stage

As we have seen in Section 6.2, the transport-diffusion stage aims to provide a first approach of the conservative variables of system (6.8)-(6.16) at time t^{n+1} using a finite volume method.

6.4.1 Finite volume discretization

The discrete approximation of the conservative variables is taken to be constant per finite volume, as it represents an integral average. By integrating (6.8), (6.11), (6.13) and (6.15) on C_i and applying Gauss' theorem, we get

$$\frac{|C_i|}{\Delta t}\left(\widetilde{\mathbf{W}}_{\mathbf{u},i}^{n+1} - \mathbf{W}_{\mathbf{u},i}^{n}\right) + \int_{\Gamma_i} \mathcal{F}^{\mathbf{w_u}}\left(\mathbf{W}_{\mathbf{u}}^{n}\right)\widetilde{\boldsymbol{\eta}}\,\mathrm{dS} + \int_{\mathrm{C_i}} \nabla\pi^{\mathrm{n}}\,\mathrm{dV} - \int_{\Gamma_\mathrm{i}} \tau^{\mathrm{n}}\,\widetilde{\boldsymbol{\eta}}\mathrm{dS} = \int_{\mathrm{C_i}} \mathbf{f}_{\mathbf{u}}^{\mathrm{n}}\,\mathrm{dV}, \tag{6.17}$$

$$\frac{|C_i|}{\Delta t}\left(\widetilde{W}_{k,i}^{n+1} - W_{k,i}^{n}\right) + \int_{\Gamma_i} \mathcal{F}^{w_k}\left(W_k^n, \mathbf{U}^n\right)\widetilde{\boldsymbol{\eta}}\,\mathrm{dS} - \int_{\Gamma_\mathrm{i}} \left[\left(\mu + \frac{\mu_\mathrm{t}^\mathrm{n}}{\sigma_\mathrm{k}}\right)\mathrm{grad}\,\frac{\mathrm{W_k^n}}{\rho}\right]\widetilde{\boldsymbol{\eta}}\,\mathrm{dS} = 0, \tag{6.18}$$

$$\frac{|C_i|}{\Delta t}\left(\widetilde{W}_{\varepsilon,i}^{n+1} - W_{\varepsilon,i}^{n}\right) + \int_{\Gamma_i} \mathcal{F}^{w_\varepsilon}\left(W_\varepsilon^n, \mathbf{U}^n\right)\widetilde{\boldsymbol{\eta}}\,\mathrm{dS} - \int_{\Gamma_\mathrm{i}} \left[\left(\mu + \frac{\mu_\mathrm{t}^\mathrm{n}}{\sigma_\varepsilon}\right)\mathrm{grad}\,\frac{\mathrm{W_\varepsilon^n}}{\rho}\right]\widetilde{\boldsymbol{\eta}}\,\mathrm{dS} = 0, \tag{6.19}$$

$$\frac{|C_i|}{\Delta t}\left(\widetilde{\mathbf{W}}_{\mathbf{y},i}^{n+1} - \mathbf{W}_{\mathbf{y},i}^{n}\right) + \int_{\Gamma_i} \mathcal{F}^{\mathbf{w_y}}\left(\mathbf{W}_{\mathbf{y}}^n, \mathbf{U}^n\right)\widetilde{\boldsymbol{\eta}}\,\mathrm{dS} - \int_{\Gamma_\mathrm{i}} \left[\left(\rho\mathcal{D} + \frac{\mu_\mathrm{t}^\mathrm{n}}{\mathrm{Sc_t}}\right)\mathrm{grad}\left(\frac{1}{\rho}\mathbf{W}_{\mathbf{y}}^{\mathrm{n}}\right)\right]\widetilde{\boldsymbol{\eta}}\,\mathrm{dS} = 0, \tag{6.20}$$

where $|C_i|$ denotes the volume of C_i and $\tilde{\boldsymbol{\eta}}_i$ is the outward unit normal of Γ_i at each point. Within the following sections we detail how to approximate the former integrals.

6.4.2 Numerical flux

We define the global normal flux on Γ_i as $\mathcal{Z}(\mathbf{W}^n, \tilde{\boldsymbol{\eta}}_i) := \mathcal{F}(\mathbf{W}^n)\tilde{\boldsymbol{\eta}}_i$. Thanks to the shape of the convective terms in equations (6.17)-(6.20) their integrals can be computed globally. We first split Γ_i into the cell interfaces Γ_{ij}, namely

$$\int_{\Gamma_i} \mathcal{F}(\mathbf{W}^n)\tilde{\boldsymbol{\eta}}_i \, \mathrm{dS} = \sum_{N_j \in \mathcal{K}_i} \int_{\Gamma_{ij}} \mathcal{Z}(\mathbf{W}^n, \tilde{\boldsymbol{\eta}}_{ij}) \, \mathrm{dS}. \tag{6.21}$$

Then, in order to obtain a stable discretization, the integral on Γ_{ij} is approximated by an upwind scheme using a numerical flux function $\boldsymbol{\phi}$:

$$\int_{\Gamma_{ij}} \mathcal{Z}(\mathbf{W}^n, \tilde{\boldsymbol{\eta}}_{ij}) \mathrm{dS} \approx \boldsymbol{\phi}\left(\mathbf{W}_i^n, \mathbf{W}_j^n, \boldsymbol{\eta}_{ij}\right). \tag{6.22}$$

The expression of $\boldsymbol{\phi}$ depends on the upwind scheme. In this thesis, we consider the Rusanov scheme (see [Rus62]),

$$\boldsymbol{\phi}\left(\mathbf{W}_i^n, \mathbf{W}_j^n, \boldsymbol{\eta}_{ij}\right) = \frac{1}{2}(\mathcal{Z}(\mathbf{W}_i^n, \boldsymbol{\eta}_{ij}) + \mathcal{Z}(\mathbf{W}_j^n, \boldsymbol{\eta}_{ij})) - \frac{1}{2}\alpha_{RS}(\mathbf{W}_i^n, \mathbf{W}_j^n, \boldsymbol{\eta}_{ij})\left(\mathbf{W}_j^n - \mathbf{W}_i^n\right). \tag{6.23}$$

To obtain the value of α_{RS}, we start by computing the jacobian matrix of $\mathcal{Z}\left(\mathbf{W}_\mathbf{u}, \rho, \boldsymbol{\eta}\right)$,

$$\mathcal{A}\left(\mathbf{W}, \rho, \boldsymbol{\eta}\right) = \begin{pmatrix} U_1\eta_1 + \mathbf{U}\cdot\boldsymbol{\eta} & U_1\eta_2 & U_1\eta_3 \\ U_2\eta_1 & U_2\eta_2 + \mathbf{U}\cdot\boldsymbol{\eta} & U_2\eta_3 \\ U_3\eta_1 & U_3\eta_2 & U_3\eta_3 + \mathbf{U}\cdot\boldsymbol{\eta} \end{pmatrix}. \tag{6.24}$$

The corresponding eigenvalues are $\lambda_1 = \lambda_2 = \mathbf{U}\cdot\boldsymbol{\eta}$ and $\lambda_3 = 2\mathbf{U}\cdot\boldsymbol{\eta}$. Similarly, the eigenvalues related to the species transport, the turbulent kinetic energy and the mean dissipation rate conservation equations result $\mathbf{U}\cdot\boldsymbol{\eta}$. Therefore, the coefficient α_{RS} could be computed in a coupled way for all the equations, so that, it would be defined by

$$\alpha_{RS}(\mathbf{W}_i^n, \mathbf{W}_j^n, \boldsymbol{\eta}_{ij}) := \max\left\{2\left|\mathbf{U}_i^n \cdot \boldsymbol{\eta}_{ij}\right|, 2\left|\mathbf{U}_j^n \cdot \boldsymbol{\eta}_{ij}\right|\right\} \tag{6.25}$$

or, we could consider

$$\alpha_{RS}^{\mathbf{w_u}}(\mathbf{W}_i^n, \mathbf{W}_j^n, \boldsymbol{\eta}_{ij}) := \max\left\{2\left|\mathbf{U}_i^n \cdot \boldsymbol{\eta}_{ij}\right|, 2\left|\mathbf{U}_j^n \cdot \boldsymbol{\eta}_{ij}\right|\right\} \tag{6.26}$$

for momentum equations and

$$\hat{\alpha}_{RS}(\mathbf{W}_i^n, \mathbf{W}_j^n, \boldsymbol{\eta}_{ij}) := \max\left\{\left|\mathbf{U}_i^n \cdot \boldsymbol{\eta}_{ij}\right|, \left|\mathbf{U}_j^n \cdot \boldsymbol{\eta}_{ij}\right|\right\} \tag{6.27}$$

for the remaining equations.

Directly using the value obtained for the conservative variables at each node at the previous time step, Rusanov scheme is first-order in space and time. Two different methodologies will be proposed in order to obtain second-order schemes: the CVC Kolgan-type scheme and the LADER scheme.

CVC Kolgan-type scheme

The CVC Kolgan-type scheme introduced in Section 3.3.1, which is second-order accurate in space and first-order in time, can be extended to the resolution of the incompressible Navier-stokes equations. In the numerical viscosity, the conservative values $\mathbf{W}_i^n$, $\mathbf{W}_j^n$ are replaced by the improved interpolations given by $\mathbf{W}_{iL}^n$, $\mathbf{W}_{jR}^n$ at both sides of each face Γ_{ij}, namely

$$\mathbf{W}_{iL}^n = \mathbf{W}_i^n + \Delta^{ijL}, \quad \mathbf{W}_{jR}^n = \mathbf{W}_j^n - \Delta^{ijR}.$$

The left and right limited slopes at the face, Δ^{ijL} and Δ^{ijR}, are defined through the Galerkin gradients computed on the upwind tetrahedra, T_{ijL} and T_{ijR}, respectively (see Figure 6.2 for the 2D case). Moreover, we avoid spurious oscillations by taking into account the minmod-type limiter

$$\Delta^{ijL} = Lim\left(\frac{1}{2}\left(\nabla \mathbf{W}^n\right)_{T_{ijL}} \overline{N_i N_j}\,, \mathbf{W}_j^n - \mathbf{W}_i^n\right), \tag{6.28}$$

$$\Delta^{ijR} = Lim\left(\frac{1}{2}\left(\nabla \mathbf{W}^n\right)_{T_{ijR}} \overline{N_i N_j}\,, \mathbf{W}_j^n - \mathbf{W}_i^n\right). \tag{6.29}$$

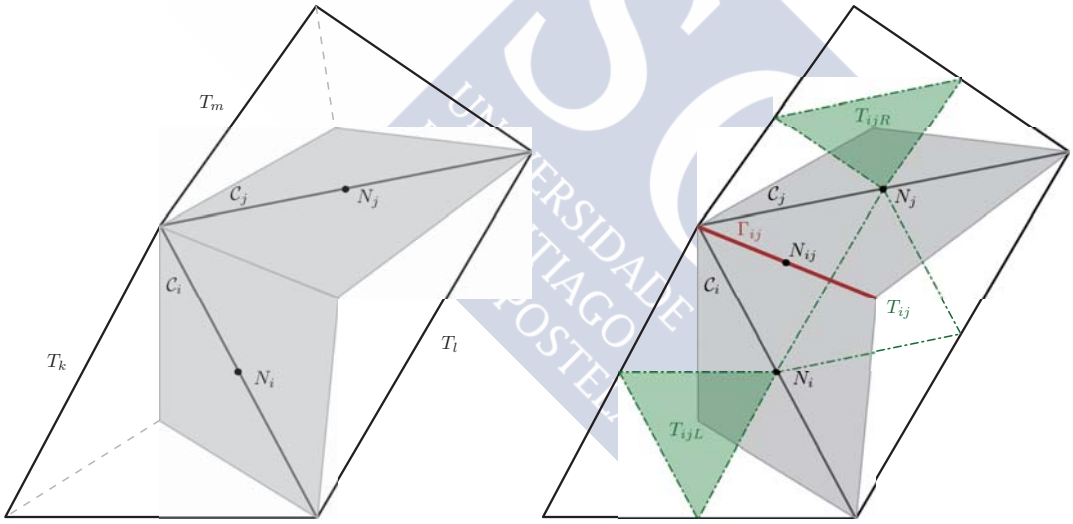

Figure 6.2: 2D mesh structure. Left: construction of the dual mesh (FV shadowed in grey). Right: auxiliary triangles related to face Γ_{ij} (upwind triangles shadowed in green).

Following [CVC12], this high-order extrapolation is used only in the upwind contribution of the numerical flux retaining the conservative variables in the centred part. So that, the numerical flux reads

$$\begin{aligned}\boldsymbol{\phi}\left(\mathbf{W}_i^n, \mathbf{W}_j^n, \mathbf{W}_{iL}^n, \mathbf{W}_{jR}^n, \boldsymbol{\eta}_{ij}\right) = \frac{1}{2}\left(\mathcal{Z}(\mathbf{W}_i^n, \boldsymbol{\eta}_{ij}) + \mathcal{Z}(\mathbf{W}_j^n, \boldsymbol{\eta}_{ij})\right) \\ -\frac{1}{2}\alpha_{RS}\left(\mathbf{W}_{iL}^n, \mathbf{W}_{jR}^n, \boldsymbol{\eta}_{ij}\right)\left(\mathbf{W}_{jR}^n - \mathbf{W}_{iL}^n\right).\end{aligned} \tag{6.30}$$

LADER approach

In Part II we have presented and analysed LADER methodology applied to the scalar advection-diffusion-reaction equation. That methodology was developed taking into account the dual mesh structure of the three-dimensional discretization. The main goal was to reduce the stencil and, hence, the computational cost of a second-order in space and time accuracy method. Moreover, the extension to 3D profits from the structure of the mesh of finite elements and uses a Galerkin approach in order to approximate the gradients involved in the computation of the evolved variables.

In this section, for easy of presentation, we will assume that the diffusion term only accounts for the velocity gradient, the remaining terms can be computed analogously. Let us consider W the approximation of a scalar conservative variable and α the related diffusion coefficient, known at each node at the previous time step, the proposed method includes the following steps:

Step 1. Data reconstruction.

Reconstruction of the data in terms of first degree polynomials is considered. At each finite volume we define four polynomials each of them at the neighbourhood of one of the boundary faces. Focusing on a face Γ_{ij}, its two related reconstruction polynomials are

$$p_{ij}^{i}(N) = W_i + (N - N_i)\,(\nabla W)_{ij}^{i}\,, \quad p_{ij}^{j}(N) = W_j + (N - N_j)\,(\nabla W)_{ij}^{j}\,. \tag{6.31}$$

A possible election of the gradients is

$$(\nabla W)_{ij}^{i} = \nabla W_{T_{ijL}}, \quad (\nabla W)_{ij}^{j} = \nabla W_{T_{ijR}} \tag{6.32}$$

which will result on a linear reconstruction as it is based on a fixed stencil.

In order to circumvent Godunov's theorem and prevent spurious oscillations, a non-linear reconstruction is considered (see [Tor09]). More precisely, the ENO (Essentially Non-Oscillatory) interpolation method is applied. The slopes are adaptively chosen as follows:

$$(\nabla W)_{ij}^{i} = \begin{cases} (\nabla W)_{T_{ijL}}\,, & \text{if } \left|(\nabla W)_{T_{ijL}} \cdot (N_{ij} - N_i)\right| \leq \left|(\nabla W)_{T_{ij}} \cdot (N_{ij} - N_i)\right|, \\ (\nabla W)_{T_{ij}}\,, & \text{if } \left|(\nabla W)_{T_{ijL}} \cdot (N_{ij} - N_i)\right| > \left|(\nabla W)_{T_{ij}} \cdot (N_{ij} - N_i)\right|; \end{cases} \tag{6.33}$$

$$(\nabla W)_{ij}^{j} = \begin{cases} (\nabla W)_{T_{ijR}}\,, & \text{if } \left|(\nabla W)_{T_{ijR}} \cdot (N_{ij} - N_j)\right| \leq \left|(\nabla W)_{T_{ij}} \cdot (N_{ij} - N_j)\right|, \\ (\nabla W)_{T_{ij}}\,, & \text{if } \left|(\nabla W)_{T_{ijR}} \cdot (N_{ij} - N_j)\right| > \left|(\nabla W)_{T_{ij}} \cdot (N_{ij} - N_j)\right|; \end{cases} \tag{6.34}$$

where $(\nabla W)_{T_{ij}}$ is the gradient of the velocity at the auxiliary tetrahedra which intersects the face.

Step 2. Computation of boundary extrapolated values at the barycenter of the faces, N_{ij}.

$$W_{i\,N_{ij}} = p_{ij}^{i}(N_{ij}) = W_i + (N_{ij} - N_i)\,(\nabla W)_{ij}^{i}\,, \tag{6.35}$$

$$W_{j\,N_{ij}} = p_{ij}^{j}(N_{ij}) = W_j + (N_{ij} - N_j)\,(\nabla W)_{ij}^{j}\,. \tag{6.36}$$

Step 3. Computation of the flux terms with second-order of accuracy using the midpoint rule.

Taylor series expansion in time and Cauchy - Kovalevskaya procedure are applied to locally approximate the conservative variables at time $\frac{\Delta t}{2}$. This methodology accounts for the contribution of the advection and diffusion terms to the time evolution of the flux term. The resulting evolved variables read

$$\begin{aligned}\overline{W_{i\,N_{ij}}} =& W_{i\,N_{ij}} - \frac{\Delta t}{2\mathcal{L}_{ij}}\left(\mathcal{Z}(W_{i\,N_{ij}}, \boldsymbol{\eta}_{ij}) + \mathcal{Z}(W_{j\,N_{ij}}, \boldsymbol{\eta}_{ij})\right) \\ &+ \frac{\Delta t}{2\mathcal{L}_{ij}^2}\left(\alpha_i\,(\nabla W)_{ij}^{i}\,\boldsymbol{\eta}_{ij} + \alpha_j\,(\nabla W)_{ij}^{j}\,\boldsymbol{\eta}_{ij}\right), \end{aligned} \tag{6.37}$$

$$\begin{aligned}\overline{W_{j\,N_{ij}}} =& W_{j\,N_{ij}} - \frac{\Delta t}{2\mathcal{L}_{ij}}\left(\mathcal{Z}(W_{i\,N_{ij}}, \boldsymbol{\eta}_{ij}) + \mathcal{Z}(W_{j\,N_{ij}}, \boldsymbol{\eta}_{ij})\right) \\ &+ \frac{\Delta t}{2\mathcal{L}_{ij}^2}\left(\alpha_i\,(\nabla W)_{ij}^{i}\,\boldsymbol{\eta}_{ij} + \alpha_j\,(\nabla W)_{ij}^{j}\,\boldsymbol{\eta}_{ij}\right). \end{aligned} \tag{6.38}$$

We have denoted $\mathcal{L}_{ij} = \min\left\{\frac{|C_i|}{\mathrm{S}(C_i)}, \frac{|C_j|}{\mathrm{S}(C_j)}\right\}$ with $\mathrm{S}(C_i)$ the area of the surface of cell C_i. Two different options will be considered in the scheme concerning the evolved variables. The first one corresponds to the previous definition of the evolved variables. Meanwhile, the second one neglects the evolution of the diffusion term.

Step 4. Computation of the numerical flux considering Rusanov scheme.

$$\begin{aligned}\phi\left(\overline{W_{i\,N_{ij}}^{n}}, \overline{W_{j\,N_{ij}}^{n}}, \boldsymbol{\eta}_{ij}\right) =& \frac{1}{2}\left(\mathcal{Z}\left(\overline{W_{i\,N_{ij}}^{n}}, \boldsymbol{\eta}_{ij}\right) + \mathcal{Z}\left(\overline{W_{j\,N_{ij}}^{n}}, \boldsymbol{\eta}_{ij}\right)\right) \\ &- \frac{1}{2}\alpha_{RS}\left(\overline{W_{i\,N_{ij}}^{n}}, \overline{W_{j\,N_{ij}}^{n}}, \boldsymbol{\eta}_{ij}\right)\left(\overline{W_{j\,N_{ij}}^{n}} - \overline{W_{i\,N_{ij}}^{n}}\right). \end{aligned} \tag{6.39}$$

6.4.3 Viscous terms

We come next to describe the computation of the integrals involving the viscous terms, (2.51). First, applying Gauss' theorem we relate the volume integral of the diffusion term with a surface integral over the boundary, Γ_i. Next, this integral is split into the integrals over the cell interfaces Γ_{ij}. Thus, the viscous term of the momentum conservation equation reads

$$\int_{C_i} \operatorname{div} \tau^n dV = \sum_{N_j \in \mathcal{K}_i} \int_{\Gamma_{ij}} \tau^n \widetilde{\boldsymbol{\eta}}_{ij}\,\mathrm{dS}$$

$$= \sum_{N_j \in \mathcal{K}_i} \int_{\Gamma_{ij}} \left[(\mu + \mu_t^n) \left(\operatorname{grad} \mathbf{U}^n + (\operatorname{grad} \mathbf{U}^n)^T \right) - \frac{2}{3} \rho K^n I \right] \tilde{\boldsymbol{\eta}}_{ij} \, \mathrm{dS}. \tag{6.40}$$

Two different approaches can be considered in order to compute the above integral.

On the one hand, decomposition with semi-implicit and explicit discretizations can be applied when using the CVC Kolgan-type scheme. This methodology splits the diffusion flux into its orthogonal and non-orthogonal parts and relaxes the stability condition on the time step size (see [BFSVC14] for further details).

On the other hand, the dual mesh eases the use of Galerkin approach to compute the derivatives involved in (6.40). We introduce a numerical diffusion function $\boldsymbol{\varphi}_{\mathbf{u}}$ such that

$$\int_{\Gamma_{ij}} (\mu + \mu_t^n) \operatorname{grad} \mathbf{U}^n \tilde{\eta}_{ij} \mathrm{dS} \approx \boldsymbol{\varphi}_{\mathbf{u}} \left(\mathbf{U}_i^n, \mathbf{U}_j^n, \mu_{t,i}^n, \mu_{t,j}^n, \boldsymbol{\eta}_{ij} \right) \tag{6.41}$$

and we consider

$$\boldsymbol{\varphi}_{\mathbf{u}} \left(\mathbf{U}_i^n, \mathbf{U}_j^n, \mu_{t,i}^n, \mu_{t,j}^n, \boldsymbol{\eta}_{ij} \right) = \left(\mu + \mu_{t,ij}^n \right) \left(\operatorname{grad} \mathbf{U}^n \right)_{T_{ij}} \boldsymbol{\eta}_{ij}, \tag{6.42}$$

with

$$\mu_{t,ij}^n = \frac{1}{2} \left(\mu_{t,i}^n + \mu_{t,j}^n \right). \tag{6.43}$$

Since we know the value of the turbulent kinetic energy at the nodes of the finite volumes, we approximate the turbulent kinetic energy term as the average of the values obtained at the two nodes related to the face

$$- \int_{\Gamma_{ij}} \frac{2}{3} W_k^n \tilde{\boldsymbol{\eta}}_{ij} \mathrm{dS} = -\frac{1}{3} \left(W_{k,i}^n + W_{k,j}^n \right) \boldsymbol{\eta}_{ij}. \tag{6.44}$$

Finally, the viscous terms for the remaining equations are obtained equally to the gradient term of the momentum equation:

$$\int_{C_i} \frac{1}{\rho} \operatorname{div} \left(\boldsymbol{\mathcal{D}}^n \operatorname{grad} \widehat{\mathbf{W}}^n \right) dV = \frac{1}{\rho} \sum_{N_j \in \mathcal{K}_i} \int_{\Gamma_{ij}} \boldsymbol{\mathcal{D}}^n \operatorname{grad} \widehat{\mathbf{W}}^n \, \tilde{\boldsymbol{\eta}}_{ij} \, dS, \tag{6.45}$$

where

$$\boldsymbol{\mathcal{D}}^n = \begin{pmatrix} \mathcal{D}_k^n & 0 & 0 \\ 0 & \mathcal{D}_\varepsilon^n & 0 \\ 0 & 0 & \mathcal{D}_{\mathbf{y}}^n \end{pmatrix} = \begin{pmatrix} \mu + \dfrac{\mu_t^n}{\sigma_k} & 0 & 0 \\ 0 & \mu + \dfrac{\mu_t^n}{\sigma_\varepsilon} & 0 \\ 0 & 0 & \rho \mathcal{D} + \dfrac{\mu_t^n}{Sc_t} \end{pmatrix}. \tag{6.46}$$

Thus, we can introduce the diffusion flux function, $\boldsymbol{\varphi}_{\widehat{\mathbf{w}}}$, verifying

$$\begin{aligned} &\int_{\Gamma_{ij}} \boldsymbol{\mathcal{D}}^n \operatorname{grad} \widehat{\mathbf{W}}^n \tilde{\boldsymbol{\eta}}_{ij} dS \approx \boldsymbol{\varphi}_{\widehat{\mathbf{w}}} \left(\widehat{\mathbf{W}}_i^n, \widehat{\mathbf{W}}_j^n, \mu_{t,i}^n, \mu_{t,j}^n, \boldsymbol{\eta}_{ij} \right), \\ &\boldsymbol{\varphi}_{\widehat{\mathbf{w}}} \left(\widehat{\mathbf{W}}_i^n, \widehat{\mathbf{W}}_j^n, \mu_{t,i}^n, \mu_{t,j}^n, \boldsymbol{\eta}_{ij} \right) = \boldsymbol{\mathcal{D}}_{ij}^n \left(\operatorname{grad} \widehat{\mathbf{W}^n} \right)_{T_{ij}} \boldsymbol{\eta}_{ij}. \end{aligned} \tag{6.47}$$

The above methodologies are used to approximate the viscous terms when choosing a first-order method or the CVC Kolgan-type scheme to compute the advection term. Nevertheless, the LADER methodology requires a special treatment.

LADER approach: the viscous terms

To apply LADER in order to obtain a second-order in space and time scheme, instead of computing the diffusion flux functions, $\boldsymbol{\varphi}_{\mathbf{u}}$ and $\boldsymbol{\varphi}_{\widehat{\mathbf{W}}}$, with the value of the variables at the previous time step, $\mathbf{U}^n$, K^n, E^n and $\mathbf{Y}^n$, it is necessary to use some evolved values, $\overline{\mathbf{U}^n}$, $\overline{K^n}$, $\overline{E^n}$ and $\overline{\mathbf{Y}^n}$.

It is important to remark that the former evolved variables do not match the already computed for the flux term. Taylor series expansion in time and Cauchy-Kovalevskaya procedure are applied neglecting the advection term so that a second-order in space and time scheme is attained:

$$\overline{\mathbf{U}^n} = \mathbf{U}^n + \frac{\Delta t}{2}\left\{\operatorname{div}\left[(\mu+\mu_t^n)\operatorname{grad}\mathbf{U}^n - \frac{2}{3}\rho K^n\mathbf{I}\right]\right\}, \tag{6.48}$$

$$\overline{K^n} = K^n + \frac{\Delta t}{2}\left[\left(\mu+\frac{\mu_t^n}{\sigma_k}\right)\operatorname{grad}K^n\right], \tag{6.49}$$

$$\overline{E^n} = E^n + \frac{\Delta t}{2}\left[\left(\mu+\frac{\mu_t^n}{\sigma_\varepsilon}\right)\operatorname{grad}E^n\right], \tag{6.50}$$

$$\overline{\mathbf{Y}^n} = \mathbf{Y}^n + \frac{\Delta t}{2}\left[\left(\rho\mathcal{D}+\frac{\mu_t^n}{Sc_t}\right)\operatorname{grad}\mathbf{Y}^n\right]. \tag{6.51}$$

In what follows, we describe the computation of the evolved velocities at an arbitrary node N_i:

1. The gradients of the original variables are computed at each auxiliary tetrahedra of the primal mesh, T_{ij} (see, on the 2D representation in Figure 6.2, the triangle with green contour). The value of the gradient at each node, N_i, is obtained as the average of the values on the two tetrahedra containing the node, T_{ijL} (green filled triangle in Figure 6.2) and T_{ij}. Taking into account the viscosity coefficients and the turbulent kinetic energy term, we introduce the auxiliary variable

$$\mathbf{V}_i^n := \left(\mu+\mu_{t,i}^n\right)\frac{1}{2}\left(\left(\operatorname{grad}\mathbf{U}^n\right)_{T_{ijL}} + \left(\operatorname{grad}\mathbf{U}^n\right)_{T_{ij}}\right) - \frac{2}{3}\rho K_i^n I. \tag{6.52}$$

2. The divergence is computed as the average of the divergences of $\mathbf{V}^n$ obtained on the auxiliary tetrahedra as

$$\overline{\mathbf{U}_i^n} = \mathbf{U}_i^n + \frac{\Delta t}{4}\operatorname{tr}\left(\left(\operatorname{grad}\mathbf{V}^n\right)_{T_{ijL}} + \left(\operatorname{grad}\mathbf{V}^n\right)_{T_{ij}}\right). \tag{6.53}$$

3. The diffusion function $\boldsymbol{\varphi}_{\mathbf{u}}$ is evaluated on the evolved variables, namely,

$$\boldsymbol{\varphi}_{\mathbf{u}}\left(\overline{\mathbf{U}_i^n}, \overline{\mathbf{U}_j^n}, \mu_{t,i}^n, \mu_{t,j}^n, \boldsymbol{\eta}_{ij}\right) = \left(\mu+\mu_{t,ij}^n\right)\left(\operatorname{grad}\overline{\mathbf{U}^n}\right)_{T_{ij}}\boldsymbol{\eta}_{ij}. \tag{6.54}$$

The remaining evolved variables are similarly obtained and the related diffusion function reads

$$\boldsymbol{\varphi}_{\widehat{\mathbf{w}}}\left(\overline{\widehat{\mathbf{W}}_i^n}, \overline{\widehat{\mathbf{W}}_j^n}, \mu_{t,i}^n, \mu_{t,j}^n, \boldsymbol{\eta}_{ij}\right) = \boldsymbol{\mathcal{D}}_{ij}^n\left(\operatorname{grad}\overline{\widehat{\mathbf{W}}^n}\right)_{T_{ij}}\boldsymbol{\eta}_{ij}. \tag{6.55}$$

6.4.4 Pressure term

For the integral of the pressure gradient we follow [BFSVC14]. We split the boundary Γ_i into the cell interfaces Γ_{ij} using Gauss' theorem and we compute the pressure as the arithmetic mean of its values at the three vertices of face Γ_{ij} and the barycenter of the tetrahedra to which the face belongs. Then, the corresponding approximation of the integral is given by

$$\int_{\Gamma_{ij}} \pi^n \, \widetilde{\boldsymbol{\eta}}_{ij} \mathrm{dS} \approx \left[\frac{5}{12} \left(\pi^n(V_1) + \pi^n(V_2) \right) + \frac{1}{12} \left(\pi^n(V_3) + \pi^n(V_4) \right) \right] \boldsymbol{\eta}_{ij}. \tag{6.56}$$

6.5 Projection stage

The incremental projection method presented in [GMS06] is adapted to solve system (6.9)-(6.10). Moreover, the pressure is computed using a standard finite element method.

Let $z \in V_0$ be a test function, $V_0 := \{z \in H^1(\Omega) : \int_\Omega z dV = 0\}$. Multiplying equation (6.9) by the gradient of the test function and integrating over Ω, we have

$$\int_\Omega \mathrm{grad}\left(\pi^{n+1} - \pi^n\right) \cdot \mathrm{grad} z dV = \frac{1}{\Delta t} \int_\Omega \widetilde{\mathbf{W}}_{\mathbf{u}}^{n+1} \cdot \mathrm{grad} z dV - \frac{1}{\Delta t} \int_\Omega \mathbf{W}_{\mathbf{u}}^{n+1} \cdot \mathrm{grad} z dV. \tag{6.57}$$

Besides, applying Green's formula to the divergence free condition (6.10), we get

$$\int_\Omega \mathbf{W}_{\mathbf{u}}^{n+1} \cdot \mathrm{grad} z dV = \int_\Gamma \mathbf{W}_{\mathbf{u}}^{n+1} \cdot \boldsymbol{\eta} \, \mathrm{grad} z dS - \int_\Omega \mathrm{div}\left(\mathbf{W}_{\mathbf{u}}^{n+1}\right) z dV = \int_\Gamma G^{n+1} z, \tag{6.58}$$

where

$$G^{n+1} = \mathbf{W}_{\mathbf{u}}^{n+1} \cdot \boldsymbol{\eta}. \tag{6.59}$$

By introducing the variable $\delta^{n+1} := \pi^{n+1} - \pi^n$ and taking into account relation (6.58) onto the variational formulation, (6.57), we obtain the weak problem:

Weak problem. Find $\delta^{n+1} \in V_0 := \{z \in H^1(\Omega) : \int_\Omega z = 0\}$ verifying

$$\int_\Omega \mathrm{grad}\delta^{n+1} \cdot \mathrm{grad} z dV = \frac{1}{\Delta t} \int_\Omega \widetilde{\mathbf{W}}_{\mathbf{u}}^{n+1} \cdot \mathrm{grad} z dV - \frac{1}{\Delta t} \int_\Gamma G^{n+1} z dS. \tag{6.60}$$

for all $z \in V_0$.

Moreover, it can be seen as corresponding to the following Laplace problem with Neumann boundary conditions

$$\Delta \delta^{n+1} = \frac{1}{\Delta t} \mathrm{div}\, \widetilde{\mathbf{W}}_{\mathbf{u}}^{n+1} \quad \text{in } \Omega, \tag{6.61}$$

$$\frac{\partial \delta^{n+1}}{\partial \boldsymbol{\eta}} = \frac{1}{\Delta t} \left(\widetilde{\mathbf{W}}_{\mathbf{u}}^{n+1} \cdot \boldsymbol{\eta} - G^{n+1} \right) \quad \text{in } \Gamma. \tag{6.62}$$

Further details about the projection stage and the coupling between the transport-diffusion stage and the projection stage can be seen in [BFSVC14].

6.6 Post-projection stage

Once the pressure is obtained, we can update $\mathbf{W}_{\mathbf{u}}^{n+1}$ with $\operatorname{grad}\delta_i^{n+1}$, that is,

$$\mathbf{W}_{\mathbf{u},\,i}^{n+1} = \widetilde{\mathbf{W}}_{\mathbf{u},\,i}^{n+1} + \Delta t \operatorname{grad}\delta_i^{n+1}. \tag{6.63}$$

The previous computation of the updated velocities allows for an implicit approach of the production term G_k on the turbulence equations. Meanwhile, for the dissipative terms a semi-implicit scheme is used:

$$\frac{W_{k,\,i}^{n+1} - \widetilde{W}_{k,\,i}^{n+1}}{\Delta t} + W_{\varepsilon,\,i}^{n} - G_{k,\,i}(\mathbf{U}^{n+1}) = f_{k,\,i}^{n}, \tag{6.64}$$

$$\frac{W_{\varepsilon,\,i}^{n+1} - \widetilde{W}_{\varepsilon,\,i}^{n+1}}{\Delta t} + C_{2\varepsilon}\frac{W_{\varepsilon,\,i}^{n}}{W_{k,\,i}^{n}} W_{\varepsilon,\,i}^{n+1} - C_{1\varepsilon}\frac{W_{\varepsilon,\,i}^{n}}{W_{k,\,i}^{n}} G_{k,\,i}(\mathbf{U}^{n+1}) = f_{\varepsilon,\,i}^{n}. \tag{6.65}$$

The derivatives involved in the production term, $G_{k,\,i}(\mathbf{U}^{n+1})$, are computed as the averaged of the auxiliary tetrahedra related to the node N_i. Finally, the source terms $\mathbf{f}_{\widehat{\mathbf{w}}}$ are pointwise evaluated.

6.7 Boundary conditions

The boundary conditions are defined following [BFSVC14] and [BFTVC18]:

- Dirichlet boundary conditions for inviscid fluids: the normal component of the conservative variable $\mathbf{w}_{\mathbf{u}}$ is set at the boundary nodes. The values of the remaining conservative variables, $\hat{\mathbf{w}}$, are set at the boundary nodes.
- Dirichlet boundary conditions for viscous fluids: the value of the conservative variables is imposed at the boundary nodes.
- Neumann boundary conditions: the definition of $\widetilde{\mathbf{W}}^{n+1}$ takes into account the inflow/outflow boundary condition with no need for any additional treatment.

Moreover, in the manufactured tests designed to analyse the order of accuracy of the numerical discretizations, it is a usual practice to impose the values of the exact solution at the boundary nodes. This practice avoids that the accuracy of the method can be affected by the treatment of the boundary conditions. From the mathematical point of view, it is like considering Dirichlet boundary conditions.

The boundary conditions defined above can be combined in diverse ways depending on the data supplied at the boundary. A more detailed description of the different types employed and the data provided is included in Table 6.1. Let us remark that if the turbulence intensity, I, and the hydraulic diameter, L, are provided then, the turbulence variables, k and ε, are computed from

$$k = \frac{3}{2}\left(u_{\text{avg}} I\right)^2, \quad \varepsilon = C_\mu^{3/4}\frac{k^{3/2}}{\ell} \tag{6.66}$$

	Velocity	Species	Energy	Turbulence	Pressure
Mass flow inlet	$\rho\mathbf{u}$	$\mathbf{y}$	θ	L, I	$\frac{\partial \pi}{\partial \boldsymbol{\eta}} = 0$
Velocity inlet	$\mathbf{u}$	$\mathbf{y}$	θ	L, I	$\frac{\partial \pi}{\partial \boldsymbol{\eta}} = 0$
Outflow	$\frac{\partial \mathbf{w_u}}{\partial \boldsymbol{\eta}} = 0$	$\frac{\partial \mathbf{w_y}}{\partial \boldsymbol{\eta}} = 0$	$\frac{\partial w_h}{\partial \boldsymbol{\eta}} = 0$	$\frac{\partial w_k}{\partial \boldsymbol{\eta}} = 0$, $\frac{\partial w_\varepsilon}{\partial \boldsymbol{\eta}} = 0$	$\frac{\partial \pi}{\partial \boldsymbol{\eta}} = 0$
Dirichlet	$\rho\mathbf{u}$	$\mathbf{y}$	h	ρk, $\rho\varepsilon$	$\frac{\partial \pi}{\partial \boldsymbol{\eta}} = 0$
Neumann	$\frac{\partial \mathbf{w_u}}{\partial \boldsymbol{\eta}}$	$\frac{\partial \mathbf{w_y}}{\partial \boldsymbol{\eta}}$	$\frac{\partial w_h}{\partial \boldsymbol{\eta}}$	$\frac{\partial w_k}{\partial \boldsymbol{\eta}}$, $\frac{\partial w_\varepsilon}{\partial \boldsymbol{\eta}}$	π

Table 6.1: Boundary conditions.

with $\ell = 0.07L$ the turbulence length scale and u_{avg} taken to be the averaged value of the normal velocity at the boundary, Γ, namely,

$$u_{\text{avg}} = \frac{1}{\text{Area}\,(\Gamma)} \sum_{N_i \in \Gamma} \mathbf{U}_i \cdot \boldsymbol{\eta}. \tag{6.67}$$

6.8 Numerical results

In this section, we present the results obtained for several test problems. In order to define the time step, two different options are implemented in the code. On the one hand, we can simply introduce a fixed time step. On the other hand, we can provide the CFL from which the code will compute the time step at each time iteration. The latest option is the one chosen to run the test cases presented in this thesis. Therefore, to determine the time step at each time iteration, we compute a local value for the time step at each cell C_i,

$$\Delta t_{C_i} = \frac{\text{CFL}\ \mathcal{L}_i^2}{2\,|\mathbf{U}_i|\,\mathcal{L}_i + \max\left\{\mu + \mu_{t,\,i}, \rho\mathcal{D} + \dfrac{\mu_{t,\,i}}{Sc_t}\right\}} \tag{6.68}$$

with $\mathcal{L}_i := \frac{|C_i|}{\text{S}(C_i)}$. Finally, as global time step at each time iteration, Δt, we choose the minimum of the time steps obtained at each cell.

Remark 6.8.1. The above definition of Δt_{C_i} is valid if the equation for the transport of species is solved; otherwise its value is given by

$$\Delta t_{C_i} = \frac{\text{CFL}\ \mathcal{L}_i^2}{2\,|\mathbf{U}_i|\,\mathcal{L}_i + \mu + \mu_{t,\,i}}. \tag{6.69}$$

6.8.1 Test 1. Laminar flow (MMS)

The first test to be posed was obtained using the method of manufactured solutions (MMS). We consider the computational domain $\Omega = [0,1]^3$ and we assume the flow being defined by

$$\rho = 1, \tag{6.70}$$

$$\pi(x,y,z,t) = \cos(\pi t(x+y+z)), \tag{6.71}$$

$$\mathbf{u}(x,y,z,t) = \left(\sin(\pi yt)\cos(\pi zt),\ -\cos(\pi z^3 t),\ \exp(-2\pi x t^2)\right)^T, \tag{6.72}$$

with $\mu = 10^{-2}$ and the source terms given by

$$\begin{aligned}
\mathbf{f}_{\mathbf{u}_1}(x,y,z,t) &= \pi y\cos(\pi ty)\cos(\pi tz) - \pi t\sin(\pi t(x+y+z)) \\
&\quad -\pi z\sin(\pi ty)\sin(\pi tz) + 2\pi^2 t^2\mu\sin(\pi ty)\cos(\pi tz) \\
&\quad -\pi t\cos(\pi tz^3)\cos(\pi ty)\cos(\pi tz) \\
&\quad -\pi t\sin(\pi ty)\sin(\pi tz)\exp(-2\pi t^2 x), \qquad (6.73)\\
\mathbf{f}_{\mathbf{u}_2}(x,y,z,t) &= \pi z^3\sin(\pi tz^3) - \pi t\sin(\pi t(x+y+z)) - 6\pi tz\mu\sin(\pi tz^3) \\
&\quad -9\pi^2 t^2 z^4\mu\cos(\pi tz^3) + 3\pi tz^2\exp(-2\pi t^2 x)\sin(\pi tz^3), \qquad (6.74)\\
\mathbf{f}_{\mathbf{u}_3}(x,y,z,t) &= -\pi t\sin(\pi t(x+y+z)) - 4\pi^2 t^4\mu\exp(-2\pi t^2 x) \\
&\quad -4\pi tx\exp(-2\pi t^2 x) \\
&\quad -2\pi t^2\sin(\pi ty)\exp(-2\pi t^2 x)\cos(\pi tz). \qquad (6.75)
\end{aligned}$$

To perform the error and order of accuracy analysis, we employ the three uniform meshes with different cell sizes presented in Table 6.2. We have denoted $N+1$ the

Mesh	N	Elements	Vertices	Nodes	V_h^m (m^3)	V_h^M (m^3)
M_1	4	384	125	864	$6.51E-04$	$1.30E-03$
M_2	8	3072	729	6528	$8.14E-05$	$1.63E-04$
M_3	16	24576	4913	50688	$1.02E-05$	$2.03E-05$

Table 6.2: Test 1. Laminar flow (MMS). Mesh features.

number of points along the edges, $h = 1/N$, V_h^m the minimum volume of the finite volumes and V_h^M the maximum volume of the finite volumes.

Four different methods are used to solve the problem: the first-order method presented in [BFSVC14], CVC Kolgan-type method with an orthogonal decomposition of the diffusion term (CVC-orth), CVC Kolgan-type method combined with a Galerkin

approach for the diffusion term (CVC-G) and LADER. The errors and orders, depicted in Table 6.3, were computed as follows:

$$E(\pi)_{M_i} = \|\pi - \pi_{M_i}\|_{l^2(L^2(\Omega))}\,, \quad E(\mathbf{w_u})_{M_i} = \|\mathbf{w_u} - \mathbf{w_u}_{M_i}\|_{l^2(L^2(\Omega)^3)}\,, \tag{6.76}$$

$$o_{\pi_{M_i/M_j}} = \frac{\ln\left(E(\pi)_{M_i}/E(\pi)_{M_j}\right)}{\ln\left(h_{M_i}/h_{M_j}\right)}, \quad o_{\mathbf{w_u}\,M_i/M_j} = \frac{\ln\left(E(\mathbf{w_u})_{M_i}/E(\mathbf{w_u})_{M_j}\right)}{\ln\left(h_{M_i}/h_{M_j}\right)}. \tag{6.77}$$

Method	Variable	E_{M_1}	E_{M_2}	E_{M_3}	o_{M_1/M_2}	o_{M_2/M_3}
Order 1	π	$1.24E-01$	$5.70E-02$	$2.96E-02$	1.12	0.95
	$\mathbf{w_u}$	$6.40E-02$	$3.32E-02$	$1.78E-02$	0.95	0.90
CVC-orth.	π	$6.30E-02$	$1.91E-02$	$8.84E-03$	1.72	1.11
	$\mathbf{w_u}$	$5.51E-02$	$2.06E-02$	$8.95E-03$	1.42	1.20
CVC-G	π	$5.98E-02$	$1.58E-02$	$4.58E-03$	1.92	1.78
	$\mathbf{w_u}$	$5.41E-02$	$1.88E-02$	$6.52E-03$	1.52	1.53
LADER	π	$4.10E-02$	$8.74E-03$	$2.03E-03$	2.23	2.11
	$\mathbf{w_u}$	$2.61E-02$	$5.76E-03$	$1.24E-03$	2.18	2.22

Table 6.3: Test 1. Laminar flow (MMS). Observed errors and convergence rates. $CFL = 1$.

We can observe that CVC-G method provides an order of convergence close to two for the pressure and 1.5 for the conservative velocities. This is in accordance with the theoretical order of this scheme, first-order in time and second-order in space, and the high time-dependency of the solution. Whereas, with LADER scheme the expected second-order of accuracy is achieved.

6.8.2 Test 2. Turbulent flow with species transport (MMS)

The second academic test to be considered is a modification of the previous test to account for the turbulence and species transport equations. Let us define the flow as

$$\rho = 1, \tag{6.78}$$

$$\pi(x, y, z, t) = \cos(\pi t(x + y + z)), \tag{6.79}$$

$$\mathbf{u}(x, y, z, t) = \left(\sin(\pi y t)\cos(\pi z t),\ -\cos(\pi z^3 t),\ \exp(-2\pi x t^2)\right)^T, \tag{6.80}$$

$$k(x, y, z, t) = \sin(\pi x t) + 2, \tag{6.81}$$

$$\varepsilon(x,y,z,t) = \exp(-\pi z t) + 1, \tag{6.82}$$
$$\mathrm{y}(x,y,z,t) = \sin(\pi x t) + 2, \tag{6.83}$$

with parameters $\mu = 10^{-2}$, $\mathcal{D} = 10^{-3}$. For the exact solution to verify the equations, the following source terms have to be taken:

$$\begin{aligned}
\mathbf{f}_{\mathbf{u}_1}(x,y,z,t) &= (2\pi t\cos(\pi t x))/3 - \pi t\sin(\pi t(x+y+z)) + \pi y\cos(\pi t y)\cos(\pi t z)\\
&\quad -\pi z\sin(\pi t y)\sin(\pi t z) + 2\pi^2 t^2\mu\sin(\pi t y)\cos(\pi t z)\\
&\quad -\pi t\cos(\pi t z^3)\cos(\pi t y)\cos(\pi t z) - \pi t\sin(\pi t y)\sin(\pi t z)\exp(-2\pi t^2 x)\\
&\quad +(2\pi^2 C_\mu t^2\sin(\pi t y)\cos(\pi t z)(\sin(\pi t x)+2)^2)/(\exp(-\pi t z)+1)\\
&\quad +(\pi^2 C_\mu t^2\sin(\pi t y)\sin(\pi t z)\exp(-\pi t z)\\
&\quad (\sin(\pi t x)+2)^2)/(\exp(-\pi t z)+1)^2, \qquad (6.84)\\
\mathbf{f}_{\mathbf{u}_2}(x,y,z,t) &= \pi z^3\sin(\pi t z^3) - \pi t\sin(\pi t(x+y+z)) - 6\pi t z\mu\sin(\pi t z^3)\\
&\quad 9\pi^2 t^2 z^4\mu\cos(\pi t z^3) + 3\pi t z^2\exp(-2\pi t^2 x)\sin(\pi t z^3)\\
&\quad -(9\pi^2 C_\mu t^2 z^4\cos(\pi t z^3)(\sin(\pi t x)+2)^2)/(\exp(-\pi t z)+1)\\
&\quad -(6\pi C_\mu t z\sin(\pi t z^3)(\sin(\pi t x)+2)^2)/(\exp(-\pi t z)+1)\\
&\quad -(3\pi^2 C_\mu t^2 z^2\exp(-\pi t z)\sin(\pi t z^3)\\
&\quad (\sin(\pi t x)+2)^2)/(\exp(-\pi t z)+1)^2, \qquad (6.85)\\
\mathbf{f}_{\mathbf{u}_3}(x,y,z,t) &= (4\pi^2 C_\mu t^3\exp(-2\pi t^2 x)\cos(\pi t x)(\sin(\pi t x)+2))/(\exp(-\pi t z)+1)\\
&\quad -4\pi^2 t^4\mu\exp(-2\pi t^2 x) - 4\pi t x\exp(-2\pi t^2 x)\\
&\quad -2\pi t^2\sin(\pi t y)\exp(-2\pi t^2 x)\cos(\pi t z) - \pi t\sin(\pi t(x+y+z))\\
&\quad -(4\pi^2 C_\mu t^4\exp(-2\pi t^2 x)(\sin(\pi t x)+2)^2)/(\exp(-\pi t z)+1), \qquad (6.86)\\
f_k(x,y,z,t) &= \exp(-\pi t z) + \pi x\cos(\pi t x)\\
&\quad -(C_\mu(\sin(\pi t x)+2)^2(2\pi t^2\exp(-2\pi t^2 x)\\
&\quad +\pi t\sin(\pi t y)\sin(\pi t z))^2)/(\exp(-\pi t z)+1)\\
&\quad +\pi^2 t^2\mu\sin(\pi t x) + \pi t\sin(\pi t y)\cos(\pi t x)\cos(\pi t z)\\
&\quad -(9\pi^2 C_\mu t^2 z^4\sin(\pi t z^3)^2(\sin(\pi t x)+2)^2)/(\exp(-\pi t z)+1)\\
&\quad -(\pi^2 C_\mu t^2\cos(\pi t y)^2\cos(\pi t z)^2(\sin(\pi t x)+2)^2)/(\exp(-\pi t z)+1)\\
&\quad -(2\pi^2 C_\mu t^2\cos(\pi t x)^2(\sin(\pi t x)+2))/(\sigma_k(\exp(-\pi t z)+1))\\
&\quad +(\pi^2 C_\mu t^2\sin(\pi t x)(\sin(\pi t x)+2)^2)/(\sigma_k(\exp(-\pi t z)+1))+1, \qquad (6.87)\\
f_\varepsilon(x,y,z,t) &= (C_{2\,\varepsilon}(\exp(-\pi t z)+1)^2)/(\sin(\pi t x)+2) - \pi z\exp(-\pi t z)\\
&\quad -\pi^2 t^2\mu\exp(-\pi t z) - \pi t\exp(-\pi t z)\exp(-2\pi t^2 x)\\
&\quad -(C_{1\,\varepsilon}(\exp(-\pi t z)+1)((C_\mu(\sin(\pi t x)+2)^2(2\pi t^2\exp(-2\pi t^2 x)\\
&\quad +\pi t\sin(\pi t y)\sin(\pi t z))^2)/(\exp(-\pi t z)+1)\\
&\quad +(9\pi^2 C_\mu t^2 z^4\sin(\pi t z^3)^2(\sin(\pi t x)+2)^2)/(\exp(-\pi t z)+1)\\
&\quad +(\pi^2 C_\mu t^2\cos(\pi t y)^2\cos(\pi t z)^2(\sin(\pi t x)\\
&\quad +2)^2)/(\exp(-\pi t z)+1)))/(\sin(\pi t x)+2)
\end{aligned}$$

$$-(\pi^2 C_\mu t^2 \exp(-\pi tz)(\sin(\pi tx)+2)^2)/(\sigma_\varepsilon(\exp(-\pi tz)+1))$$
$$+(\pi^2 C_\mu t^2 \exp(-2\pi tz)(\sin(\pi tx)+2)^2)/(\sigma_\varepsilon(\exp(-\pi tz)+1)^2), \quad (6.88)$$

$$f_y(x,y,z,t) = \pi x\cos(\pi tx)+\pi t\sin(\pi ty)\cos(\pi tx)\cos(\pi tz)$$
$$+\pi^2 t^2\sin(\pi tx)(\mathcal{D}+(C_\mu(\sin(\pi tx)+2)^2)/(Sc_t(\exp(-\pi tz)+1)))$$
$$-(2\pi^2 C_\mu t^2\cos(\pi tx)^2(\sin(\pi tx)+2))/(Sc_t(\exp(-\pi tz)+1)). \quad (6.89)$$

Method	Variable	E_{M_1}	E_{M_2}	E_{M_3}	o_{M_1/M_2}	o_{M_2/M_3}
Order 1	π	$6.97E-01$	$5.52E-01$	$4.93E-01$	0.34	0.16
	$\mathbf{w_u}$	$4.40E-02$	$2.80E-02$	$2.18E-02$	0.65	0.36
	w_k	$3.85E-02$	$2.45E-02$	$2.09E-02$	0.65	0.23
	w_ε	$1.53E-02$	$8.47E-03$	$6.40E-03$	0.85	0.40
	w_y	$2.93E-02$	$2.04E-02$	$1.76E-02$	0.52	0.21
CVC-orth.	π	$6.23E-01$	$5.13E-01$	$4.75E-01$	0.28	0.11
	$\mathbf{w_u}$	$4.08E-02$	$2.65E-02$	$2.10E-02$	0.62	0.33
	w_k	$3.18E-02$	$2.13E-02$	$1.95E-02$	0.58	0.13
	w_ε	$1.51E-02$	$8.17E-03$	$6.15E-03$	0.89	0.41
	w_y	$2.51E-02$	$1.85E-02$	$1.68E-02$	0.44	0.14
CVC-G	π	$2.70E-01$	$7.60E-02$	$2.09E-02$	1.83	1.86
	$\mathbf{w_u}$	$1.50E-02$	$5.18E-03$	$1.49E-03$	1.54	1.80
	w_k	$1.54E-02$	$3.24E-03$	$8.22E-04$	2.25	1.98
	w_ε	$1.06E-02$	$2.39E-03$	$6.35E-04$	2.15	1.91
	w_y	$7.27E-03$	$1.89E-03$	$4.86E-04$	1.94	1.96
LADER	π	$2.68E-01$	$7.61E-02$	$2.10E-02$	1.82	1.86
	$\mathbf{w_u}$	$1.51E-02$	$5.17E-03$	$1.50E-03$	1.55	1.79
	w_k	$1.37E-02$	$2.51E-03$	$5.89E-04$	2.45	2.09
	w_ε	$9.87E-03$	$1.80E-03$	$4.09E-04$	2.46	2.14
	w_y	$7.25E-03$	$1.60E-03$	$3.79E-04$	2.18	2.08

Table 6.4: Test 2. Turbulent flow (MMS). Observed errors and convergence rates. $CFL = 10$.

We consider the meshes already defined in Table 6.2 and a $CFL = 10$ (the reason why this large value of CFL is admitted was studied in [BTVC16]). Dirichlet boundary conditions are set for all the equations. The computed errors are presented in Table 6.4. The results obtained for CVC-orth confirm that using only second-order in space for computing the flux terms and neglecting the non orthogonal component will not capture properly the turbulence. Second-order in space must also be used to approximate the diffusion terms and the whole flux should be computed. Furthermore, a second-order in time scheme improve the results and order attained.

6.8.3 Test 3. Euler flow around a sphere

As a third test, we have solved the stationary inviscid Euler flow around a sphere. This problem is discussed, for instance, in [LL87] and [BFSVC14].

The statement of the problem is as follows: a sphere of radius $R = 1$ centered at the origin is surrounded by the computational domain of the flow, consisting of a cube of dimensions $\Omega = [-4, 4]^3$. The parameters of the flow are the following:

$$M_\infty = 10^{-2},\ \gamma = 1.4,\ \rho_\infty = 1,\ \pi_\infty = \frac{1}{\gamma},\ c_\infty = 1,\ u_\infty = M_\infty c_\infty = 10^{-2}. \tag{6.90}$$

The analytic solution, expressed in Cartesian coordinates is given by

$$\mathbf{u}(x, y, z, t) = \mathbf{u}_\infty + \frac{1}{2}\left(\frac{R}{r(x, y, z)}\right)^3 \left[-3\frac{\mathbf{r}(x, y, z)}{r^2(x, y, z)}\mathbf{u}_\infty \cdot \mathbf{r}(x, y, z) + \mathbf{u}_\infty\right], \tag{6.91}$$

where $\mathbf{r}$ is the position vector, $r = \|\mathbf{r}\|$ and $\mathbf{u}_\infty = u_\infty \mathbf{e}_1$. Since in this problem we consider $\rho = \rho_\infty = 1$, the physical and conservative variables coincide.

In virtue of Bernoulli's theorem, the pressure is derived from the velocity field as:

$$\pi(x, y, z, t) = \pi_\infty + \rho_0\left(\frac{1}{2}u_\infty^2 - \frac{1}{2}\|\mathbf{u}(x, y, z)\|^2\right). \tag{6.92}$$

We use the code VolFEM3D to solve the evolutionary problem until a steady state is attained. The algorithm is started with $\pi_0(x, y, z) = p_\infty$ and

$$\mathbf{u}_0(x, y, z) \quad = \quad \begin{cases} u_\infty \mathbf{e_1}, & \text{if } (x, y, z) \in \Gamma_I, \\ 0, & \text{otherwise.} \end{cases} \tag{6.93}$$

The boundary conditions of the problem are shown in Table 6.5. Function $g = \mathbf{w} \cdot \mathbf{n}$ appearing in Dirichlet boundary conditions is defined from the exact solution $\mathbf{w} = \rho\mathbf{u} = \mathbf{u}$, given by (6.91).

The unstructured mesh M employed in this test has 318684 tetrahedra, 55022 vertices and 641149 finite volumes.

Computations are carried out until time $t_{\text{end}} = 10$. Two different methods are applied, the first-order scheme and LADER-ENO methodology. The numerical results

Boundary	Surface	Type (TD-stage)	Condition
Γ_I, inlet	$x = -4$	Dirichlet	$\mathbf{w} \cdot \mathbf{n} = g$
Γ_W, wall	$r = 1$, $y = -4$, $y = 4$, $z = -4$ and $z = 4$	Dirichlet	$\mathbf{w} \cdot \mathbf{n} = g$
Γ_O, outlet	$x = 4$	Neumann	$\frac{\partial \mathbf{w}}{\partial \mathbf{n}} = 0$

Table 6.5: Test3. Boundary conditions for the flow around a sphere. $t_{\text{end}} = 10$.

obtained for different values of Δt are shown in Table 6.6. The CFL numbers related to each time step are also depicted. Furthermore, to confirm that the steady state is reached, we compute

$$\frac{\Delta \mathbf{w_u}}{\Delta t} = \frac{1}{\Delta t} \left\| \mathbf{W_u}^{n_{\text{end}}} - \mathbf{W_u}^{n_{\text{end}}-1} \right\|_{\mathcal{L}^2(\Omega)}. \tag{6.94}$$

Both methods provide similar errors due to the rough spatial discretization considered. To obtain improved results and analyse the order of accuracy we would need not only to decrease the time step but also to refine the spatial mesh. Analysing the CPU time required, we observe that the first-order method demands almost a half of the time employed by LADER.

Method	Δt	CFL	real time	$\Delta \mathbf{w_u}/\Delta t$	$E_{\mathcal{L}_2(\Omega)}(\pi)$	$E_{\mathcal{L}_2(\Omega)}(\mathbf{w_u})$
Order 1	0.4	4.12	00 : 15 : 50	$3.79E-4$	$1.38E-5$	$7.33E-4$
	0.3	3.09	00 : 16 : 36	$3.47E-4$	$1.37E-5$	$7.32E-4$
	0.2	2.06	00 : 24 : 11	$3.33E-4$	$1.37E-5$	$7.31E-4$
	0.1	1.03	00 : 46 : 33	$3.16E-4$	$1.36E-5$	$7.30E-4$
	0.05	0.51	01 : 34 : 51	$3.09E-4$	$1.36E-5$	$7.31E-4$
LADER	0.4	4.12	00 : 24 : 54	$1.02E-3$	$1.05E-5$	$8.88E-4$
	0.3	3.08	00 : 34 : 06	$9.22E-4$	$1.04E-5$	$8.80E-4$
	0.2	2.05	00 : 41 : 18	$8.63E-4$	$1.04E-5$	$8.76E-4$
	0.1	1.02	01 : 37 : 01	$8.09E-4$	$1.04E-5$	$8.72E-4$
	0.05	0.51	03 : 13 : 22	$7.87E-4$	$1.04E-5$	$8.71E-4$

Table 6.6: Test 3. Euler flow around a sphere. Observed errors. $t_{\text{end}} = 10$.

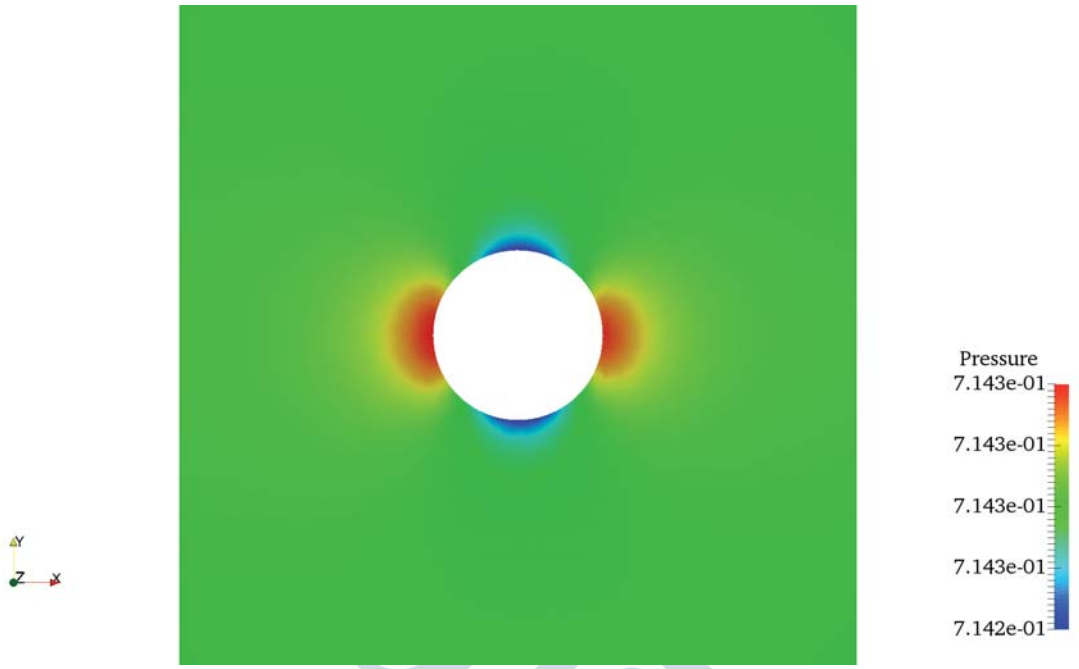

Figure 6.3: Test 3. Euler flow around a sphere. Pressure on $z = 0$, $t_{\text{end}} = 10$. Order 1.

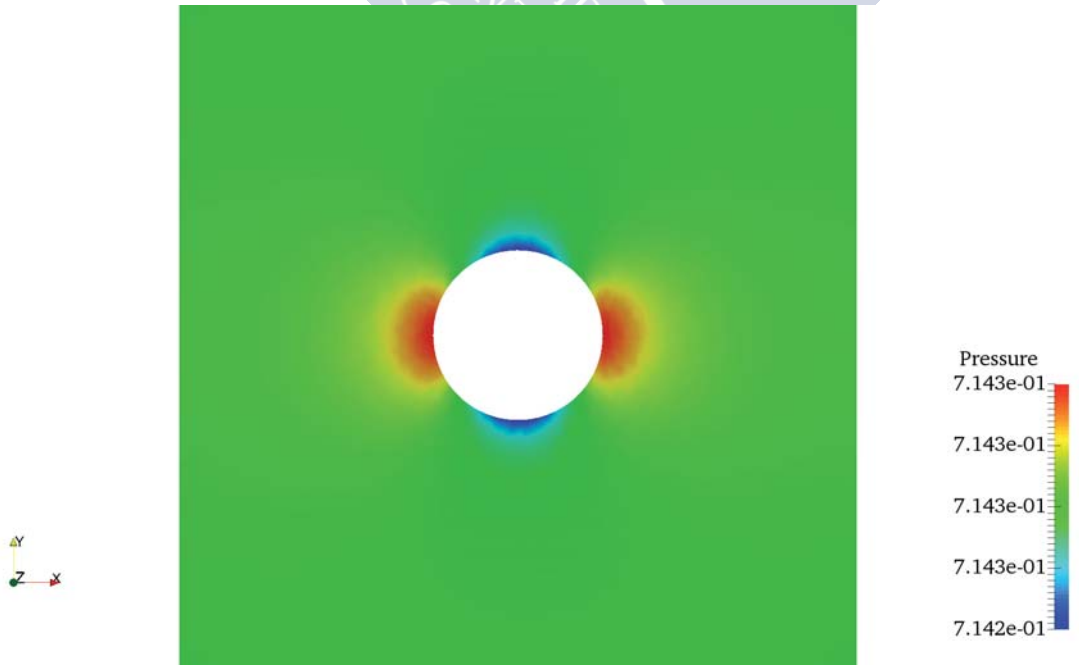

Figure 6.4: Test 3. Euler flow around a sphere. Pressure on $z = 0$, $t_{\text{end}} = 10$. LADER.

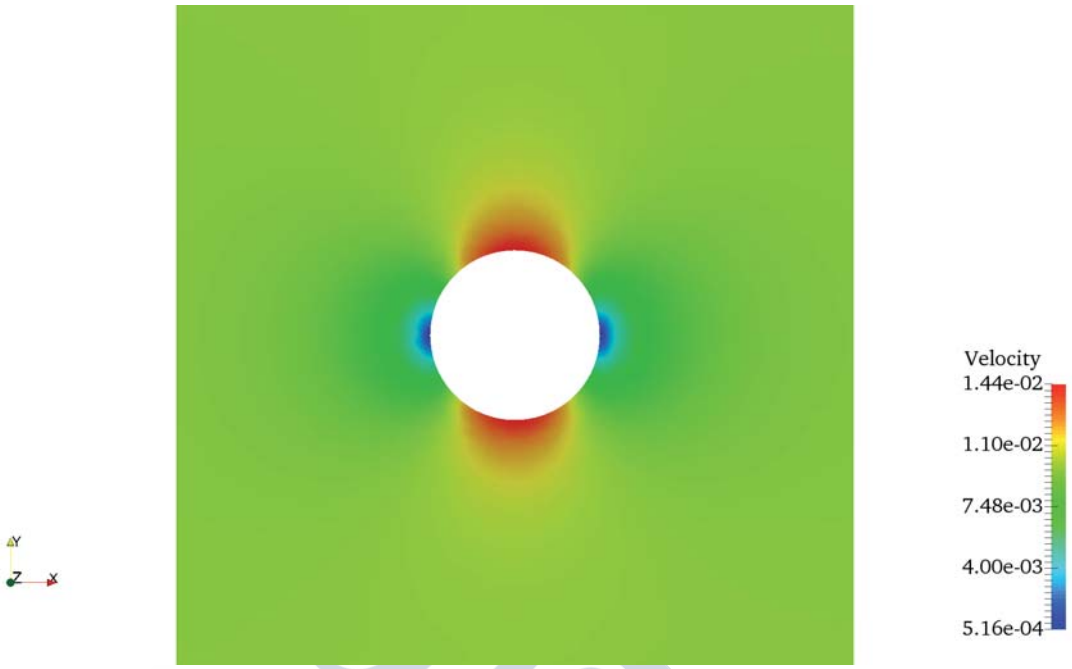

Figure 6.5: Test 3. Euler flow around a sphere. Velocity magnitude on $z = 0$, $t_{\text{end}} = 10$. Order 1.

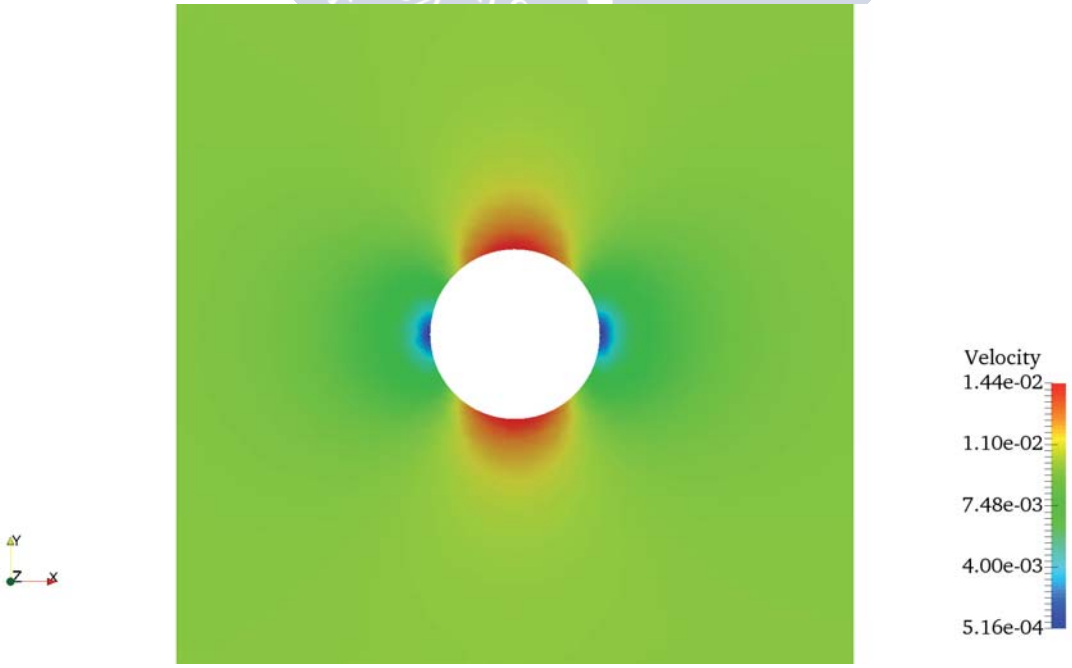

Figure 6.6: Test 3. Euler flow around a sphere. Velocity magnitude on $z = 0$, $t_{\text{end}} = 10$. LADER.

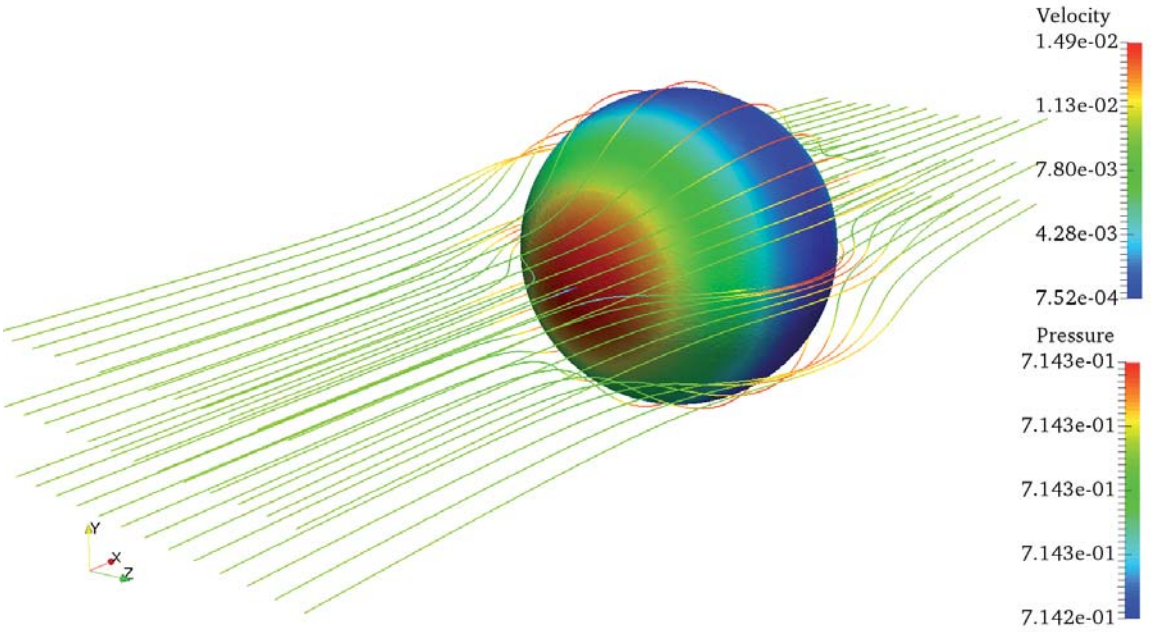

Figure 6.7: Test 3. Euler flow around a sphere. Pressure over the sphere and streamlines coloured by velocity magnitude. $t_{\text{end}} = 10$. Order 1.

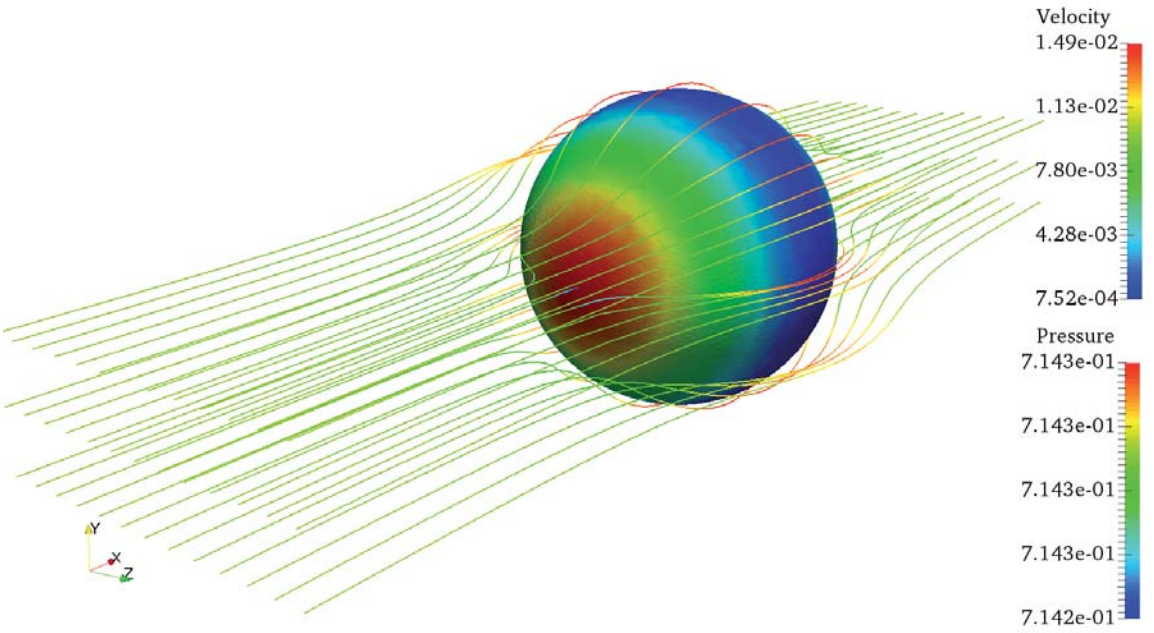

Figure 6.8: Test 3. Euler flow around a sphere. Pressure over the sphere and streamlines coloured by velocity magnitude. $t_{\text{end}} = 10$. LADER.

Results for the pressure and the modulus of the velocity are shown in Figures 6.3-6.6 at $z = 0$ for $\Delta t = 0.4$. Figures 6.7 and 6.8 show the streamlines corresponding to the approximate solution. Moreover, the approximate values of the pressure are depicted over the sphere. As can be seen, the solution is independent of the spherical coordinate θ and owing to this the result is the same on the planes $y = 0$ and $z = 0$. Therefore, we present the solutions for pressure and speed, on the plane $z = 0$, since in the present setup this variable coincides with the conservative variable.

6.8.4 Test 4. Gaussian sphere

The next problem to be analysed is the Gaussian sphere test introduced in [BS12] and [Saa11]. We consider a normal distribution function in the computational domain $\Omega = [-0.9, 0.9] \times [-0.9, 0.9] \times [-0.3, 0.3]$ with standard deviation 0.08 and mean 0.25. The density is set to one, the velocity vector is defined as $\mathbf{u}(x, y, z, t) = (-y,\ x,\ 0)^T$ and we assume that the diffusion matrix is given by $\mathcal{D} = \mu$. Hence, the solution of the problem is given by

$$\mathrm{y}(x, y, z, t) = \left(\frac{\sigma_0}{\sigma(t)}\right)^3 \exp\left(\frac{-r}{2\sigma(t)^2}\right) \tag{6.95}$$

with

$$r(x, y, z, t) = (\bar{x} + 0.25)^2 + \bar{y}^2 + z^2, \quad \sigma(t) = \sqrt{\sigma_0^2 + 2t\mathcal{D}}, \tag{6.96}$$

$$\bar{x} = x\cos(t) + y\sin(t), \quad \bar{y} = -x\sin(t) + y\cos(t). \tag{6.97}$$

The flow definition is completed setting the source terms

$$\mathbf{f}_{\mathbf{u}}(x, y, z, t) = (-x, -y, 0)^T, \quad f_{\mathrm{y}}(x, y, z, t) = 0 \tag{6.98}$$

and considering Dirichlet boundary conditions.

In order to analyse the accuracy in time and space, five structured meshes were generated. The properties of these meshes can be seen in Table 6.7, where h denotes the size of the cubes used to generate the tetrahedra of the finite element mesh.

Table 6.8 shows the results obtained for the test considering $\mu = 10^{-3}$. On the other hand, in Table 6.9 the errors and orders of accuracy for $\mu = 10^{-2}$ are presented. In both test cases we have assumed a final time $t_{\text{end}} = 2\pi$ so that the sphere completes one revolution. Two different methodologies were considered to run these tests: CVC-G and LADER. We can observe that for $\mu = 10^{-3}$ CVC-G scheme only achieves first-order and for $\mu = 10^{-2}$ the order obtained is a bit greater but still lower than two for the velocities approach. Meanwhile, using LADER we obtain the expected second-order in both tests cases and the errors obtained decrease. These improvements derive from considering a second-order method in time. The high diffusivity of the test makes necessary to consider second-order in both, time and space, to achieve good approaches for all the unknowns of the problem.

Mesh	Finite elements	Vertices	Nodes	h
M_1	11664	2527	24408	0.1
M_2	18522	3872	38514	0.0857
M_3	54000	10571	111000	0.06
M_4	93312	17797	190944	0.05
M_5	182250	33856	256711	0.04

Table 6.7: Test 4. Gaussian sphere. Mesh features.

The previous discussion is also consistent with the graphical results presented in Figures 6.9-6.14.

		π		$\mathbf{w_u}$		w_y	
		E_{M_i}	o_{M_{i-1}/M_i}	E_{M_i}	o_{M_{i-1}/M_i}	E_{M_i}	o_{M_{i-1}/M_i}
CVC-G	M_1	$7.48E{-}02$		$1.33E{-}01$		$4.00E{-}02$	
	M_2	$6.59E{-}02$	0.82	$1.17E{-}01$	0.84	$3.56E{-}02$	0.75
	M_3	$4.75E{-}02$	0.92	$8.52E{-}02$	0.89	$2.63E{-}02$	0.85
	M_4	$4.02E{-}02$	0.92	$7.21E{-}02$	0.91	$2.20E{-}02$	0.99
	M_5	$3.24E{-}02$	0.96	$5.82E{-}02$	0.96	$1.73E{-}02$	1.08
LADER	M_1	$1.02E{-}03$		$2.48E{-}03$		$2.31E{-}02$	
	M_2	$7.25E{-}04$	2.19	$1.81E{-}03$	2.02	$1.83E{-}02$	1.50
	M_3	$3.23E{-}04$	2.27	$8.17E{-}04$	2.24	$1.00E{-}02$	1.70
	M_4	$2.12E{-}04$	2.32	$5.41E{-}04$	2.26	$7.11E{-}03$	1.88
	M_5	$1.25E{-}04$	2.36	$3.24E{-}04$	2.30	$4.59E{-}03$	1.97

Table 6.8: Test 4. Gaussian sphere, $\mu = 10^{-3}$. Observed errors and convergence rates. CFL = 5 for CVC-G and CFL = 0.5 for LADER.

		π		$\mathbf{w_u}$		w_y	
		E_{M_i}	o_{M_{i-1}/M_i}	E_{M_i}	o_{M_{i-1}/M_i}	E_{M_i}	o_{M_{i-1}/M_i}
CVC-G	M_1	$3.31E{-}02$		$5.13E{-}02$		$2.19E{-}03$	
	M_2	$2.74E{-}02$	1.22	$4.29E{-}02$	1.16	$1.67E{-}03$	1.77
	M_3	$1.72E{-}02$	1.31	$2.74E{-}02$	1.26	$9.02E{-}04$	1.73
	M_4	$1.34E{-}02$	1.39	$2.15E{-}02$	1.34	$6.62E{-}04$	1.70
	M_5	$9.69E{-}03$	1.44	$1.57E{-}02$	1.40	$4.54E{-}04$	1.69
LADER	M_1	$3.68E{-}04$		$9.02E{-}04$		$1.61E{-}03$	
	M_2	$2.54E{-}04$	2.41	$6.24E{-}04$	2.02	$1.16E{-}03$	2.12
	M_3	$1.12E{-}04$	2.29	$2.60E{-}04$	2.24	$5.55E{-}04$	2.07
	M_4	$7.57E{-}05$	2.15	$1.66E{-}04$	2.26	$3.85E{-}04$	2.01
	M_5	$4.78E{-}05$	2.06	$9.54E{-}05$	2.30	$2.48E{-}04$	1.97

Table 6.9: Test 4. Gaussian sphere, $\mu = 10^{-2}$. Observed errors and convergence rates. CFL = 5 for CVC-G and CFL = 0.5 for LADER.

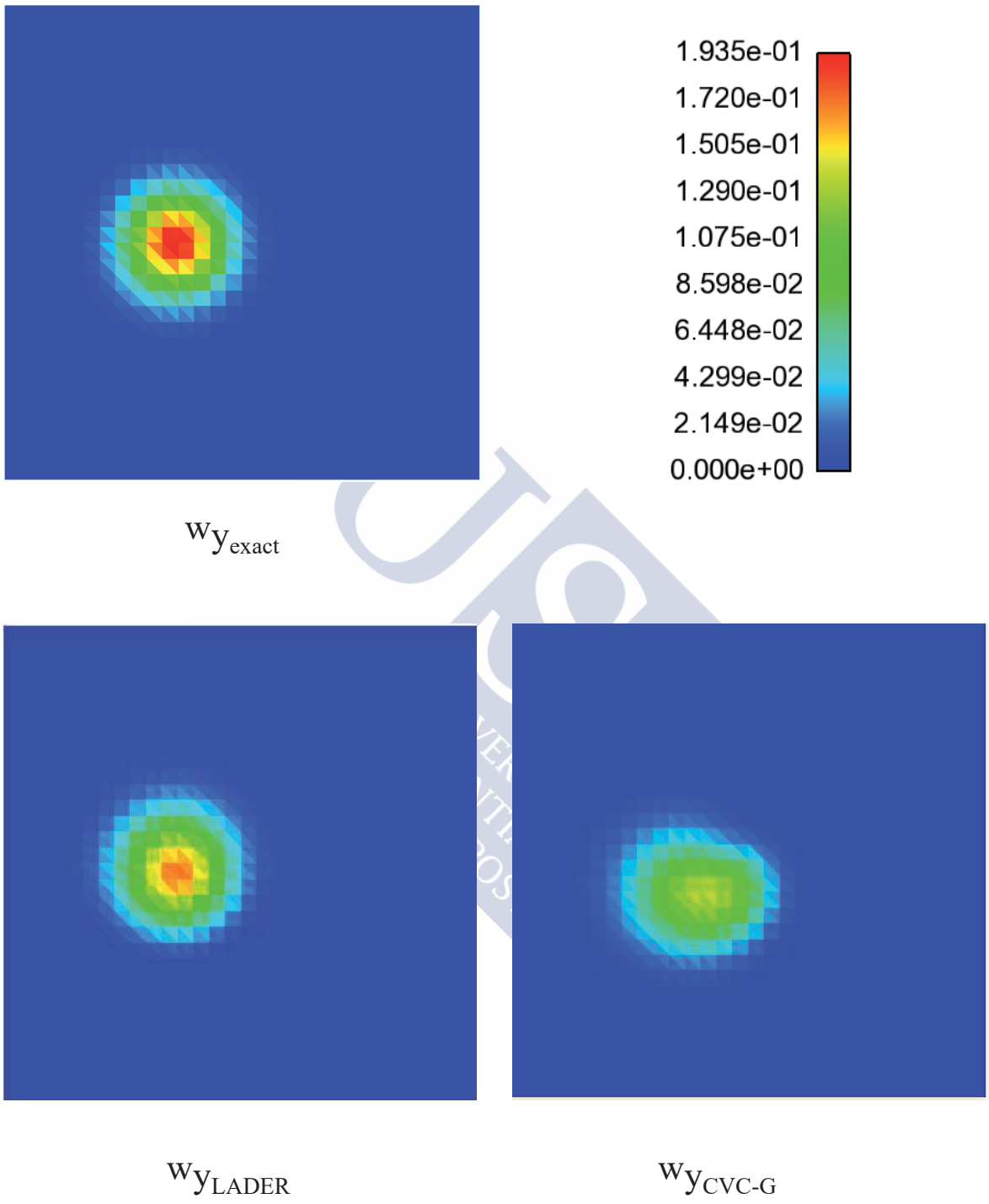

Figure 6.9: Test 4. Gaussian sphere, $\mu = 10^{-3}$. Contours of w_y at plane $z = 0$ using Mesh M_3. Above left: exact solution; below left: LADER; below right: CVC-G.

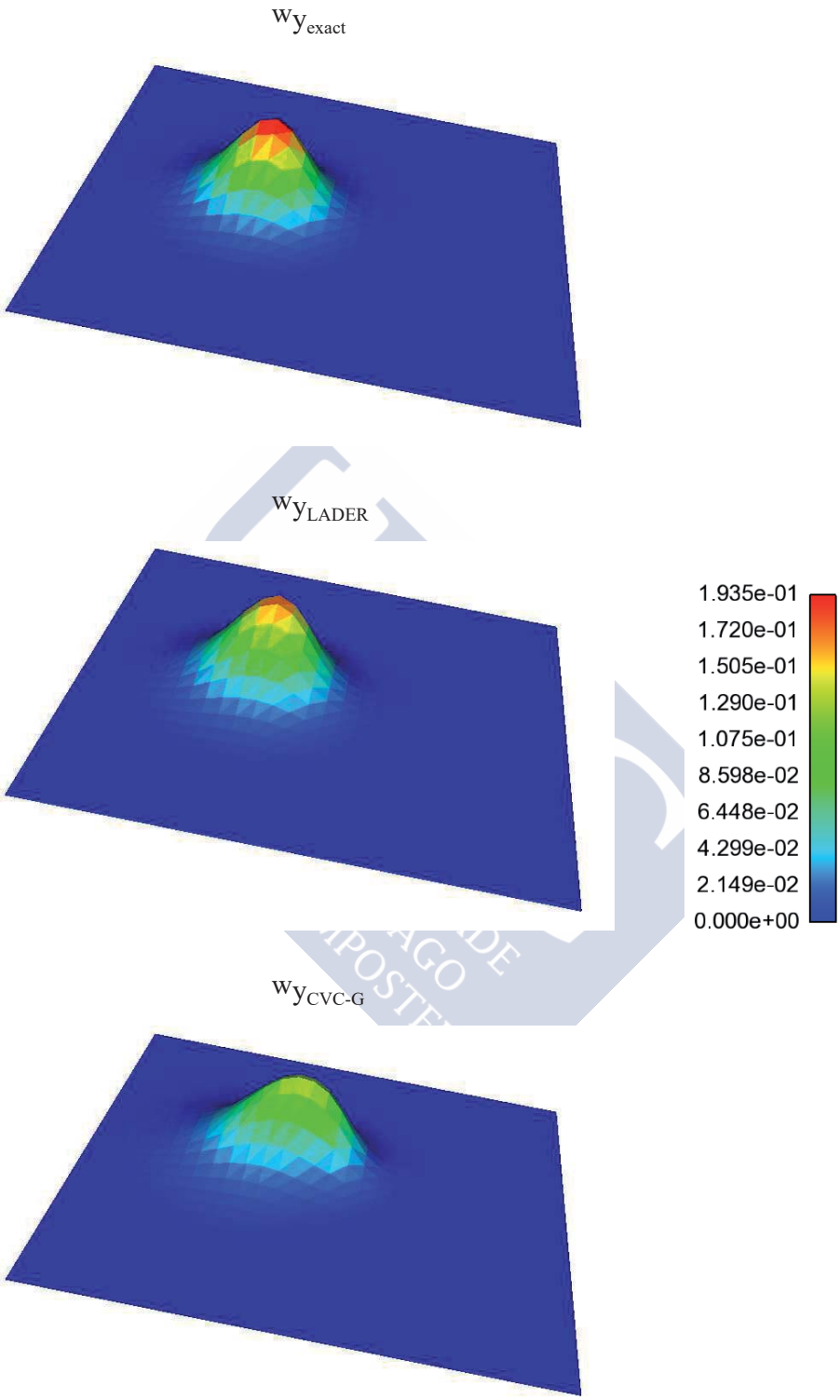

Figure 6.10: Test 4. Gaussian sphere, $\mu = 10^{-3}$. Elevated surfaces of w_y at plane $z = 0$ using Mesh M_3. Above: exact solution; centred: LADER; below: CVC-G.

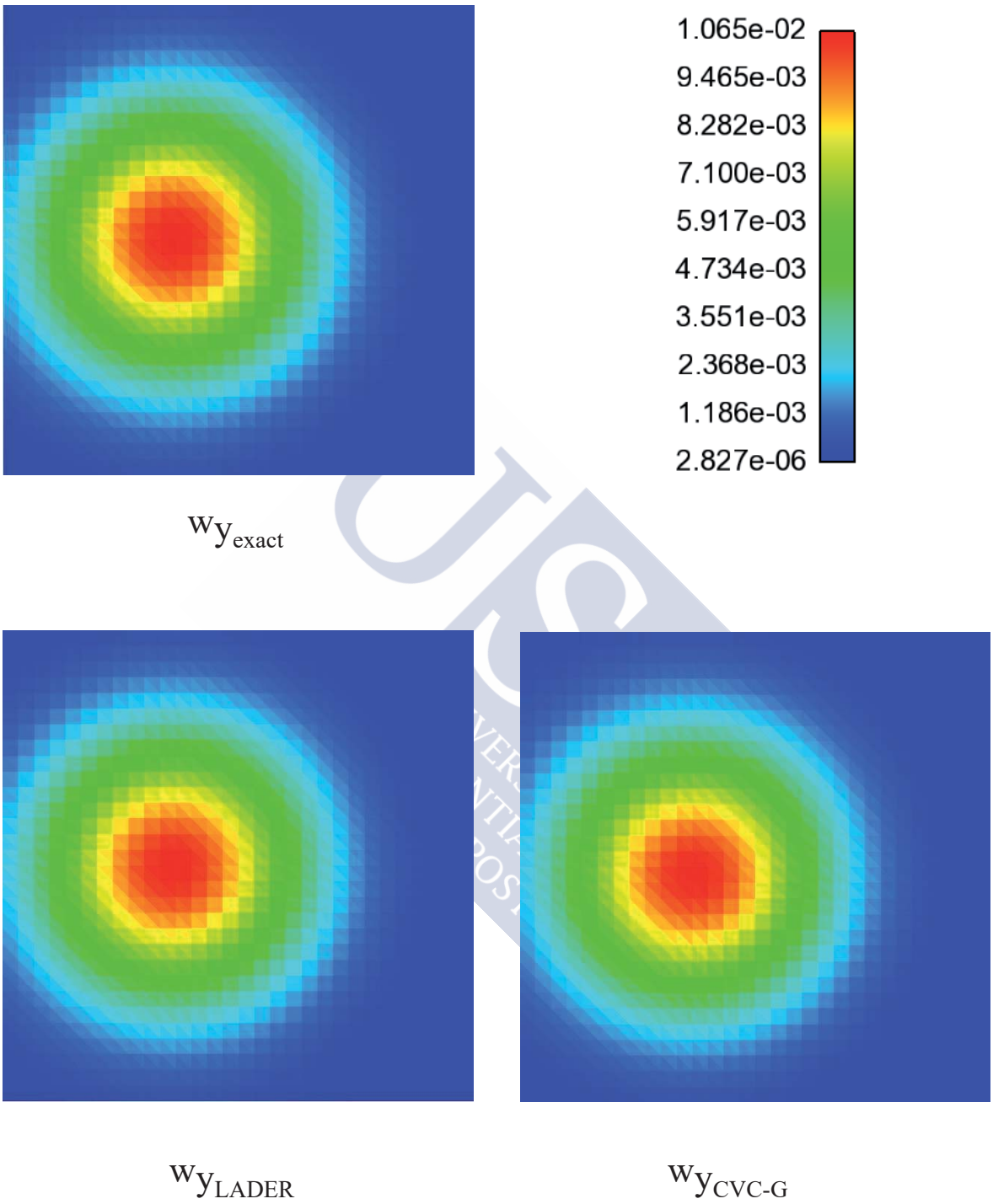

Figure 6.11: Test 4. Gaussian sphere, $\mu = 10^{-2}$. Contours of w_y at plane $z = 0$ using Mesh M_3. Above left: exact solution; below left: LADER; below right: CVC-G.

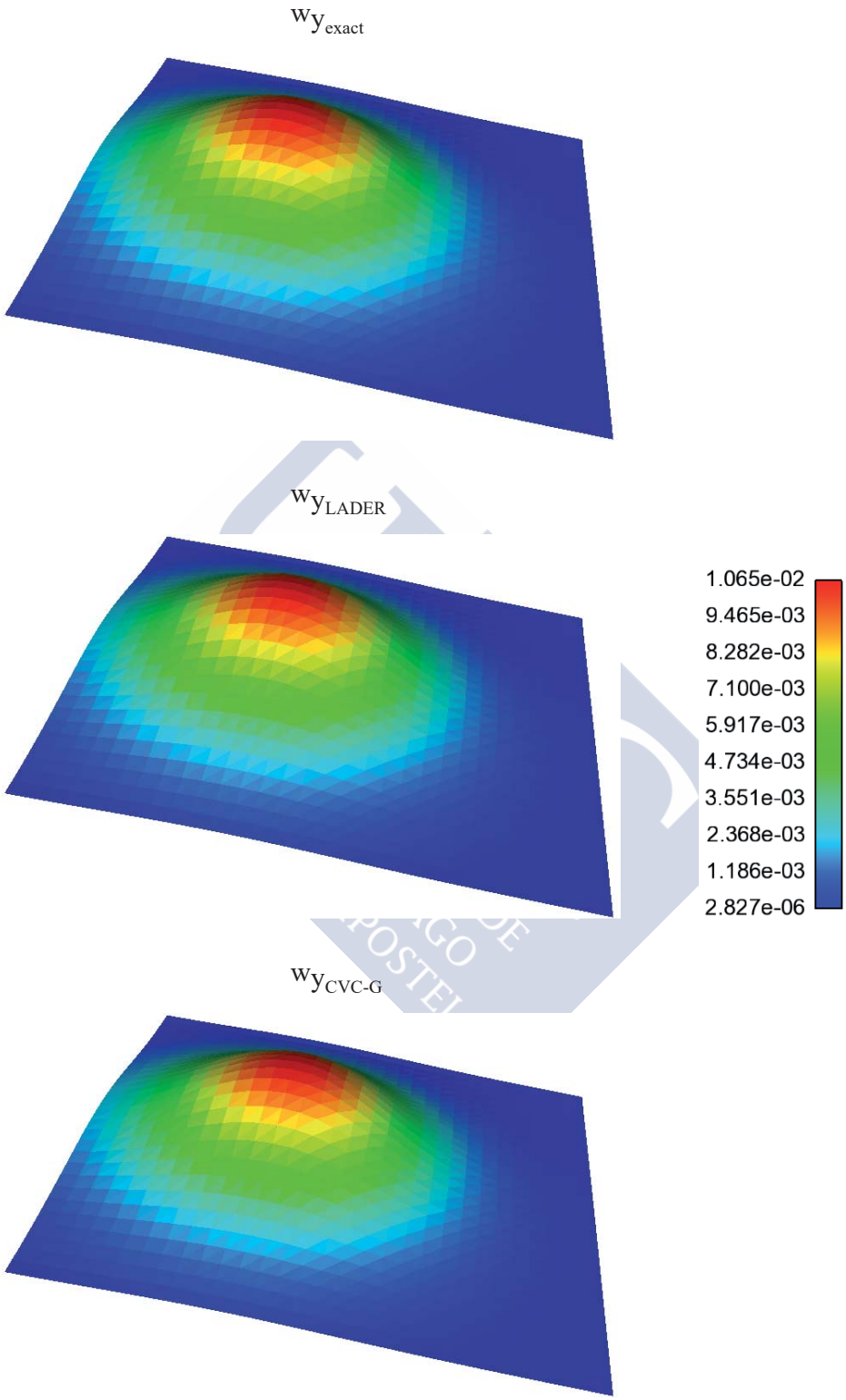

Figure 6.12: Test 4. Gaussian sphere, $\mu = 10^{-2}$. Elevated surfaces of w_y at plane $z = 0$ using Mesh M_3. Above: exact solution; centred: LADER; below: CVC-G.

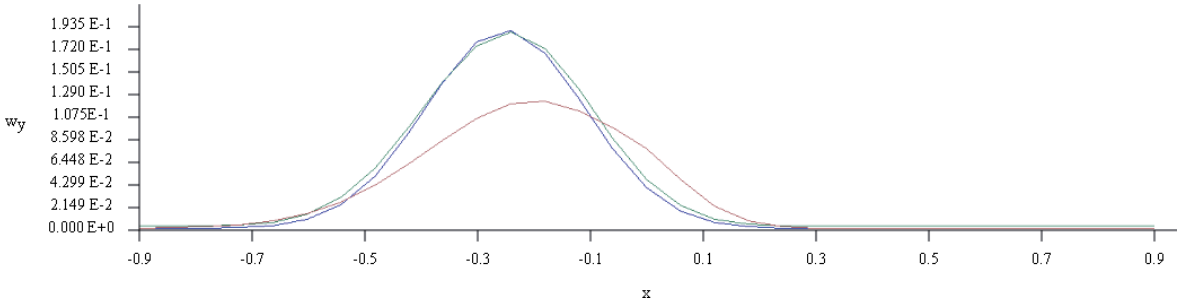

Figure 6.13: Test 4. Gaussian sphere, $\mu = 10^{-3}$. Profile of the exact solution (blue) and the computed solutions using LADER (green) and CVC-G (red) at plane $y = 0$.

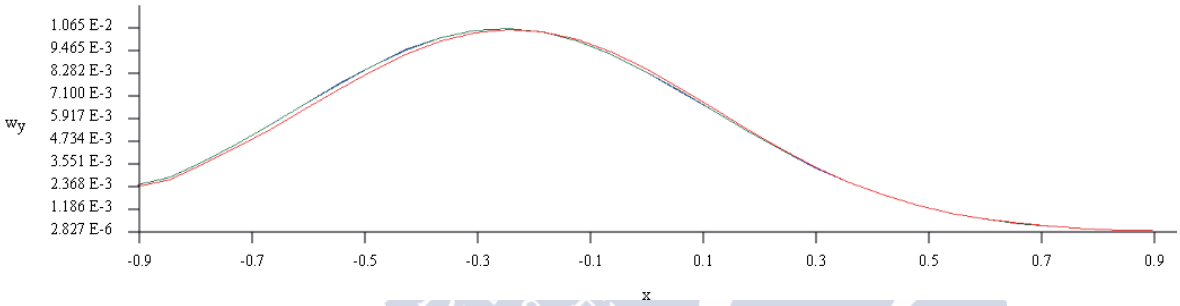

Figure 6.14: Test 4. Gaussian sphere, $\mu = 10^{-2}$. Profile of the exact solution (blue) and the computed solutions using LADER (green) and CVC-G (red) at plane $y = 0$.

6.8.5 Test 5. Flow around a cylinder

We consider the steady-state problem of a flow around a cylinder which has been introduced in [STD+96] and employed, for instance, in [BFSVC14] and [Vol02] as a benchmark problem. The computational domain consists of a solid cylinder surrounded by a rectangular channel in which the flow evolves (see Figure 6.15). The dynamic viscosity of the fluid is $\mu = 10^{-3}$(kg m)/s and the inlet velocity has the form

$$\mathbf{u}(x, y, z, t) = \left(16Uyz(H - y)(H - z)/H^4, 0, 0\right)^T, \tag{6.99}$$

with $U = 0.45$m/s, $H = 0.41$m. Based on the viscosity, the cylinder diameter, $D = 0.1$m, and an estimate of 0.2m/s for the mean inflow velocity, the flow has a Reynolds number of 20. At the outlet Neumann boundary conditions are considered. The mesh employed to obtain the numerical solution consists of 449746 finite elements and 909004 finite volumes.

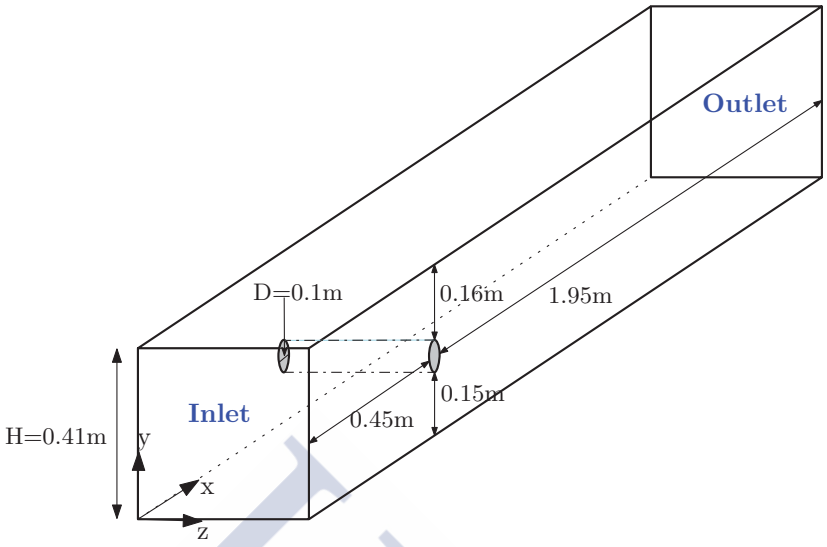

Figure 6.15: Test 5. Flow around a cylinder. Geometry.

The drag and lift coefficients for this problem are expressed by

$$c_d = \frac{500}{0.41} F_d, \; c_l = \frac{500}{0.41} F_l, \tag{6.100}$$

where F_d and F_l are the drag and lift forces, respectively:

$$F_d = \int_S \left(\mu \frac{\partial \mathbf{u}_\tau}{\partial \mathbf{n}_S} n_y - \pi n_x \right) \mathrm{dS}, \quad F_l = \int_S \left(-\mu \frac{\partial \mathbf{u}_\tau}{\partial \mathbf{n}_S} n_x - \pi n_y \right) \mathrm{dS} \tag{6.101}$$

with $\mathbf{n}_S = (n_x, n_y, 0)^t$ the inward pointing unit normal with respect to Ω, S the surface of the cylinder, and $\mathbf{n}_\tau = (n_y, -n_x, 0)^t$ one of the tangential vectors, the other one being $(0, 0, 1)^T$. The drag and lift forces were computed following [BFSVC14]. As convergence criterion, at iteration k, we consider,

$$\frac{1}{\Delta t} \| \mathbf{W}_M^k - \mathbf{W}_M^{k-1} \|_{L^\infty(\Omega)^3} \leq 10^{-4}. \tag{6.102}$$

Four different simulations regarding the method employed were run:

Method 1: the first-order method presented in [BFSVC14], which considers the Rusanov numerical flux,

Method 2: the second-order in space and first-order in time CVC-orth,

Method 3: CVC-G, also second-order in space and first-order in time,

Method 4: the second-order method given by LADER.

The numerical results are summarized in Table 6.10. Along with the aerodynamic

Method	Time iterations	C_D	C_L	$D\pi$
Experimental		$(6.05, 6.25)$	$(0.008, 0.01)$	$(0.165, 0.175)$
1. Order 1	1745	6.79	0.0062	0.1656
2. CVC-orth	72442	6.2463	-0.0007	0.1651
3. CVC-G	73994	6.1619	0.02	0.1616
4. LADER	85638	6.1249	0.0161	0.1662

Table 6.10: Test 5. Flow around a cylinder. Obtained values for the aerodynamic coefficients and the pressure difference.

coefficients, the pressure difference $D\pi$ between the points $\mathbf{p}_1 = (0.45, 0.2, 0.205)$ and $\mathbf{p}_2 = (0.55, 0.2, 0.205)$, has been computed. We observe that the solutions obtained with the higher order method, as expected theoretically, are the most accurate with respect to the reference intervals obtained from the experimental data on [STD+96]. Finally, Figures 6.16, 6.17 and 6.18 show the results obtained using LADER methodology.

Figure 6.16: Test 5. Flow around a cylinder. Pressure on $z = 0.205$.

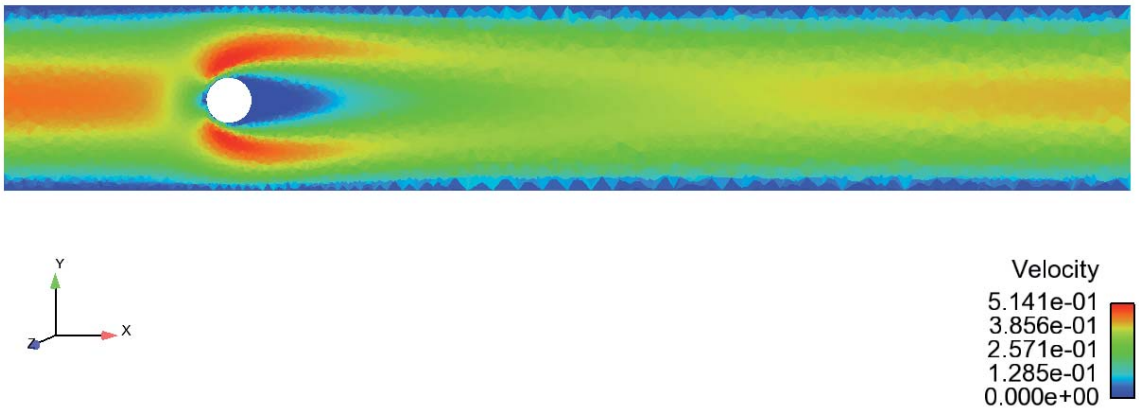

Figure 6.17: Test 5. Flow around a cylinder. Velocity magnitude on $z = 0.205$.

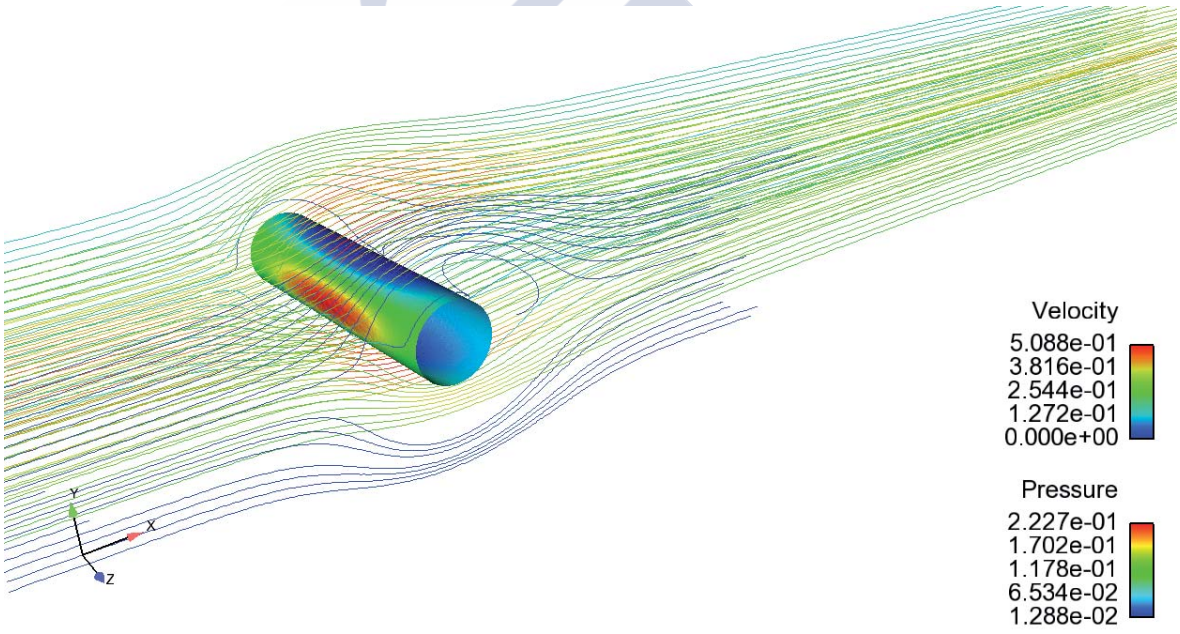

Figure 6.18: Test 5. Flow around a cylinder. Pressure over the cylinder and streamlines coloured by velocity magnitude.

USC
UNIVERSIDADE
DE SANTIAGO
DE COMPOSTELA

Chapter 7

Compressible low Mach number flows

In this chapter, the methodology previously introduced for incompressible flows is extended to solve compressible low Mach number flows. We suppose the temperature and the composition of the mixture to be known. Therefore, the system of equations to be solved involves the mass and momentum equations as well as the equation of state. This is a well known problem with several applications in industry, for instance, in gas networks. Furthermore, we can assume that the analytical expressions for the aforementioned variables are provided or that they have been computed by using another numerical method.

From the algorithm point of view, one of the main difficulties regards the proper approximation of the source term of the Laplace problem set within the projection stage. Moreover, in the flux term, the spatial dependency of the density entails the computation of a new artificial viscosity.

This chapter is organized as follows. In Section 7.1, we recall the system of equations which models low Mach number flows. Section 7.2 is devoted to the discretization of the equations and the description of the algorithm stages. In Section 7.3, the transport-diffusion stage is analysed highlighting the main differences with the incompressible case. The computation of the source term for the projection stage is detailed in Section 7.4. The projection and post-projection stages are depicted in Section 7.5. Eventually, some of the numerical results obtained are shown in Section 7.6.

7.1 Governing equations

Assuming that the mass fractions of the species and the temperature are given, the system of equations to be solved results

$$\operatorname{div} \mathbf{w_u} = q, \tag{7.1}$$

$$\frac{\partial \mathbf{w_u}}{\partial t} + \operatorname{div} \mathcal{F}^{\mathbf{w_u}}(\mathbf{w_u}, \rho) + \operatorname{grad} \pi - \operatorname{div}\left[\mu\left(\operatorname{grad}\mathbf{u} + \operatorname{grad}\mathbf{u}^T\right) - \frac{2}{3}\mu \operatorname{div}\mathbf{u}\, I\right] = 0, \tag{7.2}$$

$$q = -\frac{\partial}{\partial t}\left(\frac{\bar{\pi}}{R\theta}\right). \tag{7.3}$$

Remark 7.1.1. When the data provided is the enthalpy, we apply Corollary 1.3.5 which states that the temperature can be recovered by taking into account the specific heat at constant pressure:

$$h(\theta) = h_{\theta_0} + \int_{\theta_0}^{\theta} c_\pi(r)dr. \tag{7.4}$$

7.2 Numerical discretization

Following Section 6.2, we denote $\mathbf{W}_{\mathbf{u}}^n$, ρ^n, π^n the approximations of $\mathbf{w}_{\mathbf{u}}(x, y, z, t^n)$, $\rho(x, y, z, t^n)$, and $\pi(x, y, z, t^n)$. Then $\mathbf{W}_{\mathbf{u}}^{n+1}$, ρ^{n+1} and π^{n+1} are defined from the following system of equations:

$$\frac{1}{\Delta t}\left(\widetilde{\mathbf{W}}_{\mathbf{u}}^{n+1} - \mathbf{W}_{\mathbf{u}}^n\right) + \operatorname{div}\left(\mathcal{F}^{\mathbf{w_u}}\left(\mathbf{W}_{\mathbf{u}}^n, \rho^n\right)\right) + \operatorname{grad}\pi^n - \operatorname{div}\,\tau^n = 0, \tag{7.5}$$

$$\rho^{n+1} = \frac{\overline{\pi}}{\mathcal{R}\theta^{n+1}\displaystyle\sum_{i=1}^{N_e}\frac{Y_i^{n+1}}{\mathcal{M}_i}}, \tag{7.6}$$

$$\frac{1}{\Delta t}\left(\mathbf{W}_{\mathbf{u}}^{n+1} - \widetilde{\mathbf{W}}_{\mathbf{u}}^{n+1}\right) + \operatorname{grad}\left(\pi^{n+1} - \pi^n\right) = 0, \tag{7.7}$$

$$\operatorname{div}\mathbf{W}_{\mathbf{u}}^{n+1} = Q^{n+1}, \tag{7.8}$$

where $\mathbf{Y}^{n+1}$ and θ^{n+1} are the evaluations of $\mathbf{y}(x, y, z, t^{n+1})$ and $\theta(x, y, z, t^{n+1})$, respectively, and Q^{n+1} is an approximation of $q(x, y, z, t^{n+1})$. Let us notice that $q(x, y, z, t^{n+1})$ may also be a provided function so that Q^{n+1} would be its evaluation. The procedure to determine the solution of the above system is similar to the already presented for the incompressible case. Firstly, we solve equation (7.5) to obtain an intermediate approach of the conservative variables $\widetilde{\mathbf{W}}_{\mathbf{u}}^{n+1}$. Let us notice that, in order to get Q^{n+1}, we need to compute the density before the projection stage. Herein, we set a new stage, the pre-projection stage, where equation (7.6) is used to obtain ρ^{n+1}. Once we get the approximation of the density, we calculate its time derivative to approximate Q^{n+1} and we apply a finite element method to estimate the pressure correction. Summarizing, the global algorithm involves four stages:

- *Transport-difusion stage:* equation (7.5) is solved through a FVM.
- *Pre-projection stage:* the density is computed from the mass fractions of the species and the temperature using (7.6). Next, Q^{n+1} is obtained. If we are given the enthalpy, the temperature is recovered by solving (7.4).
- *Projection stage:* a FEM is applied to (7.7)-(7.8) in order to determine the pressure correction, δ^{n+1}.

- *Post-projection stage:* the conservative velocities are updated by using the pressure correction.

The following sections are devoted to the description of the previous stages highlighting the main differences with the incompressible methodology. Regarding the spacial discretization, the staggered mesh used corresponds to the one described in Section 6.3.

7.3 Transport-diffusion stage

Within the transport diffusion stage a finite volume method is applied in order to provide a first approximation of the conservative variables related to the velocity. Integrating equation (7.5) over the finite volume C_i and applying Gauss' theorem we get

$$\frac{|C_i|}{\Delta t}\left(\widetilde{\mathbf{W}}_{\mathbf{u},\,i}^{n+1}-\mathbf{W}_{\mathbf{u},\,i}^{n}\right)+\int_{\Gamma_i}\mathcal{F}^{\mathbf{w_u}}\left(\mathbf{W}_{\mathbf{u}}^{n},\rho^{n}\right)\widetilde{\boldsymbol{\eta}}\mathrm{dS}+\int_{C_i}\mathrm{grad}\,\pi^{n}\mathrm{dV}-\int_{\Gamma_i}\tau^{n}\,\widetilde{\boldsymbol{\eta}}\mathrm{dS}=0. \quad (7.9)$$

The above integrals can be computed analogously to the ones related to the incompressible model (see Section 6.4). Though, the time and space dependency of the density and the compressibility condition produce several changes on advection and viscous terms. Moreover, when willing to obtain a second-order in space and time scheme using LADER methodology, special attention must be paid to the density approximation.

The former concerns also appear when solving a scalar advection equation with a time and space dependent advection coefficient. Therefore, this simplified model has been used to develop the numerical schemes presented in this chapter (see Section 3.7 for further details). Subsequently, they have been extended to solve compressible Navier-Stokes equations.

7.3.1 Advection term

In Section 6.4.2, we have seen that the flux term related to the momentum equation can be approximated via a numerical flux function $\boldsymbol{\phi}_{\mathbf{u}}$. Besides, considering Rusanov scheme, we have

$$\begin{aligned}\boldsymbol{\phi}_{\mathbf{u}}\left(\mathbf{W}_{\mathbf{u},\,i}^{n},\mathbf{W}_{\mathbf{u},\,j}^{n},\rho_i^{n},\rho_j^{n},\boldsymbol{\eta}_{ij}\right)=&\frac{1}{2}(\mathcal{Z}(\mathbf{W}_{\mathbf{u},\,i}^{n},\rho_i^{n},\boldsymbol{\eta}_{ij})+\mathcal{Z}(\mathbf{W}_{\mathbf{u},\,j}^{n},\rho_j^{n},\boldsymbol{\eta}_{ij}))\\&-\frac{1}{2}\alpha_{RS,\,ij}^{\mathbf{w_u},\,n}\left(\mathbf{W}_{\mathbf{u},\,j}^{n}-\mathbf{W}_{\mathbf{u},\,i}^{n}\right)\end{aligned} \quad (7.10)$$

with

$$\mathcal{Z}\left(\mathbf{W}_{\mathbf{u},\,i}^{n},\rho_i^{n},\boldsymbol{\eta}_{ij}\right):=\mathcal{F}^{\mathbf{w_u}}\left(\mathbf{W}_{\mathbf{u},\,i}^{n},\rho_i^{n}\right)\boldsymbol{\eta}_{ij}, \quad (7.11)$$

$$\alpha_{RS,\,ij}^{\mathbf{w_u},\,n}=\alpha_{RS}^{\mathbf{w_u}}(\mathbf{W}_{\mathbf{u},\,i}^{n},\mathbf{W}_{\mathbf{u},\,j}^{n},\rho_i^{n},\rho_j^{n},\boldsymbol{\eta}_{ij}):=\max\left\{2\left|\mathbf{U}_i^{n}\cdot\boldsymbol{\eta}_{ij}\right|,2\left|\mathbf{U}_j^{n}\cdot\boldsymbol{\eta}_{ij}\right|\right\}. \quad (7.12)$$

Then, equation (7.9) can be rewritten as

$$\frac{1}{\Delta t}\left(\widetilde{\mathbf{W}}_{\mathbf{u},i}^{n+1}-\mathbf{W}_{\mathbf{u},i}^{n}\right)+\frac{1}{|C_i|}\sum_{\mathcal{N}_j\in\mathcal{K}_i}\boldsymbol{\phi}_{\mathbf{u}}\left(\mathbf{W}_{\mathbf{u},i}^{n},\mathbf{W}_{\mathbf{u},j}^{n},\rho_i^n,\rho_j^n,\boldsymbol{\eta}_{ij}\right)$$
$$+\frac{1}{|C_i|}\int_{C_i}\operatorname{grad}\pi^n\mathrm{dV}-\frac{1}{|C_i|}\sum_{\mathcal{N}_j\in\mathcal{K}_i}\boldsymbol{\varphi}_{\mathbf{u}}\left(\mathbf{U}_i^n,\mathbf{U}_j^n,\boldsymbol{\eta}_{ij}\right)=0 \tag{7.13}$$

where $\boldsymbol{\varphi}_{\mathbf{u}}$ denotes the diffusion flux function to be detailed in Section 7.3.2. This scheme may produce spurious oscillations on the solutions. We come now to propose a modification of it willing to avoid this bad behaviour.

Artificial viscosity related to the density

As it is well known, the numerical flux of Rusanov scheme splits into a centred approximation of the whole flux and a numerical viscosity needed for the stability of the scheme. This upwind term is built with the Jacobian matrix of the flux, namely,

$$\frac{\partial\mathcal{F}^{\mathbf{w_u}}\left(\mathbf{w_u},\rho\right)}{\partial\mathbf{w_u}}\mathrm{div}\mathbf{w_u}. \tag{7.14}$$

For incompressible flows, it corresponds with the spatial derivative of the flux. However, for compressible flows, the flux also depends on the spatial variable through the density:

$$\mathrm{div}\mathcal{F}^{\mathbf{w_u}}\left(\mathbf{w_u},\rho\right)=\frac{\partial\mathcal{F}^{\mathbf{w_u}}\left(\mathbf{w_u},\rho\right)}{\partial\mathbf{w_u}}\mathrm{div}\mathbf{w_u}+\frac{\partial\mathcal{F}^{\mathbf{w_u}}\left(\mathbf{w_u},\rho\right)}{\partial\rho}\operatorname{grad}\rho. \tag{7.15}$$

Therefore, when applying (7.12) we are taking into account just the numerical viscosity related to the first term at the right-hand side of (7.15). Whereas, the second term is considered only in the centred part of the flux. This lack of upwind may produce spurious oscillations on the solution of the compressible model. Consequently, the bad behaviour of (7.13) can be corrected by adding a new artificial viscosity term to get an upwind discretization of

$$\frac{\partial\mathcal{F}^{\mathbf{w_u}}\left(\mathbf{w_u},\rho\right)}{\partial\rho}\operatorname{grad}\rho. \tag{7.16}$$

To this end, we present two different approaches extending the treatment first put forward in [BLVC17a] for the unidimensional case. The first one consists in subtracting the integral on the control volume of (7.16) from both sides of (7.13). Next, a centred discretization is used to compute the integral introduced in the left term and the inserted in the right term is approximated in an upwind fashion. The second approach incorporates the upwind term into the Rusanov scheme by considering an approximation of the derivative of the normal flux with respect to the density.

Remark 7.3.1. For an incompressible flow the density gradient is zero and so the term (7.16).

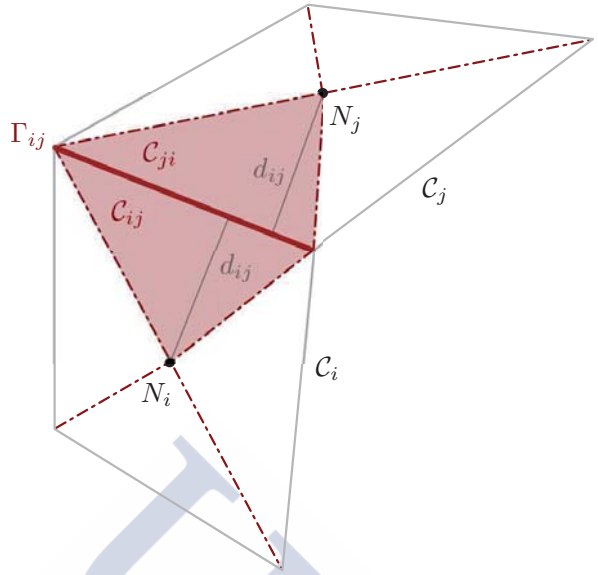

Figure 7.1: Subtriangles related to face Γ_{ij} (shadowed in red) for a bi-dimensional grid.

Approach 1. Denoting

$$\mathbf{V}\left(\mathbf{W}_{\mathbf{u}},\rho\right) := \frac{\partial \mathcal{F}^{\mathbf{w}_{\mathbf{u}}}\left(\mathbf{w}_{\mathbf{u}},\rho\right)}{\partial \rho}\operatorname{grad}\rho = -\frac{1}{\rho^2}\mathbf{W}_{\mathbf{u}}\otimes\mathbf{W}_{\mathbf{u}}\operatorname{grad}\rho, \tag{7.17}$$

$$\mathbf{G}\left(\mathbf{W}_{\mathbf{u}},\rho\right) := -\frac{\partial \mathcal{F}^{\mathbf{w}_{\mathbf{u}}}\left(\mathbf{w}_{\mathbf{u}},\rho\right)}{\partial \rho}\operatorname{grad}\rho = \frac{1}{\rho^2}\mathbf{W}_{\mathbf{u}}\otimes\mathbf{W}_{\mathbf{u}}\operatorname{grad}\rho \tag{7.18}$$

and incorporating both terms in the discrete equation (7.13), we get

$$\begin{aligned}\frac{1}{\Delta t}\left(\widetilde{\mathbf{W}}_{\mathbf{u},i}^{n+1}-\mathbf{W}_{\mathbf{u},i}^{n}\right)+\frac{1}{|C_i|}\sum_{\mathcal{N}_j\in\mathcal{K}_i}\boldsymbol{\phi}_{\mathbf{u}}\left(\mathbf{W}_{\mathbf{u},i}^{n},\mathbf{W}_{\mathbf{u},j}^{n},\rho_i^n,\rho_j^n,\boldsymbol{\eta}_{ij}\right)\\ +\frac{1}{|C_i|}\int_{C_i}\operatorname{grad}\pi^n\mathrm{dV}-\frac{1}{|C_i|}\sum_{\mathcal{N}_j\in\mathcal{K}_i}\boldsymbol{\varphi}_{\mathbf{u}}\left(\mathbf{U}_i^n,\mathbf{U}_j^n,\boldsymbol{\eta}_{ij}\right)\\ -\frac{1}{|C_i|}\int_{C_i}\mathbf{V}\left(\mathbf{W}_{\mathbf{u}}^n,\rho^n\right)\mathrm{dV}=\frac{1}{|C_i|}\int_{C_i}\mathbf{G}\left(\mathbf{W}_{\mathbf{u}}^n,\rho^n\right)\mathrm{dV}.\end{aligned} \tag{7.19}$$

To compute these new terms, we propose to divide each interior finite volume into six sub-tetrahedra denoted by C_{ij}. Each one of them has a face, Γ_{ij}, of the original finite volume, C_i, as basis and the opposed vertex is taken to be the barycenter of the finite volume, that is, the node N_i. Similarly, boundary volumes are split into three sub-tetrahedra. Besides, we denote d_{ij} the distance between Γ_{ij} and N_i. Let us remark that $d_{ij}=d_{ji}$, due to the construction of the staggered mesh, and $|C_{ij}|=\frac{1}{3}d_{ij}\|\boldsymbol{\eta}_{ij}\|$. In Figure 7.1 the 2D sub-triangles correspondent to the 3D sub-tetrahedra are depicted. We observe that in 2D we divide each interior cell onto four sub-triangles instead of the six sub-tetrahedra needed in 3D.

Using this new structure, we can split the integral on the finite volume as the sum of the integrals on the subtetrahedra, C_{ij}:

$$\frac{1}{|C_i|}\int_{C_i}\mathbf{V}\left(\mathbf{W}_{\mathbf{u}},\rho\right)\mathrm{dV}=\frac{1}{|C_i|}\sum_{N_j\in\mathcal{K}_i}\int_{C_{ij}}\mathbf{V}\left(\mathbf{W}_{\mathbf{u}},\rho\right)\mathrm{dV}. \tag{7.20}$$

Next, we denote $\mathbf{V}_i^n$ an approximation of (7.20),

$$\mathbf{V}_i^n:=\frac{1}{|C_i|}\sum_{N_j\in\mathcal{K}_i}\mathbf{V}_{i,ij}^n, \tag{7.21}$$

where

$$\mathbf{V}_{i,ij}^n\approx\int_{C_{ij}}\mathbf{V}\left(\mathbf{W}_{\mathbf{u}}^n,\rho^n\right)\mathrm{dV}. \tag{7.22}$$

To approximate these new integrals we consider the conservative variables to be constant by sub-tetrahedra and its value is set as the average velocity on the two nodes related to the face. On the other hand, the density gradient is approximated by its orthogonal part in such a way it is consistent with the approach used in the viscous term of Rusanov's flux to compute the divergence of the velocities (see [BVC94] and [VC94]). Therefore, we obtain

$$\begin{aligned}\mathbf{V}_{i,ij}&=-\left|C_{ij}\right|\frac{1}{4}\left[\left(\mathbf{W}_{\mathbf{u},i}^n+\mathbf{W}_{\mathbf{u},j}^n\right)\otimes\left(\mathbf{W}_{\mathbf{u},i}^n+\mathbf{W}_{\mathbf{u},j}^n\right)\right]\frac{1}{\frac{1}{4}\left(\rho_i^n+\rho_j^n\right)^2}\frac{\rho_j^n-\rho_i^n}{d_{ij}}\widetilde{\boldsymbol{\eta}}_{ij}\\&=-\frac{d_{ij}\|\boldsymbol{\eta}_{ij}\|}{3}\left[\left(\mathbf{W}_{\mathbf{u},i}^n+\mathbf{W}_{\mathbf{u},j}^n\right)\otimes\left(\mathbf{W}_{\mathbf{u},i}^n+\mathbf{W}_{\mathbf{u},j}^n\right)\right]\left(\rho_i^n+\rho_j^n\right)^{-2}\frac{\rho_j^n-\rho_i^n}{d_{ij}}\widetilde{\boldsymbol{\eta}}_{ij}\\&=-\frac{1}{3}\left(\mathbf{W}_{\mathbf{u},i}^n+\mathbf{W}_{\mathbf{u},j}^n\right)\left(\mathbf{W}_{\mathbf{u},i}^n+\mathbf{W}_{\mathbf{u},j}^n\right)\cdot\boldsymbol{\eta}_{ij}\frac{\rho_j^n-\rho_i^n}{\left(\rho_i^n+\rho_j^n\right)^2}.\end{aligned} \tag{7.23}$$

Substituting (7.23) in (7.21) we get

$$\mathbf{V}_i^n=-\frac{1}{3\left|C_i\right|}\sum_{N_j\in\mathcal{K}_i}\left[\left(\mathbf{W}_{\mathbf{u},i}^n+\mathbf{W}_{\mathbf{u},j}^n\right)\left(\mathbf{W}_{\mathbf{u},i}^n+\mathbf{W}_{\mathbf{u},j}^n\right)\cdot\boldsymbol{\eta}_{ij}\frac{\rho_j^n-\rho_i^n}{\left(\rho_i^n+\rho_j^n\right)^2}\right]. \tag{7.24}$$

Let us denote $\mathbf{G}_i^n$ the upwind approximation of $\frac{1}{|C_i|}\int_{C_i}\mathbf{G}\left(\mathbf{W}_{\mathbf{u}},\rho\right)\mathrm{dV}$. Then, taking into account the procedure to upwind source terms when using Rusanov flux, we obtain

$$\begin{aligned}\mathbf{G}_i^n&=\frac{1}{|C_i|}\sum_{N_j\in\mathcal{K}_i}\boldsymbol{\psi}_{i,j}\left(\mathbf{W}_{\mathbf{u},i}^n,\mathbf{W}_{\mathbf{u},j}^n,\rho_i^n,\rho_j^n,\boldsymbol{\eta}_{ij}\right)=-\frac{1}{|C_i|}\sum_{N_j\in\mathcal{K}_i}\left[1-\operatorname{sign}\left(\breve{\alpha}_{RS}^{\mathbf{w}_{\mathbf{u}},n}\right)\right]\mathbf{V}_{i,ij}^n\\&=\frac{1}{3\left|C_i\right|}\sum_{N_j\in\mathcal{K}_i}\left[1-\operatorname{sign}\left(\breve{\alpha}_{RS}^{\mathbf{w}_{\mathbf{u}},n}\right)\right]\left(\mathbf{W}_{\mathbf{u},i}^n+\mathbf{W}_{\mathbf{u},j}^n\right)\left(\mathbf{W}_{\mathbf{u},i}^n+\mathbf{W}_{\mathbf{u},j}^n\right)\cdot\boldsymbol{\eta}_{ij}\frac{\rho_j^n-\rho_i^n}{\left(\rho_i^n+\rho_j^n\right)^2},\end{aligned} \tag{7.25}$$

where we have denoted by $\text{sign}\left(\breve{\alpha}_{RS,\,ij}^{\mathbf{w_u},\,n}\right)$ the sign of the eigenvalue considered in Rusanov constant. Moreover, we have introduced the mappings

$$\boldsymbol{\psi}_{i,\,j} = \left[1 - \text{sign}\left(\breve{\alpha}_{RS,\,ij}^{\mathbf{w_u},\,n}\right)\right] \mathbf{V}_{i,\,ij}^{n} \tag{7.26}$$

which extend the procedure to upwind source terms presented in [VC94] and [BLVC17a] to the upwind of $\mathbf{G}$.

Substituting (7.21) and (7.25) in (7.19) it results

$$\begin{aligned}
&\frac{1}{\Delta t}\left(\widetilde{\mathbf{W}}_{\mathbf{u},\,i}^{n+1} - \mathbf{W}_{\mathbf{u},\,i}^{n}\right) + \frac{1}{|C_i|}\sum_{\mathcal{N}_j \in \mathcal{K}_i} \boldsymbol{\phi}_{\mathbf{u}}\left(\mathbf{W}_{\mathbf{u},\,i}^{n}, \mathbf{W}_{\mathbf{u},\,j}^{n}, \rho_i^n, \rho_j^n, \boldsymbol{\eta}_{ij}\right) \\
&\quad + \frac{1}{|C_i|}\int_{C_i} \text{grad}\,\pi^n \text{dV} - \frac{1}{|C_i|}\sum_{\mathcal{N}_j \in \mathcal{K}_i} \boldsymbol{\varphi}_{\mathbf{u}}\left(\mathbf{U}_i^n, \mathbf{U}_j^n, \boldsymbol{\eta}_{ij}\right) \\
&\quad - \frac{1}{|C_i|}\sum_{N_j \in \mathcal{K}_i} \mathbf{V}_{i,\,ij}^{n} = -\frac{1}{|C_i|}\sum_{N_j \in \mathcal{K}_i} \left[1 - \text{sign}\left(\breve{\alpha}_{RS}^{\mathbf{w_u},\,n}\right)\right] \mathbf{V}_{i,\,ij}^{n}.
\end{aligned} \tag{7.27}$$

Hence, the discretized equation reads

$$\begin{aligned}
&\frac{1}{\Delta t}\left(\widetilde{\mathbf{W}}_{\mathbf{u},\,i}^{n+1} - \mathbf{W}_{\mathbf{u},\,i}^{n}\right) + \frac{1}{|C_i|}\sum_{\mathcal{N}_j \in \mathcal{K}_i} \boldsymbol{\phi}_{\mathbf{u}}\left(\mathbf{W}_{\mathbf{u},\,i}^{n}, \mathbf{W}_{\mathbf{u},\,j}^{n}, \rho_i^n, \rho_j^n, \boldsymbol{\eta}_{ij}\right) \\
&\quad + \frac{1}{|C_i|}\int_{C_i} \text{grad}\,\pi^n \text{dV} - \frac{1}{|C_i|}\sum_{\mathcal{N}_j \in \mathcal{K}_i} \boldsymbol{\varphi}_{\mathbf{u}}\left(\mathbf{U}_i^n, \mathbf{U}_j^n, \boldsymbol{\eta}_{ij}\right) \\
&\quad - \frac{1}{|C_i|}\sum_{N_j \in \mathcal{K}_i} \text{sign}\left(\breve{\alpha}_{RS}^{\mathbf{w_u},\,n}\right) \mathbf{V}_{i,\,ij}^{n} = 0.
\end{aligned} \tag{7.28}$$

Approach 2. Operating with the increment of the normal flux, we get

$$\Delta \mathcal{Z}\left(\mathbf{w_u}, \rho, \boldsymbol{\eta}\right) = \mathcal{A}\Delta \mathbf{w_u} + \mathcal{R}\Delta\rho \tag{7.29}$$

where $\mathcal{A}$ denotes the jacobian matrix of the normal flux and

$$\mathcal{R} = \frac{\partial \mathcal{Z}\left(\mathbf{w_u}, \rho, \boldsymbol{\eta}\right)}{\partial \rho}. \tag{7.30}$$

Analysing expression (7.29), we notice that the first term is related to the upwind term of Rusanov scheme. Whereas, the second term,

$$\frac{\partial \mathcal{F}^{\mathbf{w_u}}\left(\mathbf{w_u}, \rho\right)\boldsymbol{\eta}}{\partial \rho}\Delta\rho = -\mathbf{w_u}\left(\mathbf{w_u}\cdot\boldsymbol{\eta}\right)\rho^{-2}\Delta\rho, \tag{7.31}$$

is not included. Thus, we propose a modification of the scheme consisting on incorporating the term

$$\left[-\mathbf{W}_{\mathbf{u}}^{n}\left(\mathbf{W}_{\mathbf{u}}^{n}\cdot\boldsymbol{\eta}\right)\left(\rho^n\right)^{-2}\Delta\rho^n\right]_{|\Gamma_{ij}}$$

$$\approx -\left[\frac{1}{2}\left(\mathbf{W}^n_{\mathbf{u},i}+\mathbf{W}^n_{\mathbf{u},j}\right)\right]\left[\frac{1}{2}\left(\mathbf{W}^n_{\mathbf{u},i}+\mathbf{W}^n_{\mathbf{u},j}\right)\cdot\boldsymbol{\eta}_{ij}\right]\left[\frac{1}{2}\left(\rho^n_i+\rho^n_j\right)\right]^{-2}\left(\rho^n_j-\rho^n_i\right)$$
$$= -\left[\left(\mathbf{W}^n_{\mathbf{u},i}+\mathbf{W}^n_{\mathbf{u},j}\right)\right]\left[\left(\mathbf{W}^n_{\mathbf{u},i}+\mathbf{W}^n_{\mathbf{u},j}\right)\cdot\boldsymbol{\eta}_{ij}\right]\left(\rho^n_i+\rho^n_j\right)^{-2}\left(\rho^n_j-\rho^n_i\right) \tag{7.32}$$

to the flux function. Since the approximation must be consistent, we multiply the above expression by a constant $\beta=\frac{1}{3}$. Furthermore, we use the sign of the eigenvalue considered in the Rusanov constant, $\breve{\alpha}^{\mathbf{w_u},n}_{RS,ij}$, to account for the sense of the flux. Therefore, the term reads

$$-\beta\text{sign}\left(\breve{\alpha}^{\mathbf{w_u},n}_{RS,ij}\right)\left(\mathbf{W}^n_{\mathbf{u},i}+\mathbf{W}^n_{\mathbf{u},j}\right)\left(\mathbf{W}^n_{\mathbf{u},i}+\mathbf{W}^n_{\mathbf{u},j}\right)\cdot\boldsymbol{\eta}_{ij}\left(\rho^n_i+\rho^n_j\right)^{-2}\left(\rho^n_j-\rho^n_i\right) \tag{7.33}$$

and the new flux function, to be substituted in (7.13), results

$$\boldsymbol{\phi}_{\mathbf{u}}\left(\mathbf{W}^n_{\mathbf{u},i},\mathbf{W}^n_{\mathbf{u},j},\rho^n_i,\rho^n_j,\boldsymbol{\eta}_{ij}\right)$$
$$=\frac{1}{2}\left[\mathcal{Z}(\mathbf{W}^n_{\mathbf{u},i},\rho^n_i,\boldsymbol{\eta}_{ij})+\mathcal{Z}(\mathbf{W}^n_{\mathbf{u},j},\rho^n_j,\boldsymbol{\eta}_{ij})\right]-\frac{1}{2}\alpha^{\mathbf{w_u},n}_{RS,ij}\left(\mathbf{W}^n_j-\mathbf{W}^n_i\right)$$
$$-\frac{1}{3}\text{sign}\left(\breve{\alpha}^{\mathbf{w_u},n}_{RS,ij}\right)\left(\mathbf{W}^n_{\mathbf{u},i}+\mathbf{W}^n_{\mathbf{u},j}\right)\left(\mathbf{W}^n_{\mathbf{u},i}+\mathbf{W}^n_{\mathbf{u},j}\right)\cdot\boldsymbol{\eta}_{ij}\left(\rho^n_i+\rho^n_j\right)^{-2}\left(\rho^n_j-\rho^n_i\right). \tag{7.34}$$

Remark 7.3.2. Both approaches produce the same numerical scheme.

LADER methodology

To achieve a second-order in space and time scheme we apply LADER methodology. We follow the steps described in Section 6.4.2 taking into account the dependency of the density on time and space. Accordingly, we need to compute the evolved values of the density at the neighbouring of the faces, Γ_{ij}. Moreover, the variables involved in the computation of the latest term added to the flux must also be evolved. We come now to detail the new computations to be performed at each step of the method:

Step 1. ENO-based reconstruction of the density in terms of first degree polynomials:

$$p^i_{ij}(N)=\rho_i+(N-N_i)\,(\nabla\rho)^i_{ij}\,,\quad p^j_{ij}(N)=\rho_j+(N-N_j)\,(\nabla\rho)^j_{ij} \tag{7.35}$$

with

$$(\nabla\rho)^i_{ij}=\begin{cases}(\nabla\rho)_{T_{ijL}}\,, & \text{if } \left|(\nabla\rho)_{T_{ijL}}\cdot(N_{ij}-N_i)\right|\leq\left|(\nabla\rho)_{T_{ij}}\cdot(N_{ij}-N_i)\right|,\\ (\nabla\rho)_{T_{ij}}\,, & \text{if } \left|(\nabla\rho)_{T_{ijL}}\cdot(N_{ij}-N_i)\right|>\left|(\nabla\rho)_{T_{ij}}\cdot(N_{ij}-N_i)\right|;\end{cases} \tag{7.36}$$

$$(\nabla\rho)^j_{ij}=\begin{cases}(\nabla\rho)_{T_{ijR}}\,, & \text{if } \left|(\nabla\rho)_{T_{ijR}}\cdot(N_{ij}-N_j)\right|\leq\left|(\nabla\rho)_{T_{ij}}\cdot(N_{ij}-N_j)\right|,\\ (\nabla\rho)_{T_{ij}}\,, & \text{if } \left|(\nabla\rho)_{T_{ijR}}\cdot(N_{ij}-N_j)\right|>\left|(\nabla\rho)_{T_{ij}}\cdot(N_{ij}-N_j)\right|.\end{cases} \tag{7.37}$$

Step 2. Computation of the boundary extrapolated values at the barycenter of the faces:

$$\rho_{i\,N_{ij}} = p_{ij}^{i}(N_{ij}) = \rho_i + (N_{ij} - N_i)\,(\nabla\rho)_{ij}^{i}\,, \tag{7.38}$$

$$\rho_{j\,N_{ij}} = p_{ij}^{j}(N_{ij}) = \rho_j + (N_{ij} - N_j)\,(\nabla\rho)_{ij}^{j}\,. \tag{7.39}$$

Step 3. Computation of the variables involved in the flux term with second-order of accuracy using the mid-point rule:

$$\overline{\rho_{i\,N_{ij}}} = \rho_{i\,N_{ij}} - \frac{\Delta t\|\boldsymbol{\eta}_{ij}\|}{2\mathcal{L}_{ij}}\left(\operatorname{div}\mathbf{W}_{\mathbf{u},\,i\,N_{ij}} + \operatorname{div}\mathbf{W}_{\mathbf{u},\,j\,N_{ij}}\right), \tag{7.40}$$

$$\overline{\rho_{j\,N_{ij}}} = \rho_{j\,N_{ij}} - \frac{\Delta t\|\boldsymbol{\eta}_{ij}\|}{2\mathcal{L}_{ij}}\left(\operatorname{div}\mathbf{W}_{\mathbf{u},\,i\,N_{ij}} + \operatorname{div}\mathbf{W}_{\mathbf{u},\,j\,N_{ij}}\right). \tag{7.41}$$

Step 4. Computation of the numerical flux:

$$\begin{aligned}\boldsymbol{\phi}_{\mathbf{u}}\left(\overline{\mathbf{W}^n_{\mathbf{u},\,i\,N_{ij}}}, .\overline{\mathbf{W}^n_{\mathbf{u},\,j\,N_{ij}}}, \overline{\rho^n_{i\,N_{ij}}}, \overline{\rho^n_{j\,N_{ij}}}, \boldsymbol{\eta}_{ij}\right) &= -\frac{1}{2}\overline{\alpha^{\mathbf{w}_{\mathbf{u}},\,n}_{RS,\,ij}}\left(\overline{\mathbf{W}^n_{\mathbf{u},\,j\,N_{ij}}} - \overline{\mathbf{W}^n_{\mathbf{u},\,i\,N_{ij}}}\right)\\ &+\frac{1}{2}\left[\mathcal{Z}(\overline{\mathbf{W}^n_{\mathbf{u},\,i\,N_{ij}}}, \overline{\rho^n_{i\,N_{ij}}}, \boldsymbol{\eta}_{ij}) + \mathcal{Z}(\overline{\mathbf{W}^n_{\mathbf{u},\,j\,N_{ij}}}, \overline{\rho^n_{j\,N_{ij}}}, \boldsymbol{\eta}_{ij})\right]\\ -\frac{1}{3}\operatorname{sign}&\left(\overline{\alpha^{\mathbf{w}_{\mathbf{u}},\,n}_{RS,\,ij}}\right)\left(\overline{\rho^n_{i\,N_{ij}}} + \overline{\rho^n_{j\,N_{ij}}}\right)^{-2}\left(\overline{\mathbf{W}^n_{\mathbf{u},\,i\,N_{ij}}} + \overline{\mathbf{W}^n_{\mathbf{u},\,j\,N_{ij}}}\right)\\ &\left(\overline{\mathbf{W}^n_{\mathbf{u},\,i\,N_{ij}}} + \overline{\mathbf{W}^n_{\mathbf{u},\,j\,N_{ij}}}\right)\cdot\boldsymbol{\eta}_{ij}\left(\overline{\rho^n_{j\,N_{ij}}} - \overline{\rho^n_{i\,N_{ij}}}\right).\end{aligned} \tag{7.42}$$

7.3.2 Viscous term

The approximation of the integrals related to the diffusion term is done following Section 6.4.3. Since the shape of these terms is slightly different from the obtained for the incompressible model, we will further detail it.

Considering the momentum equation, (7.9), we have

$$\begin{aligned}\int_{C_i}\operatorname{div}\tau^n dV &= \sum_{N_j\in\mathcal{K}_i}\int_{\Gamma_{ij}}\tau^n\widetilde{\boldsymbol{\eta}}_{ij}\,\mathrm{dS}\\ &= \sum_{N_j\in\mathcal{K}_i}\int_{\Gamma_{ij}}\left[\mu\operatorname{grad}\mathbf{U}^n + \mu\left(\operatorname{grad}\mathbf{U}^n\right)^T - \frac{2}{3}\mu\operatorname{div}\mathbf{U}^n I\right]\widetilde{\boldsymbol{\eta}}_{ij}\,\mathrm{dS},\end{aligned} \tag{7.43}$$

where a new divergence term has appeared. Accounting for the velocity gradient treatment we compute this divergence through a Galerkin approach. Thus, the diffusion flux function reads

$$\boldsymbol{\varphi}_{\mathbf{u}}\left(\mathbf{U}^n_i, \mathbf{U}^n_j, \boldsymbol{\eta}_{ij}\right) = \mu\left(\operatorname{grad}\mathbf{U}^n\right)_{T_{ij}}\boldsymbol{\eta}_{ij} + \mu\left(\operatorname{grad}\mathbf{U}^{n\,T}\right)_{T_{ij}}\boldsymbol{\eta}_{ij} - \frac{2}{3}\mu\left(\operatorname{div}\mathbf{U}^n\right)_{T_{ij}}\boldsymbol{\eta}_{ij}. \tag{7.44}$$

Remark 7.3.3. A second-order in space and time approach can be attained applying LADER method:

$$\boldsymbol{\varphi}_{\mathbf{u}}\left(\overline{\mathbf{U}_i^n}, \overline{\mathbf{U}_j^n}, \boldsymbol{\eta}_{ij}\right) = \mu\left(\operatorname{grad}\overline{\mathbf{U}^n}\right)_{T_{ij}} \boldsymbol{\eta}_{ij} + \mu\left(\operatorname{grad}\overline{\mathbf{U}^{n\,T}}\right)_{T_{ij}} \boldsymbol{\eta}_{ij} - \frac{2}{3}\mu\left(\operatorname{div}\overline{\mathbf{U}^n}\right)_{T_{ij}} \boldsymbol{\eta}_{ij}. \tag{7.45}$$

for further details on the computation of the evolved variables, see Section 6.4.3.

7.4 Pre-projection stage

The pre-projection stage is devoted to the computation of the source term of equation (7.8), Q_i^{n+1}. Since we are assuming that we are given the mass fraction of the species and the temperature, we compute the density, ρ_i^{n+1}, by substituting $\mathbf{Y}_i^{n+1}$ and θ_i^{n+1} in the state equation, namely,

$$\rho_i^{n+1} = \frac{\overline{\pi}^{n+1}}{\mathcal{R}\theta_i^{n+1}\displaystyle\sum_{l=1}^{N_e} \frac{Y_{l,i}^{n+1}}{\mathcal{M}_l}}. \tag{7.46}$$

Finally, the source term of the projection stage results

$$Q_i^{n+1} = \frac{\rho_i^{n+1} - \rho_i^n}{\Delta t}. \tag{7.47}$$

Remark 7.4.1. Let us notice that if an analytical expression of the densities is known then, we can directly evaluate the term

$$q(x, y, z, t^n) = \frac{\partial \rho(x, y, z, t^n)}{\partial t} \tag{7.48}$$

so that the exact value of Q_i^{n+1} is provided to the mass conservation equation.

Remark 7.4.2. If the data supplied is no more the temperature but the enthalpy, we apply Newton's method to equation (7.4),

$$H_i^{n+1} = h_{\theta_0} + \int_{\theta_0}^{\theta_i^{n+1}} c_\pi(r)\, dr, \tag{7.49}$$

obtaining the value of the temperature at the node N_i at the new time step, θ_i^{n+1}.

7.5 Projection and post-projection stages

Following the methodology already introduced in Section 6.5 for incompressible flows, equations (7.7)-(7.8) are solved via a finite element method. The weak problem below is obtained.

Weak problem. Find $\delta^{n+1} \in V_0 := \{z \in H^1(\Omega) : \int_\Omega z = 0\}$ verifying

$$\int_\Omega \text{grad}\delta^{n+1} \cdot \text{grad}z \, dV = \frac{1}{\Delta t}\int_\Omega \widetilde{\mathbf{W}}_{\mathbf{u}}^{n+1} \cdot \text{grad}z \, dV + \frac{1}{\Delta t}\int_\Omega Q^{n+1} z dV - \frac{1}{\Delta t}\int_{\partial\Omega} G^{n+1} z \, dA \tag{7.50}$$

for all $z \in V_0$.

It corresponds to the Laplace problem:

$$\Delta\delta^{n+1} = \frac{1}{\Delta t}\left(\text{div}\, \widetilde{\mathbf{W}}_{\mathbf{u}}^{n+1} - Q^{n+1}\right) \quad \text{in } \Omega, \tag{7.51}$$

$$\frac{\partial\delta^{n+1}}{\partial\boldsymbol{\eta}} = \frac{1}{\Delta t}\left(\widetilde{\mathbf{W}}_{\mathbf{u}}^{n+1} \cdot \boldsymbol{\eta} - G^{n+1}\right) \quad \text{in } \Gamma. \tag{7.52}$$

Finally, at the post-projection stage, $\mathbf{W}_{\mathbf{u}}^{n+1}$ is calculated by substituting δ^{n+1} in

$$\mathbf{W}_{\mathbf{u},i}^{n+1} = \widetilde{\mathbf{W}}_{\mathbf{u},i}^{n+1} + \Delta t \text{ grad } \delta_i^{n+1}. \tag{7.53}$$

7.6 Numerical results

Several test problems will be presented willing to asses the performance of the methodology. The errors are computed likewise in the incompressible case (see Section 6.8.1).

7.6.1 Test 1. Euler flow (MMS)

As first compressible test, we consider the computational domain $\Omega = [0,1]^3$ and we define the flow as

$$\rho(x,y,z,t) = \cos(t) + x + 1, \tag{7.54}$$

$$\pi(x,y,z,t) = 1, \tag{7.55}$$

$$\mathbf{u}(x,y,z,t) = \left(\frac{x\sin(t)+1}{\cos(t)+x+1}, 0, 0\right)^T, \tag{7.56}$$

$$\mathrm{y}(x,y,z,t) = 1, \tag{7.57}$$

$$\theta(x,y,z,t) = \frac{10^3}{\cos(t)+x+1} \tag{7.58}$$

with $\mu = 0$ and

$$f_{u_1} = f_{u_2} = 0, \tag{7.59}$$

$$f_{u_3} = x\cos(t) - \frac{(x\sin(t)+1)^2}{(x+\cos(t)+1)^2} + \frac{(2\sin(t)(x\sin(t)+1))}{x+\cos(t)+1} \tag{7.60}$$

the source terms related to the momentum equation. Dirichlet boundary conditions are set on the boundary.

The numerical simulations were run on the meshes already introduced in Table 6.2. We present the results obtained at time $t_{end} = 1$ and for a $CFL = 1$. In Table 7.1, the errors and the convergence rates are depicted. We have consider three different schemes:

- The first-order scheme constructed by substituting (6.56), (7.34) and (7.44) in (7.13).
- LADER scheme built gathering together (6.56), (7.42), (7.45) and (7.13).
- LADER scheme without the evolution of the density, $\overline{\rho_{iN_{ij}}}$.

We can conclude that, as we have seen in Section 3.7 for the unidimensional advection-diffusion reaction equation, applying LADER methodology to compute the density is crucial to achieve a second-order scheme.

Method	Variable	E_{M_1}	E_{M_2}	E_{M_3}	o_{M_1/M_2}	o_{M_2/M_3}
Order 1	π	$3.73E-03$	$1.44E-03$	$5.29E-04$	1.37	1.44
	$\mathbf{w_u}$	$7.30E-03$	$4.05E-03$	$2.13E-03$	0.85	0.93
LADER	π	$4.13E-03$	$1.60E-03$	$6.15E-04$	1.37	1.38
without $\overline{\rho_{iN_{ij}}}$	$\mathbf{w_u}$	$6.11E-03$	$3.23E-03$	$1.71E-03$	0.92	0.91
LADER	π	$4.64E-04$	$1.93E-04$	$9.21E-05$	1.26	1.07
	$\mathbf{w_u}$	$6.31E-04$	$1.62E-04$	$4.15E-05$	1.97	1.96

Table 7.1: Test 1. Euler flow (MMS). Observed errors and convergence rates. $CFL = 1$.

7.6.2 Test 2. Navier-Stokes flow (MMS)

The flow of the second academic test posed reads

$$\rho(x, y, z, t) = \sin(\pi y t) + 2, \tag{7.61}$$

$$\pi(x, y, z, t) = \exp(xyz)\cos(t), \tag{7.62}$$

$$\mathbf{u}(x, y, z, t) = \Big((\cos(\pi x t))^2, \exp(-2\pi y t), -\cos(\pi x y t)\Big)^T, \tag{7.63}$$

$$\mathrm{y}(x, y, z, t) = 1, \tag{7.64}$$

$$\theta(x, y, z, t) = \frac{10^3}{\sin(\pi y t) + 2}. \tag{7.65}$$

Assuming $\mu = 10^{-2}$ the source terms for the momentum equations result

$$f_{u_1} = \pi y \cos(\pi t x)^2 \cos(\pi t y) - 4\pi t \sin(\pi t x)\cos(\pi t x)^3(\sin(\pi t y)+2) \\ -(2\mu(2\pi^2 t^2\cos(\pi t x)^2 - 2\pi^2 t^2 \sin(\pi t x)^2))/3 + 2\pi^2 t^2 \mu \cos(\pi t x)^2 \\ -2\pi^2 t^2 \mu \sin(\pi t x)^2 + \pi t \exp(-2\pi t y)\cos(\pi t x)^2 \cos(\pi t y) + yz\exp(xyz)\cos(t) \\ -2\pi x \sin(\pi t x)\cos(\pi t x)(\sin(\pi t y)+2) - 2\pi t \exp(-2\pi t y)\cos(\pi t x)^2(\sin(\pi t y)+2), \tag{7.66}$$

$$f_{u_2} = \pi t \exp(-4\pi t y)\cos(\pi t y) + \pi y \exp(-2\pi t y)\cos(\pi t y) \\ -(4\pi^2 t^2 \mu \exp(-2\pi t y))/3 - 4\pi t \exp(-4\pi t y)(\sin(\pi t y)+2) + xz\exp(xyz)\cos(t) \\ -2\pi y \exp(-2\pi t y)(\sin(\pi t y)+2) - 2\pi t \sin(\pi t x)\exp(-2\pi t y)\cos(\pi t x)(\sin(\pi t y)+2), \tag{7.67}$$

$$f_{u_3} = 2\pi t \exp(-2\pi t y)\cos(\pi t x y)(\sin(\pi t y)+2) - \pi y \cos(\pi t x y)\cos(\pi t y) \\ +\pi x y \sin(\pi t x y)(\sin(\pi t y)+2) - \pi t \exp(-2\pi t y)\cos(\pi t x y)\cos(\pi t y) - \pi^2 t^2 x^2 \mu \cos(\pi t x y) \\ -\pi^2 t^2 y^2 \mu \cos(\pi t x y) + 2\pi t \sin(\pi t x)\cos(\pi t x y)\cos(\pi t x)(\sin(\pi t y)+2) + xy\exp(xyz)\cos(t) \\ +\pi t x \exp(-2\pi t y)\sin(\pi t x y)(\sin(\pi t y)+2) + \pi t y \sin(\pi t x y)\cos(\pi t x)^2(\sin(\pi t y)+2). \tag{7.68}$$

Besides, to verify the mass conservation equation we also define a source term for it:

$$f_\rho = \pi y \cos(\pi t y) + \pi t \exp(-2\pi t y)\cos(\pi t y) \\ -2\pi t \exp(-2\pi t y)(\sin(\pi t y)+2) - \pi t \sin(2\pi t x)(\sin(\pi t y)+2). \tag{7.69}$$

We consider the computational domain used in the previous test as well as the three uniform meshes formerly introduced. Computations were carried out until time $t_{end} = 1$ with $CFL = 1$.

The numerical results obtained are shown in Table 7.2. To analyse the performance of the proposed methodology we have run several simulations slightly modifying the proposed schemes.

On the one hand, Order 1 $(\partial_t \rho)_{\text{exact}}$ and LADER $(\partial_t \rho)_{\text{exact}}$ provide the results obtained when the exact value of the time derivative of the density is imposed in the computation of the pressure correction. We observe that the errors obtained are close to the ones corresponding with the simulations in which the former derivative is approximated.

On the other hand, in LADER $\rho_{i_{\text{exact}}}^{n+\frac{1}{2}\Delta t}$ we assume that the exact value of the density at half in time steps is known and so, instead of approximating $\overline{\rho_{iN_{ij}}}$ we set $\rho_i^{n+\frac{1}{2}\Delta t}$. The decrease on the exactitude of the method compared with LADER scheme can be explained by the fact that when applying LADER methodology we are not only half in time evolving the densities but we are also extrapolating them in a vicinity of the face. Indeed, the errors obtained when applying LADER almost match the ones corresponding with LADER $\overline{\rho_{i\,N_{ij}}}_{\text{exact}}$ where an extrapolation of the density considering

Method	Variable	E_{M_1}	E_{M_2}	E_{M_3}	o_{M_1/M_2}	o_{M_2/M_3}
Order 1	π	$3.32E-01$	$1.52E-01$	$6.76E-02$	1.13	1.17
	$\mathbf{w_u}$	$1.45E-01$	$7.80E-02$	$4.27E-02$	0.89	0.87
Order 1	π	$3.33E-01$	$1.52E-01$	$6.76E-02$	1.13	1.17
$(\partial_t\rho)_{\text{exact}}$	$\mathbf{w_u}$	$1.45E-01$	$7.80E-02$	$4.27E-02$	0.89	0.87
LADER	π	$8.65E-02$	$1.72E-02$	$4.40E-03$	2.33	1.97
	$\mathbf{w_u}$	$7.43E-02$	$1.76E-02$	$4.33E-03$	2.08	2.02
LADER	π	$8.55E-02$	$1.66E-02$	$3.77E-03$	2.36	2.14
$(\partial_t\rho)_{\text{exact}}$	$\mathbf{w_u}$	$7.40E-02$	$1.75E-02$	$4.30E-03$	2.08	2.02
LADER	π	$1.02E-01$	$2.68E-02$	$1.06E-02$	1.93	1.33
$\rho_{i_{\text{exact}}}^{n+\frac{1}{2}\Delta t}$	$\mathbf{w_u}$	$8.29E-02$	$2.78E-02$	$1.23E-02$	1.58	1.18
LADER	π	$8.81E-02$	$1.74E-02$	$4.43E-03$	2.34	1.98
$\overline{\rho_{iN_{ij}}}_{\text{exact}}$	$\mathbf{w_u}$	$7.44E-02$	$1.76E-02$	$4.33E-03$	2.08	2.02

Table 7.2: Test 2. Navier-Stokes flow (MMS). Observed errors and convergence rates. $CFL = 1$.

its exact gradient for the computation of the first degree polynomials and the exact value of the density at the half in time step was performed. Therefore, we confirm that coupling both techniques is necessary to attain the order of accuracy sought. This conclusion is reinforced by the studies presented in Part II for the advection-diffusion-reaction equation with time and space dependent advection coefficient.

Conclusions

In this part, a projection hybrid high-order finite volume - finite element method for incompressible and low Mach number flows has been presented. Incompressible Navier-Stokes equations have been coupled with the $k - \varepsilon$ model in order to simulate turbulent flows. The system to be solved was enlarged with respect to [BFSVC14] also by considering species transport. High-order of accuracy has shown necessary for the proper computation of turbulent effects. Two different methodologies to achieve second-order were presented. Firstly, CVC Kolgan provided a second-order in space and first-order in time scheme. To attain second-order in both space and time, LADER methodology was used. Godunov's theorem was circumvented thanks to an ENO-based approach. The computation of the gradients involved on the diffusion terms was done via Galerkin. Regarding compressible low Mach number flows we have assumed the temperature and the composition of the mixture to be known. Therefore, we have approximated the time derivative of the density involved in the mass conservation equation by considering the equation of state. The density dependency on time and space generates a new numerical viscosity to be added to the flux term. LADER methodology was extended to properly account for the density obtaining a second-order scheme. The former methods for solving incompressible and compressible low Mach number flows were applied to manufactured test problems in order to asses their accuracy. Furthermore, for incompressible flows, different benchmarks were considered and the results obtained were successfully confronted with experimental data.

USC
UNIVERSIDADE
DE SANTIAGO
DE COMPOSTELA

USC
UNIVERSIDADE
DE SANTIAGO
DE COMPOSTELA

USC
UNIVERSIDADE
DE SANTIAGO
DE COMPOSTELA

Further research

To conclude the dissertation of this thesis, we briefly introduce some of the research lines that we would like to develop as part of future research:

- Implementation of wall laws.

  The presence of walls in viscous flows can generate a boundary layer where turbulence arises. The issue here are the small scales of the eddies generated which yield a high computational complexity. To avoid the exact computation of these chaotic structures a classical approach is the use of wall laws. They provide information about the average velocity at the vicinity of the wall which can be used in the approximation of the velocities at the nodes placed close to the boundary. The inclusion of wall laws would enlarge the amount of physical problems that the developed code may be able to solve.

- Incorporation of a numerical method which allows the simulation of movement.

  Numerous industrial problems involve the movement of bodies embedding in flows. We propose to start by studying translational and rotational movements. Accordingly, the domain would be divided into several regions with interfaces between them. Inside each sub-domain the methods already presented would be directly applied whereas special care must be taken at the interface.

- Computation of the mass fraction of the species and the enthalpy in the low Mach number model.

  The method presented in this thesis assumes the temperature and the composition of the mixture to be known. However, these data is not always available and, sometimes, needs to be computed. Taking into account the transport equations of species and energy we can derive equations for the physical variables. Solving these equations results on approximations for the enthalpy and the mixture composition that may be used at the pre-projection stage to compute the time derivative of the density.

  Some preliminary results on this research line have already been presented in [BBF+17a] and [BBF+17b].

- Development of reduced order models.

  In many industrial applications the same problem with different values for a set of parameters must be solved in real time. Since the method we have presented is really time consuming we need to develop a computational tool allowing us to reduce the computational cost. To this end, we propose the use of reduced order models (MOR). The main idea behind this technique is to decompose the computation of the solution into an offline and an online stages. Within the offline stage, the full order model, in our case VolFEM3D, is used to compute the solution of the problem for a large set of values of the parameters. Then, we assume that the approximated solutions can be expressed as a linear combination of spatial modes and we perform a proper orthogonal decomposition (POD) to select the most energetic and construct the basis. Regarding the online stage, we set the dynamical system which has as solution the values of the coefficients of the linear combination which corresponds with the values of the parameters chosen. Finally, we reconstruct the solution by using the computed coefficients and the modes included in the POD basis.

  During the research stage at SISSA mathLab, we have started to investigate on the application of MOR to the incompressible Navier-Stokes equations. To this end, we have mainly followed the works presented in [LCLR16] and [HRS16].

- Design of an interface and parallelization.

  To make VolFEM3D become friendly to new users an OpenNum based interface is underdevelopment (see [PPS17]). The parallelization of the code would largely reduce the computational cost of the method.

Appendices

USC
UNIVERSIDADE
DE SANTIAGO
DE COMPOSTELA

Appendix A

Truncation error analysis

This appendix includes the accuracy analysis of Kolgan and CVC Kolgan-type schemes.

A.1 Branches of Kolgan scheme

We analyse the accuracy of the branches of Kolgan scheme one by one:

- Branch 1, (3.30):

$$\begin{aligned}\tau_j^n =& \frac{1}{\Delta t}\left[q(x_j,t^{n+1})-q(x_j,t^n)\right]-\frac{\lambda}{2\Delta x}\left[q(x_{j-1},t^n)-q(x_{j+1},t^n)\right]\\ =& \frac{1}{\Delta t}\left[\partial_t q(x_j,t^n)\Delta t+\frac{1}{2}\partial_t^{(2)}q(x_j,t^n)\Delta t^2+\mathcal{O}\left(\Delta t^3\right)\right]\\ &-\frac{\lambda}{2\Delta x}\left[q(x_j,t^n)-\partial_x q(x_j,t^n)\Delta x+\frac{1}{2}\partial_x^{(2)}q(x_j,t^n)\Delta x^2+\mathcal{O}\left(\Delta x^3\right)\right.\\ &\left.-q(x_j,t^n)-\partial_x q(x_j,t^n)\Delta x-\frac{1}{2}\partial_x^{(2)}q(x_j,t^n)\Delta x^2+\mathcal{O}\left(\Delta x^3\right)\right]\\ =&\partial_t q(x_j,t^n)+\lambda\partial_x q(x_j,t^n)+\mathcal{O}\left(\Delta t\right)+\mathcal{O}\left(\Delta x^2\right)\\ =&\mathcal{O}\left(\Delta t\right)+\mathcal{O}\left(\Delta x^2\right).\end{aligned}$$

- Branch 2, (3.31):

  This branch matches (3.34) so its accuracy has been proved in Proposition 4.4.1.

- Branch 3, (3.32):

$$\begin{aligned}\tau_j^n =& \frac{1}{\Delta t}\left[q(x_j,t^{n+1})-q(x_j,t^n)\right]-\frac{\lambda}{\Delta x}\left[q(x_{j-1},t^n)-q(x_j,t^n)\right]\\ =& \frac{1}{\Delta t}\left[\partial_t q(x_j,t^n)\Delta t+\frac{1}{2}\partial_t^{(2)}q(x_j,t^n)\Delta t^2+\mathcal{O}\left(\Delta t^3\right)\right]\end{aligned}$$

$$
\begin{aligned}
&-\frac{\lambda}{\Delta x}\left[q(x_j,t^n)-\partial_x q(x_j,t^n)\Delta x+\mathcal{O}\left(\Delta x^2\right)-q(x_j,t^n)\right]\\
=&\partial_t q(x_j,t^n)+\lambda\partial_x q(x_j,t^n)+\mathcal{O}\left(\Delta t\right)+\mathcal{O}\left(\Delta x\right)\\
=&\mathcal{O}\left(\Delta t\right)+\mathcal{O}\left(\Delta x\right).
\end{aligned}
$$

- Branch 4, (3.33):

$$
\begin{aligned}
\tau_j^n =&\frac{1}{\Delta t}\left[q(x_j,t^{n+1})-q(x_j,t^n)\right]-\frac{\lambda}{2\Delta x}\left[q(x_{j-2},t^n)\right.\\
&\left.+3q(x_{j-1},t^n)-q(x_j,t^n)-q(x_{j+1},t^n)\right]\\
=&\partial_t q(x_j,t^n)+\mathcal{O}\left(\Delta t\right)-\frac{\lambda}{2\Delta x}\left[-q(x_j,t^n)+2\partial_x q(x_j,t^n)\Delta x\right.\\
&-2\partial_x^{(2)}q(x_j,t^n)\Delta x^2+\mathcal{O}(\Delta x^3)+3q(x_j,t^n)-3\partial_x q(x_j,t^n)\Delta x\\
&+\frac{3}{2}\partial_x^{(2)}q(x_j,t^n)\Delta x^2+\mathcal{O}(\Delta x^3)-q(x_j,t^n)-q(x_j,t^n)\\
&\left.-\partial_x q(x_j,t^n)\Delta x-\frac{1}{2}\partial_x^{(2)}q(x_j,t^n)\Delta x^2+\mathcal{O}(\Delta x^3)\right]\\
=&\partial_t q(x_j,t^n)+\lambda\partial_x q(x_j,t^n)+\mathcal{O}\left(\Delta t\right)+\mathcal{O}\left(\Delta x\right)\\
=&\mathcal{O}\left(\Delta t\right)+\mathcal{O}\left(\Delta x\right).
\end{aligned}
$$

A.2 Branches of CVC Kolgan-type scheme

To complete accuracy analysis of CVC Kolgan-type scheme, truncation error of each branch is studied:

- Branch 1, (3.37):

$$
\begin{aligned}
\tau_j^n =&\frac{1}{\Delta t}\left[q(x_j,t^{n+1})-q(x_j,t^n)\right]+\frac{\lambda}{4\Delta x}\left[q(x_{j-2},t^n)\right.\\
&\left.-5q(x_{j-1},t^n)+3q(x_j,t^n)+q(x_{j+1},t^n)\right]\\
=&\partial_t q(x_j,t^n)+\mathcal{O}\left(\Delta t\right)+\frac{\lambda}{4\Delta x}\left[q(x_j,t^n)-2\partial_x q(x_j,t^n)\Delta x\right.\\
&+2\partial_x^{(2)}q(x_j,t^n)\Delta x^2-5q(x_j,t^n)+5\partial_x q(x_j,t^n)\Delta x-\frac{5}{2}\partial_x^{(2)}q(x_j,t^n)\Delta x^2\\
&\left.+3q(x_j,t^n)+q(x_j,t^n)+\partial_x q(x_j,t^n)\Delta x+\frac{1}{2}\partial_x^{(2)}q(x_j,t^n)\Delta x^2+\mathcal{O}(\Delta x^3)\right]\\
=&\partial_t q(x_j,t^n)+\lambda\partial_x q(x_j,t^n)+\mathcal{O}\left(\Delta t\right)+\mathcal{O}\left(\Delta x^2\right)\\
=&\mathcal{O}\left(\Delta t\right)+\mathcal{O}\left(\Delta x^2\right).
\end{aligned}
$$

- Branch 2, (3.38):

$$\begin{aligned}\tau_j^n =&\frac{1}{\Delta t}\left[q(x_j,t^{n+1})-q(x_j,t^n)\right]+\frac{\lambda}{4\Delta x}\left[q(x_{j-2},t^n)\right.\\&\left.-5q(x_{j-1},t^n)+4q(x_j,t^n)-q(x_{j+1},t^n)+q(x_{j+2},t^n)\right]\\=&\partial_t q(x_j,t^n)+\mathcal{O}\left(\Delta t\right)+\frac{\lambda}{4\Delta x}\Big[q(x_j,t^n)-2\partial_x q(x_j,t^n)\Delta x\\&+2\partial_x^{(2)}q(x_j,t^n)\Delta x^2-5q(x_j,t^n)+5\partial_x q(x_j,t^n)\Delta x-\frac{5}{2}\partial_x^{(2)}q(x_j,t^n)\Delta x^2\\&+4q(x_j,t^n)-q(x_j,t^n)-\partial_x q(x_j,t^n)\Delta x-\frac{1}{2}\partial_x^{(2)}q(x_j,t^n)\Delta x^2+q(x_j,t^n)\\&+2\partial_x q(x_j,t^n)\Delta x+2\partial_x^{(2)}q(x_j,t^n)\Delta x^2+\mathcal{O}(\Delta x^3)\Big]\\=&\partial_t q(x_j,t^n)+\lambda\partial_x q(x_j,t^n)+\mathcal{O}\left(\Delta t\right)+\mathcal{O}\left(\Delta x\right)\\=&\mathcal{O}\left(\Delta t\right)+\mathcal{O}\left(\Delta x\right).\end{aligned}$$

- Branch 3, (3.39):

$$\begin{aligned}\tau_j^n =&\frac{1}{\Delta t}\left[q(x_j,t^{n+1})-q(x_j,t^n)\right]+\frac{\lambda}{4\Delta x}\left[q(x_{j-2},t^n)\right.\\&\left.-5q(x_{j-1},t^n)+4q(x_j,t^n)\right]\\=&\partial_t q(x_j,t^n)+\mathcal{O}\left(\Delta t\right)+\frac{\lambda}{4\Delta x}\Big[q(x_j,t^n)-2\partial_x q(x_j,t^n)\Delta x\\&+2\partial_x^{(2)}q(x_j,t^n)\Delta x^2-5q(x_j,t^n)+5\partial_x q(x_j,t^n)\Delta x\\&-\frac{5}{2}\partial_x^{(2)}q(x_j,t^n)\Delta x^2+4q(x_j,t^n)+\mathcal{O}(\Delta x^3)\Big]\\=&\partial_t q(x_j,t^n)+\frac{3}{4}\lambda\partial_x q(x_j,t^n)+\mathcal{O}\left(\Delta t\right)+\mathcal{O}\left(\Delta x\right)\\=&-\frac{1}{4}\lambda\partial_x q(x_j,t^n)+\mathcal{O}\left(\Delta t\right)+\mathcal{O}\left(\Delta x\right).\end{aligned}$$

- Branch 4, (3.40):

$$\begin{aligned}\tau_j^n =&\frac{1}{\Delta t}\left[q(x_j,t^{n+1})-q(x_j,t^n)\right]+\frac{\lambda}{4\Delta x}\left[-3q(x_{j-1},t^n)+2q(x_j,t^n)+q(x_{j+1},t^n)\right]\\=&\partial_t q(x_j,t^n)+\mathcal{O}\left(\Delta t\right)+\frac{\lambda}{4\Delta x}\Big[-3q(x_j,t^n)+3\partial_x q(x_j,t^n)\Delta x\\&-\frac{3}{2}\partial_x^{(2)}q(x_j,t^n)\Delta x^2+2q(x_j,t^n)+q(x_j,t^n)+\partial_x q(x_j,t^n)\Delta x\\&+\frac{1}{2}\partial_x^{(2)}q(x_j,t^n)\Delta x^2+\mathcal{O}(\Delta x^3)\Big]\\=&\partial_t q(x_j,t^n)+\lambda\partial_x q(x_j,t^n)+\mathcal{O}\left(\Delta t\right)+\mathcal{O}\left(\Delta x\right)\\=&\mathcal{O}\left(\Delta t\right)+\mathcal{O}\left(\Delta x\right).\end{aligned}$$

- Branch 5, (3.3.1):

$$\begin{aligned}\tau_j^n =&\frac{1}{\Delta t}\left[q(x_j,t^{n+1})-q(x_j,t^n)\right]+\frac{\lambda}{4\Delta x}\left[-3q(x_{j-1},t^n)+3q(x_j,t^n)\right.\\&\left.-q(x_{j+1},t^n)+q(x_{j+2},t^n)\right]\\=&\partial_t q(x_j,t^n)+\mathcal{O}\left(\Delta t\right)+\frac{\lambda}{4\Delta x}\left[3q(x_j,t^n)-3q(x_j,t^n)+3\partial_x q(x_j,t^n)\Delta x\right.\\&-\frac{3}{2}\partial_x^{(2)}q(x_j,t^n)\Delta x^2-q(x_j,t^n)-\partial_x q(x_j,t^n)\Delta x-\frac{1}{2}\partial_x^{(2)}q(x_j,t^n)\Delta x^2\\&\left.+q(x_j,t^n)+2\partial_x q(x_j,t^n)\Delta x+2\partial_x^{(2)}q(x_j,t^n)\Delta x^2+\mathcal{O}(\Delta x^3)\right]\\=&\partial_t q(x_j,t^n)+\lambda\partial_x q(x_j,t^n)+\mathcal{O}\left(\Delta t\right)+\mathcal{O}\left(\Delta x^2\right)\\=&\mathcal{O}\left(\Delta t\right)+\mathcal{O}\left(\Delta x^2\right).\end{aligned}$$

- Branch 6, (3.42):

$$\begin{aligned}\tau_j^n =&\frac{1}{\Delta t}\left[q(x_j,t^{n+1})-q(x_j,t^n)\right]+\frac{3\lambda}{4\Delta x}\left[-q(x_{j-1},t^n)+q(x_j,t^n)\right]\\=&\partial_t q(x_j,t^n)+\mathcal{O}\left(\Delta t\right)+\frac{\lambda}{4\Delta x}\left[3q(x_j,t^n)-3q(x_j,t^n)\right.\\&\left.+3\partial_x q(x_j,t^n)\Delta x-\frac{3}{2}\partial_x^{(2)}q(x_j,t^n)\Delta x^2+\mathcal{O}(\Delta x^3)\right]\\=&\partial_t q(x_j,t^n)+\frac{3}{4}\lambda\partial_x q(x_j,t^n)+\mathcal{O}\left(\Delta t\right)+\mathcal{O}\left(\Delta x\right)\\=&-\frac{1}{4}\lambda\partial_x q(x_j,t^n)+\mathcal{O}\left(\Delta t\right)+\mathcal{O}\left(\Delta x\right).\end{aligned}$$

- Branch 7, (3.43):

$$\begin{aligned}\tau_j^n =&\frac{1}{\Delta t}\left[q(x_j,t^{n+1})-q(x_j,t^n)\right]+\frac{\lambda}{4\Delta x}\left[-4q(x_{j-1},t^n)+3q(x_j,t^n)+q(x_{j+1},t^n)\right]\\=&\partial_t q(x_j,t^n)+\mathcal{O}\left(\Delta t\right)+\frac{\lambda}{4\Delta x}\left[-4q(x_j,t^n)+4\partial_x q(x_j,t^n)\Delta x\right.\\&-2\partial_x^{(2)}q(x_j,t^n)\Delta x^2+3q(x_j,t^n)+q(x_j,t^n)+\partial_x q(x_j,t^n)\Delta x\\&\left.+\frac{1}{2}\partial_x^{(2)}q(x_j,t^n)\Delta x^2+\mathcal{O}(\Delta x^3)\right]\\=&\partial_t q(x_j,t^n)+\frac{5}{4}\lambda\partial_x q(x_j,t^n)+\mathcal{O}\left(\Delta t\right)+\mathcal{O}\left(\Delta x\right)\\=&\frac{1}{4}\lambda\partial_x q(x_j,t^n)+\mathcal{O}\left(\Delta t\right)+\mathcal{O}\left(\Delta x\right).\end{aligned}$$

- Branch 8, (3.44):

$$\begin{aligned}\tau_j^n =&\frac{1}{\Delta t}\left[q(x_j,t^{n+1})-q(x_j,t^n)\right]+\frac{\lambda}{4\Delta x}\left[-4q(x_{j-1},t^n)+4q(x_j,t^n)\right.\\&\left.-q(x_{j+1},t^n)+q(x_{j+2},t^n)\right]\\=&\partial_t q(x_j,t^n)+\mathcal{O}\left(\Delta t\right)+\frac{\lambda}{4\Delta x}\Big[-4q(x_j,t^n)+4\partial_x q(x_j,t^n)\Delta x\\&-2\partial_x^{(2)}q(x_j,t^n)\Delta x^2+4q(x_j,t^n)-q(x_j,t^n)-\partial_x q(x_j,t^n)\Delta x\\&-\frac{1}{2}\partial_x^{(2)}q(x_j,t^n)\Delta x^2+q(x_j,t^n)+2\partial_x q(x_j,t^n)\Delta x\\&+2\partial_x^{(2)}q(x_j,t^n)\Delta x^2+\mathcal{O}(\Delta x^3)\Big]\\=&\partial_t q(x_j,t^n)+\frac{5}{4}\lambda\partial_x q(x_j,t^n)+\mathcal{O}\left(\Delta t\right)+\mathcal{O}\left(\Delta x\right)\\=&\frac{1}{4}\lambda\partial_x q(x_j,t^n)+\mathcal{O}\left(\Delta t\right)+\mathcal{O}\left(\Delta x\right).\end{aligned}$$

- Branch 9, (3.45):

$$\begin{aligned}\tau_j^n =&\frac{1}{\Delta t}\left[q(x_j,t^{n+1})-q(x_j,t^n)\right]+\frac{\lambda}{2\Delta x}\left[-q(x_{j-1},t^n)+q(x_j,t^n)\right]\\=&\partial_t q(x_j,t^n)+\mathcal{O}\left(\Delta t\right)+\frac{\lambda}{2\Delta x}\Big[-q(x_j,t^n)+\partial_x q(x_j,t^n)\Delta x\\&-\frac{1}{2}\partial_x^{(2)}q(x_j,t^n)\Delta x^2+q(x_j,t^n)+\mathcal{O}(\Delta x^3)\Big]\\=&\partial_t q(x_j,t^n)+\frac{1}{2}\lambda\partial_x q(x_j,t^n)+\mathcal{O}\left(\Delta t\right)+\mathcal{O}\left(\Delta x\right)\\=&-\frac{1}{2}\lambda\partial_x q(x_j,t^n)+\mathcal{O}\left(\Delta t\right)+\mathcal{O}\left(\Delta x\right).\end{aligned}$$

USC
UNIVERSIDADE
DE SANTIAGO
DE COMPOSTELA

Appendix B

Resumo

Os fluídos forman parte de numerosos aspectos da nosa vida e inflúen en moitos dos fenómenos industriais e medioambientais da nosa contorna. Por iso, resulta primordial ser quen de predicir correctamente o seu comportamento. Así, durante as últimas décadas un gran número de investigadores centraron os seus esforzos na modelización e na simulación de fluxos.

Nesta tese, traballamos con dous tipos particulares de fluídos: os fluídos incompresibles e os fluídos compresibles a baixo número de Mach. Co obxetivo de obter un documento autocontido, comezamos modelando ambos os dous tipos derivando as ecuacións de Navier-Stokes incompresibles e compresibles. Inspirándonos en traballos de investigación previos, podemos constatar que moitos dos fluxos que nos ocupan, como poden ser o fluxo nun entorno dun dispositivo de xeración de enerxía ou dun avión, son de carácter turbulento. Isto lévanos a engadir, ao noso modelo inicial, unha nova parella de ecuacións en derivadas parciais que nos permiten recoller a pegada que os remuíños de menor tamaño teñen sobre o fluxo medio.

Por outra banda, problemas coma o transporte de gas a través dunha rede de gaseoductos ou a mestura de especies nun forno, fannos incorporar ao modelo as ecuacións de transporte de especies.

Unha vez definido o modelo tridimensional, pasamos a desenvolver un método numérico para a súa resolución. En concreto, centrámonos na extensión, aos novos sistemas de ecuacións, do método híbrido de proxección volúmes finitos - elementos finitos presentado en [BFSVC14].

Para realizar correctamente o axuste entre as distintas ecuacións do modelo precisamos aplicar métodos de alta orde. Porén, o seu desenvolvemento e estudo para o modelo tridimensional resulta demasiado complexo. Este feito lévanos a traballar cunha ecuación escalar simplificada. Concretamente, estudamos a ecuación de convección-difusión-reacción que busca recoller as principais características das ecuacións do modelo tridimensional. De cara á resolución do novo problema, podemos establecer diversas metodoloxías e desenvolver os correspondentes estudos de estabilidade e de análise da magnitude dos erros cometidos. Unha vez teñamos validada a nova metodoloxía pasaremos a estendela ao caso tridimensional.

O método híbrido de proxección escollido permítenos realizar de xeito independente

o cálculo das variables conservativas do das presións. Así, aproveitamos as principais vantaxes das dúas familias de métodos numéricos consideradas. O método de volumes finitos encárgase da tarefa de resolución das ecuacións de convección-difusión-reacción que nos proporcionan a aproximación dos valores das variables conservativas. Por outra banda, para resolver de xeito eficaz o problema tipo laplaciano que xorde no cálculo das presións, empregamos un método de elementos finitos. Dentro de cada un destes métodos, prestamos especial atención ás discetizacións utilizadas para os distintos termos involucrados nas ecuacións.

O método resultante foi programado en Fortran dando lugar ao código VolFEM3D. No deseño de tests, que nos permiten a validación da metodoloxía desenvolvida e a realización de estudos de converxencia, empregamos o método das solucións manufacturadas. Abórdanse, ademais, tests clásicos da dinámica de fluídos computacional comparando os resultados obtidos con datos presentes na bibliografía.

A continuación, realizamos unha descrición pormenorizada dos contidos incluídos en cada parte da memoria.

Parte I. Modelos matemáticos

A primeira parte da tese está adicada á obtención dos modelos matemáticos que permiten estudar fluxos a baixo número de Mach. Abórdase tanto o caso de fluxos incompresibles coma compresibles.

O primeiro capítulo comeza coa revisión dalgúns conceptos básicos da mecánica dos medios continuos que serven como base para introducir a ecuación de conservación de masa e os balances de momentos e enerxía (ver [Ber05]). Posteriormente, os fluídos compresibles caracterízanse grazas á definición de materiais de Coleman-Noll. Para a simulación do comportamento de fluídos constituídos por varias especies empregamos as mesturas de fluídos de Coleman-Noll. Ademais, detállanse as expresións das ecuacións de conservación de masa, momentos e enerxía para ditos fluxos. O sistema de ecuacións obtido péchase coa ecuación de estado. Por outra banda, os fluídos incompresibles caracterízanse empregando a definición de proceso termodinámico isocórico. Finalmente, realízase a análise dimensional dos dous sistemas de ecuacións considerados. Os modelos simplificados resultantes correspóndense coas ecuacións de Navier-Stokes para fluxos compresibles e incompresibles.

Por mor do elevado coste computacional que supón a resolución numérica de fluxos turbulentos, é preciso achegar un modelo de turbulencia que permita capturar o efecto que teñen os remuíños de menor tamaño sobre o fluxo medio (ver [CL14]). Así, no segundo capítulo, realizamos unha breve introdución ás diversas técnicas empregadas na bibliografía facendo especial fincapé nos modelos tipo RANS. Concretamente, centrámonos no modelo $k - \varepsilon$ standard derivando as ecuacións que modelan a enerxía cinética turbulenta e a taxa de disipación viscosa.

Parte II. Análise numérica da ecuación de convección-difusión-reacción

O estudo teórico de métodos de volumes finitos para a resolución das ecuacións de Navier-Stokes tridimensionais resulta demasiado custoso. Por iso, nesta parte da tese centrámonos no desenvolvemento de métodos de alta orde aplicados á ecuación de convección-difusión-reacción escalar. Este problema simplificado permítenos realizar as análises de estabilidade e os cálculos asociados aos erros de truncadura dos métodos propostos. Na terceira parte da memoria, preséntase a extensión dos mesmos para a resolución dos modelos matemáticos introducidos na primeira parte.

O terceiro capítulo da tese ocúpase do desenvolvemento de métodos de alta orde para a resolución do problema escalar. Centrámonos principalmente en dúas familias de métodos: os métodos tipo Kolgan e a metodoloxía ADER.

Kolgan, [Kol11], foi o primeiro en sortear o teorema de Godunov presentando un método de volumes finitos estable de orde dúas. Para iso, realizou unha reconstrución non lineal dos gradientes involucrados na aproximación do termo de fluxo. Numerosos métodos non lineais xurdiron a raíz desta aportación. Entre eles, destacamos o método CVC tipo Kolgan, [CVC12], que ten como principal diferenza co esquema de Kolgan orixinal a utilización das reconstrucións unicamente na parte viscosa do fluxo numérico mantendo, na centrada, os valores obtidos no paso de tempo anterior. Como resultado, obtense un esquema constituído por nove ramas diferentes que se calculan considerando as distintas combinacións viables para a aproximación dos gradientes.

Tamén fundamentada no deseño de métodos non lineais, atopamos a metodoloxía ADER. Ditos métodos baséanse na resolución de problemas de Riemann xeralizados e permiten obter esquemas de orde de exactitude arbitraria. Neste traballo, estendemos o método orixinalmente proposto en [TMN01] para a ecuación de convección-reacción á ecuación de convección-difusión-reacción cun coeficiente difusivo dependente de espazo e tempo. Os principais pasos a seguir para a construción destes esquemas son:

Paso 1. Reconstrución da solución mediante polinomios de primera orde definidos en cada volume finito. Co obxectivo de evitar solucións espurias, combinamos este método cunha interpolación tipo ENO para o cálculo dos gradientes dos polinomios.

Paso 2. Resolución do problema de Riemann xeneralizado. Este problema é unha xeneralización do problema de Riemann clásico por dous motivos. Por unha banda considérase unha condición inicial definida mediante polinomios. Por outra banda, a ecuación en derivadas parciais a resolver inclúe os termos difusivos e reactivos.

Para a consecución deste paso, é preciso ter en conta as expansións en series de Taylor en tempo. Ademais, as derivadas temporais son substituídas por unha combinación lineal das derivadas espaciais seguindo o procedemento de Cauchy-Kovalevskaya.

Paso 3. Cálculo dos termos difusivos e reactivos mediante a regra de integración do punto medio. De novo, neste paso, facemos uso das expansións en series de Taylor de xeito que as aproximacións de tódolos termos teñan conta das contribucións dos restantes termos da ecuación.

Unha vantaxe importante que presenta esta metodoloxía é a facilidade de estendela a esquemas de orde superior. Se, por exemplo, quixésemos un esquema de orde tres, bastaría con incrementar en un a orde dos polinomios do primeiro paso e considerar o desenvolvemento de Taylor de grado dous en tempo.

Un terceiro método estudado nesta tese é o método MUSCL-Hancock, [vL84]. Orixinalmente prantexado para a resolución de ecuacións de convección, estendémolo ao caso dunha ecuación de convección-difusión-reacción. O método pódese dividir nos seguintes pasos:

Paso 1. Reconstrución polinómica.

Paso 2. Cálculo dos valores extrapolados nas fronteiras da cela.

Paso 3. Evolución en medio paso de tempo dos valores extrapolados.

Paso 4. Resolución do problema de Riemann definido en cada cara fronteira a partires dos valores extrapolados.

É importante destacar que, na evolución en medio paso de tempo, é preciso ter en conta, non só a contribución dos termos convectivos, senón, tamén, dos difusivos e dos reactivos. O esquema final obtido resulta alxebricamente idéntico ao construído empregando ADER.

Finalmente, desenvolvemos unha cuarta metodoloxía á que denominamos ADER local (LADER). Con ela buscamos obter esquemas máis sinxelos de extrapolar á resolución das ecuacións de Navier-Stokes tridimensionais pero que manteñan as boas propiedades que presenta o método ADER. A maior diferenza entre ambos métodos atópase na aproximación usada para calcular os gradientes involucrados na reconstrución polinómica. Como consecuencia, LADER non precisa lembrar a presencia do termo de fluxo na aproximación do termo difusivo. Así e todo, ambas metodoloxías obrigan a incluír o termo difusivo no problema de Riemann xeneralizado definido para o cálculo do termo convectivo. Deste xeito, en LADER temos dous tipos distintos de variables evolucionadas, as relativas ao fluxo e aquelas empregadas no termo difusivo. Por último, estendemos esta metodoloxía á resolución de ecuacións de convección-difusión-reacción con coeficiente de convección dependente de espazo e tempo. Este novo paso lévanos a incluír un novo termo de viscosidade artificial na aproximación do termo do fluxo que evite a xeración de oscilacións espurias nas solucións.

O cuarto capítulo focalízase no estudo teórico dos métodos presentados no capítulo anterior. Formúlanse e demóstranse os resultados de estabilidade para a ecuación de convección. No caso das ecuacións de convección-reacción e convección-difusión-reacción, a elevada complexidade das expresións analíticas obtidas para o factor de

amplificación, lévanos a propoñer unha nova metodoloxía que permita definir gráficamente as rexións de estabilidade. A continuación, analízase o erro de truncadura dos esquemas obtidos comprobando que os esquemas tipo Kolgan son de orde dúas en espazo e orde unha en tempo mentres que ADER e LADER acadan orde dúas tanto en espazo coma en tempo.

A validación da metodoloxía proposta realízase no capítulo cinco. O método de solucións manufacturadas proporciónanos tests analíticos con solucións coñecidas que permiten estudar a orde de converxencia dos diversos esquemas introducidos. Realízase unha comparación dos métodos Kolgan, CVC tipo Kolgan, ADER e LADER para a resolución da ecuación de convección-reacción. Posteriormente, analízase a aplicación das dúas últimas metodoloxías propostas ás ecuacións de convección-difusión-reacción e de difusión-reacción. Ademais, xustifícase, mediante os resultados numéricos obtidos, a necesidade de utilizar reconstrucións tipo ENO para os métodos ADER e LADER co obxectivo de evitar oscilacións espurias. Os resultados acadados confirman as ordes de converxencia calculadas analiticamente e proban a utilidade dos métodos propostos para a resolución de ecuacións de convección-difusión-reacción dependentes de espazo e tempo.

A extensión dos métodos ADER e MUSCL-Hancock para a resolución da ecuación de convección-difusión-reacción escalar foron publicados en [BTVC16]. A metodoloxía LADER foi parcialmente incluída en [BFTVC18].

Parte III. O método híbrido de proxección volumes finitos - elementos finitos para as ecuacións de Navier-Stokes

Nos anos oitenta comezaron a xurdir numerosos casos de éxito nos que se combinaban métodos de volumes finitos con resolvedores de Riemann para diversos tipos de fluídos. Centrándonos nos fluxos incompresibles, os algoritmos propostos garanten a condición de incompresibilidade para as velocidades grazas ao uso de multiplicadores de Lagrange nas presións. Así, a tradicional etapa explícita dos métodos de volumes finitos, na que se obtén unha primeira aproximación do cálculo das velocidades, vese completada coa chamada etapa de proxección na que se calcula a corrección das presións que garante unha diverxencia de velocidades nula. No caso das ecuacións de Navier-Stokes, existe un gran número de referencias bibliográficas que analizan diversos tipos de métodos de proxección de volumes finitos. Co obxectivo de garantir a estabilidade dos mesmos deséñanse mallas encaixadas que permiten resolver as presións e as velocidades de xeito independente sobre distintos nodos. O problema que presenta esta metodoloxía é a súa complexidade de cara ao seu uso en mallas non estruturadas.

Por outra banda, os métodos de proxección tamén foron amplamente empregados no marco dos métodos de elementos finitos. Neste caso, a condición de diverxencia

nula para as velocidades substitúese por unha ecuación que prescribe a diverxencia da variable conservativa das velocidades.

Estes precedentes na aplicación de métodos de proxección tanto empregando métodos de elementos finitos coma de volumes finitos, fixeron que en [BFSVC14] se propuxese un algoritmo de proxección que combinase ambas metodoloxías. O propósito desta parte da memoria consiste na extensión de dito método á resolución de fluxos incompresibles en réxime turbulento e de fluxos compresibles a baixo número de Mach. Ademais, contémplase a incorporación, ao modelo, das ecuacións de transporte de especies. Ter en conta fluxos turbulentos lévanos a engadir o modelo de turbulencia $k-\varepsilon$ standard. Debido á dependencia entre as distintas ecuacións introducida pola viscosidade turbulenta, obsérvase a necesidade de dispoñer de métodos de alta orde para poder resolver correctamente este tipo de fluxos. De aquí xorde outro dos principais obxetivos de esta tese doutoral: o desenvolvemento de métodos de alta orde en espazo e tempo.

No capítulo seis da memoria, descríbese o método de proxección desenvolvido para a resolución de fluxos incompresibles. Dito método permite calcular as presións independentemente das restantes variables conservativas e pode dividirse en tres etapas:

- Etapa de transporte-difusión: calcúlase unha primeira aproximación das variables conservativas asociadas ao modelo empregando un método de volumes finitos.
- Etapa de proxección: utilízase un método de elementos finitos para calcular a corrección das presións.
- Etapa de posproxección: modifícanse os valores das velocidades obtidos na primeira etapa grazas á corrección das presións o que garante que a diverxencia da velocidade sexa nula. Ademais, as restantes variables conservativas do sistema actualízanse tendo en conta os termos de produción e os termos fonte.

Un dos aspectos clave, para o correcto funcionamento da metodoloxía proposta, é a definición das mallas que se utilizan para resolver as presións e as variables conservativas. Inicialmente, divídese o dominio computacional empregando un mallado de tetraedros a partir do cal se constrúe a malla de volumes finitos dual cuxos nodos se sitúan sobre os baricentros das caras da malla primal. Deste xeito, os nodos dos volumes finitos fronteira atópanse sobre a propia fronteira facilitando a implementación das condicións de contorno o que constitúe unha das principais vantaxes das mallas tipo cara. Estas mallas, xa foron satisfactoriamente utilizadas na resolución das ecuacións das augas someras bidimensionais (ver [BDDVC98]) e para a resolución das ecuacións de Navier-Stokes mediante o uso de esquemas Galerkin descontinuos (ver [THD09] e [DHC$^+$10]). No que se refire á discretización temporal, empregamos un esquema de Euler explícito.

A etapa de transporte difusión céntrase na aproximación dos termos convectivos e difusivos involucrados nas ecuacións do modelo. Emprégase o esquema de Rusanov para a aproximación do fluxo numérico (ver [Tor09] e [VC15]). Co obxectivo de mellorar a orde de exactitude, propóñense dúas aproximacións diferentes que poden ser combinadas co esquema de Rusanov: o esquema tipo Kolgan CVC e o método LADER.

O esquema tipo Kolgan CVC, xa introducido para a ecuación escalar, é de segunda orde en espazo e primeira orde en tempo e pode combinarse con dúas discretizacións distintas para o termo viscoso. A primeira foi presentada en [BFSVC14] e baséase na descomposición do fluxo como suma dunha parte ortogonal e unha non ortogonal. A segunda opción fai uso da malla de elementos finitos primal para calcular as derivadas empregando unha aproximación tipo Galerkin. Pódese observar que esta segunda aproximación proporciona un método de maior orde que a primeira.

Coa finalidade de desenvolver un método de segunda orde tanto en espazo coma en tempo, a metodoloxía LADER, introducida na segunda parte desta memoria, esténdese á resolución do modelo tridimensional. É, neste caso, cando se percibe unha das principais vantaxes que presenta LADER fronte ao método ADER clásico. Ao ter sido deseñado pensando na estrutura de mallas do problema tridimensional, aproveitamos a existencia da malla dual para reducir o *stencil* e, dese xeito, diminuír o custe computacional do método. Esta metodoloxía afecta tamén aos termos difusivos que deberán ser calculados empregando unhas variables conservativas evolucionadas de forma análoga ao feito no caso escalar. Por outra banda, para evitar posibles oscilacións espurias, no paso de construción dos polinomios de orde unha de LADER, utilízase unha reconstrución tipo ENO congruente coa estrutura da malla primal.

Na etapa de proxección, a corrección das presións é calculada mediante un método de elementos finitos $\mathbb{P}^1$ asociado á malla de tetraedros primal. O uso das mallas encaixadas definidas anteriormente, xunto cun método simple de transvase de información entre ambas, proporcionan un algoritmo estable. En concreto, as variables conservativas defínense constantes por tetraedro e a corrección as presións fíxase constante sobre cada cara de volume finito.

A etapa de posproxección comeza coa actualización, utilizando a corrección das presións, dos valores das variables conservativas asociadas á velocidade. Así, pódense tratar de forma implícita os termos de produción asociados ao modelo de turbulencia. Os termos de disipación restantes trátanse de forma semi-implícita. Finalmente, os termos fonte son avaliados proporcionando as aproximacións das variables conservativas asociadas á turbulencia e ao transporte de especies.

A validación da metodoloxía presentada realízase mediante diversos test obtidos empregando o método de solucións manufacturadas. Nos distintos problemas considerados observamos que as ordes de converxencia obtidas numericamente coinciden coas esperadas teoricamente. Alén, realízanse tests clásicos da mecánica de fluídos computacional comparando os resultados con datos experimentais recollidos na bibliografía (ver [Saa11] e [BFSVC14]).

No último capítulo, esténdese a metodoloxía empregada no capítulo anterior á resolución de fluxos compresibles a baixo número de Mach. Asúmese que as temperaturas e a composición do fluído son coñecidas o que nos permite utilizar a ecuación de estado para obter o valor das presións en cada instante de tempo. Como consecuencia é preciso engadir unha nova etapa ao algoritmo proposto inicialmente para fluxos incompresibles:

- Etapa de transporte-difusión: calcúlase unha primeira aproximación das variables conservativas asociadas ás velocidades empregando un método de volumes finitos.

- Etapa de preproxección: obtense a aproximación das densidades, no novo instante de tempo, utilizando a temperatura e as fraccións másicas das especies. No caso de que a variable proporcionada orixinalmente sexa a entalpía, resólvese a ecuación da entalpía interna para un gas perfecto mediante o método de Newton.
- Etapa de proxección: emprégase un método de elementos finitos para calcular a corrección das presións.
- Etapa de posproxección: modifícanse os valores das velocidades obtidos na primeira etapa grazas á corrección das presións de xeito que as novas aproximacións verifiquen a ecuación de conservación da masa.

É importante destacar que a dependencia espazo-temporal da densidade supón a aparición de novos termos nas ecuacións de transporte. En particular, se estudamos o termo de fluxo involucrado na ecuación dos momentos, observamos que a viscosidade numérica non ten en conta a derivada da densidade respecto da variable espacial. Como consecuencia, podemos obter solucións espurias. Seguindo [BLVC17a], proponse engadir unha nova viscosidade artificial que corrixa este erro.

Na última sección do capítulo, preséntanse os resultados para algúns tests analíticos empregados na validación do código para fluxos compresibles a baixo número de Mach.

Os contidos desta parte da memoria relativos a fluxos incompresibles foron incluídos nas publicacións [BBC+15], [BBF+17c] e [BFTVC18]. A contribución correspondente a fluxos compresibles a baixo número de Mach atópase en preparación.

USC
UNIVERSIDADE
DE SANTIAGO
DE COMPOSTELA

USC
UNIVERSIDADE
DE SANTIAGO
DE COMPOSTELA

Bibliography

[Bat53] G. K. Batchelor. *The theory of homogeneous turbulence*. Cambridge university press, 1953.

[BBC+15] A. Bermúdez, S. Busto, M. Cobas, J. L. Ferrín, L. Saavedra and M. E. Vázquez-Cendón. Paths from mathematical problem to technology transfer related with finite volume methods. In *Proceedings of the XXIV Congress on Differential Equations and Aplications / XIV Congress on Applied Mathematics*, 45–56, 2015.

[BBF+17a] A. Bermúdez, S. Busto, J. L. Ferín, Toro E. F. and Vázquez-Cendón M. E. A high order FV/FE projection method for Navier-Stokes equations. In *Book of abstracts of the IV Congreso de Jóvenes Investigadores de la Real Sociedad Matemática Española*, page 242, 2017.

[BBF+17b] A. Bermúdez, S. Busto, J. L. Ferrín, Toro E. F. and M. E. Vázquez-Cendón. A high order FV/FE projection method for compressible low-Mach number flos. In *Book of abstracts of the SHARK-FV 2017 conference*, page 35, 2017.

[BBF+17c] A. Bermúdez, S. Busto, J. L. Ferrín, L. Saavedra, E. F. Toro and M. E. Vázquez-Cendón. *SEMA SIMAI Springer Series. Computational Mathematics, Numerical Analysis and Applications*, chapter A projection hybrid finite volume-ADER/finite element method for turbulent Navier-Stokes, 201–206. Springer, 2017.

[BBFF15] A. Bermúdez, S. Busto, J. L. Ferrín and P. Fontán. A first approach to the design of tidal turbines. In *Proceedings of the XXIV Congress on Differential Equations and Aplications / XIV Congress on Applied Mathematics*, 909–914, 2015.

[BD14] W. Boscheri and M. Dumbser. A direct arbitrary-lagrangian-eulerian ADER-WENO finite volume scheme on unstructured tetrahedral meshes for conservative and non-conservative hyperbolic systems in 3D. *J. Comput. Phys.*, 275:484–523, 2014.

[BDA+02] J. B. Bell, A. S. Day, A. S. Almgren, M. J. Lijewski and C. A. Rendleman. A parallel adaptive projection method for low Mach number flows. *Int. J. Numer. Methods Fluids*, 40:209–216, 2002.

[BDDVC98] A. Bermúdez, A. Dervieux, J. A. Desideri and M. E. Vázquez-Cendón. Upwind schemes for the two-dimensional shallow water equations with variable depth using unstructured meshes. *Comput. Methods Appl. Mech. Eng.*, 155(1):49–72, 1998.

[BDL16] W. Boscheri, M. Dumbser and R. Loubère. Cell centered direct Arbitrary-Lagrangian-Eulerian ADER-WENO finite volume schemes for nonlinear hyperelasticity. *Computers & Fluids*, 134-135(Supplement C):111 – 129, 2016.

[Ber05] A. Bermúdez. *Continuum thermomechanics*, volume 43 of *Progress in Mathematical Physics*. Birkhäuser Verlag, Basel, 2005.

[Ber06] C. Berthon. Why the MUSCL-Hancock scheme is L1-stable. *Numer. Math.*, 104:27–46, 2006.

[BFSVC14] A. Bermúdez, J. L. Ferrín, L. Saavedra and M. E. Vázquez-Cendón. A projection hybrid finite volume/element method for low-Mach number flows. *J. Comp. Phys.*, 271:360–378, 2014.

[BFTVC18] S. Busto, J. L. Ferrín, E. F. Toro and M. E. Vázquez-Cendón. A projection hybrid high order finite volume/finite element method for incompressible turbulent flows. *J. Comput. Phys.*, 353:169–192, 2018.

[BLVC16] A. Bermúdez, X. López and M. E. Vázquez-Cendón. Numerical solution of non-isothermal non-adiabatic flow of real gases in pipelines. *J. Comput. Phys.*, 323(Supplement C):126 – 148, 2016.

[BLVC17a] A. Bermúdez, X. López and M. E. Vázquez-Cendón. Finite volume methods for multi-component Euler equations with source terms. *Computers & Fluids*, 156:113 – 134, 2017.

[BLVC17b] A. Bermúdez, X. López and M. E. Vázquez-Cendón. Treating network junctions in finite volume solution of transient gas flow models. *J. Comput. Phys.*, 344(Supplement C):187 – 209, 2017.

[BS12] R. Bermejo and L. Saavedra. Modified Lagrange-Galerkin methods of first and second order in time for convection-diffusion problems. *Numer. Math.*, 120:601–638, 2012.

[BTVC16] S. Busto, E. F. Toro and M. E. Vázquez-Cendón. Design and analisis of ADER–type schemes for model advection–diffusion–reaction equations. *J. Comp. Phys.*, 327:553–575, 2016.

[Bus14] S. Busto. Análisis mediante CFD de un dispositivo de generación de energía de corrientes. Master's thesis, Universidade de Santiago de Compostela, 2014.

[Bus15] S. Busto. Diseñando generadores. *As matemáticas do veciño. Actas do Seminario de Iniciación á Investigación*, 35–40, 2015.

[BVC94] A. Bermúdez and M. E. Vázquez-Cendón. Upwind methods for hyperbolic conservation laws with source terms. *Computers & Fluids*, 23(8):1049–1071, 1994.

[CCM15] R. Costa, S. Clain and G. Machado. A sixth-order finite volume scheme for the steady-state incompressible Stokes equations on staggered unstructured meshes. *J. Comput. Phys.*, 349:501–527, 2015.

[CCML17] R. Costa, S. Clain, G. J. Machado and R. Loubère. A very high-order accurate staggered finite volume scheme for the stationary incompressible Navier-Stokes and Euler equations on unstructured meshes. *J. Sci. Comput.*, 71(3):1375–1411, Jun 2017.

[Cea05] L. Cea. *An unstructure finite volume model for unsteady turbulent shallow water flow with wet-dry fronts: Numerical solver and experimental validation.* PhD thesis, UDC, 2005.

[CFL28] R. Courant, K. Friedrichs and H. Lewy. On the partial difference equations of mathematical physics. *Mathematische Annalem*, 100:32–74, 1928.

[CFS13] I. Constenla, J. L. Ferrín and L. Saavedra. Numerical study of a 350MWe tangentially fired pulverized coal furnace of the As Pontes power plant. *Fuel Process. Technol.*, 116(Supplement C):189 – 200, 2013.

[CFVC06] L. Cea, J. R. French and M. E. Vázquez-Cendón. Numerical modelling of tidal flows in complex estuaries including turbulence: An unstructured finite volume solver and experimental validation. *Int. J. Numer. Meth. Engng.*, 67:1909–1932, 2006.

[CFVN50] J. G. Charney, R. Fjörtoft and J. Von Neumann. Numerical integration of the barotropic vorticity equation. *Tellus*, 2(4):237–254, 1950.

[CL14] T. Chacón and R. Lewandowski. *Mathematical and numerical foundations of turbulence models and applications.* Modeling and simulation in science, engineering and technology. Birkhauser, 2014.

[CN63] B. D. Coleman and W. Noll. The thermodynamics of elastic materials with heat conduction and viscosity. *Arch. Ration. Mech. Anal.*, 13(1):167–178, 1963.

[CN96] J. Crank and P. Nicolson. A practical method for numerical evaluation of solutions of partial differential equations of the heat-conduction type. *Adv. Comput. Math.*, 6(1):207–226, 1996.

[CT08] C. E. Castro and E. F. Toro. Solvers for the high-order Riemann problem for hyperbolic balance laws. *J. Comp. Phys.*, 227(4):2481–2513, 2008.

[CVC10] L. Cea and M. E. Vázquez-Cendón. Unstructured finite volume discretization of two-dimensional depth-averaged shallow water equations with porosity. *Int. J. Numer. Methods Fluids*, 63(8):903–930, 2010.

[CVC12] L. Cea and M. E. Vázquez-Cendón. Analysis of a new Kolgan-type scheme motivated by the shallow water equations. *Appl. Num. Math.*, 62(4):489–506, 2012.

[DBTM08] M. Dumbser, D. S. Balsara, E. F. Toro and C.-D. Munz. A unified framework for the construction of one-step finite volume and discontinuous Galerkin schemes on unstructured meshes. *J. Comput. Phys.*, 227(18):8209–8253, 2008.

[DD92] A. Dervieux and J. A. Desideri. Compressible flow solvers using unstructured grids. Technical report, Rapports de Recherche 1732, INRIA, 1992.

[DET08] M. Dumbser, C. Enaux and E. F. Toro. Finite volume schemes of very high order of accuracy for stiff hyperbolic balance laws. *J. Comput. Phys.*, 227(8):3971 – 4001, 2008.

[DHC+10] M. Dumbser, A. Hidalgo, M. Castro, C. Parés and E. F. Toro. FORCE schemes on unstructured meshes II: Non-conservative hyperbolic systems. *Comput. Methods Appl. Mech. Eng.*, 199:625–647, 2010.

[DM05] M. Dumbser and C. D. Munz. ADER discontinuous Galerkin schemes for aeroacoustics. *CR Acad. Sci. II B*, 333(9):683–687, 2005.

[Dum10] M. Dumbser. Arbitrary high order PNPM schemes on unstructured meshes for the compressible Navier-Stokes equations. *Comput. Fluids*, 39(1):60–76, 2010.

[Fav65] A. Favre. Equations des gaz turbulents compressibles. *Journal de Mecanique*, 4(3):361–390, 1965.

[Fro68] J. E. Fromm. A method for reducing dispersion in convective difference schemes. *J. Comput. Phys.*, 3(2):176 – 189, 1968.

[FS13] J. L. Ferrín and L. Saavedra. Distribution of the coal flow in the mill-duct system of the As Pontes power plant using CFD modeling. *Fuel Process. Technol.*, 106(Supplement C):84 – 94, 2013.

[GGHL08] T. Gallouët, L. Gastaldo, R. Herbin and J.-C. Latché. An unconditionally stable pressure correction scheme for the compressible barotropic Navier-Stokes equations. *ESAIM: Mathematical Modelling and Numerical Analysis*, 42(2):303–331, 2008.

[GLL12] W. Gao, H. Li and R. Liu. An unstructured finite volume projection method for pulsatile flows through an asymmetric stenosis. *J. Eng. Math.*, 72(1):125–140, 2012.

[GMS06] J. L. Guermond, P. Minev and J. Shen. An overview of projection methods for incompressible flows. *Comput. Methods Appl. Mech. Eng.*, 195:6011–6045, 2006.

[God59] S. K. Godunov. A finite difference method for the computation of discontinuous solutions of the equations of fluid dynamics. *Mat. Sb.*, 47:357–393, 1959.

[GR96] E. Godlewski and P.-A. Raviart. *Numerical Approximation of Hyperbolic Systems of Conservation Laws*, volume 118 of *Applied Mathematical Sciences*. Springer-Verlag New York, 1996.

[Gur81] M. E. Gurtin. *An introduction to continuum mechanics*, volume 158 of *Mathematics in Science and Engineering*. Academic Press Inc., New York, 1981.

[HD11] A. Hidalgo and M. Dumbser. ADER schemes for nonlinear systems of stiff advection–diffusion–reaction equations. *J. Sci. Comput.*, 48(1-3):173–189, 2011.

[HEOC87] A. Harten, B. Engquist, S. Osher and S. R. Chakravarthy. Uniformly high order accurate essentially non-oscillatory schemes, III. In *Upwind and High-Resolution Schemes*, 218–290. Springer, 1987.

[Hir07] C. Hirsch. *Numerical computation of internal and external flows: The fundamentals of computational fluid dynamics*. Butterworth-Heinemann, 2007.

[HLvL83] A. Harten, P. Lax and A. van Leer. volume 25, chapter On upstream differencing and Godunov-type schemes for hyperbolic conservation laws, 35–61. SIAM Rev., 1983.

[Hof89] K. A. Hoffmann. *Computational fluid dynamics for engineers*. EES, 1989.

[HRS16] J. S. Hesthaven, G. Rozza and B. Stamm. *Certified Reduced Basis Methods for Parametrized Partial Differential Equations*. Springer, 2016.

[Kol11] V.P. Kolgan. Application of the principle of minimizing the derivative to the construction of finite-difference schemes for computing discontinuous solutions of gas dynamics. *J. Comput. Phys.*, 230(7):2384–2390, 2011.

[Lax57] P. D. Lax. Hyperbolic systems of conservation laws II. *Commun. Pur. Appl. Math.*, 10(4):537–566, 1957.

[LCLR16] S. Lorenzi, A. Cammi, L. Luzzi and G. Rozza. POD-Galerkin method for finite volume approximation of Navier-Stokes and RANS equations. *Computer Methods in Applied Mechanics and Engineering*, 311:151 – 179, 2016.

[LeV92] R. J. LeVeque. *Numerical Methods for Conservation Laws*. Lectures in Mathematics. ETH Zürich. Birkhäuser Basel, 1992.

[LeV02] R. J. LeVeque. *Finite Volume Methods for Hyperbolic Problems*. Cambridge Texts in Applied Mathematics. August 2002.

[LL87] L. D Landau and E M Lifshitz. *Course of theoretical physics*, volume 6. Elsevier, second edition, 1987.

[LOC94] X.-D. Liu, S. Osher and T. Chan. Weighted essentially non-oscillatory schemes. *J. Comp. Phys.*, 115(1):200–212, 1994.

[LS72] B. E. Launder and D. B. Spalding. *Mathematical models of turbulence*. Academic Press, 1972.

[LW60] P. Lax and B. Wendroff. Systems of conservation laws. *Commun. Pur. Appl. Math.*, 13(2):217–237, 1960.

[MP94] B. Mohammadi and O. Pironneau. *Analysis of the k-epsilon turbulence model*, volume 31 of *Research in applied mathematics*. Wiley-Masson, 1994.

[MT14] G. I. Montecinos and E. F. Toro. Reformulations for general advection–diffusion–reaction equations and locally implicit ADER schemes. *J. Comput. Phys.*, 275:415–442, 2014.

[PAB+95] R. B. Pember, A. S. Almgren, J. B. Bell, P. Colella, M. Howell and M. Lai. A high order projection method for the simulation of unsteady turbulent non premixed combustion in an industrial burner. In *Proceedings of the 8th International Symposium on Transport Phenomena in Combustion*, 16–20, 1995.

[PBH04] S. Perron, S. Boivin and J.-M. Hérard. A finite volume method to solve the 3D Navier-Stokes equations on unstructured collocated meshes. *Computers & fluids*, 33(10):1305–1333, 2004.

[PPS17] F. Pena, F. Prieto and V. Sande. Opennum. `https://sourceforge.net/projects/opennum/`, 2017. Accessed: 02-11-2017.

[Pra52] L. Prandtl. *Guide à traversle mécanique des fluides*. Dunod, 1952.

[Rey95] Osborne Reynolds. IV. on the dynamical theory of incompressible viscous fluids and the determination of the criterion. *Phil. Trans. R. Soc. Lond. A*, 186:123–164, 1895.

[Rus62] V. V. Rusanov. The calculation of the interaction of non-stationary shock waves and obstacles. *USSR Computational Mathematics and Mathematical Physics*, 1:304–320, 1962.

[Saa11] L. Saavedra. *Modelización Matemática y resolución numérica de problemas de combustión de carbón pulverizado*. PhD thesis, Departamento de Matemática Aplicada Universidade de Santiago de Compostela, 2011.

[Shu98] Chi-Wang Shu. Essentially non-oscillatory and weighted essentially non-oscillatory schemes for hyperbolic conservation laws. In *Advanced numerical approximation of nonlinear hyperbolic equations*, 325–432. Springer, 1998.

[SO88] C.-W. Shu and S. Osher. Efficient implementation of essentially non-oscillatory shock-capturing schemes. *J. Comp. Phys.*, 77(2):439–471, 1988.

[STD+96] M. Schäfer, S. Turek, F. Durst, E. Krause and R. Rannacher. *Benchmark Computations of Laminar Flow Around a Cylinder*, 547–566. Vieweg+Teubner Verlag, Wiesbaden, 1996.

[Str04] J. C. Strikwerda. *Finite difference schemes and partial differential equations*. SIAM, 2004.

[Swe84] P. K. Sweby. High resolution schemes using flux limiters for hyperbolic conservation laws. *SIAM J. Num. Anal.*, 21(5):995–1011, 1984.

[TA07] S. Tu and S. Aliabadi. Development of a hybrid finite volume/element solver for incompressible flows. *Int. J. Numer. Methods Fluids*, 55(2):177–203, 2007.

[Tak06] Y. Takakura. Direct-expansion forms of ADER schemes for conservation laws and their verification. *J. Comp. Phys.*, 219(2):855–878, 2006.

[TAPW09] S. Tu, S. Aliabadi, R. Patel and M. Watts. An implementation of the Spalart-Allmaras DES model in an implicit unstructured hybrid finite volume/element solver for incompressible turbulent flow. *Int. J. Numer. Methods Fluids*, 59(9):1051–1062, 2009.

[TD14] M. Tavelli and M. Dumbser. A staggered semi-implicit discontinuous Galerkin method for the two dimensional incompressible Navier-Stokes equations. *Appl. Math. Comput.*, 248:70 – 92, 2014.

[TD15] M. Tavelli and M. Dumbser. A staggered space-time discontinuous Galerkin method for the incompressible Navier-Stokes equations on two-dimensional triangular meshes. *Computers & Fluids*, 119:235 – 249, 2015.

[TD16] M. Tavelli and M. Dumbser. A staggered space-time discontinuous Galerkin method for the three-dimensional incompressible Navier-Stokes equations on unstructured tetrahedral meshes. *J. Comput. Phys.*, 319:294 – 323, 2016.

[TD17] M. Tavelli and M. Dumbser. A pressure-based semi-implicit space-time discontinuous Galerkin method on staggered unstructured meshes for the solution of the compressible Navier-Stokes equations at all Mach numbers. *J. Comput. Phys.*, 341:341 – 376, 2017.

[TDTK06] E. F. Toro, M. Dumbser, V. A. Titarev and M. Käser. The derivative Riemann problem: the basis for high order ADER schemes. In *ECCOMAS CFD 2006: Proceedings of the European Conference on Computational Fluid Dynamics, Egmond aan Zee, The Netherlands, September 5-8, 2006.* Delft University of Technology; European Community on Computational Methods in Applied Sciences (ECCOMAS), 2006.

[TH09] E. F. Toro and A. Hidalgo. ADER finite volume schemes for nonlinear reaction-diffusion equations. *Appl. Num. Math.*, 59:73–100, 2009.

[THD09] E. F. Toro, A. Hidalgo and M. Dumbser. FORCE schemes on unstructured meshes I: Conservative hyperbolic systems. *J. Comput. Phys.*, 228(9):3368 – 3389, 2009.

[Tit05] V. Titarev. *Derivative Riemann Problem and ADER schemes.* PhD thesis, Università degli studi di Trento, 2005.

[TM14] E. F. Toro and G. I. Montecinos. Advection-diffusion-reaction equations: hyperbolization and high-order ADER discretizations. *SIAM J. Sci. Comp.*, 36(5):A2423–A2457, 2014.

[TMN01] E. F. Toro, R. C. Millington and L. A. M. Nejad. *Godunov methods*, chapter Towards very high order Godunov schemes. Springer, 2001.

[Tor09] E. F. Toro. *Riemann solvers and numerical methods for fluid dynamics: A practical introduction.* Springer, 2009.

[TT01] E. F. Toro and V. A. Titarev. ADER: Towards arbitrary order non-oscillatory schemes for advection-diffusion-reaction. *Proceedings of 8th Taiwan National Conference on Computational Fluid Dynamics*, 2001.

[TT05a] V. A. Titarev and E. F. Toro. ADER schemes for three-dimensional non-linear hyperbolic systems. *J. Comp. Phys.*, 204(2):715–736, 2005.

[TT05b] E. F. Toro and V. A. Titarev. ADER schemes for scalar non-linear hyperbolic conservation laws with source terms in three-space dimensions. *J. of Comp. Phys.*, 202(1):196–215, 2005.

[TT05c] E. F. Toro and V. A. Titarev. TVD fluxes for the high-order ADER schemes. *J. Sci. Comp.*, 24(3):285–309, 2005.

[TT06a] V. A. Titarev and E. F. Toro. ADER schemes for hyperbolic conservation laws with reactive terms. In *ECCOMAS CFD 2006: Proceedings of the European Conference on Computational Fluid Dynamics, Egmond aan Zee, The Netherlands, September 5-8, 2006*. Delft University of Technology; European Community on Computational Methods in Applied Sciences (ECCOMAS), 2006.

[TT06b] E. F. Toro and V. A. Titarev. Derivative Riemann solvers for systems of conservation laws and ADER methods. *J. Comp. Phys.*, 212(1):150–165, 2006.

[TT07] V. A. Titarev and E. F. Toro. Analysis of ADER and ADER-WAF schemes. *IMA J Num. Anal.*, 27(3):616–630, 2007.

[Van83] D. Vandromme. *Contribution à la modélisation et la prédiction d'ècoulements turbulents à masse volumique variable*. PhD thesis, University of Lille, 1983.

[VC94] M. E. Vázquez-Cendón. *Estudio de esquemas descentrados para su aplicación a las leyes de conservación hiperbólicas con términos fuente*. PhD thesis, Universidade de Santiago de Compostela, 1994.

[VC15] M. E. Vázquez-Cendón. *Solving Hyperbolic Equations with Finite Volume Methods*. Springer, 2015.

[vL84] B. van Leer. On the relation between the upwind-differencing schemes of Godunov, Engquist-Osher and Roe. *SIAM J. Sci. Stat. Comp.*, 5(1):1–20, 1984.

[vL97] B. van Leer. Towards the ultimate conservative difference scheme. *J. Comp. Phys.*, 135(2):229–248, 1997.

[Vol02] J. Volker. Higher order finite element methods and multigrid solvers in a benchmark problem for the 3D Navier-Stokes equations. *Int. J. Numer. Methods Fluids*, 40(6):775–798, 2002.

[WB76] R. F. Warming and R. M. Beam. Upwind second-order difference schemes and applications in aerodynamic flows. *AIAA Journal*, 14(9):1241–1249, 1976.

[Wil88] D.C. Wilcox. *Turbulence modelling for CFD*. DCW Industries, 1988.

[Zah08] H.Y. Zahran. Central ADER schemes for hyperbolic conservation laws. *J. Math. Anal. Appl.*, 346(1):120–140, 2008.

[ZZB14] S. Zhang, X. Zhao and S. Bayyuk. Generalized formulations for the Rhie-Chow interpolation. *Journal of Computational Physics*, 258:880–914, 2014.

Nomenclature

We include a list of the main notations used in this thesis.

Part I

Geometrical notation

Notation	Description
$\mathcal{V}$	euclidean vector space
$\mathcal{E}$	affine space
$\mathcal{B}$	body
$\mathcal{P}$	part of a body
$\mathcal{R}$	control volume
$\partial\mathcal{R}$	control volume boundary
$\boldsymbol{\eta}$	outwards unit normal vector
$\mathcal{N}$	set of unit normal vectors

Physical variables

Notation	Description	Units
ρ	density	$\mathrm{kg/m^3}$
p	pressure	Pa

Notation	Description	Units
$\overline{\pi}$	mean pressure	Pa
π	pressure perturbation	Pa
$\mathbf{u}$	velocity	m/s
$\mathbf{f_u}$	source term of momentum equations	N/m^3
$\mathbf{s}$	surface force	$Pa=N/m^2$
$\mathbf{b}$	body force	N/m^3
$\mathcal{T}$	Cauchy stress tensor	Pa
τ	viscous part of the Cauchy stress tensor	Pa
μ	dynamic viscosity	kg/(m s)
ξ	second viscosity coefficient	kg/(m s)
E	specific total energy	$J/kg=m^2/s^2$
g	surface heat	kg/s^3
f	body heat	$kg/(m\ s^3)$
$\mathbf{q}$	heat flux	W/m^2
$\mathbf{e}$	specific internal energy	m^2/s^2
s	specific entropy	J/(kg K)
h	specific enthalpy	J/kg
h_{θ_0}	standard enthalpy formation	J/kg
θ	absolute temperature	K
y_i	mass fraction (i^{th} species)	-
R	gas constant	J/(K kg)
$\mathcal{M}$	molar mass	g/mol

Notation	Description	Units
c	concentration	$\mathrm{mol/m^3}$
c_p	specific heat at constant pressure	J/(kg K)
c_v	specific heat at constant volume	J/(kg K)
$\mathcal{D}$	mass diffusion coefficient	$\mathrm{m^2/s}$
$\mathbf{q}_r$	radiation heat flux	$\mathrm{W/m^2}$
$\mathbf{q}_c$	convection heat flux	$\mathrm{W/m^2}$
k_T	diffusion term coefficient	W/(m K)
τ^R	Reynolds stress tensor	Pa
τ^F	Favre stress tensor	Pa
μ_t	turbulent viscosity	kg/(m s)
k	turbulent kinetic energy	J/kg
ε	mean dissipation rate	J/(kg s)

Part II

Variables for the scalar advection-diffusion-reaction equation

Notation	Description
$\lambda(x,t)$	advection coefficient, characteristic speed
$\alpha(x,t)$	diffusion coefficient
β	reaction term coefficient
$q(x,t)$	scalar conservative variable
c	Courant number
r	radiation number
d	diffusion number

Notation	Description
C_j	finite volume cell
x_j	node of the finite volume C_j
Δx	cell length
Δt	time step
V	control volume
Ω	spatial domain
T	time domain
t_{end}	final time of a simulation
N	number of nodes
q_j^n	discrete scalar conservative variable
ϕ	numerical flux function
α_{RS}	Rusanov coefficient
$\breve{\alpha}_{RS}$	eigenvalue related to Rusanov coefficient
Δ_j	slope related with node x_j
$\Delta_j^{L_*}$	left slope at the node x_j
$\Delta_j^{R_*}$	right slope at the node x_j

Notations used in the stability and accuracy analysis

Notation	Description
A	amplitude
θ	angle
i	complex unit
O_{c_M,d_M,r_m}	4-orthotope
τ^n	truncation error

Part III

Notation related to the discrete equations

Notation	Description
$\mathbf{w_u}$	conservative variables related to $\mathbf{u}$
$\mathbf{w}$	vector of unknowns
$\mathcal{F}^{\mathbf{w}}$	flux tensor
ρ_i^n	approximation of $\rho(x_i, t^n)$
π_i^n	approximation of $\pi(x_i, t^n)$
$\mathbf{U}_i^n$	approximation of $\mathbf{u}(x_i, t^n)$
$\mathbf{Y}_i^n$	approximation of $\mathbf{y}(x_i, t^n)$
K_i^n	approximation of $k(x_i, t^n)$
E_i^n	approximation of $\varepsilon(x_i, t^n)$
θ_i^n	approximation of $\theta(x_i, t^n)$
H_i^n	approximation of $h(x_i, t^n)$
$\mathbf{W}_i^n$	approximation of $\mathbf{w}(x_i, t^n)$
$\widetilde{\mathbf{W}}_i^n$	intermediate approximation of $\mathbf{w}(x_i, t^n)$
$\mathcal{Q}_i^n$	approximation of $q(x_i, t^n)$
δ^n	pressure correction
L	hydraulic diameter
ℓ	turbulence length scale
I	turbulence intensity
u_{avg}	averaged velocity

Numerical functions

Notation	Description
$\boldsymbol{\phi}$	numerical flux function
$\boldsymbol{\varphi}$	numerical diffusion function
$\mathcal{Z}(\mathbf{W}, \boldsymbol{\eta})$	global normal flux
$\alpha_{RS}^{\mathbf{w_u}}$	Rusanov coefficient related to $\mathbf{w_u}$
$\hat{\alpha}_{RS}$	Rusanov coefficient related to $\hat{\mathbf{w}}$
$\breve{\alpha}_{RS}^{\mathbf{w_u}}$	eigenvalue related to Rusanov coefficient $\alpha_{RS}^{\mathbf{w_u}}$

Mesh related notations

Notation	Description
T_k	tetrahedron of the FE mesh
B_k	barycenter of T_k
V_j	vertex of T_k
C_i	cell of the FV mesh
$\lvert C_i \rvert$	volume of cell C_i
N_i	node of C_i
$\mathcal{K}_i$	set of the neighbouring nodes of N_i
Γ_i	boundary of C_i
Γ_{ij}	interface between cells C_i and C_j
N_{ij}	barycenter of Γ_{ij}
$\widetilde{\boldsymbol{\eta}}_{ij}$	outward unit normal vector to Γ_{ij}
$\boldsymbol{\eta_{ij}}$	outward normal vector to Γ_{ij}
$\lvert\lvert \boldsymbol{\eta_{ij}} \rvert\rvert$	area of Γ_{ij}
T_{ij}	auxiliary tetrahedra related to face Γ_{ij}
T_{ijL}, T_{ijR}	upwind auxiliary tetrahedra related to face Γ_{ij}

Index

A high order projection hybrid finite volume - finite element method is developed to solve incompressible and compressible low Mach number flows. Furthermore, turbulent regimes are also considered thanks to the $k - \varepsilon$ model. The unidimensional advection-diffusion-reaction equation is used to construct, analyze and assess high order finite volume schemes. Two families of methods are studied: Kolgan-type schemes and ADER methodology. A modification of the last one is proposed providing a new numerical method called Local ADER. The designed method is extended to solve the transport-diffusion stage of the three-dimensional projection method. Within the projection stage the pressure correction is computed by a piecewise linear finite element method. Numerical results are presented, aimed at verifying the formal order of accuracy of the schemes and to assess the performance of the method on several realistic test problems.